



omni

OAK RIDGE NATIONAL LABORATORY

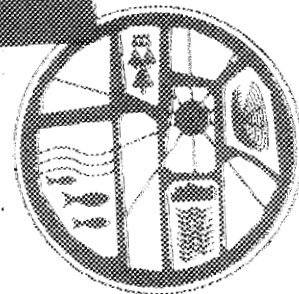
MARTIN MARIETTA

Evaluation of an In Situ Vitrification Field Demonstration of a Simulated Radioactive Liquid Waste Disposal Trench

B. P. Spalding
G. K. Jacobs

Environmental Sciences Division
Publication No. 3832

OAK RIDGE NATIONAL LABORATORY
CENTRAL RESEARCH LIBRARY
CIRCULATION SECTION
4500N ROOM 175
LIBRARY LOAN COPY
DO NOT TRANSFER TO ANOTHER PERSON.
If you wish someone else to see this report, send in
name with report and the library will arrange a loan.
ORNL-118 (6-97)



OPERATED BY
MARTIN MARIETTA ENERGY SYSTEMS, INC.
FOR THE UNITED STATES
DEPARTMENT OF ENERGY

This report has been reproduced directly from the best available copy.

Available to DOE and DOE contractors from the Office of Scientific and Technical Information, P.O. Box 62, Oak Ridge, TN 37831, prices available from (615) 576-8401, FTS 626-8401.

Available to the public from the National Technical Information Service, U.S. Department of Commerce, 5285 Port Royal Rd., Springfield, VA 22161.

NTIS price codes—Printed Copy: A12 Microfiche A01

This report was prepared as an account of work sponsored by an agency of the United States Government. Neither the United States Government nor any agency thereof, nor any of their employees, makes any warranty, express or implied, or assumes any legal liability or responsibility for the accuracy, completeness, or usefulness of any information, apparatus, product, or process disclosed, or represents that its use would not infringe privately owned rights. Reference herein to any specific commercial product, process, or service by trade name, trademark, manufacturer, or otherwise, does not necessarily constitute or imply its endorsement, recommendation, or favoring by the United States Government or any agency thereof. The views and opinions of authors expressed herein do not necessarily state or reflect those of the United States Government or any agency thereof.

ENVIRONMENTAL SCIENCES DIVISION
EVALUATION OF AN IN SITU VITRIFICATION FIELD DEMONSTRATION
OF A SIMULATED RADIOACTIVE LIQUID WASTE DISPOSAL TRENCH

Brian P. Spalding
Gary K. Jacobs

Environmental Sciences Division
Publication No. 3332

Date Published - October 1989

Prepared for the
Office of Defense Waste and Transportation Management
(Activity No. GF 11 03 00 0)

Prepared by the
OAK RIDGE NATIONAL LABORATORY
Oak Ridge, Tennessee 37831-6285
operated by
MARTIN MARIETTA ENERGY SYSTEMS, INC.
for the
U.S. Department of Energy
under contract DE-AC05-84OR21400



3 4456 0328276 6

CONTENTS

	<u>Page</u>
LIST OF FIGURES	v
LIST OF TABLES	ix
ACKNOWLEDGMENTS	xi
EXECUTIVE SUMMARY	xiii
1. INTRODUCTION	1
1.1 ISV PROCESS DESCRIPTION	5
1.2 PILOT-SCALE TEST SYSTEM	7
1.2.1 Power-Delivery System	7
1.2.2 Off-Gas Containment and Electrode-Support Hood	10
1.2.3 Off-Gas Treatment System	10
2. TEST OBJECTIVES	14
3. SITE PREPARATION AND TRENCH CONSTRUCTION	17
4. ISV RUN PERFORMANCE	27
4.1 RUN PARAMETERS AND OVERALL SYSTEM PERFORMANCE	27
4.2 ISV PROCESS TEMPERATURES	35
4.3 PROCESS OFF-GAS SYSTEM EVALUATION	43
4.3.1 Off-Gas Hood	46
4.3.2 Off-Gas Ducting	47
4.3.3 Off-Gas Scrub Solutions	49
4.3.4 Off-Gas HEPA Filters	63
4.3.5 Overall Off-Gas System	69
5. ISV PRODUCT CHARACTERIZATION	75
5.1 FIELD SAMPLING AND CHARACTERIZATION	75
5.2 PHYSICAL DESCRIPTION OF ISV PRODUCT	85
5.3 BULK CHEMICAL COMPOSITION	90
5.4 MINERALOGICAL PHASE CHARACTERIZATION	109
5.5 CHEMICAL DURABILITY OF ISV PRODUCT	113
5.5.1 MCC-1 Static Leach Test	114
5.5.2 MCC-3 Agitated Powder Leach Tests	119
5.5.3 Pulverized Product Leaching with 0.1 N HCl	126
5.5.4 Leaching of ¹³⁷ Cs-, ⁹⁰ Sr-, and ⁶⁰ Co-Labeled Soil Glasses	130
5.5.5 Retention and Leachability of ¹³⁷ Cs, ⁹⁰ Sr, and ⁶⁰ Co from Thermally Treated Soils	139

	<u>Page</u>
6. RADIOLOGICAL AND OPERATIONAL SAFETY ASSESSMENT OF ISV FOR APPLICATION TO ORNL SEEPAGE PITS AND TRENCHES	148
7. REFERENCES	156
APPENDIX--ANALYTICAL DATA	A-1

LIST OF FIGURES

<u>Figure</u>		<u>Page</u>
1	Location of radioactive liquid waste disposal pits 1-4 and trenches 5-7 at ORNL in relation to the pilot-scale ISV demonstration site	2
2	Construction details of ORNL liquid waste disposal trench 7	3
3	Schematic illustration of the ISV operating sequence	6
4	Cutaway view of the pilot-scale ISV processing components	8
5	Scott-Tee electrical connection for the pilot-scale ISV system	9
6	Schematic drawing of the pilot-scale ISV off-gas treatment system	11
7	Tandem nozzle Hydro-Sonic scrubber (Hydro Sonic Systems, Dallas, Texas)	13
8	View of stratification in the eastern wall of ORNL ISV demonstration trench showing folding, dip, and interbedded limestone and shale	18
9	Cross section and longitudinal section of ORNL pilot-scale trench with predicted shape of ISV mass	20
10	View of cesium and strontium carbonate addition to ORNL ISV demonstration trench with the central vertical array of thermocouples	21
11	ORNL ISV demonstration trench partially filled with crushed limestone	22
12	ORNL ISV demonstration trench showing final stages of filling with soil	23
13	View of pilot-scale off-gas hood, ducting, and process trailer at ORNL demonstration site	26
14	Voltage and amperage to electrodes during the ORNL ISV demonstration	30
15	Total power (kilowatts) and cumulative energy (megawatt-hours) to the electrodes during the ORNL ISV demonstration	31
16	Flow rate of off-gas at the stack during the ORNL ISV demonstration	32
17	Temperatures of the off-gas system components during the ORNL ISV demonstration	33

<u>Figure</u>	<u>Page</u>
18	The concentrations of carbon monoxide and carbon dioxide at the stack during the ORNL ISV demonstration 34
19	Top sections of the four molybdenum electrodes and graphite sleeves after the ORNL ISV demonstration illustrating the oxidation of the graphite sleeves 36
20	Temperatures in the central vertical array of type-K thermocouples in the ORNL ISV demonstration trench and derived depths of melting . . . 37
21	Temperatures along the west and east side of the ISV trench at indicated depths 2.2 m north of the center of the ORNL ISV demonstration trench 39
22	Temperatures along the west and east sides of the ISV trench at indicated depths 2.2 m south of the center of the ORNL ISV demonstration trench. 40
23	Temperatures along the west and east sides of the ISV trench at indicated depths 3.1 m north of the center of the ORNL ISV demonstration trench 41
24	Temperatures along the west and east sides of the ISV trench at indicated depths 3.1 m south of the center of the ORNL ISV demonstration trench 42
25	Amounts of cesium and strontium in off-gas system components after the ORNL ISV demonstration 45
26	Electrical conductivity and pH of the off-gas scrub solution during the ORNL ISV demonstration 54
27	Cumulative titratable acidity and alkalinity in the off-gas scrub solution during the ORNL ISV demonstration 55
28	Cumulative amounts of total, dissolved, and suspended solids in the off-gas scrub solution during the ORNL ISV demonstration 56
29	Cumulative amounts of Ca, Mg, and Sr in the off-gas scrub solution during the ORNL ISV demonstration 58
30	Cumulative amounts of Li, Na, and Cs in the off-gas scrub solution during the ORNL ISV demonstration 60
31	Cumulative amounts of Al, Fe, and Si in the off-gas scrub solution during the ORNL ISV demonstration 61

<u>Figure</u>	<u>Page</u>
32	Cumulative amounts of gross-beta radioactivity in the off-gas scrub solution during ORNL the ISV demonstration 62
33	Leaching of ¹³⁷ Cs from borosilicate glass vials following heating to indicated temperatures 65
34	Distribution of alkali metal elements in the ISV off-gas system components after the ORNL ISV demonstration 71
35	Distribution of alkaline earth elements in the off-gas system components after the ORNL ISV demonstration 73
36	Distribution of Al, Fe, Si, and solids in the off-gas system components after the ORNL ISV demonstration 74
37	View of the ORNL ISV demonstration trench after removal of the off-gas hood 76
38	Relative positions of cores into the ISV mass following the ORNL ISV demonstration 77
39	View of the vitrified mass (looking east) after excavation following the ORNL ISV demonstration 81
40	Position of the grab samples taken after excavation of vitrified mass 82
41	Dark green porous (upper) and dense (lower) glass phases found in the vitrified mass in the ORNL ISV demonstration trench 86
42	Gas cavity and spherulites found in the vitrified mass from the ORNL ISV demonstration trench 87
43	Portlandite (Ca(OH) ₂) found at the contact between the vitrified material and the limestone cobble in the ORNL ISV demonstration trench 88
44	Contact zone between the saprolite and the vitrified material near the SW electrode in the ORNL ISV demonstration trench 89
45	Cesium and strontium composition of all vitrified samples from ORNL ISV demonstration trench 106

<u>Figure</u>	<u>Page</u>
46 Photomicrograph of a single spherulite within the glass phase from the ORNL ISV demonstration trench ($\times 10$ polarized light)	110
47 Backscattered electron image of a spherulite, showing the textural relationship between the feldspar-like (dark zones) and wollastonite-like (light zones) phases in the ORNL ISV demonstration trench	112
48 Results for Al, Ca, and Mg from MCC-3 agitated powder leach tests	123
49 Results for Sr, Cs, and Si from MCC-3 agitated powder leach tests	123
50 Change in normalized concentration of Si (between NC of sample and NC of initial solution) versus log (time \times SA/V) for MCC-3 agitated powder leach tests	125
51 Leaching of elements from pulverized crystalline phase of the ORNL ISV demonstration trench product with 0.1 N HCl	127
52 Leaching of elements from pulverized glass phase of the ORNL ISV demonstration trench product with 0.1 N HCl	128
53 Leaching of radionuclides from pulverized specimens of radioisotopically labeled soil glasses	133
54 Cumulative leaching of radioisotopes from soil and pulverized soil glass with CaCl_2 and dilute acid	135
55 Leachability of ^{90}Sr from soil following treatments of increasing temperature	138
56 Retention of radioisotopes in soil following heat treatments of increasing temperature	141
57 The retention of ^{137}Cs in soil following heating to 1600°C for increasing periods of time	143
58 Weight loss of radionuclide-labeled soils following heat treatments of increasing temperature	145
59 Extraction of radionuclides from soil with 0.1 N HCl following heat treatments of increasing temperature	146

LIST OF TABLES

<u>Table</u>		<u>Page</u>
1	Comparison of predicted and actual operational results from the pilot-scale ISV demonstration	29
2	Distribution of elements in ISV off-gas system components	44
3	Average elemental composition of ISV ash deposited on off-gas system ducting	48
4	Total inventory of elements and characteristics in barrels of ISV off-gas scrub solutions	50
5	Comparison of scrub solution inventories	64
6	Elemental inventories deposited on the off-gas HEPA filters	68
7	ISV off-Gas retention factors for elements	70
8	Description of ISV cores	78
9	Description of grab samples from ISV mass	83
10	Samples from ISV cores and grab samples selected for bulk chemical analysis	91
11	Bulk composition of ISV samples	92
12	Bulk chemical composition of crushed limestone and soil from ISV trench	93
13	Bulk chemical composition of soil (duplicate and replicate analyses) from ORNL ISV demonstration trench	94
14	Bulk chemical composition of crushed limestone (duplicate and replicate analyses) from ORNL ISV demonstration trench	95
15	Bulk chemical composition of ISV core samples from ORNL ISV demonstration trench	96
16	Bulk chemical composition of ISV glass (note duplicate analyses)	98
17	Bulk chemical composition of ISV spherulites (note duplicate analyses)	99

<u>Table</u>	<u>Page</u>
18 Bulk chemical composition of ISV glass sample QG1 (note duplicate analyses)	100
19 Bulk chemical composition of ISV spherulite in thin section sample H1-1	101
20 Comparison of the average chemical compositions of ISV spherulites and glass	102
21 Average chemical composition of the ISV product	103
22 Average chemical compositions of the two major phases identified in spherulite H1-1	104
23 Calculation of limestone-to-soil mixing ratio in the ORNL ISV demonstration product	108
24 Chemical composition (milligrams per liter) of the initial leach solution use for Material Characterization Center testing of ORNL ISV demonstration products (three analyses via ICP; Cs, K, and Sr via AA)	115
25 Analytical data (milligrams per liter except where noted) from MCC-1 28-d leach tests	116
26 Normalized release (grams per square meter) values for ISV samples in MCC-1 28-d leach tests	118
27 Analytical data (milligrams per liter except where noted) from MCC-3 modified agitated powder leach tests	120
28 Extraction of cesium and strontium from ISV crystalline and glass phases by alternate leaching procedures	129
29 Characteristics of radionuclide-contaminated soils used for preparing radionuclide-labeled soil glasses	131
30 Leachability of ¹³⁷ Cs and ⁹⁰ Sr from soil and soil glass	137
31 Hypothetical Distribution of ¹³⁷ Cs activity in ISV off-gas system after vitrifying 10,000 Ci	149

ACKNOWLEDGMENTS

Staff at ORNL who contributed to the success of the demonstration included C. Abner, C. Brown, C. Bruce, C. D. Farmer, C. Thomas, R. Thomas, and R. Todd. Staff from PNL who helped to prepare the site and run the test included J. Buel, J. G. Carter, K. Eliason, T. Hinkle, S. Koegler, M. Longaker, K. Oma, T. Powell, and C. Timmerman. We gratefully acknowledge the help of numerous other persons at ORNL who helped in the preparation of the site. We thank T. E. Myrick for his programmatic support that enabled us to accomplish this demonstration. O. C. Kopp, H. Y. McSween, L. A. Taylor, and Y. Jin of the University of Tennessee provided the XRF and electron microprobe analyses. We also acknowledge the assistance of Mr. H. S. Kuo, Atomic Energy Council, Republic of China, for help in the product leaching characterization studies. Tammy Prandini patiently helped with the preparation of the manuscript.

EXECUTIVE SUMMARY

In July 1987, a field demonstration of in situ vitrification (ISV) was carried out at the Oak Ridge National Laboratory (ORNL). The project was a collaborative venture between ORNL and Battelle Pacific Northwest Laboratory (PNL) using the PNL pilot-scale processing unit. A 3/8-scale model of an ORNL radioactive liquid waste disposal trench was constructed and chemical additions of Cs_2CO_3 and SrCO_3 were used to simulate the ^{137}Cs and ^{90}Sr contained in the seven abandoned ORNL seepage disposal trenches. A 20-Mg mass of vitrified product was produced from the demonstration trench.

The objectives of the demonstration were (1) to evaluate the operational performance of ISV within the local geologic and hydrologic regime with the earthen materials used in ORNL seepage trench construction; (2) to determine the soil retention factors (i.e., the ratio of the elemental amounts in the vitrified mass to that released to the process off-gas) for Cs and Sr so that the radiological safety for ISV application to large inventories of ^{137}Cs and ^{90}Sr can be assessed; and (3) to determine the durability of the resulting ISV product as a waste form and compare it to the durability of the form of ^{137}Cs and ^{90}Sr presently in the ORNL seepage trenches.

Between 1951 and 1966, ORNL disposed of approximately a million curies of fission products, activation products, actinides, and transuranic isotopes by allowing liquid waste to seep into seven pits and trenches filled with crushed limestone. Much of the radioactivity remains in close proximity to its point of disposal and does not seem to be contributing significantly to the current discharges to surface water from ORNL. But in the long term, this relatively high inventory of radioactivity, particularly the long-lived ^{137}Cs and ^{90}Sr , is potentially mobile, and techniques for its stabilization must be considered. ISV represents a promising technique to incorporate this radioactivity into a durable waste form if the process can be shown to be applied safely.

Four molybdenum electrodes with graphite sleeves were placed in the soil formation around the demonstration trench and a specially fabricated off-gas hood placed over the trench. Electrical power (up to 400 kW during the later stages of the run) was applied to the electrodes. Power delivery system malfunctions caused two delays in the initiation of the melt. Once these problems were overcome, the ISV

operation continued uninterrupted, except for scheduled downtime, for 110 h. A total of 29 MWh of energy was delivered to the trench over the 110 h of the run. The starter path on the surface of the soil between the electrodes had to be reestablished several times due to trench surface subsidence during the melting and the delays caused by the power system malfunctions. After allowing several weeks for the ISV block to cool, core samples were taken and, later, one side of the trench was excavated to expose the product. The melt tended to proceed down the long axis of the trench to a greater degree than into the host soil formation. This effect was not anticipated but can be considered advantageous for application to seepage trenches because fewer electrode placements would be required to vitrify a given length of trench than if a symmetrical block were produced.

The retention of Sr in the vitrified zone was excellent; >99.999% of the Sr was incorporated in the ISV product and did not appear in the off-gas processing system. The retention of Cs was encouraging at 99.88%. However, this retention of Cs needs to be improved so that the application of ISV to ORNL seepage trench 7 (about 10,000 Ci of ^{137}Cs per electrode setting) does not result in 12 Ci (0.12%) of ^{137}Cs volatilizing from the melt and depositing in the off-gas system components. Measures to decrease the potential for volatilization of ^{137}Cs need to be established before application to an ORNL seepage trench. Potential techniques include addition of a melt temperature lowering flux (e.g., NaOH) to the trench prior to ISV. The NaOH addition may also allow a subsurface melt initiation which would allow for more removal of ^{137}Cs from the off-gas via filtration by the overlying soil.

The ISV product was found to be a mixture of microcrystalline and glass phases with the former dominating in the slower-cooling regions of the trench. The melt composition was a mixture of the siliceous saprolite (70 wt %) and the limestone cobble (30 wt %) used to backfill the trench and had a 100-poise viscosity temperature of 1325°C. The crystalline phase was in the form of spherulites that consisted of a mixture of feldspar-like and wollastonite-like phases. The bulk chemical compositions of the crystalline and glass phases were essentially identical at 55% SiO_2 , 13% Al_2O_3 , 4% Fe_2O_3 , 2% MgO , 18% CaO , 3% K_2O , 1% Na_2O , 1.5% SrO , and 0.4% Cs_2O . The significant Cs and Sr compositions resulted from the chemical additions to the demonstration trench.

Both Cs and Sr were quite uniformly distributed in all vitrified samples from the trench indicating that thermal convection in the molten state had been extensive.

Both the crystalline and glass phases were tested for leach resistance and durability by using standardized test methods for nuclear waste glasses. Although the crystalline phase was slightly less leach resistant than the glass phase, both phases were as durable as several vitreous forms considered for high-level radioactive waste. The leachability of Sr was greatly reduced over its ambient leachability from contaminated soil and waste by conversion from a cation-exchangeable form in soil to a solubility-controlled phase in the ISV product. The leachability of ^{137}Cs from vitrified phases increased marginally over that in soil, where its fixation by illitic minerals results in its inherently low leachability. However, the increase in ^{137}Cs leachability from the ISV product was more than offset by a decrease in surface area after vitrification, by up to five orders of magnitude, resulting in a net gain in durability. Overall, much of the improvement in waste form durability after vitrification results from a large decrease in sample surface area when soil is transformed to glass. Leaching of pulverized ISV crystalline and glass phases in standardized tests resulted in low release rates. The ISV product is, without qualification, an extremely durable waste form.

Before ISV is applied to an actual seepage trench at ORNL, it would be important to perform a "hot" test to demonstrate some of the possible techniques to minimize or further reduce the volatilization of ^{137}Cs . Control of the power delivered to the melt could be used to maintain temperatures just high enough to continue melting. Exceeding this power level superheats the melt and may cause unnecessary volatilization of ^{137}Cs . Two possible methods to monitor melt temperature (thus minimum power required) are (1) real-time monitoring of ^{137}Cs in the off-gas by using gamma detectors in the process trailer and (2) use of heat sensors in the melt itself. Establishing the ability to regulate ^{137}Cs volatilization through electrical power control would be an important safety demonstration. Additional techniques could be established in bench-scale tests prior to incorporation in a field hot test. One technique could be the addition of a flux (e.g., NaOH) to the trench prior to vitrification to lower the melting temperature of the soil-limestone mixture. Addition of NaOH also may allow melting to be initiated below the surface, which would allow for more removal of ^{137}Cs from the off-gas via filtration through the overlying soil. It is possible that prefiltration of particulates, where the ^{137}Cs

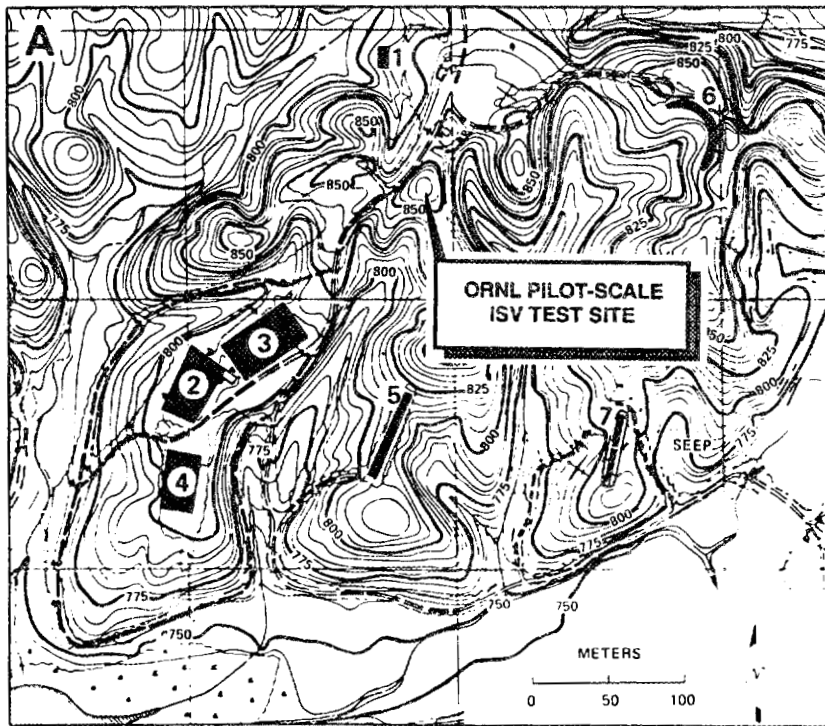
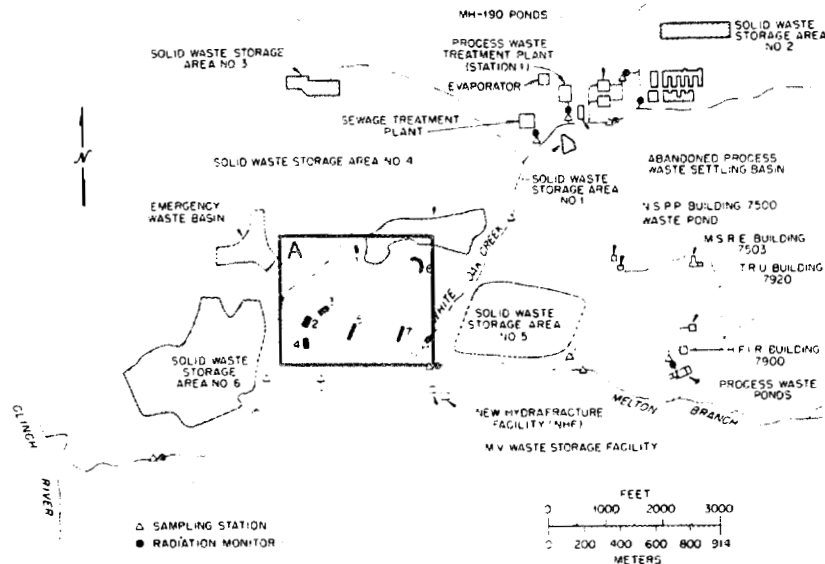
is concentrated, could be accomplished within the off-gas hood so that less ^{137}Cs reached the process trailer. Assuming the success of any or a combination of these techniques, ISV represents a safe and permanent stabilization technique for disposal trenches at ORNL. Because of its inherent costs, ISV would probably not be a cost-effective or necessary stabilization technique for lower-hazard sources such as low-level solid radioactive waste burial trenches.

1. INTRODUCTION

A series of seven seepage pits and trenches (Fig. 1) were used between 1951 and 1966 for the disposal of approximately 6.8×10^8 L of liquid radioactive wastes at Oak Ridge National Laboratory (ORNL) (Olsen et al. 1983). Over 4×10^7 GBq ($\approx 10^6$ Ci) of fission products, activation products, actinides, and transuranium nuclides were disposed of in these seepage trenches (Fig. 2). The acidic liquids were treated with NaOH to raise the pH (pH = 12). The liquids were then pumped to the trenches, which were filled with crushed limestone. To facilitate the seepage of liquids, the trenches were constructed on the tops of ridges and were oriented perpendicular to the strike of the bedding of the weathered formation (Conasauga Group). As the liquids seeped out, most radionuclides remained within close proximity of the trenches. Illite, an abundant phase in these soils, generally sorbs Cs irreversibly (Tamura and Jacobs 1960). Strontium, which is poorly sorbed by the soils, is mostly retained within the trenches as a sludge of coprecipitated $\text{Ca}(\text{Sr})\text{CO}_3$ (Lomenick et al. 1967). To further reduce the potential mobility of contaminants, the trenches were pretreated with a solution of NaOH to increase the alkalinity of the system prior to filling with the liquid wastes (Lomenick et al. 1967; Spalding 1980, 1981). All of these pits and trenches are now covered with asphalt caps to reduce the direct infiltration of precipitation into the waste.

Currently, ^{137}Cs and ^{90}Sr from the pits and trenches do not contribute significantly to surface-water contamination; most of the Cs and Sr remains near the bottom of the pits and trenches. However, near-surface groundwaters in the vicinity of one trench are contaminated with other radionuclides (e.g., ^3H , ^{99}Tc , ^{60}Co , ^{235}U) that were present in the wastes in lesser but significant quantities (Olsen et al. 1983). These researchers suggested that correlations between the activities of radionuclides in the waters with elevated pH values and high concentrations of Na^+ , Ca^{2+} , Cl^- , NO_3^- , and SO_4^{2-} along suspected flowpaths from the trench indicate that present-day leaching and neutralization of the alkalinity in the trench, which retains the ^{90}Sr , is occurring. Because Sr is not strongly sorbed by the soils in this area, the neutralization of the alkaline waste sludge by acidic waters, which creates the potential for significant releases of ^{90}Sr in the future, is a highly adverse process. Although it is not known at the present time what the

ORNL-DWG 88-8631



ILW WASTE PITS AND TRENCHES

Fig. 1. Location of radioactive liquid waste disposal pits 1-4 and trenches 5-7 at ORNL in relation to the pilot-scale ISV demonstration site.

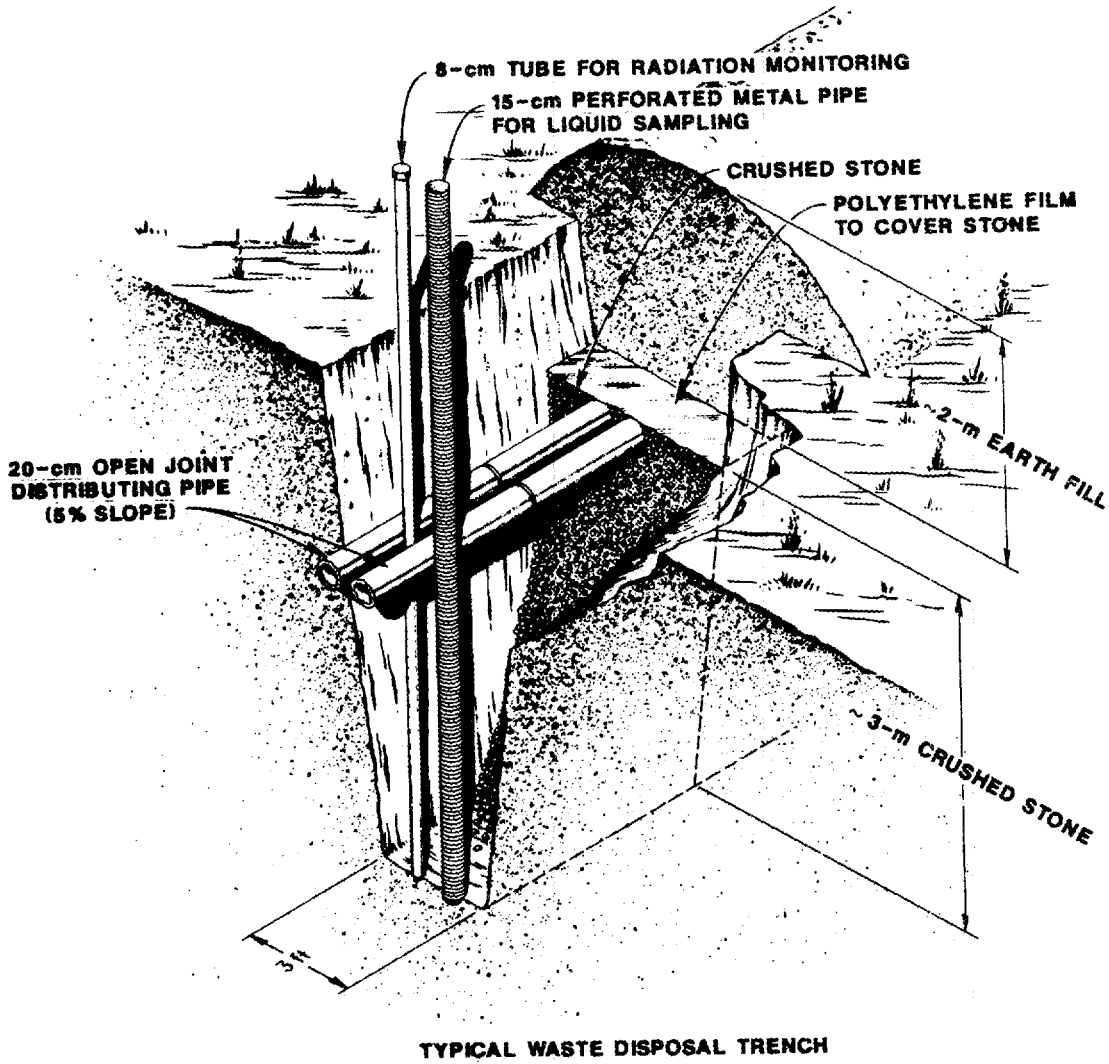


Fig. 2. Construction details of ORNL liquid waste disposal trench 7.

future impact from these sites will be on the environment, these factors, combined with the large inventories of radionuclides in close proximity to the surface, create the potential for significant releases in the future. Either a long-term site monitoring and maintenance program will be required, or remedial actions such as grouting, groundwater diversion, dynamic compaction, or vitrification need to be performed for the permanent closure of these sites.

In situ vitrification (ISV), developed and patented for the U.S. Department of Energy (DOE) by Pacific Northwest Laboratory (PNL) involves placing four electrodes around the volume of contaminated soil, applying electrical power to the electrodes, and melting the entire mass of contaminated soil into a homogeneous and durable glassy-to-microcrystalline waste form. The ISV technology has been extensively tested by PNL at a variety of scales (i.e., electrode spacings from 0.1 to 4.5 m). Tests on several types of wastes have been conducted (Buelt and Freim 1986; Buelt et al. 1987; Timmerman and Oma 1984; Timmerman et al. 1983). A large-scale ISV system capable of producing vitrified blocks of 400 to 800 Mg in a single electrode setting (up to 5.5-m electrode spacing) has been developed and tested (Buelt and Carter 1986).

The pits and trenches at ORNL are candidates for vitrification because of their small areal extent, shallow depth (<6 m), and relatively well-defined and homogeneous contents. The potential for significant personnel exposure during excavation of the contaminated pits and trenches with their high concentrations of ^{137}Cs and ^{90}Sr makes an *in situ* technology highly desirable. However, before a decision concerning the full-scale application of ISV technology to sites at ORNL can be made, several detailed studies were deemed necessary. Results from laboratory- and engineering-scale (0.23-m electrode spacing) tests that were conducted to evaluate the feasibility of ISV for ORNL conditions suggested that a pilot-scale demonstration was warranted (Carter et al. 1987). This pilot-scale demonstration, which involved no radioactivity, but rather stable analogs for ^{137}Cs and ^{90}Sr , had three main objectives: (1) to determine the retention factors (mass in melted soil divided by mass in off-gas) for Sr and Cs under field conditions, (2) to evaluate the durability of the waste form produced in the ORNL soil system, and (3) to assess the operational performance of ISV applications in heterogenous, high-carbonate soils and rocks. The third objective addressed the fact that previous tests of

ISV had been accomplished on the Hanford Site, where the soils are more homogeneous, sandy, and highly siliceous.

1.1 ISV PROCESS DESCRIPTION

The ISV process as applied to the stabilization of contaminated soils involves placing four molybdenum electrodes into a square array of augered holes that bound the contaminated zone. Figure 3 illustrates the sequence of the process. A conductive path for electrical current is formed by placing a small amount of a mixture of powdered graphite and crushed borosilicate glass between the electrodes on the surface of the soil. A molten, conductive path is established via the dissipation of power through the starter material to create a temperature high enough to melt a layer of soil. This molten zone continues to grow downward and increases in size to encompass the contaminated soil. Less-dense material sometimes creates a layer of "rock" that floats near the surface of the melt until it is eventually incorporated into the molten mass.

The high temperature (1600 to 2000°C) of the molten material causes organic materials to pyrolyze; the pyrolysis products diffuse to the surface and combust. In addition, water vapor and carbon dioxide are released from the soil. The movement of these gases through the melt produces some porosity in the final product near the surface of the melt. A hood over the vitrification zone is maintained under a slightly negative pressure to collect off-gases and the small percentage (usually <0.01 wt %) of particulates that are released with the off-gas from the molten mass. The hood also provides support for the electrodes. The off-gases from the process are collected, treated, and monitored to ensure that only environmentally safe levels of potential contaminants are released. Noncombustible materials dissolve into, or become encapsulated by, the molten soil. Thermally induced convection currents within the molten material help to homogenize the final waste form, which often physically resembles natural obsidian.

The principles of ISV are based on developments from work performed at PNL on joule-heated melters for various nuclear waste immobilization projects (Buel et al. 1979). The joule-heating principle involves internal resistance heating as electrical current passes through the molten media. In ISV the resistance decreases as the molten mass increases in size. To maintain a power level high enough to continue

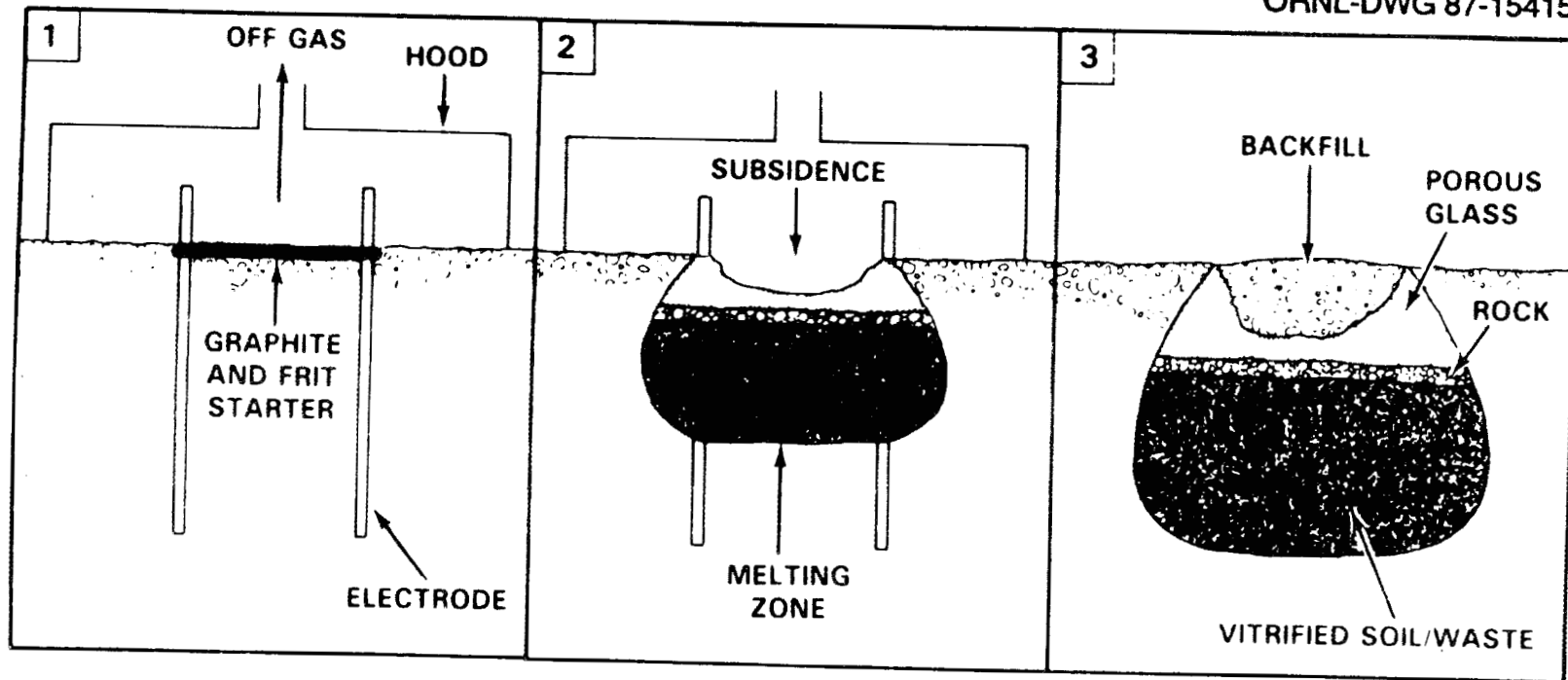


Fig. 3. Schematic illustration of the ISV operating sequence. 1) Initial setup prior to application of power, 2) configuration during operation, 3) vitrified mass after completion of run and withdrawal of electrodes.

melting additional soil, the current must be increased. To accomplish the variable current during ISV processing, a power transformer with multiple voltage taps is used. At startup the ISV process requires high voltage and low amperage. As the melt progresses and resistance decreases, the lower voltage taps on the power transformer allow increased amperage to be applied to the melt, maintaining a high power level. The process continues until heat losses from the melt approach the energy delivered to the soil via the electrodes or until power is discontinued to the electrodes.

1.2 PILOT-SCALE TEST SYSTEM

The pilot-scale test system at ORNL used four electrodes in a square array (1.2-m separation) and consisted of a power-control unit, gas-scrubbing unit, and an off-gas containment hood over the vitrification zone. A cutaway view of the pilot-scale ISV system is illustrated in Fig. 4. Prior to the ORNL test, this system had been used on 11 pilot-scale tests at the Hanford site at electrode spacings from 0.9 to 1.3 m (10 to 50 Mg of melt). The pilot-scale system has been described previously; the following discussion is included for completeness and is modified after Jacobs et al. (1988) and Carter et al. (1988).

1.2.1 Power-Delivery System

The pilot-scale power system uses a Scott-Tee connection to transform a three-phase input to a two-phase secondary load by using diagonally opposed electrodes in a square pattern. The 500-kW power supply may be either voltage or current regulated. The alternating primary current is rated at 480 V, 600 A, three phase, and 60 Hz. The three-phase input feeds a Scott-Tee connected transformer (Fig. 5), which provides a two-phase secondary load. The transformer has four separate voltage tap settings of 1000, 650, 430, and 250 V. Each voltage tap has a corresponding amperage rating of 250, 385, 580, and 1000 A per phase, respectively. The amount of three-phase input power delivered to the transformer is controlled by adjusting the conduction angle of the thyristor switches located in each of the three input lines. These switches, in conjunction with selectable taps on the transformer secondary, regulate the amount of power deliverable to both secondary phases. The Scott-Tee connection provides an even-load distribution among the three primary phases.

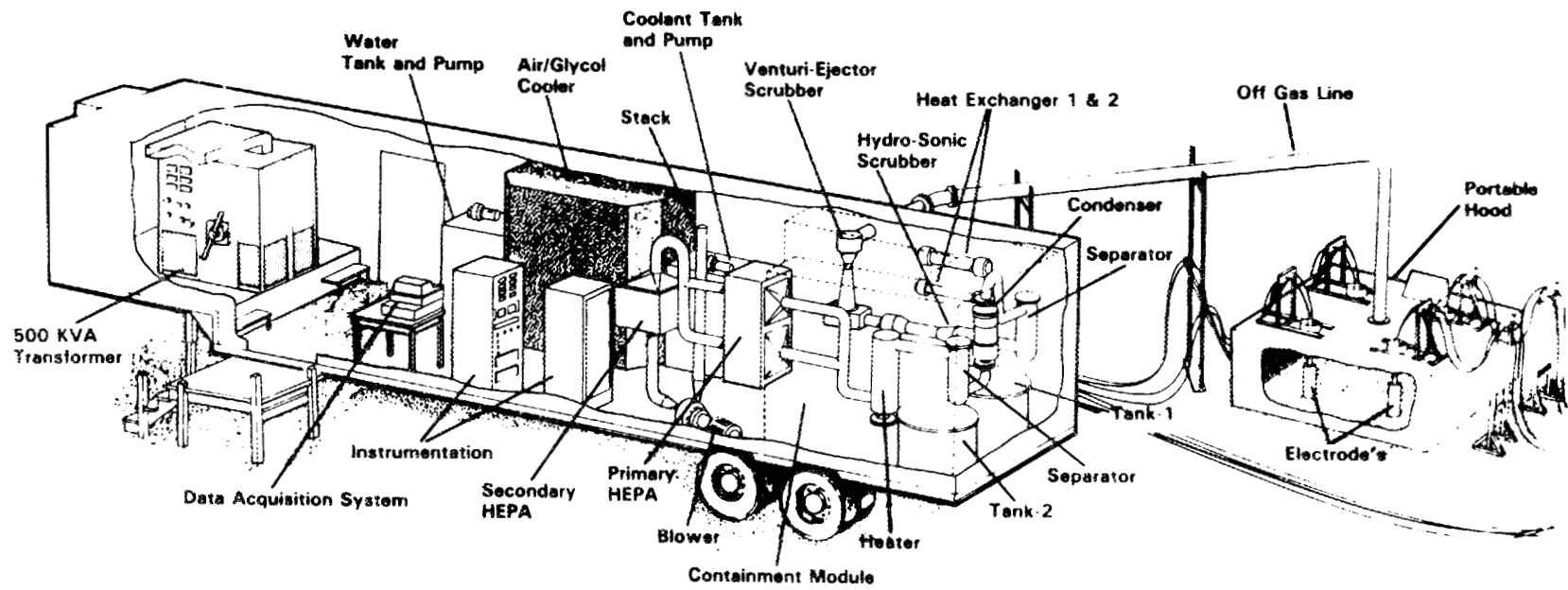


Fig. 4. Cutaway view of the pilot-scale ISV processing components.

ORNL-DWG 88-8629

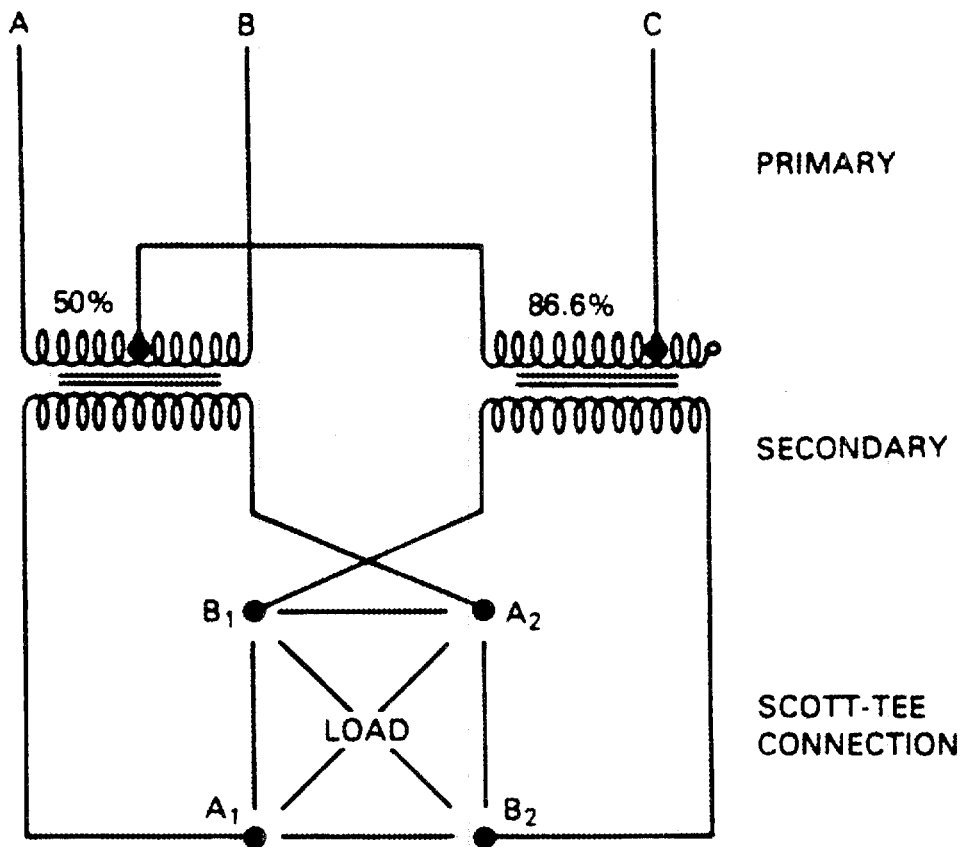


Fig. 5. Scott-Tee electrical connection for the pilot-scale ISV system.

1.2.2 Off-Gas Containment and Electrode-Support Hood

The off-gas containment and electrode-support hood, constructed from seven panels of 20-gauge stainless steel bolted together, is 3.1 m wide, 5.5 m long, and 0.9 m high. Four leveling supports are attached to the corners of the hood, which also has a port for viewing and providing access to the surface of the melt. A central off-gas port allows direct coupling of the hood to the processing trailer and off-gas treatment system. Heat fins installed on the surfaces of the panels help remove radiant heat that is transferred to the hood from the partially molten surface during processing. The hood, designed to withstand a water vacuum of 18 cm, had a flexible skirt of tightly woven, high-temperature-resistant fabric attached to the bottom of all side panels. This skirt extended approximately 0.6 m away from the hood to allow for a hood-to-ground seal when covered with a layer of soil.

The electrodes consisted of molybdenum rods (5-cm diameter) placed into graphite sleeves (15-cm diameter). To reduce the oxidation of the electrodes during processing, they were coated with MoSi_2 , and the annulus between the molybdenum rods and the graphite sleeves was filled with a molybdenum disilicide/zirconium diboride powder. The molybdenum rods of the electrodes protruded through the hood and were surrounded by electrically insulated sleeves that allowed adjustment of the electrode positions. The electrodes and bus bars were supported by insulators above the sleeves that were designed to withstand movement of the molten mass against the electrodes from convection currents and the gravitational and buoyant forces exerted on the electrodes.

1.2.3 Off-Gas Treatment System

The off-gas treatment system is shown schematically in Fig. 6. The off-gas passes through a venturi-ejector scrubber and separator, a Hydro-Sonic scrubber (Hydro Sonic Systems, Dallas, Texas), a separator, a condenser, another separator, a heater, two stages of high-efficiency particulate air (HEPA) filtration, and a blower. Liquid to the two wet scrubbers is supplied by two independent scrub recirculation tanks, each equipped with a pump and heat exchanger. The entire off-gas system has been installed in a 13.7-m-long semitrailer to facilitate transportation (see Fig. 4). All of the off-gas components except the second-stage HEPA filter and blower are housed within a removable containment

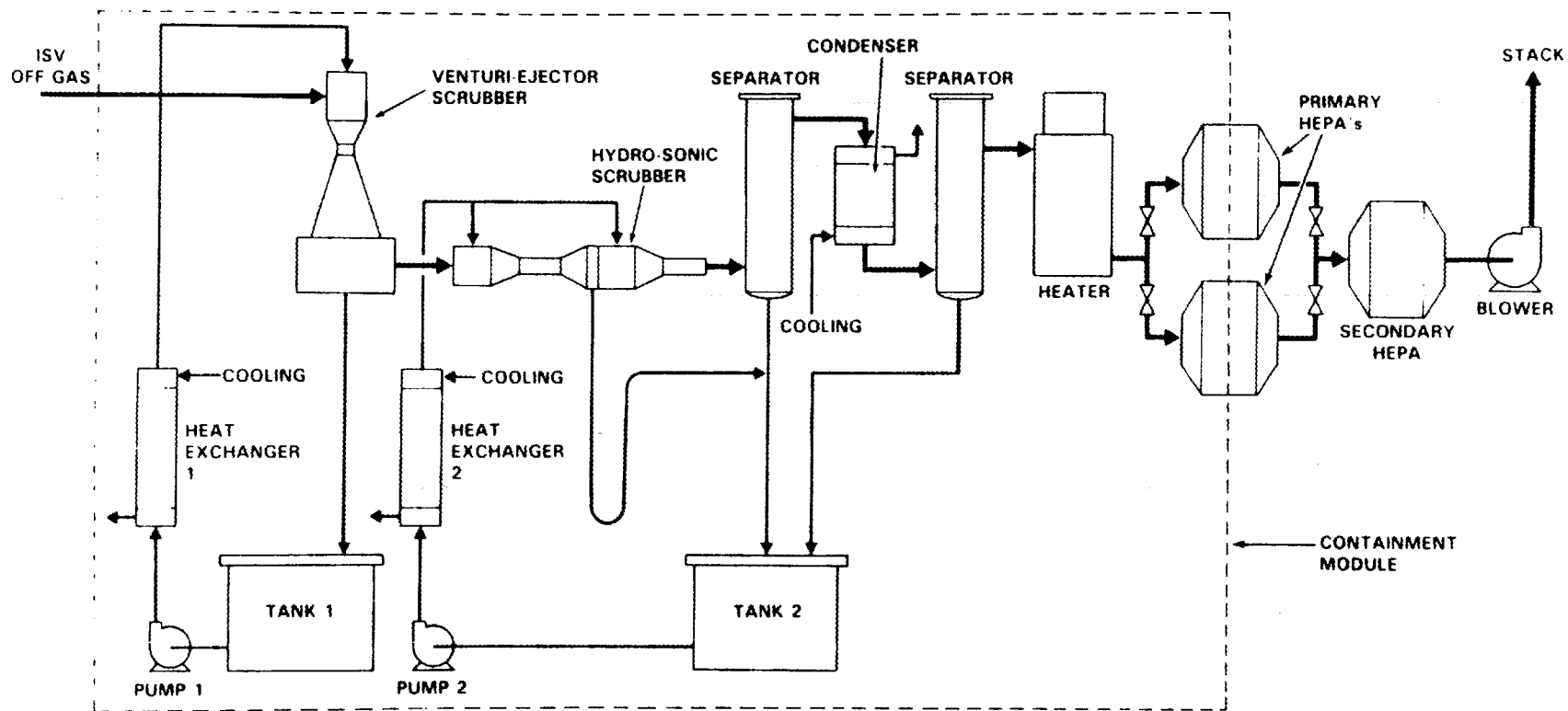


Fig. 6. Schematic drawing of the pilot-scale ISV off-gas treatment system.

module that has gloved access and is maintained under a slightly negative pressure to protect workers from potential contamination. Heat is removed from the off-gas by a closed-loop cooling system consisting of an air/liquid heat exchanger, a coolant storage tank, and a pump. A 1:1 mixture of water and ethylene glycol is pumped first from the storage tank through the shell side of the condenser and the two scrub-solution heat exchangers and then through the air/liquid exchanger, where heat is removed from the coolant.

The venturi-ejector scrubber serves both as a quencher and high-energy scrubber. The second scrubber is a two-stage Hydro-Sonic scrubber (tandem nozzle scrubber) as illustrated in Fig. 7. The first section condenses vapors, removes large particles, and initiates growth of the finer particles so that they are easily captured in the second stage. Particles are captured when the gas is mixed with fine water droplets produced by spraying water into the exhaust of the subsonic nozzle. Mixing and droplet growth continue down the length of the mixing tube. Large droplets containing the particles are then removed by a vane separator and drained back into the scrub tank. When operated at a differential pressure of 127 cm of water, the unit is designed to remove over 90% of all particles greater than 0.5 μm in diameter. Efficiency of removal increases with an increase in pressure differential.

Additional water is removed from the gas system by a condenser with heat exchange area of 8.9 m^2 and a final separator. The gases are then reheated to approximately 25°C above the dew point in a 30-kW heater to prevent condensate carryover to the HEPA filters. The first stage of filtration consists of two HEPA filters (61 × 61 × 29 cm) in parallel. During operation, one filter is used and the other remains as a backup in case the primary filter becomes loaded or fails. The primary filter can be replaced during operation.

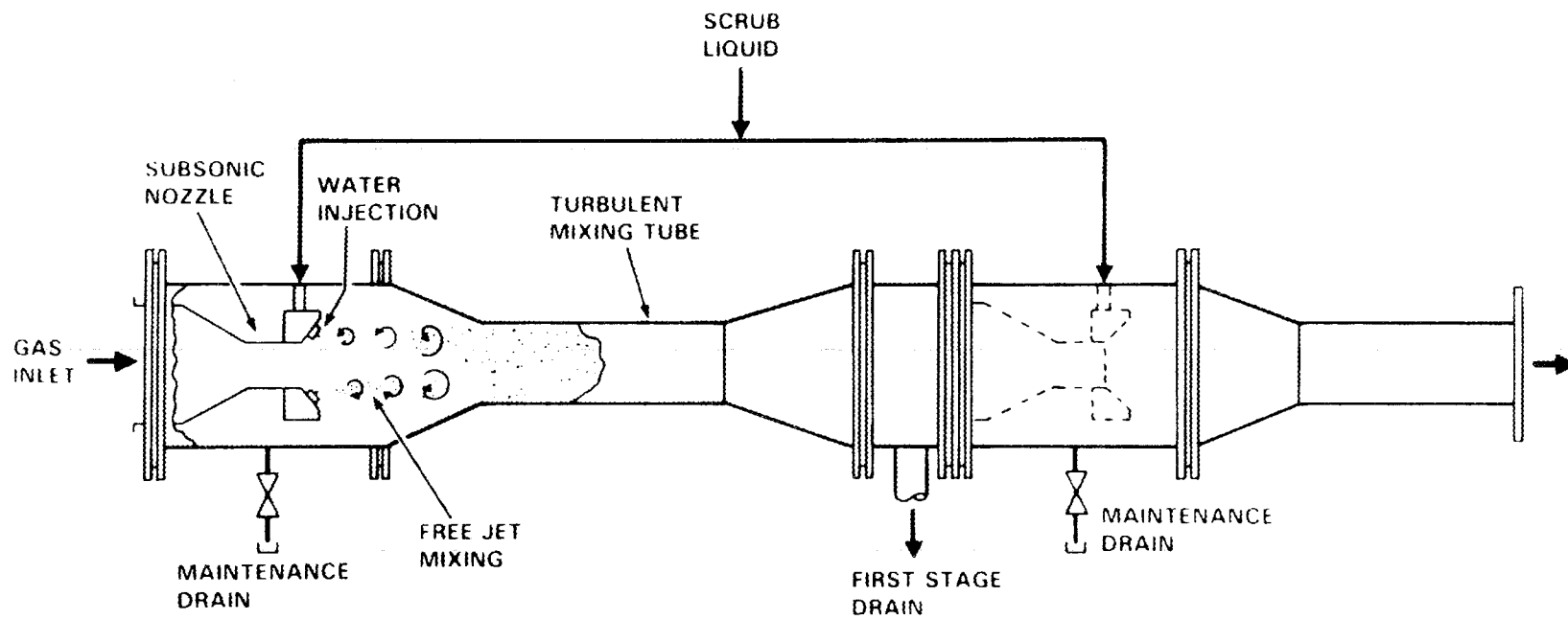


Fig. 7. Tandem nozzle Hydro-Sonic scrubber (Hydro Sonic Systems, Dallas, Texas).

2. TEST OBJECTIVES

The objectives of the pilot-scale demonstration of ISV technology at ORNL were developed to address key differences between the conditions during previous tests and those anticipated for contaminated sites at ORNL. For example, the waste trenches at ORNL contain large quantities of ^{137}Cs that could volatilize at high temperatures and be carried into the process trailer with the off-gas, resulting in excess wastes and the need for radiation shielding to prevent significant operator exposure. Also, the soils at ORNL are more structurally and chemically heterogeneous than those used in previous tests at Hanford. The trench design, with a significant quantity of crushed carbonate rock present, results in a bulk composition of the ISV product lower in silica and higher in calcium than previously studied compositions (Oma et al. 1983). Therefore, the operational performance of the ISV technology as well as the long-term durability of the resulting waste form needed to be addressed specifically for sites at ORNL. Some issues have been investigated during lab- and engineering-scale tests conducted at PNL during 1985-1986 (Carter et al. 1987), but needed field verification.

Objective 1: Evaluation of the Operational Performance of ISV

Prior to the full-scale application of ISV technology to contaminated sites at ORNL, all health, safety, radiological, and environmental concerns need to be identified and resolved. The most efficient manner to identify such concerns is to plan and execute smaller-scale demonstrations of the technology. The numerous tests of ISV conducted previously by PNL provide an excellent basis for evaluating many concerns at the pilot scale. Indeed, many of the plans and procedures developed by PNL for previous tests were directly transferable to the demonstration at ORNL. Although such background information is useful, conducting an actual test so that staff at ORNL can be familiarized with the process is an essential step in assessing the feasibility of the ISV technology for application at ORNL.

As part of this objective, the transportability of the trailer containing the off-gas treatment system, power delivery controls, and data acquisition equipment was addressed by shipping the system to ORNL and performing the tests successfully. In addition, it was important to assess the construction and installation of the electrodes and the

off-gas hood and off-gas lines. The preparation of the test site, a 3/8-scale simulated trench, was designed to demonstrate the ability to (1) auger holes in the soils close to a trench for the electrodes, (2) seal the hood to the ground, (3) have a sufficient supply of electrical power, and (4) coordinate the necessary personnel to complete preparation, construction, and installation details. The overall performance of the system during processing needed to be assessed also. For example, the quantities of off-gas and its composition needed to be determined so that a full-scale system can be properly designed. The pilot-scale demonstration allowed a more accurate determination of the power required to melt the high-carbonate soils at ORNL, which are unlike the silica-rich sandy soils used for most previous tests conducted by PNL. The potential influence of the complex structure and stratigraphy of the Conasauga Group at Oak Ridge on the ISV process and vitrification zone geometry needed to be determined in a field situation. All these activities were designed to provide a data base for more confident scale-up analyses in the design and construction of a full-scale system should the pilot-scale demonstration show that the ISV technology is feasible. The demonstration also allowed ORNL staff to directly participate in the operation of the equipment and observe its capabilities and limitations.

Objective 2: Determination of Off-Gas Retention Factors for Cs and Sr

The retention factor (RF) is defined as the ratio of the mass of an element in the solidified ISV product to the mass of the element released in the off-gas. These RF values are determined by the analysis of hood and ducting smears, scrub solutions, and HEPA filters from the process trailer and samples obtained from the ISV product. Determining reliable RF values is important because of the large inventories of ^{137}Cs and ^{90}Sr in the pits and trenches at ORNL. Trench 7 contains approximately 10^7 GBq of fission product activity (Olsen et al. 1983). Therefore, even small releases to the off-gas trailer could be of concern for operator exposure and waste generation. In laboratory- and engineering-scale tests, RF values of 2.6×10^4 and 2.7×10^4 for Cs and Sr, respectively, were obtained (Carter et al. 1987). However, these favorable values needed to be confirmed at a larger scale under field conditions so that the anticipated behavior of a full-scale system can be reliably assessed.

Objective 3: Assessment of the Durability of the ISV Product

Previous tests of ISV have produced highly durable waste forms (Oma et al. 1983). However, the bulk compositions of these materials were much higher in silica and lower in calcium than the expected composition of the ISV product resulting from the melting of a limestone-filled trench in an interlayered shale-carbonate saprolite. In addition, the viscosity and crystallization behavior will be affected by differences in bulk composition. Some of these differences were identified in the lab- and engineering-scale tests performed previously (Carter et al. 1987). Therefore, an important objective of the pilot-scale ISV demonstration was to confirm the melting and durability characteristics on a field-scale application.

3. SITE PREPARATION AND TRENCH CONSTRUCTION

Trench 7 (Figs. 1 and 2) was chosen as a model because of its size, its inventory characteristics, and the fact that much characterization of the trench has already been accomplished (Olsen et al. 1983). A 3/8-scale model of trench 7 was constructed in a pristine (i.e., uncontaminated) portion of ORNL (Fig. 1). The site was chosen for the similarity of its physical and geological characteristics to the areas used for seepage disposal in the past at ORNL (e.g., located on the top of a ridge in the saprolite of the Maryville Formation, an interlayered shale-limestone sequence). Four water table monitoring wells were constructed at the site with a 6-in. (2.4-cm-) diam auger to depths at least 20 ft (6.2 m) below the first encounter with free water. Wells were cased with 4-in. (1.5-cm) Schedule 80 PVC threaded flush-joint pipe with slotted casing on the bottom 10 ft (3.1 m). The annular space was backfilled with sand to about 5 ft (1.6 m) above the slotted section. Then, a bentonite pellet seal was emplaced for the next 5-ft (1.6-m) interval, and the remaining annular space was filled with soil. Water levels in these wells have been monitored at weekly intervals from May 20, 1987 to the present and have never been higher than 9 m below the ground surface. Thus, the ISV trench was at least 7 m above the water table, and no influence of the water table on the vitrification of the trench (or vice versa) would be possible. Samples of groundwater from each of these wells were collected in November 1987 for background water quality characteristics at the site; they were essentially a Ca-Mg-bicarbonate composition, as is typical of water in contact with limestone in the Maryville Formation, and contained no detectable hard beta or alpha activity.

After preparation of the site (clearing, leveling, electrical service, etc.), the trench was constructed perpendicular to the strike of the bedding (approximately N57°E). The dip of the saprolite layering was quite variable because of folding in the area (Fig. 8) but averaged about 45° to the south. Figure 8 also illustrates the interlayered shale-limestone stratigraphy near the center of the trench. The site was leveled to a mean elevation of 262.1 m above National Geodetic Vertical Datum (NGVD) and the center of the trench was located at ORNL Administrative Grid coordinates 18,420 ft north and 26,901 ft east. The 9.2-m-long trench was 1 m wide at the top and tapered to 0.4 m at



Fig. 8. View of stratification in the eastern wall of ORNL ISV demonstration trench showing folding, dip, and interbedded limestone and shale.

the bottom (Fig. 9). The trench was constructed to a depth of 1.5 m, except for a central section (≈ 2.5 m long), which was excavated with a backhoe to a depth of 2.5 m to allow for the placement of a vertical array of thermocouples. To simulate the contaminated sludge that is present in trench 7, a chemical addition consisting of 526 kg of a mixture of 18 wt % Cs_2CO_3 (99.9% purity, Henley Chemicals, Inc.) and 82 wt % SrCO_3 (Pyrotechnic grade, nominally 97.7% pure but analyzed as 99.4%, Hummel Chemical Corp.) was placed in the central portion of the trench (Fig. 9). Because the SrCO_3 was packaged in 50-lb bags and the Cs_2CO_3 in 1-lb plastic bottles, the mixture was prepared in 19 batches of 50 + 11 lbs, respectively, by blending the powders in a sealed drum. These quantities of Cs and Sr were selected to yield (1) a waste form with sufficient concentrations of Cs and Sr to permit determination of leach characteristics and (2) sufficient Cs and Sr in the ISV off-gas to permit determination of accurate retention factors for these elements.

The entire trench was then filled from the 0.6- to 1.5-m level with crushed limestone (4- to 5-cm-diam cobbles). Two tared 20-L buckets were filled with the limestone gravel and reweighed; the bulk density of the free-fall packing of the limestone averaged 1.44 ± 0.01 g/cm³. The width and depth of the trench was measured every 0.3 m of its length before and after each additional layer of backfill material. From the measured trench dimensions before and after addition of the limestone cobble, the limestone occupied a volume of 6.51 m³, which calculates to a weight of 9.38 Mg at 47% porosity. The upper 0.6 m of the trench was backfilled with the soil which had been excavated from the trench. Figures 10 through 12 illustrate the sequence of filling the trench. Four samples of this backfill soil were taken in 20-L buckets, whose exact volumes were determined previously by weighing before and after filling with water. The soil was placed in the buckets to its free-fall density to simulate the density of the trench cap layer. The buckets were weighed and then dried at 80°C to constant weight. The moisture content during trench construction was calculated at 7.0 ± 1.6 wt % (dry weight basis) and its bulk density was 1.41 ± 0.04 g/cm³. The trench soil cap occupied a volume of 6.43 m³ and calculated to a weight of 9.08 Mg with a total porosity of 47%.

A vertical array of eight type-K thermocouples was placed in the center of the trench (Figs. 9 and 10). These thermocouples, one at every 0.3-m depth, were used to

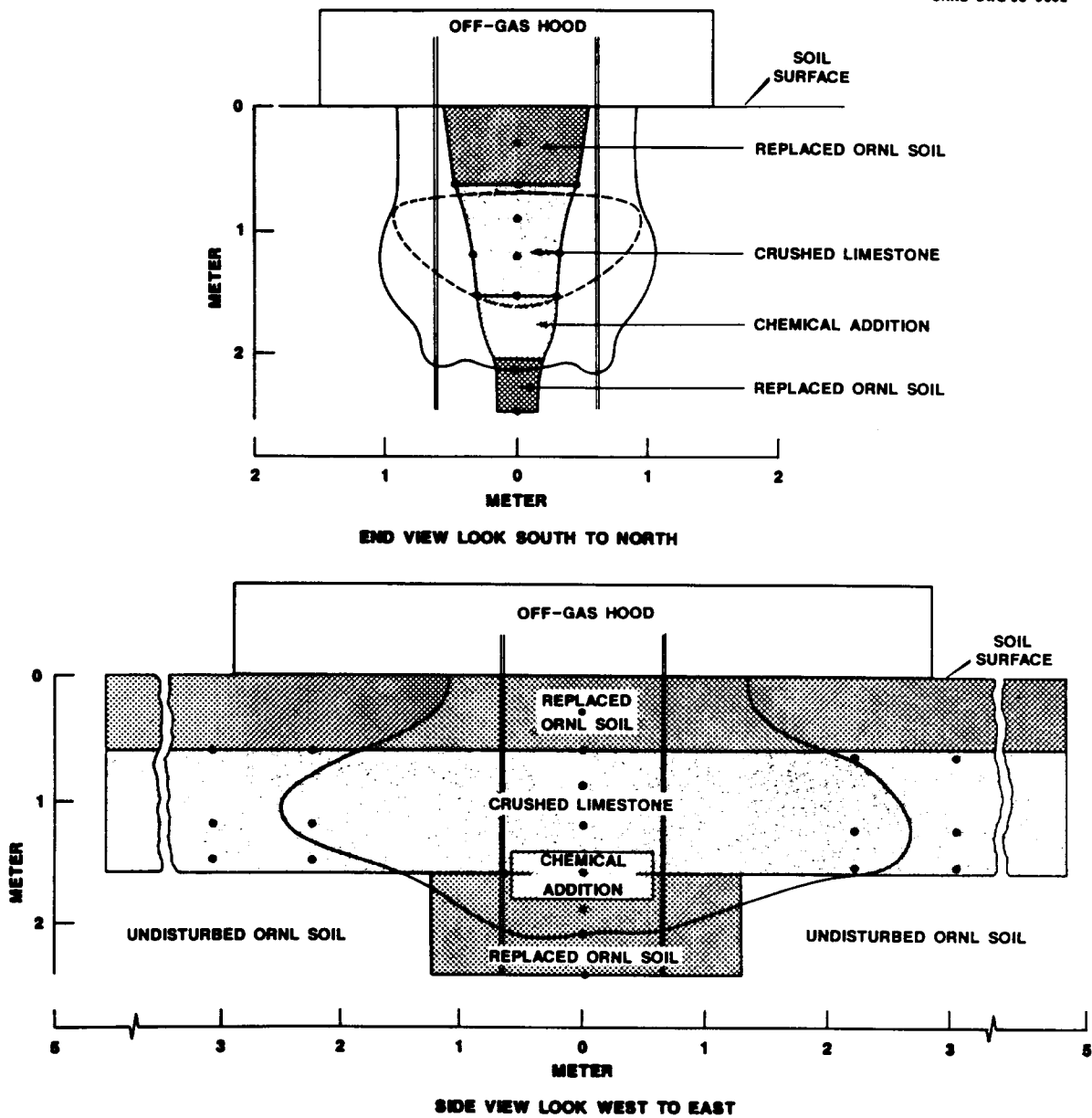


Fig. 9. Cross section and longitudinal section of ORNL pilot-scale trench with predicted shape of ISV mass. Circles denote positions of thermocouples.

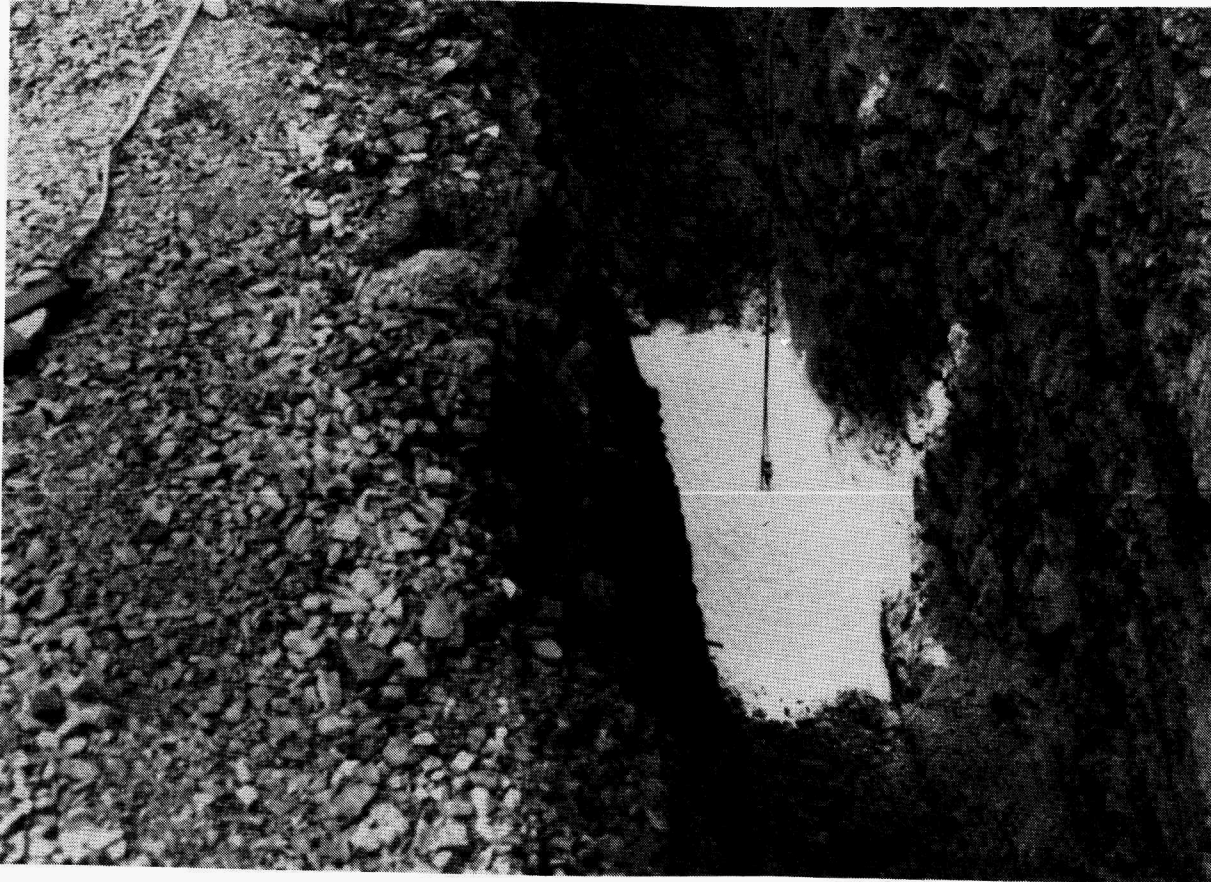


Fig. 10. View of cesium and strontium carbonate addition to ORNL ISV demonstration trench with the central vertical array of thermocouples.



Fig. 11. ORNL ISV demonstration trench partially filled with crushed limestone.



Fig. 12. ORNL ISV demonstration trench showing final stages of filling with soil.

monitor the depth of the melt during processing. As the melt approaches a thermocouple, the temperature increases to $\approx 100^{\circ}\text{C}$ as the water boils off. As the water is exhausted and the melt reaches the thermocouple, the temperature increases rapidly and goes off scale as the thermocouple exceeds its working range. In addition to the array of thermocouples in the center of the trench, type-K thermocouples were placed at depths of 0.6, 1.2, and 1.5 m along both sides of the trench at distances of 2.2 and 3.1 m north and south from the center of the trench (Fig. 9). Three type-R thermocouples in high-temperature ceramic protection tubes were placed in the center of the trench at depths of 0.9, 1.5, and 2 m in an unsuccessful attempt to monitor melt temperatures and cooling rates. Moisture detection cells were placed in the trench at several locations but did not function properly and will not be discussed further. Between the dates of trench construction, May 13, 1987, and electrode placement, June 17, 1987, the trench area was covered with plastic sheeting to prevent infiltration of rainfall into the trench.

The four molybdenum electrodes (5-cm diameter and 3.7 m long, consisting of two 1.8-m sections screwed together, Teledyne Wah Chang) were placed in graphite sleeves (15-cm OD by 6.4-cm ID, Great Lakes Carbon Corp.) and placed 1.2 m apart in a square array of 20-cm-diam augered holes approximately 2.5 m deep. To reduce the oxidation of the electrodes, they were coated with a 0.04 to 0.06-mm layer of MoSi_2 by a proprietary process (Hitempco) and painted with a molybdenum disilicide coating. The annulus between the electrodes and the graphite sleeves was filled with a powdered mixture (1:5 by weight) of molybdenum disilicide (99.5%) and zirconium diboride (99.5%, Noah Industrial Corp). The starter path was established by using a mixture of powdered graphite and crushed borosilicate glass. The path was formed by placing a thin and narrow layer (nominally 5 by 5 cm) around each electrode and between the electrodes. The path formed an X pattern between the electrodes as well as connecting each electrode in a surrounding square pattern. A ceramic insulating blanket (Kaowool) was placed over the melt zone to help reduce radiant heat loss during the processing. The off-gas hood was then placed over the trench, its skirt attached, and the off-gas lines connected to the hood and trailer. Auxiliary hoods [4 × 8 × 1 ft (1.3 × 2.5 × 0.3 m) high] were constructed of 16-gauge carbon steel and were placed over the portions of the trench that were not covered by the main hood. These hoods were not connected to the main off-gas system and were not held at a negative pressure.

However, they contained a CO₂ trap of ascarite (A. H. Thomas Corp) and gas flow meters, attached to 1/4-inch tube fittings, to detect any off-gases that may have bypassed the main hood; neither gas flow nor change in the CO₂ color indicator was observed during the ISV run. After the electrodes were connected to the power delivery system by using 750 MCM single-conductor flexible cable and several operational checklists were completed, the system was ready to be operated. Figure 13 depicts the pilot-scale system completely installed at the ORNL site. The area around the off-gas hood, containing all the electrical power delivery cable, was roped off to prevent visitors from entering the area without proper safety equipment. A permit (no. 996148P) to construct or modify an air contaminant source was issued by the Tennessee Air Pollution Control Board pursuant to Tennessee Air Quality Act to operate the ORNL pilot-scale ISV demonstration from June 12 to July 31, 1987.

Run data were recorded every 6 min and logged into a computerized data storage system. Parameters that were monitored included temperatures (soil, surface of the off-gas hood, plenum of the off-gas hood, inlet of the venturi scrubber, and the off-gas stack); off-gas flow rate; concentrations of CO₂ and CO in the off-gas; amperage; voltage; and power and cumulative energy. Samples of the scrub solutions from the off-gas treatment system were collected approximately every 2 h. (Duplicate samples were obtained for analysis at both PNL and ORNL.) After the power was shut down at the end of the test, a portable data logger was used to monitor the temperatures from thermocouples outside of the melt zone that were still functional. Samples of particulates on the inside of the hood and in the off-gas lines were taken after the system had cooled (\approx 12 h after power shutdown). After the mass had cooled sufficiently, the hood was removed and cores of the mass were obtained. The mass was partially excavated and additional samples recovered for analysis. Details of the sampling procedures and locations are discussed in Sect. 5.1.

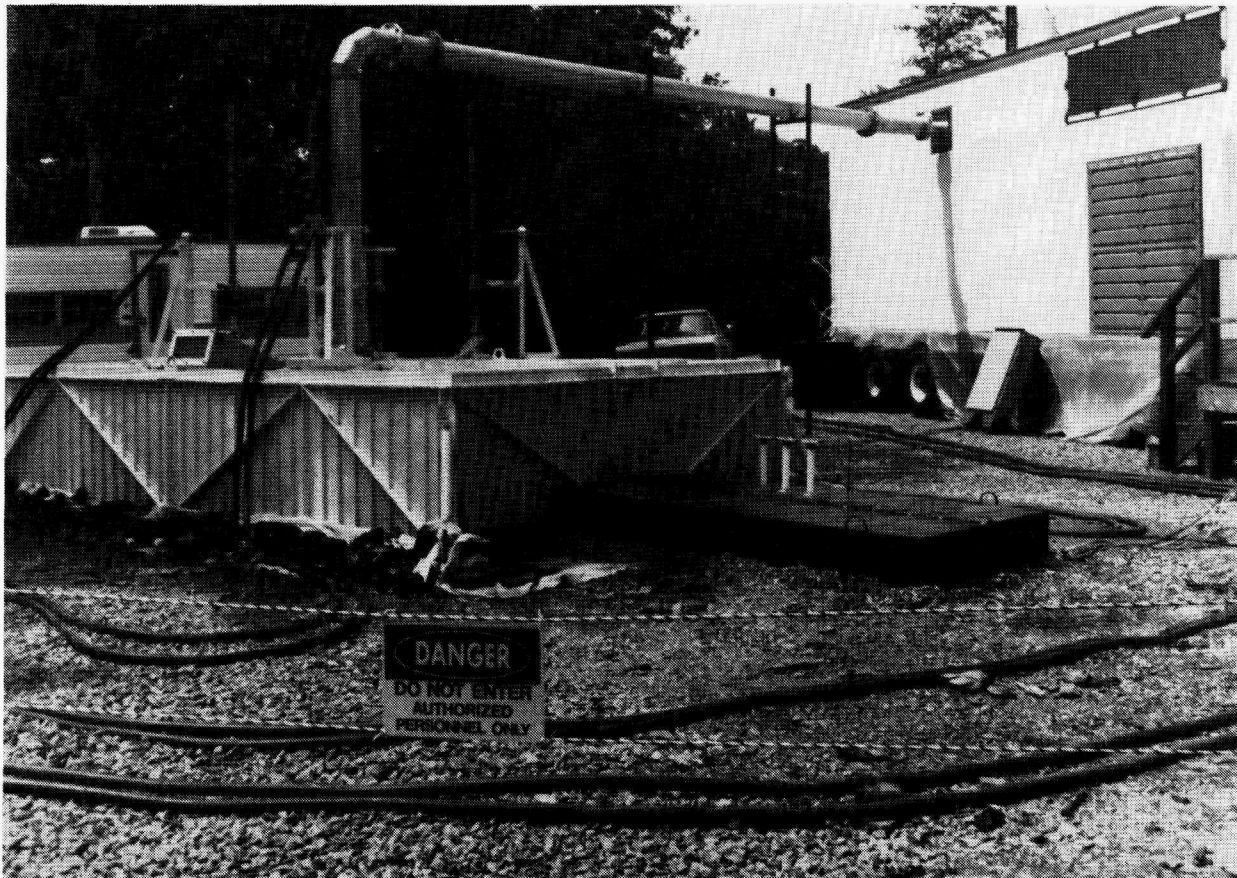


Fig. 13. View of pilot-scale off-gas hood, ducting, and process trailer at ORNL demonstration site.

4. ISV RUN PERFORMANCE

Many results from the pilot-scale ISV demonstration have been reported previously (Carter et al. 1988). Some of the results are repeated here to provide a complete record. In addition, some parameters were either not reported earlier, or samples and analyses were performed in duplicate. These results are presented and contrasted and compared where appropriate.

The ISV test was started on July 14, 1987. Previously, a start was attempted on June 26, but transformer malfunctions had to be repaired by the manufacturer. The test was restarted on July 13, but had to be shut down again because the automatic power control system was not operating correctly. Therefore, manual control was used and the test got under way at 9:28 A.M. on July 14, 1987. Approximately 5 h into the run, the starter path between electrodes was interrupted due to subsidence. Because all of the graphite and glass frit starter path material had been consumed in the previous restarts, 45.3 kg of soda ash (Na_2CO_3) was used to reestablish the starter path. The test then ran continuously, except for short planned power interrupts, for a total of 110 h until power was shut off on July 19 at midnight. Temperatures from the vertical array of thermocouples on the center of the trench and manual probing of the melt with a steel rod confirmed that the desired depth (≈ 2.1 m) of melting had been reached.

4.1 RUN PARAMETERS AND OVERALL SYSTEM PERFORMANCE

The starter path had to be regenerated several times as a result of the starting and stopping of the process during the problems with the transformer and power control units. In addition, the starter path had a tendency to break its continuity during the early stages of melting. This behavior was a result of the heterogeneous nature of the trench components and their relatively low bulk densities that allowed the initial melt path to break apart when the molten soil flowed into lower pockets. When this interruption of the conductive path occurred, the system had to be shut down and the starter path reformed. This tendency is one area that needs attention prior to a radioactive application (see Sect. 6).

In addition to the power problems mentioned above, one other equipment failure occurred. The pump to the venturi scrubber had to be shut down 5 h into the run

because of a leak in the pump surge tank. This malfunction required that the Hydro-Sonic scrubber handle the entire off-gas stream scrubbing. Carter et al. (1988) note that the single scrubber was designed to accommodate this situation and performed adequately during the demonstration. In addition, some unknown interaction occurred between the ORNL power delivery system and the PNL power regulation system. Spurious alarms of the process trailer area radiation monitors occurred during every voltage tap change to the electrodes. In addition, spurious alarms of area radiation monitors were also noted during ISV operation at the New Hydrofracture Facility and at White Oak Creek dam in Melton Valley; these facilities are supplied electrical power via the same secondary line as the ISV trailer.

Table 1 lists predicted and actual operating results for the pilot-scale test. The predicted results are from a model developed by Buelt et al. (1987). Note that the model assumes a square, symmetrical shape for the final ISV mass, but that the actual mass produced during the test was oblong in shape because of the growth of the melt down the length of the trench. The run time was governed by the time required to reach the target depth of approximately 2.1 m and was longer than predicted because of the longitudinal melting that occurred. This depth of melting was required to completely encompass the zone of chemical addition (Fig. 9) so that all of the Cs_2CO_3 and SrCO_3 would be incorporated into the melt. The longer run time is the reason that the energy use was higher than that predicted. The energy-to-mass ratio was larger than that predicted based on engineering-scale test results and may be partly attributable to differences in water and carbonate content of the trench site compared to the samples used in the engineering-scale test.

The estimated mass of the ISV product is calculated from the measured concentrations of Cs and Sr in the product. Knowing the initial quantities of these elements placed in the trench, and assuming they are homogeneously distributed throughout the final product (see Sect. 5.3), one can calculate the mass of the ISV product by dividing the mass added by the measured concentration (wt %) of the element. The calculated masses obtained with this approach are 19.4 Mg using Cs and 20.6 Mg using Sr.

Table 1. Comparison of predicted and actual operational results from the pilot-scale ISV demonstration

Parameter	Predicted	Actual
Run time, h	54.6	110
Melt depth, m	2.19	2.13
Melt width, m	2.57	2.1 ^a
Melt length, m	2.57 ^b	5.3
ISV mass, 1000 kg	16.3	≈20 ^c
Average power, kW	309	263
Energy, 1000 kWh	16.9	28.9
Energy/Mass, kWh/kg	1.04	1.44

^aEstimated maximum width at the center of the trench. Estimate because the ISV mass was not completely excavated.

^bModel assumed formation of a symmetrical block; therefore, width = length.

^cCalculated value based on Cs and Sr concentrations in the ISV mass. The mass is calculated according to (mass added to trench)/(wt % in ISV product). The actual value calculated is 19.4 Mg using Cs (77,681 g Cs₂O, 0.40 wt % Cs₂O) and 20.6 Mg using Sr (304,981 g SrO from the chemical addition and estimated contributions from the melted soil and limestone cobble, 1.48 wt % SrO). See Sect. 5.3 for details on the chemical composition of the ISV product.

Figures 14 and 15 summarize the key run parameters monitored during the ISV demonstration. The trends of increasing amperage and decreasing voltage illustrate the typical behavior necessary to maintain power levels during operation because of the decreasing electrical resistance of the melt during processing. Tap changes made during operation are indicated by the sharp increases in power at run times of approximately 10, 20, and 30 h. The manual control of the power delivery system, required because of malfunctions in the automatic control system, was adequate to successfully perform the demonstration. The total energy consumed (28.9 MWh, Table 1) was calculated from the product of the average power during operation (263 kW) and the run time (110 h).

Figures 16-18 illustrate operational data for the off-gas system. The flow rate was fairly constant at a value of approximately 11 m³/min. Figure 17 shows temperatures

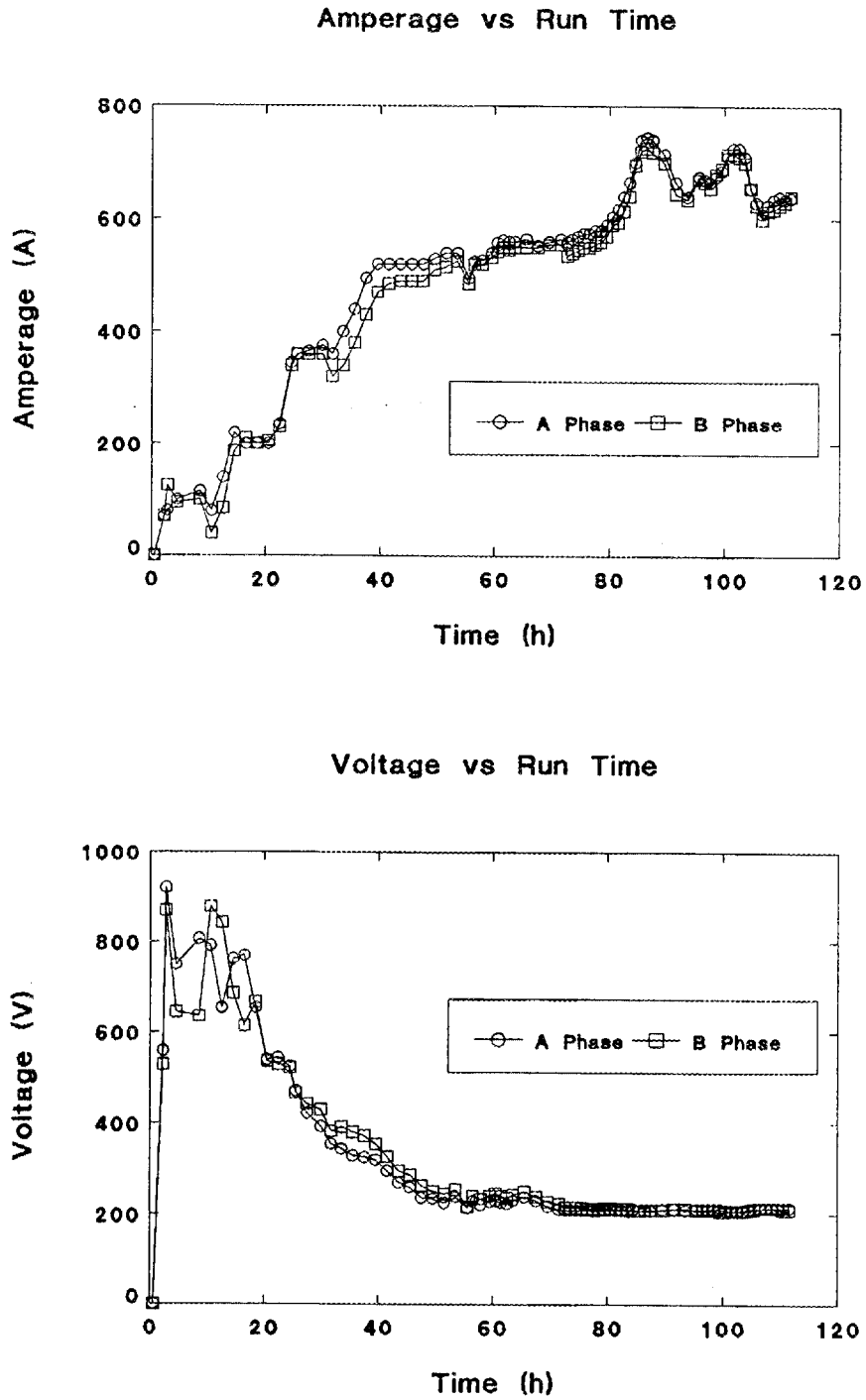


Fig. 14. Voltage and amperage to electrodes during the ORNL ISV demonstration.

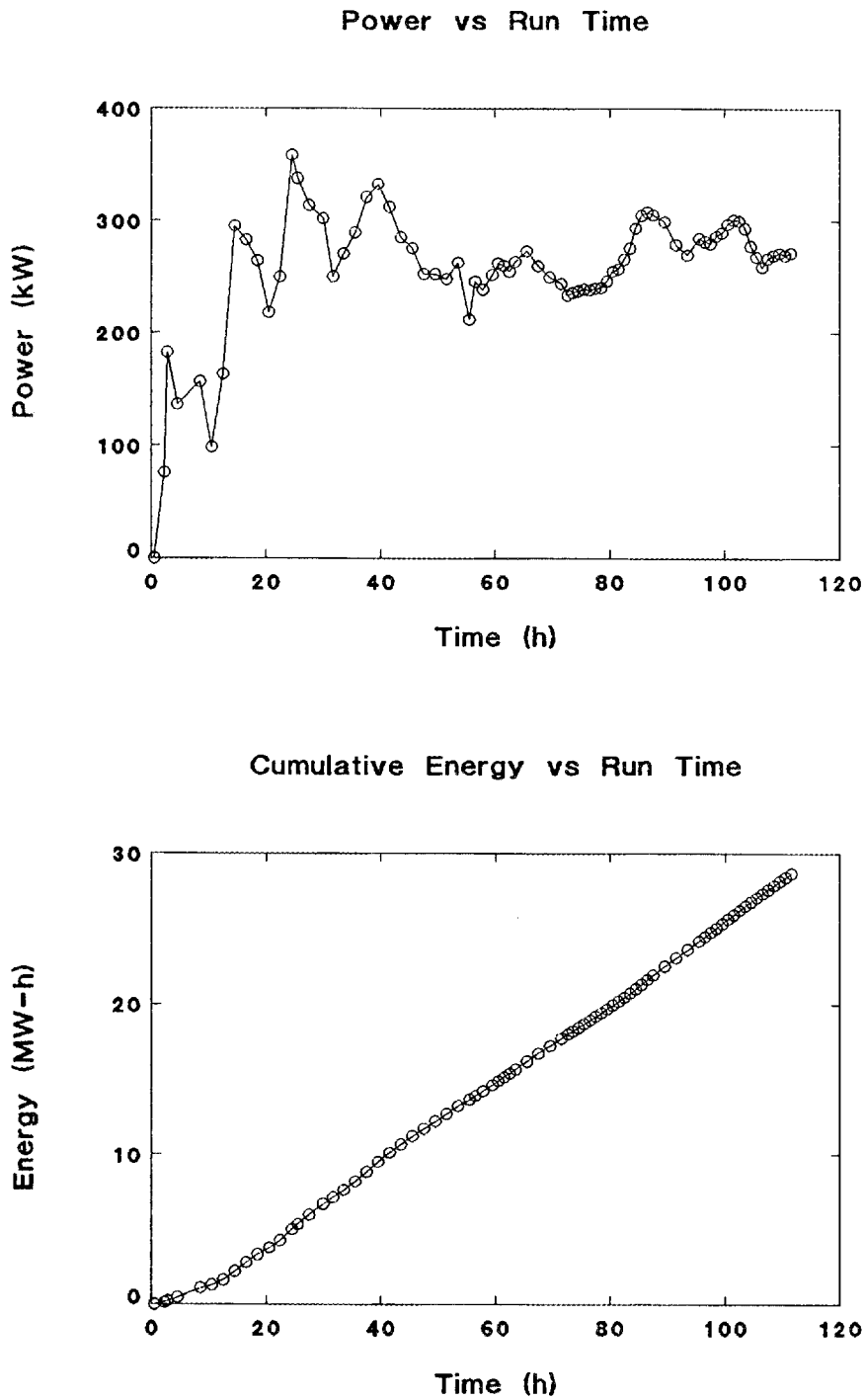


Fig. 15. Total power (kilowatts) and cumulative energy (megawatt-hours) to the electrodes during the ORNL ISV demonstration.

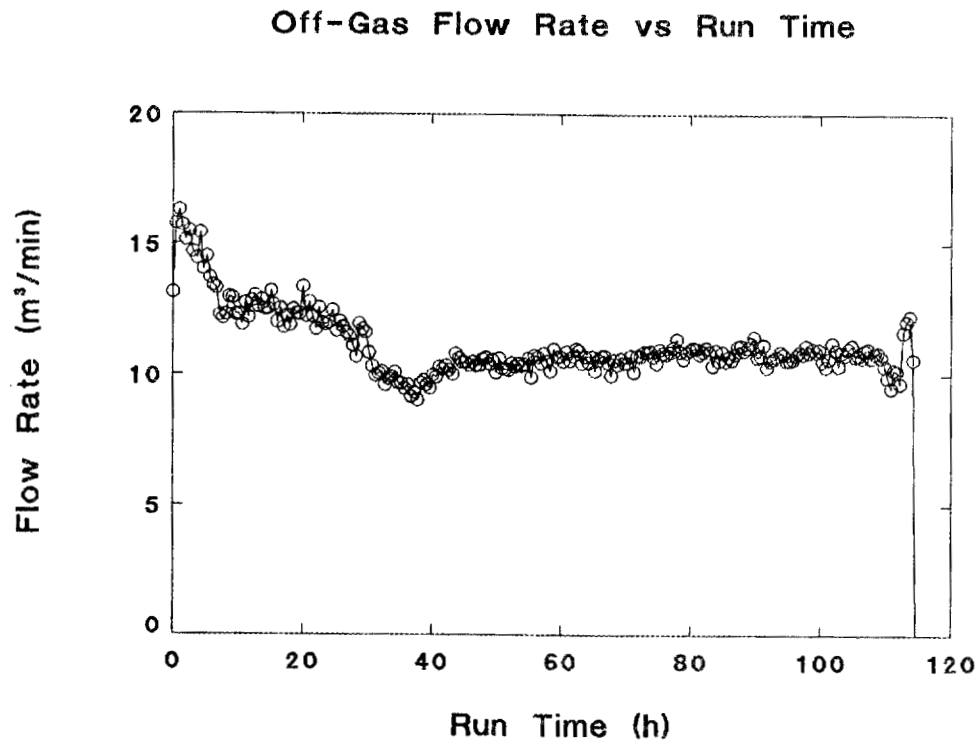


Fig. 16. Flow rate of off-gas at the stack during the ORNL ISV demonstration.

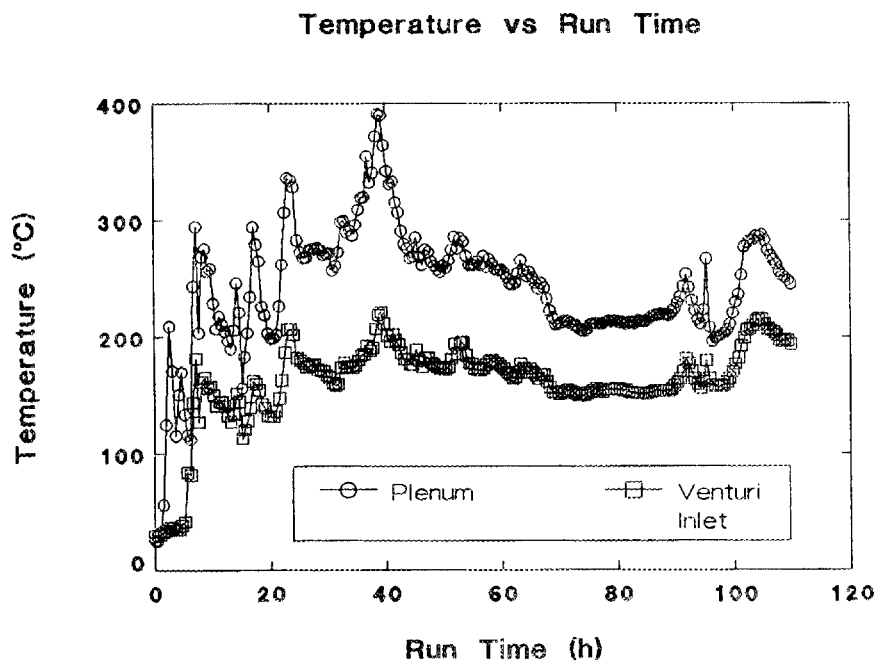
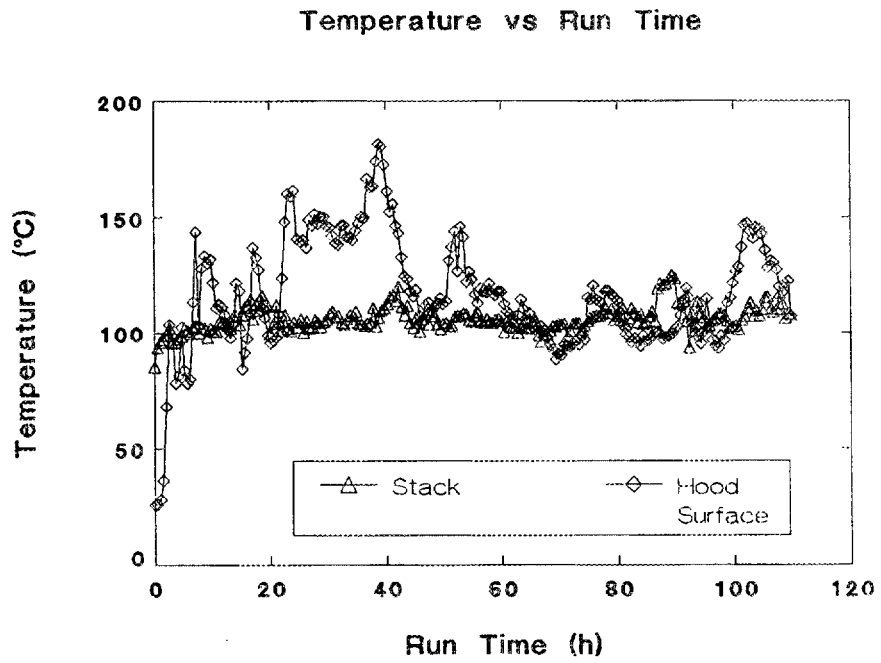


Fig. 17. Temperatures of the off-gas system components during the ORNL ISV demonstration.

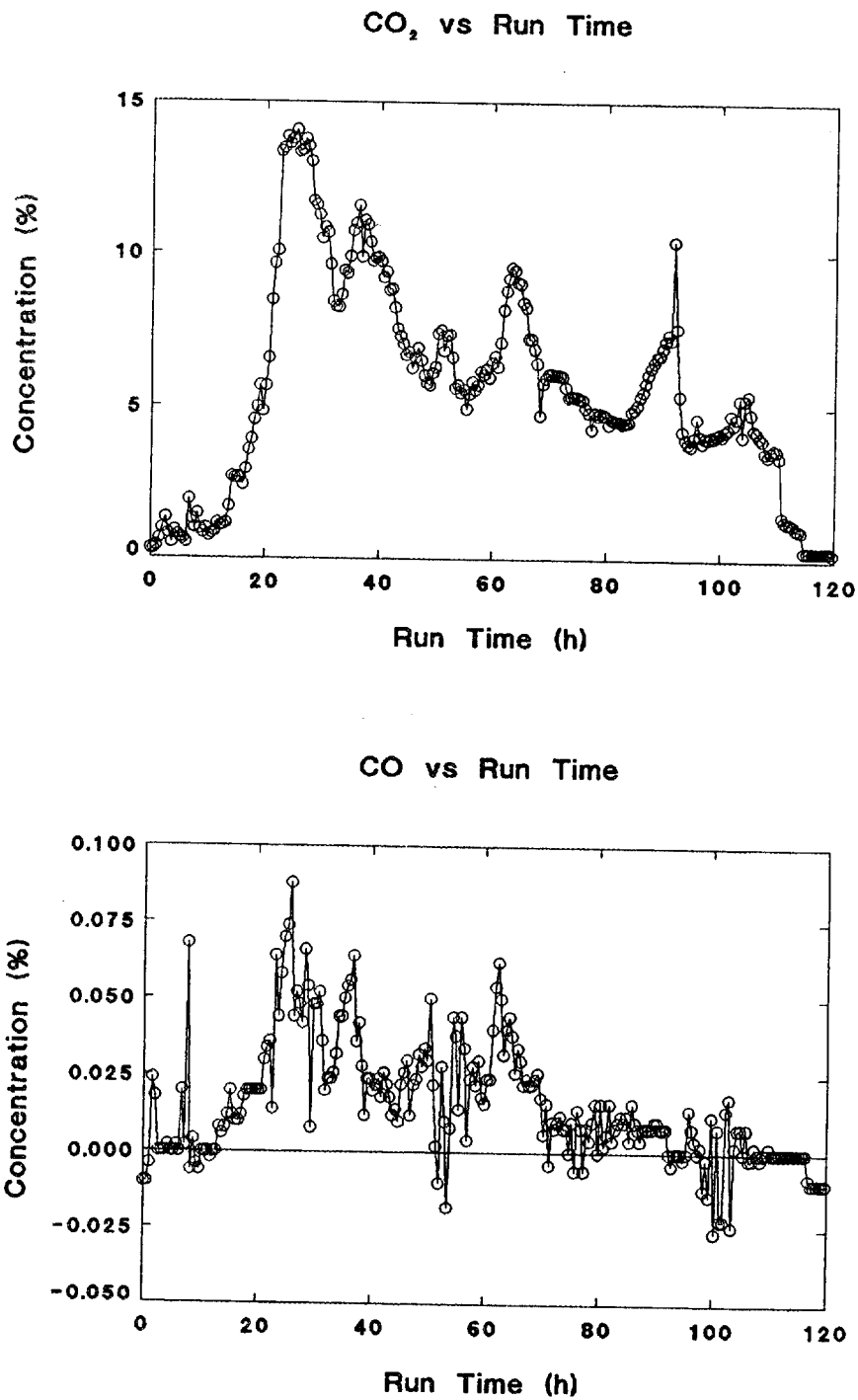


Fig. 18. The concentrations of carbon monoxide and carbon dioxide at the stack during the ORNL ISV demonstration.

during the run at various positions in the off-gas system. The concentrations of CO and CO₂ exiting the off-gas system are illustrated on Fig. 18. The time (≈ 22 h) of the increase in CO₂ concentration corresponds to the time when the depth of the crushed limestone in the trench was encountered by the melt. Although there is much scatter in the data, the CO concentrations generally parallel the CO₂ values. The melt reached a depth below the crushed limestone at approximately 80 h although the melt continued to grow longitudinally into the limestone cobble of the trench; this behavior can be seen in the somewhat reduced levels of both CO₂ and CO in the off gas.

The upper sections of the electrodes were removed prior to core sampling of the trench on October 13-15, 1987, and were inspected (Fig. 19). The graphite sleeves were heavily oxidized in the high-temperature zones where significant subsidence occurred, allowing contact between the sleeves and air. The molybdenum electrodes showed little sign of oxidation, which was inhibited by the molybdenum disilicide - zirconium diboride powder that was placed in the annulus between the electrodes and the graphite sleeves. This conductive powder formed a sintered, protective coating where the graphite had been oxidized away.

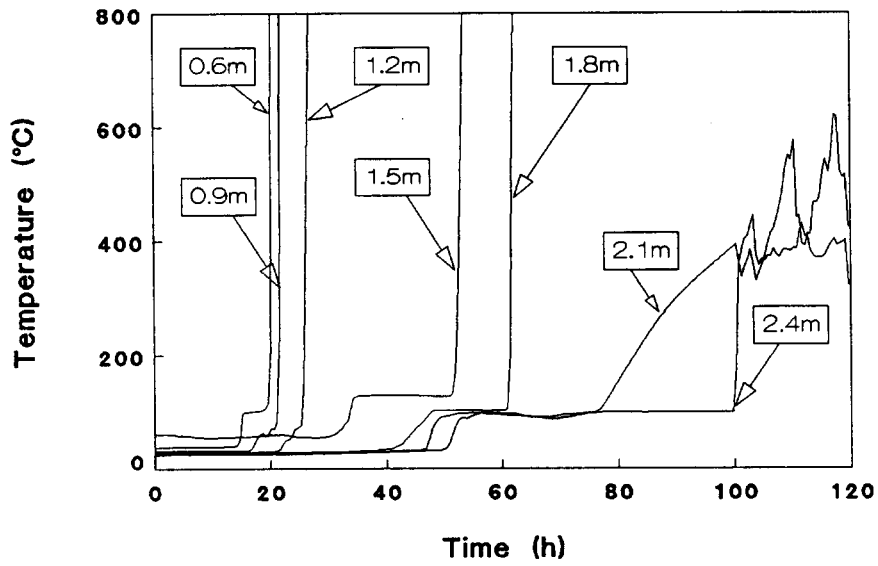
4.2 ISV PROCESS TEMPERATURES

Figure 20 illustrates the temperatures from the vertical array of type-K thermocouples as a function of run time. Temperatures from the thermocouple at the 0.3-m depth are not shown because this thermocouple burned out during the first aborted startup. The depth of melting was determined by observing the maximum temperature reached by each thermocouple in the vertical array located at the center of the trench. The sharp, near-vertical increases in temperature indicate the time when the melt reached the thermocouples. The thermocouples at depths of 2.1 and 2.4 m do not accurately reflect the depth of melting because the extension wires placed along the bottom of the trench burned out before (at ≈ 100 h) the melt reached the thermocouple itself (a result of the longitudinal melting behavior of the system). The type-R thermocouples intended to monitor melt temperatures did not function properly so this information was not available. The type-R thermocouples were 1.8 m long and were positioned so that their tip was at the center of the electrode array. However, the melt



Fig. 19. Top sections of the four molybdenum electrodes and graphite sleeves after the ORNL ISV demonstration illustrating the oxidation of the graphite sleeves.

Centerline Thermocouples



Depth vs Run Time

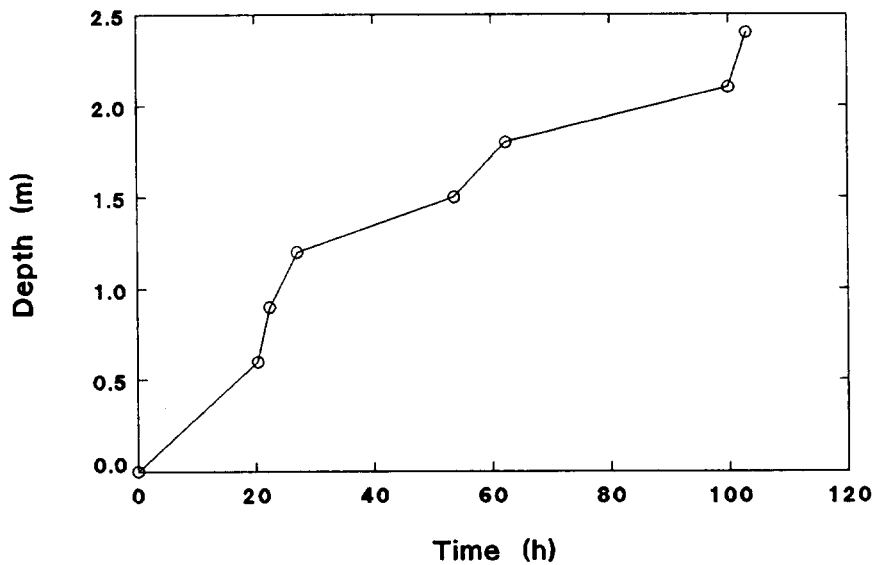


Fig. 20. Temperatures in the central vertical array of type-K thermocouples in the ORNL ISV demonstration trench and derived depths of melting.

progressed further than 1.8 m from the center along the length of the trench so that the thermocouple-wire junctions burned out. Based on previous experience with ISV, the PNL staff estimated that melt temperatures were between 1600-2000°C. In future tests, it would be highly desirable to monitor melt temperatures and correlate them with the volatilization of Cs, which is temperature dependent.

Temperatures from the thermocouples located 2.2 m along the length of the trench are illustrated in Figs. 21 and 22. The temperatures are shown for times well past the end of the melting period to illustrate the cooling behavior of the ISV mass. The temperatures of the north section reached several hundred degrees (Celsius), indicating that the melt nearly reached this distance during the longitudinal melting. Note that the northwest 1.2-m thermocouple did not function at all, so no data are available. To the south, the 1.2- and 1.5-m-deep thermocouples actually burned out, indicating the melt had reached at least this far down the length of the trench. The 0.6-m-deep thermocouples did not reach temperatures as high as the others. This behavior is consistent with the shape of the ISV mass (see Sect. 5.1), which was found to have a horizontal surface at a depth of approximately 0.9 m, well below the level of the 0.6-m thermocouples. At the 2.2-m distances, the cooling period was actually longer than the melting period as indicated by the asymmetric curves. Nearly 25 d was required for the temperatures at 2.2 m from the center of the trench to reach <100°C after power was shut down.

Temperatures 3.1 m from the center of the trench are illustrated in Figs. 23 and 24. Again, the temperatures are illustrated through 45 d to show the cooling trends. The northern section of the trench never reached 100°C at the 3.1-m distance. To the south, however, several thermocouples indicated temperatures approximately 150°C, and one approached 300°C. Nearly 15 d was required for temperatures to reach <100°C at this distance from the center of the melt after power to the melt was discontinued. Note that the southwest 1.2-m thermocouple did not function at all so no data are available.

The temperature profiles at the 2.2- and 3.1-m distances along the trench were used to predict the shape of the ISV mass that is illustrated in Fig. 9. This prediction

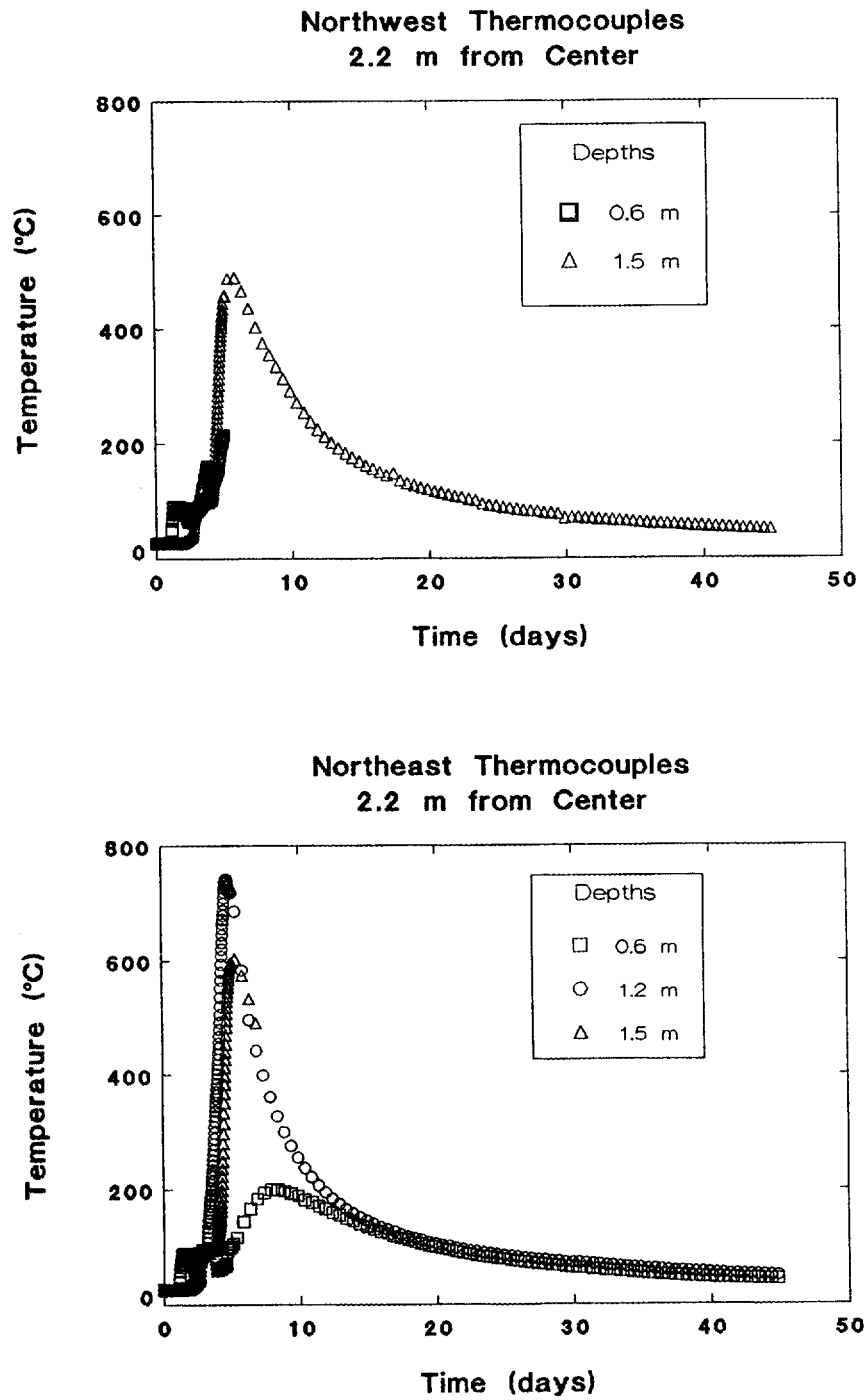


Fig. 21. Temperatures along the west and east side of the ISV trench at indicated depths 2.2 m north of the center of the ORNL ISV demonstration trench.

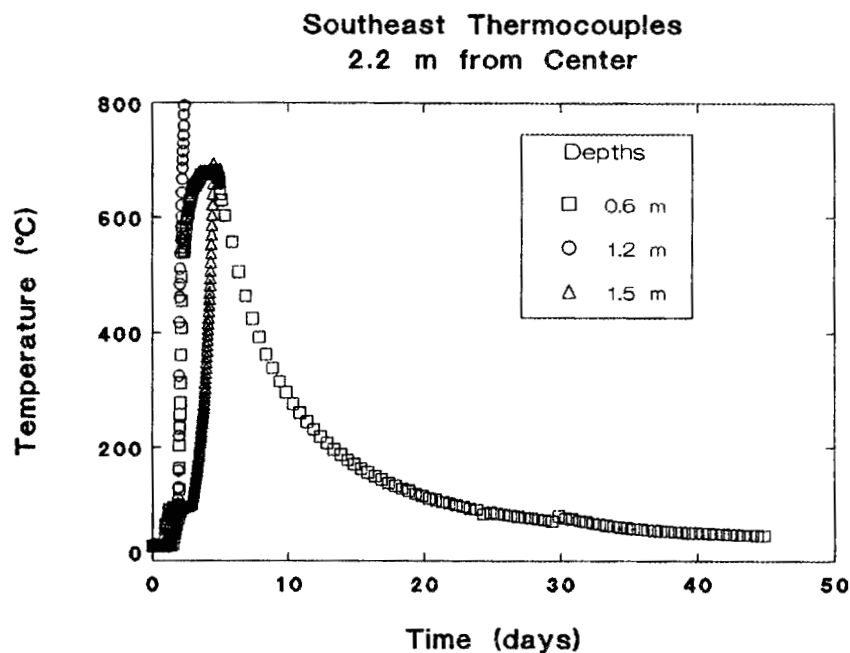
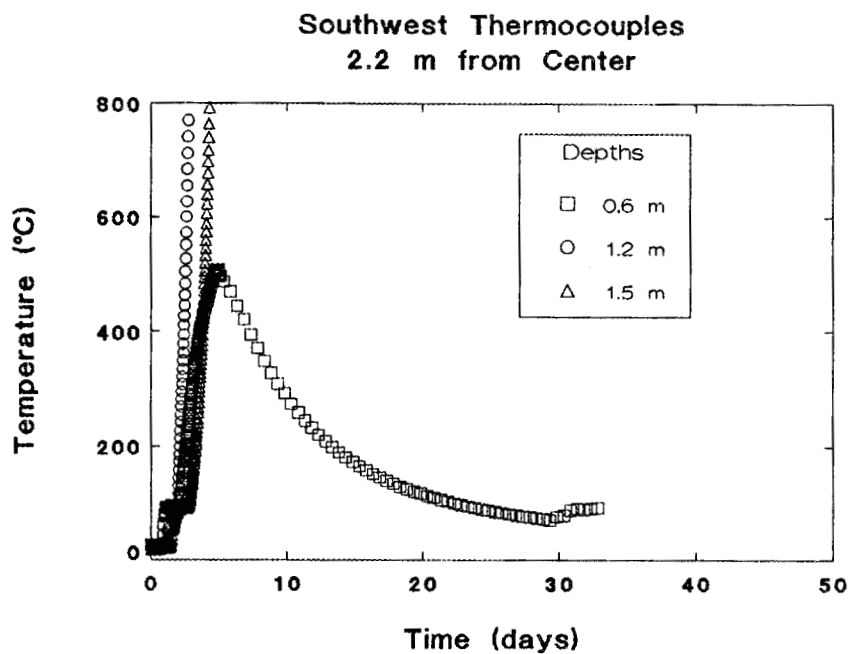


Fig. 22. Temperatures along the west and east sides of the ISV trench at indicated depths 2.2 m south of the center of the ORNL ISV demonstration trench.

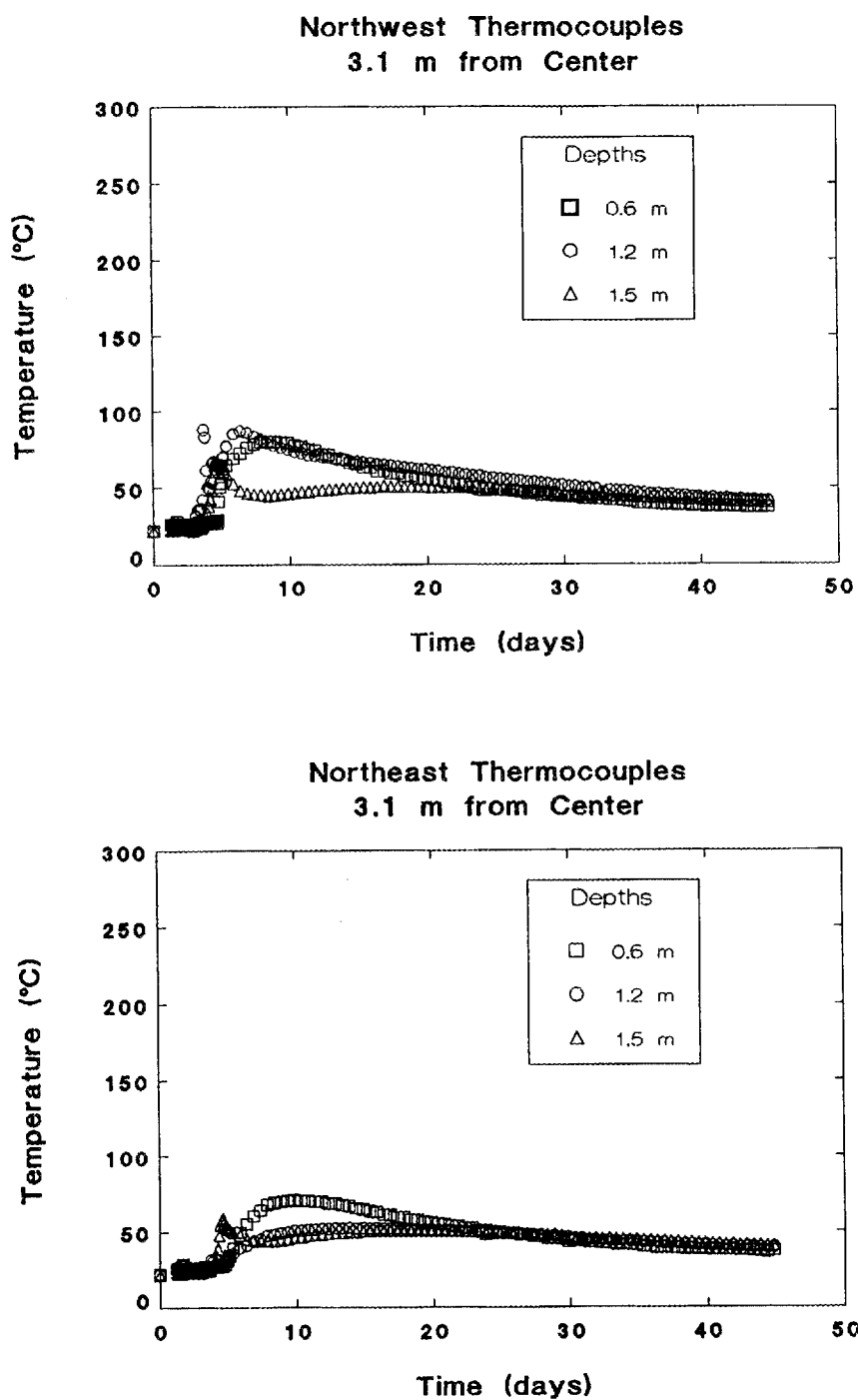


Fig. 23. Temperatures along the west and east sides of the ISV trench at indicated depths 3.1 m north of the center of the ORNL ISV demonstration trench.

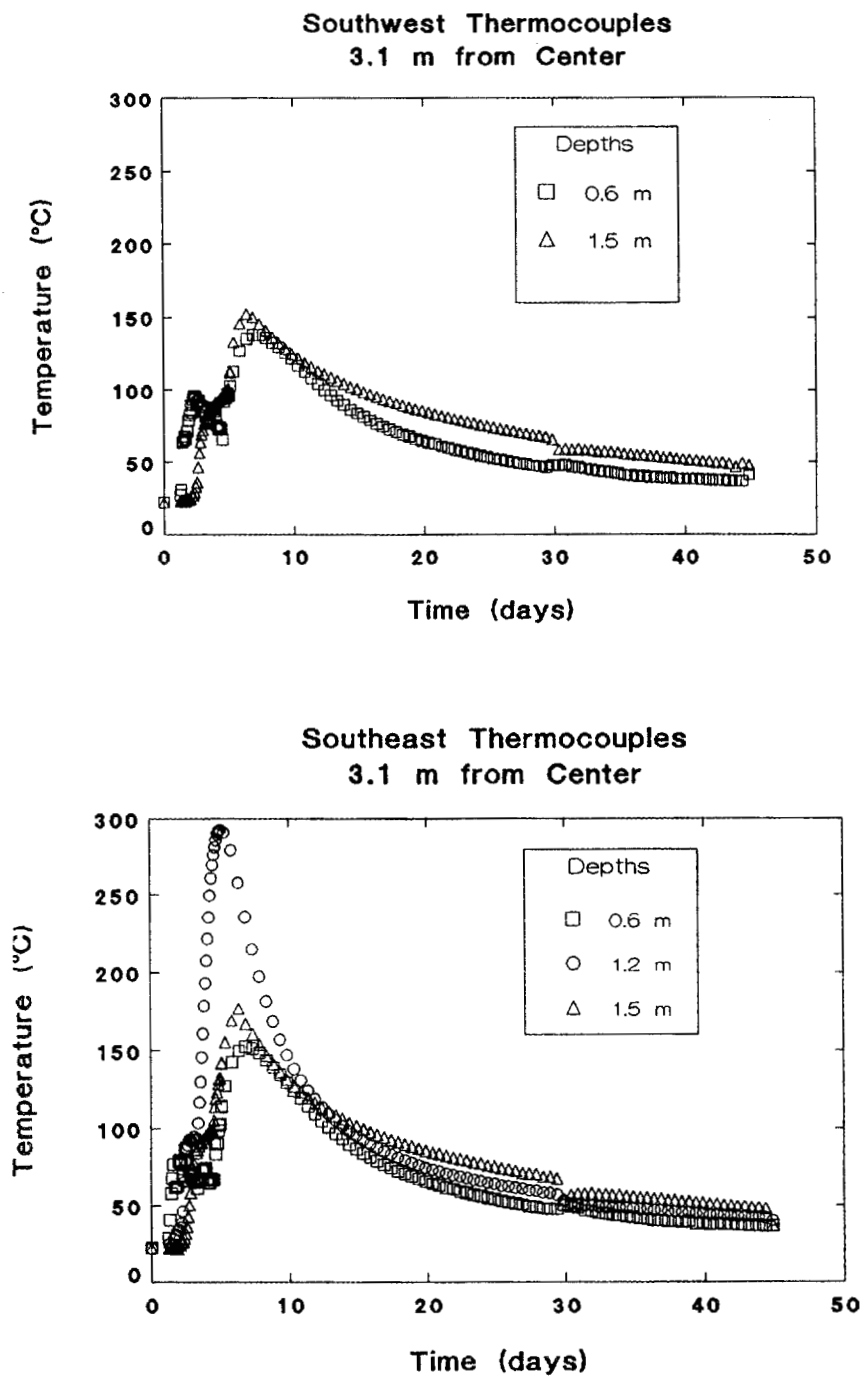


Fig. 24. Temperatures along the west and east sides of the ISV trench at indicated depths 3.1 m south of the center of the ORNL ISV demonstration trench.

was consistent with the shape of the mass as determined after partial excavation of the ISV mass (see Sect. 5.1).

4.3 PROCESS OFF-GAS SYSTEM EVALUATION

Although the process off-gas system operated continuously throughout the 110 h of this demonstration, the venturi-ejector scrubber component failed about 5 h into the run. The pump (Fig. 6), which circulates scrub solution to the scrubber, failed. The function of the venturi-ejector scrubber is to remove coarse suspended particles in the off-gas and to reduce the temperature of the off-gas. The system continued to function by relying on the Hydro-Sonic scrubber to remove particulates and prevent clogging of the HEPA filters. The system was designed to remain operative if either the Hydro-Sonic or venturi-ejector scrubbers are not functioning.

The distribution of elements and solids within the five off-gas system components provides a good summary of the system performance (Table 2). Details of the sampling, evaluation, and properties of each off-gas system component will be discussed subsequently. Determination of elemental inventories on the ISV hood and ducting were made from the amount and chemical composition of transferrable solids within defined surface areas. Scrub solution inventories were based on elemental analyses of samples of the scrub solutions taken at 2-h intervals during the run and on analyses of the eleven barrels of composite scrub solution waste. The HEPA filters were ashed and digested for total elemental analyses.

Of particular interest to the evaluation of ISV for application to seepage pits and trenches at ORNL is the distribution of Cs and Sr (Fig. 25). The distribution of these elements will predict the distribution of the two major radioisotopes, ^{137}Cs and ^{90}Sr , among off-gas system components. The total amount of Sr in all off-gas system components (0.82 g) represents such a small fraction of the total amount in the ISV product (i.e., 257,892 g, which includes the 254,212 g added as SrCO_3 , 2,000 g from the estimated 6 tons of limestone, and 1,680 g from the estimated 14 tons of soil which formed the ISV melted product). Thus, greater than 99.9997% of the Sr was retained in the melted product. Cesium, in contrast, showed a more significant degree of volatilization. A total of 91.73 g of Cs was detected in all off-gas system components. A total inventory of 73,274 g was placed into the trench as Cs_2CO_3 ; the soil and

Table 2. Distribution of elements in ISV off-gas system components

<u>Element</u>	<u>Hood</u>	<u>Ducting</u>	<u>Scrub</u> <u>Solution</u>	<u>HEPA-1</u>	<u>HEPA-2</u>
	(----- g /(fraction of total) -----)				
Al	3.83 (.14)	6.35 (.23)	17.32 (.63)	0.12 (.004)	0.06 (.002)
Ca	1.21 (.03)	2.00 (.05)	35.43 (.90)	0.54 (.01)	0.25 (.01)
Cs	0.56 (.006)	2.94 (.032)	86.02 (.94)	2.15 (.023)	0.06 (.001)
Fe	6.23 (.05)	10.33 (.08)	117.91 (.88)	0.07 (.003)	0.01 (.00)
Li	4.31 (.05)	7.15 (.08)	78.97 (.87)	0.29 (.003)	0.04 (.00)
Mg	1.10 (.04)	1.83 (.07)	22.13 (.88)	0.06 (.002)	.05 (.002)
Mo	2.01 (.14)	3.33 (.24)	8.05 (.57)	0.61 (.04)	0.01 (.00)
Na	27.93 (.02)	46.32 (.03)	1693.42 (.95)	19.62 (.01)	4.64 (.003)
Si	233.22 (.30)	386.81 (.50)	159.51 (.20)	0.95 (.001)	0.84 (.001)
Sr	0.04 (.05)	0.02 (.03)	0.67 (.83)	0.06 (.06)	0.03 (.03)
Solids	542 (.03)	899 (.05)	17138 (.92)	23.48 (.001)	0.0 (.00)

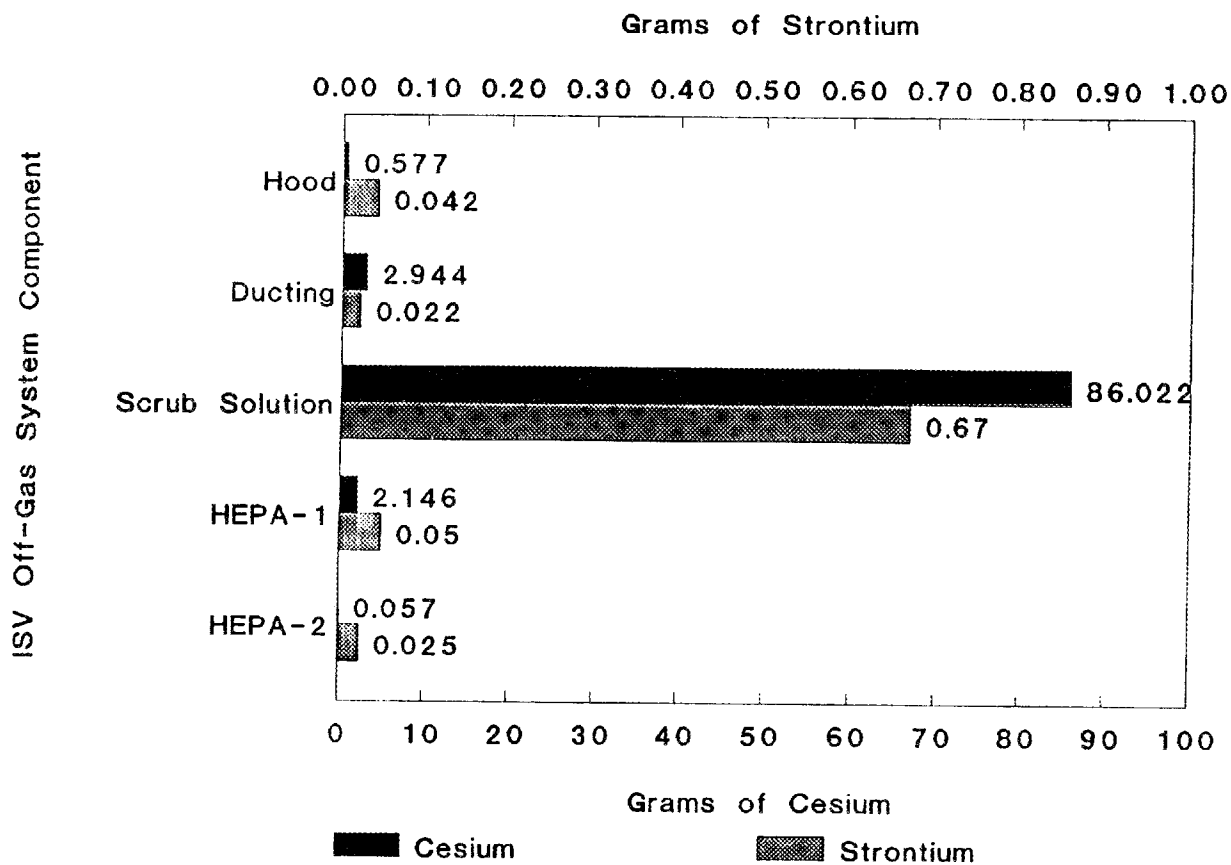


Fig. 25. Amounts of cesium and strontium in off-gas system components after the ORNL ISV demonstration.

limestone made no significant contribution to the inventory of Cs contained in the trench. Thus, the retention of Cs in the melted product was only 99.87%. Both the amount and fractionation of Cs within the off-gas system necessitates careful planning and evaluation of radiological safety for application to a seepage trench at ORNL. Details of this radiological assessment will be discussed subsequently (Sect. 6).

4.3.1 Off-Gas Hood

The deposited solids from five 10- by 10-cm areas on the ISV off-gas hood were smeared on April 27, 1988. Three areas from the top and two from the sides were wiped with a moistened paper towel, which was placed into a seal-lock polyethylene bag. Each area was wiped with a second paper towel until a shiny stainless steel surface was achieved, indicating that all ash had been removed. The towels and their plastic bags were placed into tared 250-mL beakers, covered with watch glasses, and ashed for 16 h in a muffle furnace. After cooling, the beakers were weighed to determine ash content and corrected for ash contributed by blank paper towels and polyethylene bags. The ash was then transferred to 50-mL beakers and heated to dryness with 15 mL of Ultrex HNO_3 . The residue was then extracted with hot 12% HNO_3 , filtered through Whatman no. 1 paper, and made up to 50 mL with 12% HNO_3 and submitted for Cs and Sr analyses. After these analyses indicated lower-than-expected levels of Cs, the archived samples of filter paper and ash residue were placed in Teflon beakers and digested with several aliquots of 5 mL of Ultrex HNO_3 plus 5 mL of 48% HF to dissolve all the solids. The resulting digests were rinsed three times with 10 mL of hot 12% HNO_3 and transferred to a 50-mL volumetric flask. These HF-digests were then submitted for Cs and Sr analyses.

The amounts of Cs and Sr in the HNO_3 and HF extracts were totaled to calculate the amount of Cs and Sr deposited on the hood. Only 22% of the Cs was extractable from the hood ash by hot HNO_3 , whereas about 70% of the Sr was extractable. (See Appendix for all tabulated results.) The amounts per square centimeter were then multiplied by the top and lateral areas of the hood, 167,225 and 156,038 cm^2 , respectively, to obtain the total inventory on the hood. The resulting total was 576 and 42 mg of Cs and Sr, respectively, in a total of 542 g of deposited solids (1.67 mg/cm^2). Thus, the deposited solids averaged 809 and 47 mg/kg of Cs and Sr, respectively, which

contrasts with the higher concentrations within the melted product (i.e., 3,500 and 10,700 mg/kg, respectively). Therefore, it appears that the solids deposited on the off-gas hood do not represent flaking or deposition of solids directly from the ISV melted product, but indicate some elemental fractionation.

4.3.2 Off-Gas Ducting

The ISV ducting consisted of five pieces of stainless steel 21-cm-ID pipe: a 264-cm-long upright with a right-angle turn (17,380-cm² internal surface area), a 671-cm-long straight section (44,144 cm²), a 41-cm-long straight extension (2,699 cm²), an 86-cm long elbow (5,661 cm²), and a 36-cm-long reducing adaptor (21 to 15 cm ID, 2,370 cm²). The upright, extension, straight, and elbow pieces were sampled on August 28, 1987, by the same technique described above for the off-gas hood. Unlike the samples of ash taken from the ISV hood, these samples were subjected to Li₂B₄O₇ fusion for Si analyses and HF digestion for all other elements. Thus, any fixation of Cs in the ash, resistant to HNO₃ dissolution, would not be evident in results for these samples.

A significant amount of Cs, 2.94 g, was found in the deposited solids on the ducting. (See Appendix for complete elemental analyses.) Considerably more solids were deposited on the ducting, 898 g averaging 11.1 mg/cm² of surface area, than on the hood. This increase represents about a tenfold increase in areal deposition over that found on the hood. Whereas the hood remained quite hot during the run, the ducting was sometimes cool enough to condense water vapor from the melt zone, probably enhancing the deposition of solids onto the ducting. This condensation was particularly noticeable during the first day of the run when much electrical energy was being expended to evaporate water from the melt zone. The average Cs and Sr concentrations in the ducting ash samples were 2420 and 23 mg/kg, respectively. The Sr concentration is similar to that found on the hood. The Cs concentration is higher than the 809 mg/kg found on the hood; however, this concentration is still lower than the 3500 mg/kg of the ISV product. This result seems to imply that Cs is volatilizing from the melt zone and being deposited with the solids on the ducting. The low concentration of Sr, however, implies that the deposition process is not a simple physical mechanism of Cs codepositing with solids, because this behavior would result in a Sr

concentration similar to that found in the melted material, 10,700 mg/kg. Analyses of smears of the ducting and the hood performed by Carter et al. (1988) indicated a factor of 30 less Cs deposited than the present analyses. The acid leaching procedure to extract the Cs from the PNL smear samples probably resulted in the much lower inventory found by these investigators. As discussed previously in the hood ash analysis section, thermally treated samples of ash are resistant to leaching of Cs by acid and require complete dissolution with HF. This effect will be amplified even further in the section on HEPA filter analyses.

The ducting ash itself had an unusual elemental composition (Table 3). It was quite enriched in sodium compared to the composition of the melted product, probably a result of the release of particulates from the addition of the soda ash. The depletion in Ca, Mg, and Sr was clearly indicative of the nonvolatile nature of these elements. The ash deposited on the ducting was also highly siliceous, although the 95 wt % SiO₂ was based on inductively coupled plasma emission spectroscopy (ICP) analyses and was

Table 3. Average elemental composition of ISV ash deposited on off-gas system ducting

Elemental oxide	Weight percent
Al ₂ O ₃	1.46
CaO	0.38
Cs ₂ O	0.26
Fe ₂ O ₃	3.07
K ₂ O	1.48
Li ₂ O	1.52
MgO	0.35
MnO	0.04
MoO ₂	0.62
Na ₂ O	5.24
SiO ₂	95.01
SrO	0.03
Total	109.43

probably high. The significant concentration of Mo was a result of the volatilization from the electrodes and the $\text{MoSi}_2/\text{ZrB}_2$ powder between the Mo electrodes and the graphite sleeves.

4.3.3 Off-Gas Scrub Solutions

The temporal variation of the inventory of any element in the off-gas scrub solution during the ISV run can be calculated from the chemical composition of samples, usually taken at 2 h intervals during the run, and the recorded feed tank and transfer volumes. However, due to the large number of chemical analyses performed and the large number of volumetric measurements required for this calculation, the calculated inventory is subject to a great many uncertainties. Fortunately, however, all of the scrub solutions were transferred into 11 barrels (208-L capacity) during and after the run. Thus, the total elemental inventory can be calculated from a relatively small number of chemical analyses and volumetric measurements. A high degree of confidence, therefore, can be placed in the inventories calculated from the barrel samples. These inventories can then be used as a guide in the various methods of calculating temporal inventories during the course of the ISV run.

Barrels were sampled on two occasions: August 5, 1987, and again on November 13, 1987. Drum contents were recirculated for 2 min at 20 gal/min using an electric drum pump with its intake pipe extending to the bottom of the barrel. This pumping was performed to resuspend any settled solids at the barrel bottom. An approximately one-liter sample was taken into a polypropylene bottle. The elevation of liquid in each drum was measured using a dipstick, and the volume of liquid was calculated by multiplying the fractional liquid level by the barrel capacity (208 L). Samples were taken to the laboratory for analyses. Approximately half the sample was filtered through a $0.45 \mu\text{m}$ nitrocellulose membrane in a disposable polystyrene filtering unit to remove suspended solids. Samples of the filtrate were analyzed for pH, electrical conductivity, alkalinity, acidity, and gross alpha and beta activity by standard methods (APHA 1980). A 5-mL aliquot of the filtrate was dried onto a tared 2-in- (5-cm-) diam stainless steel planchet for the gross beta and alpha analyses, and the dried weight was also used to calculate total dissolved solids. A 5-mL aliquot of the unfiltered sample was used to calculate total solids, and the difference was used to calculate total

suspended solids. Additional 100-mL aliquots of the unfiltered samples were submitted for elemental analyses with ICP. These analyses were performed on 50-mL aliquots that had been evaporated to dryness, digested with HNO₃, and reconstituted to 50 mL with 12% HNO₃ [U.S. Environmental Protection Agency (EPA method 200.7)]. This method would tend to underestimate the contribution of suspended siliceous materials to the inventory of elements such as Si and Al. After the ICP analyses, the same samples were analyzed for Cs and Sr via atomic absorption spectroscopy (EPA method 200.7). The total inventories of selected elements and characteristics for the 11 barrels are presented in Table 4, and the analytical results for each barrel are contained in the Appendix.

Table 4. Total inventory of elements and characteristics
in barrels of ISV off-gas scrub solutions
(All quantities given are in grams unless otherwise indicated)

Characteristic	Quantity	Ratio of amount in off-gas to amount in vitrified mass
Al	17.32	0.000011
B	281.72	0.0518
Ba	0.11	0.000009
Ca	35.43	0.000014
Co	0.49	0.0015
Cs	86.02	0.00120
Fe	487.08	0.00074
Li	78.97	0.00157
Mg	22.13	0.000087
Mo	8.05	0.0601
Na	1693.	0.0070
P	22.98	0.00154
Si	160.80	0.000029
Sr	0.67	0.000002
Zn	45.80	0.0332
Zr	3.41	0.00088
Total Solids	17.14 kg	0.00087
Dissolved Solids	10.16 kg	-
Alkalinity	292. g CaCO ₃	-
Acidity	1663. g CaCO ₃	-
Gross Beta	823. kBq	-

A number of caveats need to be established to interpret these inventories correctly. First, the inventories of Si and Al are probably low because the acid digestion of samples would not dissolve all the suspended solids as discussed above. In the investigation of Carter et al. (1988), significantly greater amounts of Si and Al were found in duplicate samples of off-gas scrub solutions than were found in the ORNL samples. The PNL samples were filtered, and the suspended solids were fused with KOH; elemental analyses include these suspended solids. Second, the amount of Fe reported in Table 4 is probably largely an artifact of the strongly acidic scrub solution (i.e., $\text{pH} < 3$) dissolving Fe from the mild-steel barrels during storage. Third, the apparently contradictory coexistence of alkalinity and acidity resulted from early barrels having alkalinity and later barrels having acidity. These later barrels also contained most of the Fe; several of these barrels also swelled and were significantly pressurized if the bungs were tightly closed, presumably due to outgassing of CO_2 or perhaps the formation of $\text{H}_{2(g)}$ from the corrosion of the steel ($\text{Fe} + 2\text{H}^+ = \text{Fe}^{2+} + \text{H}_{2(g)}$). Fourth, the relatively large amounts of B, Mo, and Zr in the scrub solution, and, hence, their large ratios to the amounts in the vitrified product, are a result of the inclusion of ZrB_2 and MoSi_2 as a protective powder filling the annular space between the Mo rod and the graphite sleeve of each electrode. Fifth, the presence of gross beta activity (and gross alpha not shown) was due to residual contamination within the off-gas processing train from previous tests in Richland, Washington; the major radionuclides were ^{90}Sr and ^{239}Pu with estimated inventories of 960 and 10 kBq, respectively. Because over 800 kBq of gross beta activity was found in the scrub solution barrels, considerable decontamination of the off-gas train must have been achieved during the pilot-scale operation. Sixth, the relatively large amount of Na in the off-gas is also largely an artifact. Approximately five hours from the initiation of the run on July 14, 1987, electrical continuity of the starter path material between the electrodes was interrupted due to subsidence of the ground surface. Because the usual starter path material, a mixture of glass frit and graphite, had been used up in several previous reestablishments of the starter path, a 100-lb bag of light soda ash (Na_2CO_3) was used to fabricate a new starter path. The subsequent heating and decomposition of the soda ash lead to a pulse of Na, high pH, dissolved solids, and alkalinity over the next several hours into the scrub solutions. Most

of the Na in the off-gas scrub solution resulted from this spike from the soda ash and will be discussed subsequently.

The amount of Cs in the barrels, 86.02 g, was considerably greater than the Cs inventory, 69.53 g, calculated by Carter et al. (1988). Although there were some minor differences in the concentrations of Cs in duplicate time-series samples of the off-gas scrub solutions between ORNL and PNL, most of the difference probably resulted from the estimates of volumes used in the calculation. Carter et al. (1988) computed a standing inventory of Cs based on volumes of liquid transferred to waste barrels and concentrations of Cs in samples taken immediately before and/or after transfer. The total volume recorded for 19 liquid transfers was only 1357 L. However, the 11 barrels had a total volume of 1990 L (or 1656 L, if the 334 L transferred during the abortive June ISV start is subtracted). Thus, the PNL solution transfer volume estimates were low enough to account for most of the discrepancy between the Cs inventories [(i.e., $(1656/1357) \times 69.53 = 84.8$ g]. The PNL estimates were based on the liquid level measurements on Tank 2 (the Hydro-Sonic scrubber) before and after transfer to Tank 1 (the venturi-ejector scrubber). From Tank 1, the waste solution was then transferred to the barrels. However, the liquid levels in Tank 1 also were recorded before and after each transfer from Tank 2, and the resulting volume estimates are significantly larger than those based on measurements of Tank 2. Using the Tank 1 solution transfer volumes, a total volume of 1894 L of scrub solution was calculated, which is approximately 95% of the 1990 L contained in the barrels. Thus, the Tank 1 liquid level measurements appear to be more accurate than the Tank 2 liquid level measurements used by Carter et al. (1988).

In the following discussion of the temporal changes in the off-gas scrub solution composition, the transfer volumes were based on the measurement of liquid levels in Tank 1. Duplicate samples of each scrubber tank were taken every 2 h during the ISV run. Analytical procedures for the characterization of these samples were identical to those described previously for the samples from the 11 barrels of scrub solution waste. By using (1) the laboratory determinations (see Appendix for a complete listing of analytical results), (2) the ambient liquid levels in both scrubber tanks, and (3) the solution transfer volumes, the time dependence of the accumulation of elements and

characteristics of the scrub solutions can be computed [analogous to the calculation method employed by Carter et al. (1988)].

The time dependence of the scrub solution pH indicates several changes that occurred during the course of the ISV run (Fig. 26). Initially near neutral, the pH rose to above 10 within a few hours of the start of the run. This increase was due to the volatilization of the alkaline Na_2CO_3 used to reinitiate the starter path between electrodes as discussed previously. Concurrently, there was a dramatic increase in the electrical conductivity of the scrub solution also associated with the volatilization of Na_2CO_3 . At ~ 24 h into the run, the electrical conductivity began to decline and the pH of the scrub solution began to decrease rapidly. Also at this time, the titratable alkalinity disappeared from the scrub solution and titratable acidity began to appear (Fig. 27). This dramatic change in character of the scrub solution from basic to acidic conditions occurred at the time when the melt depth began to encounter the limestone gravel. The increase in the concentration of CO_2 in the off-gas (Fig. 18) was indicative that the melt had reached this depth [i.e., 2 ft (0.6 m)] as corroborated by the thermocouple data. This increased evolution of CO_2 would produce significant carbonic acid in the scrub solution and would result in the neutralization of the alkalinity and further production of acidity. However, the pH of the scrub solution continued to fall well below $\text{pH} = 4.0$, which is about as low as carbonic acidity, even in equilibrium with 100% CO_2 , can go. The rise in pH at the end of the run was associated with an alkaline wash solution placed in the scrub tanks to protect them from corrosion. The depression of pH below $\text{pH} = 4$ must be associated with strong mineral acidity. Samples from the waste barrels were analyzed for anions which indicated that sulfate was the predominant anion present (see Appendix). Thus, the off-gas likely contained SO_2 , which is the likely source of the stronger mineral acidity that lowered the pH below 4.0. The sulfur content and chemical form in the soil and limestone of the trench is not known at this time.

The behavior of total, suspended, and dissolved solids in the scrub solution (Fig. 28) allows an assessment of the radiological consequences of an ISV operation on a seepage pit at ORNL. The amount of total solids in the scrub solution rose rapidly during the first 18 h of operation and rose slowly thereafter. Some of this rapid

Electrical Conductivity and pH of ISV Off-Gas Scrub Solutions

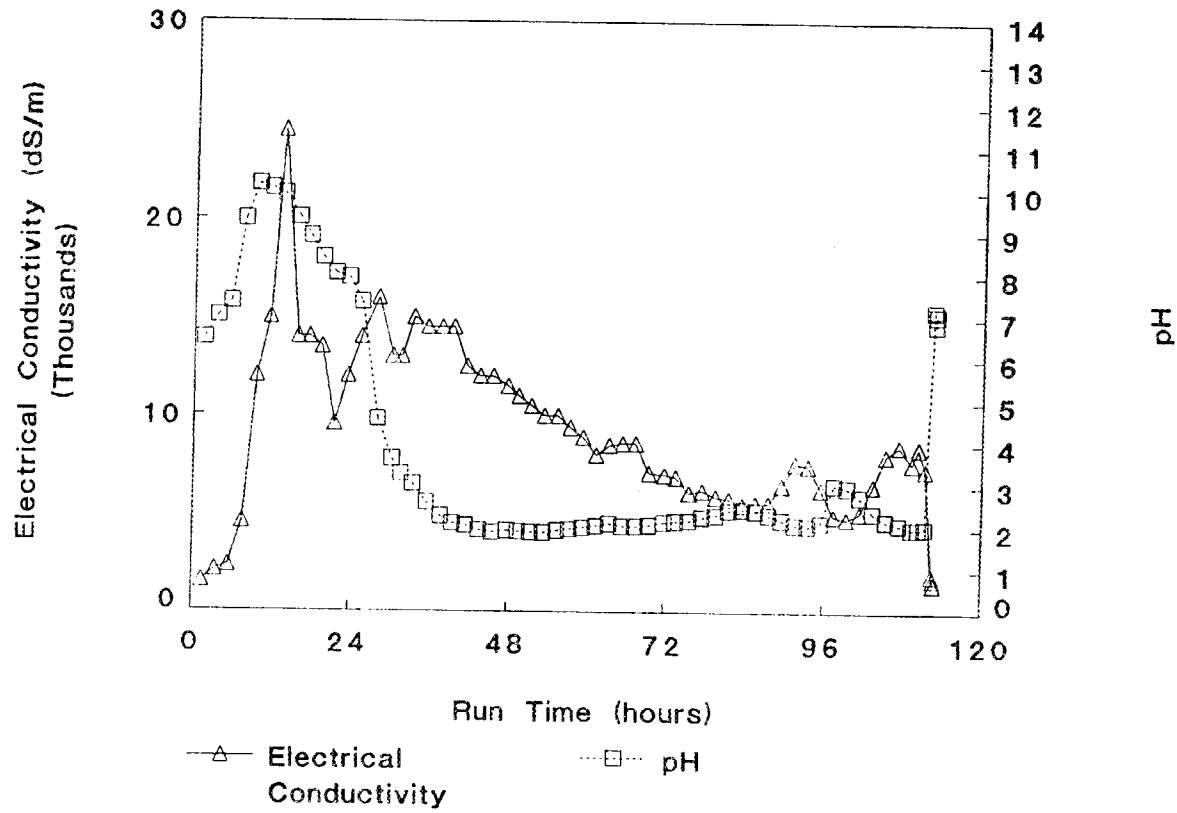


Fig. 26. Electrical conductivity and pH of the off-gas scrub solution during the ORNL ISV demonstration.

Soluble Acidity and Alkalinity in ISV Off-Gas Scrub Solutions

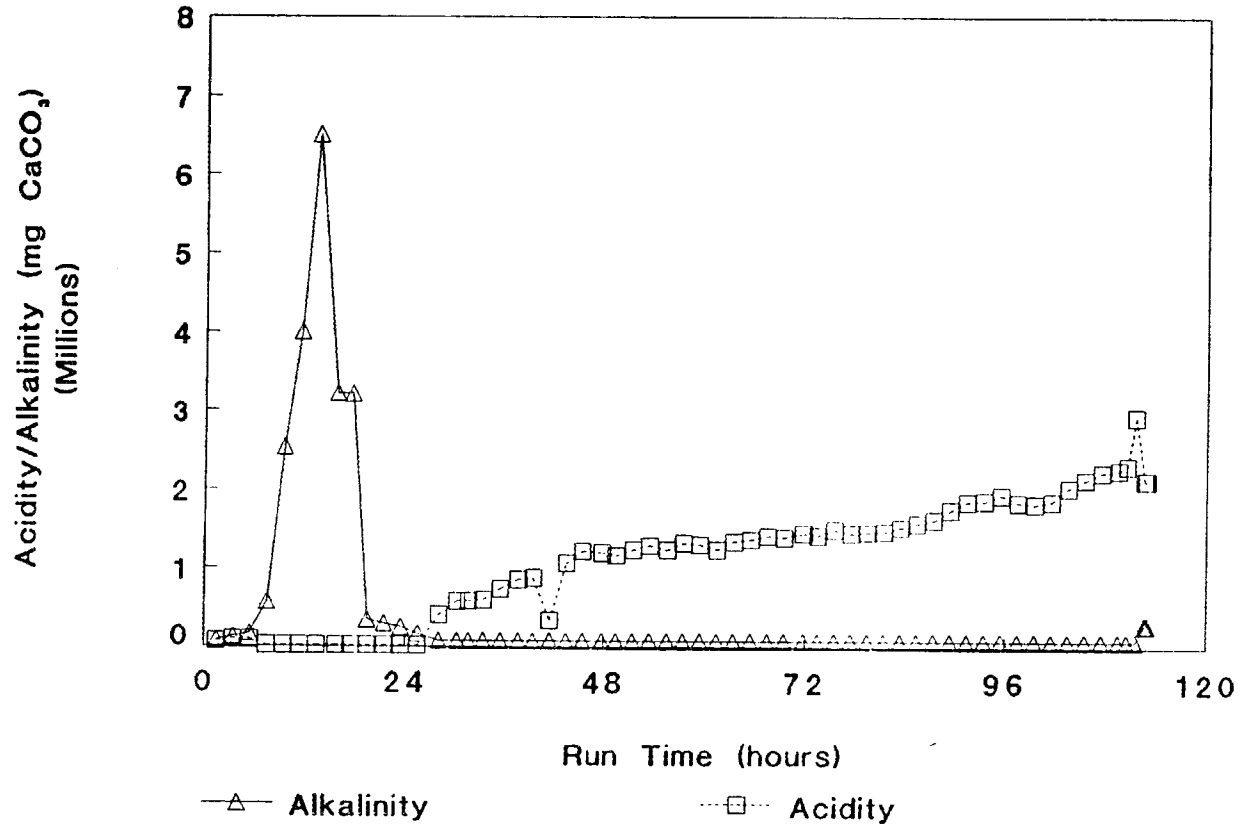


Fig. 27. Cumulative titratable acidity and alkalinity in the off-gas scrub solution during the ORNL ISV demonstration.

Total, Dissolved, and Suspended Solids in ISV Off-Gas Scrub Solutions

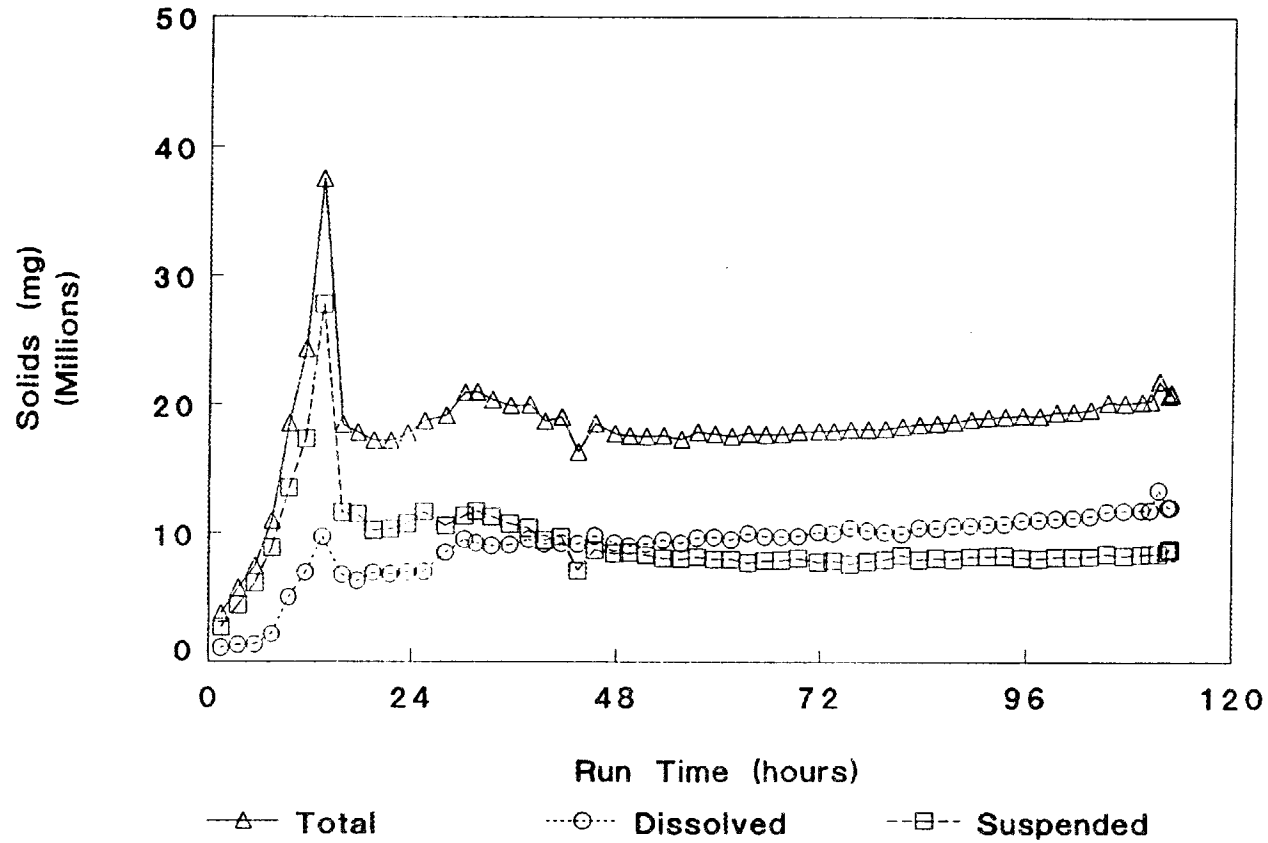


Fig. 28. Cumulative amounts of total, dissolved, and suspended solids in the off-gas scrub solution during the ORNL ISV demonstration.

increase was probably a result of the entrainment of the Na_2CO_3 powder in the air stream, but the majority of solids probably result from entrainment of soil particles in the air flow. This behavior is expected because the ground surface over which the hood lies would become depleted of air-suspendible solids as the air flow continues without further ground surface disturbance. Secondly, a cold cap begins to form over the surface of the melt zone as it progresses downward. This cold cap aids in the removal of particulates that might otherwise become entrained in the off-gas due to turbulence on an exposed melt surface. The off-gas scrubbers are designed to remove particulates from the off-gas so that the HEPA filters do not become clogged. However, after about a day of operation, relatively few particulates needed to be removed by the scrubbers. Thus, there is a potential technique to minimize ^{137}Cs accumulation in the processing trailer components. At this point in the run, a HEPA filter might work well if placed directly at the intake of the ducting within the off-gas hood. Notably, at this point in the run, significant amounts of Cs had yet to appear in the off-gas because the melt had not progressed to the burial depth of the Cs. This situation is identical to that expected in the vitrification of a seepage trench at ORNL. Insertion of a HEPA filter in the hood at this point in the ISV operation would minimize the deposition of Cs on the ducting and its accumulation in the scrub solutions and trailer HEPA filters. Near the end of the run, the HEPA filter, in a remote-controlled housing within the hood, could be dropped into the melt.

The behavior of individual elemental accumulations in the off-gas scrub solution provides further indications as to what might be expected during an actual application to a seepage trench at ORNL. The behaviors of Ca, Mg, and Sr (Fig. 29) were quite similar although the actual inventories varied. All three elements started with significant accumulations due to their initial concentrations in the makeup water for the scrub tanks. After the pulse of each element during the initial 18 h of operation, accumulation was much more gradual and the ratio of all three alkaline earth elements remained constant throughout the run. Thus, perhaps all of the accumulated Sr was due to entrainment of Ca and Mg particulates from the soil and limestone. No demonstrative change in slope of the Sr accumulation curve occurred when the melt zone reached the depth of tracer burial [~ 4 ft (1.3 m)] at about 30 h into the run.

Cumulative Alkaline Earth Elements in ISV Off-Gas Scrub Solutions

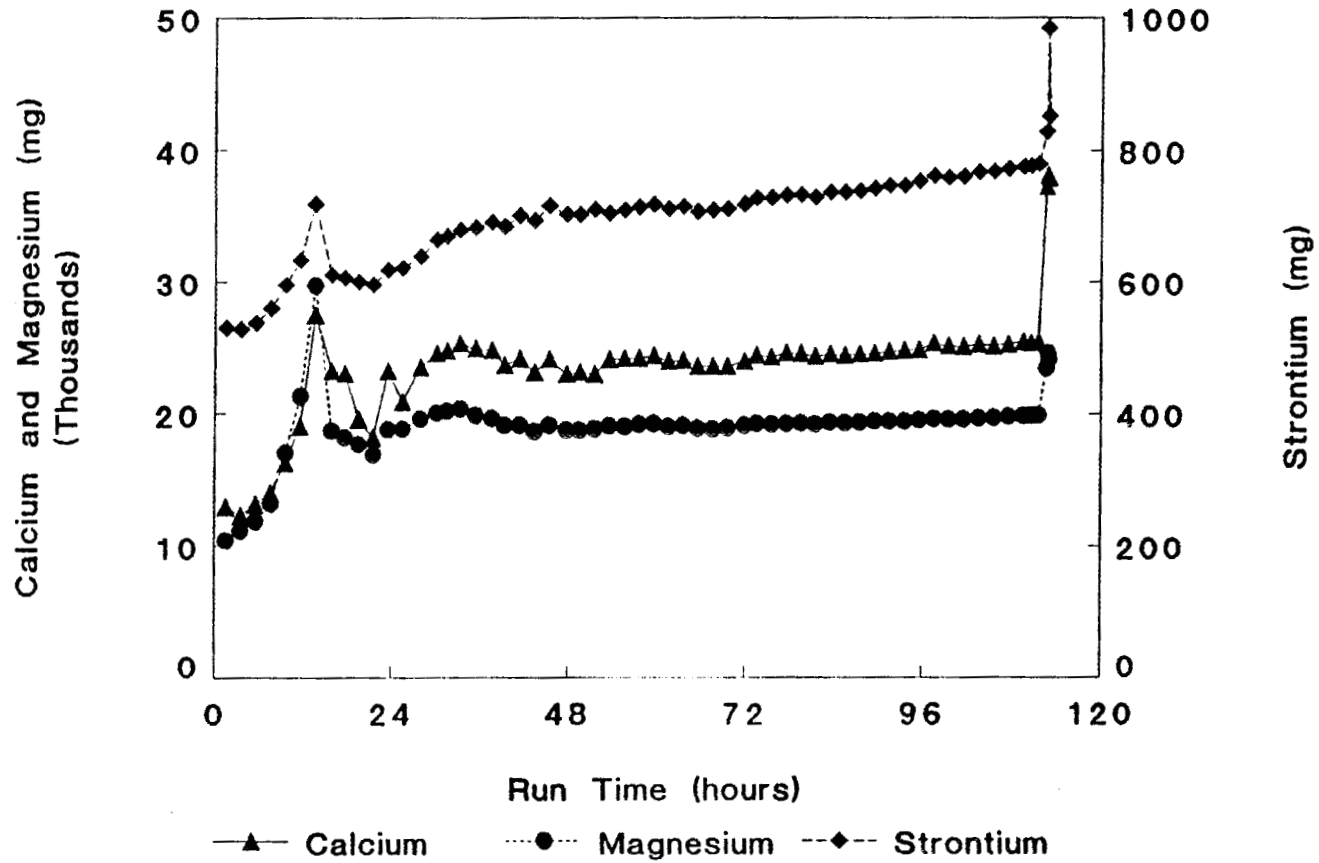


Fig. 29. Cumulative amounts of Ca, Mg, and Sr in the off-gas scrub solution during the ORNL ISV demonstration.

This behavior of Sr contrasts with that of Cs (Fig. 30), where the slope of the Cs accumulation significantly increased at 30 h, when the melt zone entered the burial depth of the Cs_2CO_3 and SrCO_3 . The behavior of Cs was also different from that of the other alkali metal elements, reflecting its different source. Sodium and lithium accumulated early in the run due to the addition of Na_2CO_3 to reinitiate soil melting within 8 h of the start. It would be incorrect to assume that Na additions would not carry or affect the volatilization of Cs because of the different responses of Na or Li to that of Cs. Addition of NaOH to a seepage trench is being considered as a method to lower the viscosity and melt temperature of the ISV material (hence, lowering Cs volatilization by lowering operating temperatures) and as a means to initiate trench melting in the subsurface. However, the effects of any potential Na additions on Cs volatilization must be determined through laboratory tests before attempting any field tests. Again, the observation that Cs volatilization did not become significant until after the pulse of total solids had entered the off-gas scrub system points to the potential to minimize Cs accumulation in the processing trailer. Removal of Cs by a HEPA filter within the hood during the later stages of the ISV run may be a method to control Cs contamination.

The accumulation of Al, Fe, and Si in the off-gas scrub solution (Fig. 31) appears to be steadier than that of the alkaline earths or alkali metals. These apparent trends may be somewhat artifactual. These elements would all be largely constitutive or bound to particulates in the off-gas. Particulate elements would be underestimated in the analytical procedure employed because only acid digestion was employed rather than complete sample dissolution. The increasing acidity of the scrub solution may also have affected an increase in the solubility of Al, Fe, and Si contained in entrained water droplets carried into the Hydro-Sonic scrubber.

The behavior of the gross beta activity (Fig. 32) shows the expected accumulation of an element, given no input from the hood or ducting. The ^{90}Sr contamination within the off-gas processing system was residual from previous test of the pilot-scale unit on the Hanford reservation. Because there were no inputs of beta activity to the process system, the accumulation represents self-scrubbing of residual contamination from the various inaccessible components of the system (e.g., the heat exchangers and piping). Thus, its slope, expressed as a percent increase per unit time, would be expected

Accumulation of Alkali Metal Elements in ISV Off-Gas Scrub Solutions

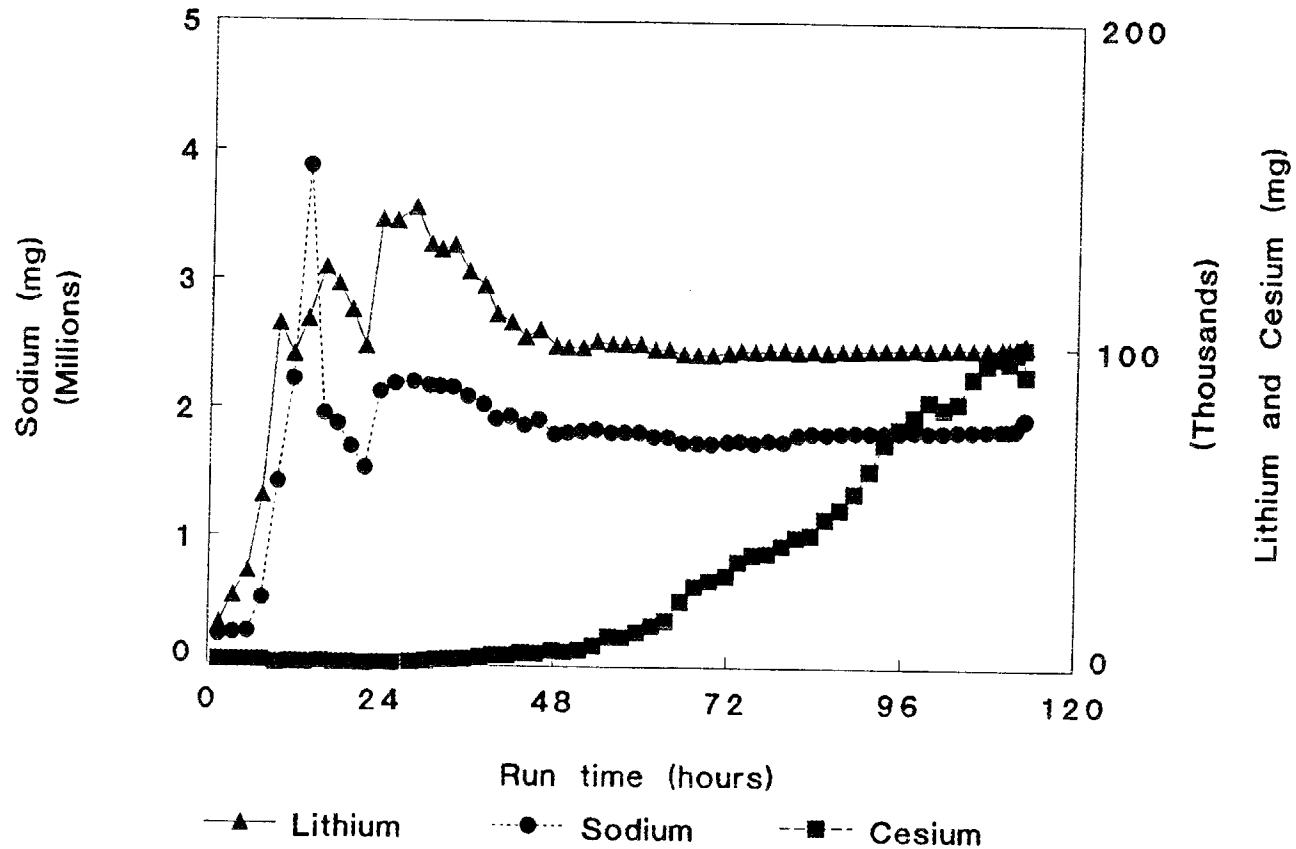


Fig. 30. Cumulative amounts of Li, Na, and Cs in the off-gas scrub solution during the ORNL ISV demonstration.

Aluminum, Iron, and Silicon Totals in ISV Off-Gas Scrub Solutions

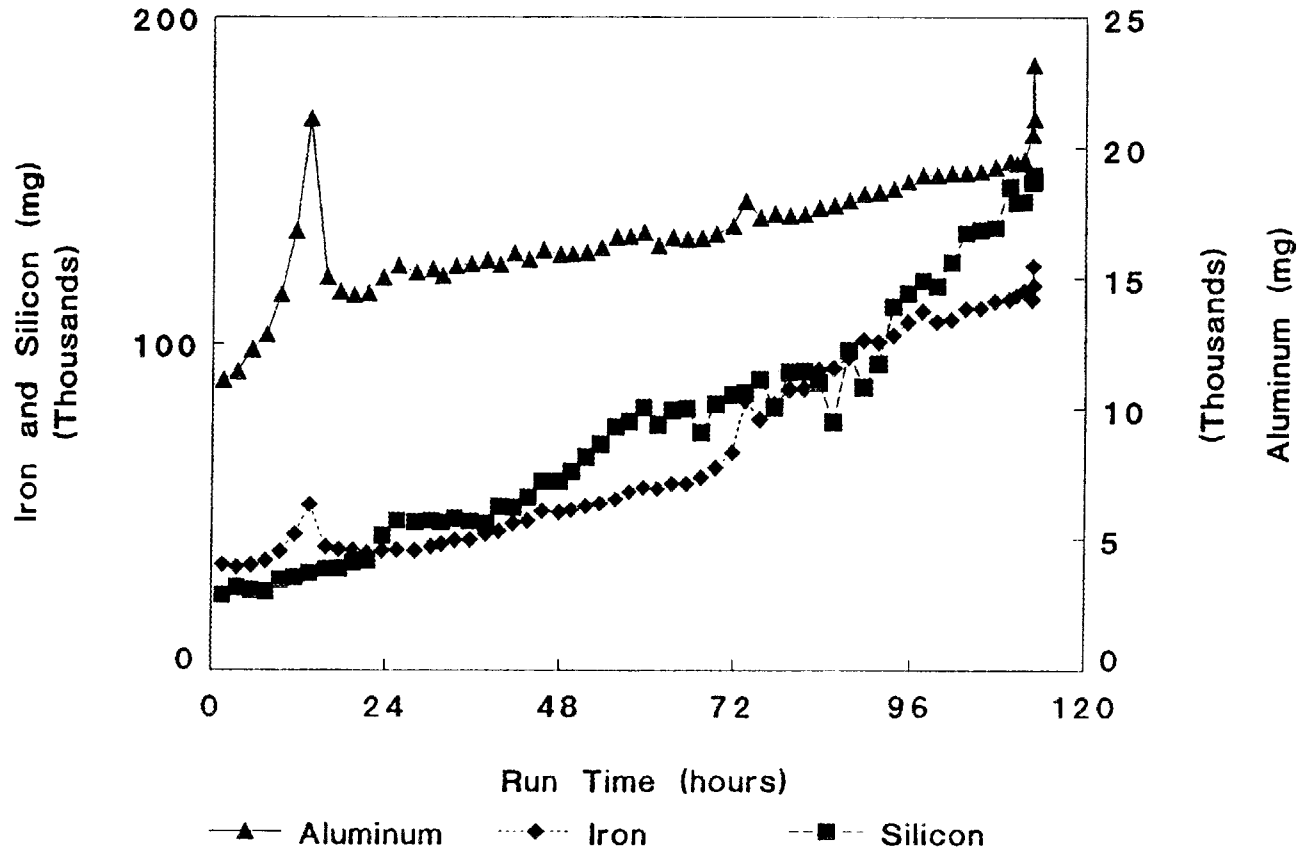


Fig. 31. Cumulative amounts of Al, Fe, and Si in the off-gas scrub solution during the ORNL ISV demonstration.

Gross Beta Radioactivity Inventory in ISV Off-Gas Scrub Solutions

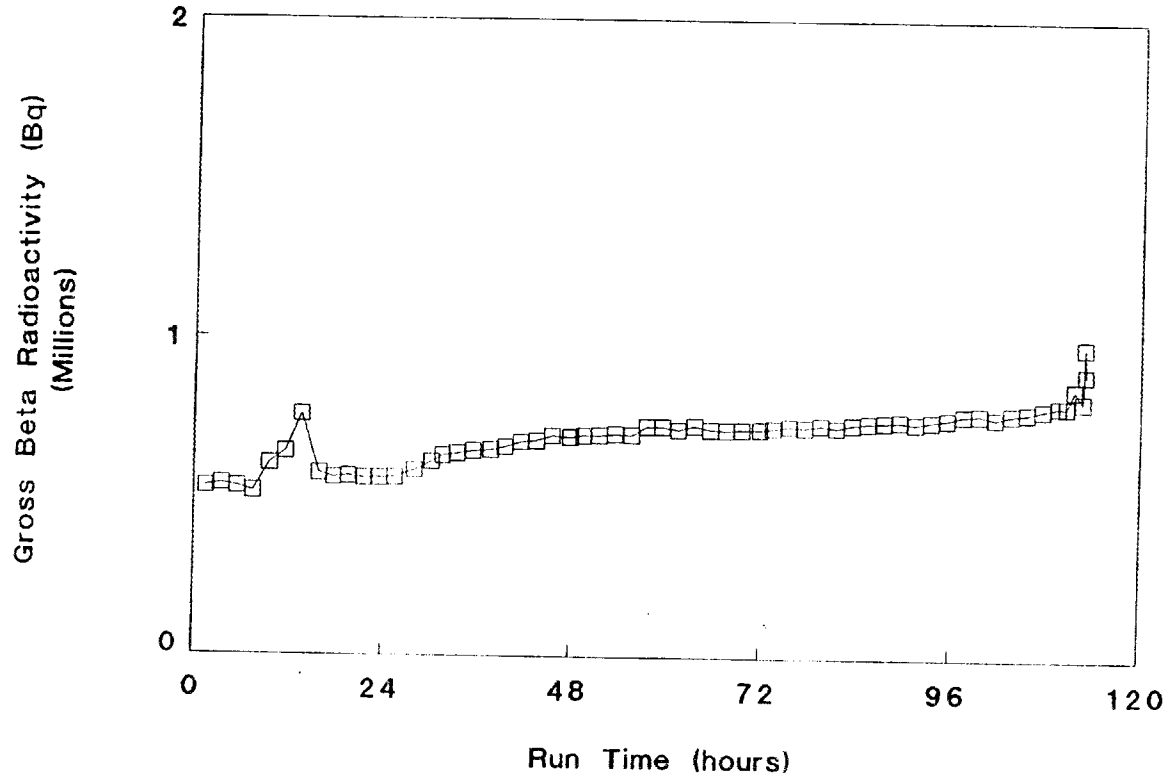


Fig. 32. Cumulative amounts of gross-beta radioactivity in the off-gas scrub solution during ORNL the ISV demonstration.

for any element or conservative characteristic of the scrub solution. Thus, any elemental accumulation showing a similar gentle slope probably does not represent a net accumulation but rather a washing out of that element from other parts of the scrub solution system into the tank (e.g., the alkaline earth elements).

The final inventories of each element can be compared with the inventories calculated from the barrels (Table 5). The average inventory of all properties in the system inventory was 14% greater than that calculated from the analyses of the 11 barrels. As discussed previously, these system inventories were calculated by using the Tank 1 (venturi-ejector scrubber tank) volume measurements for all tank transfers. The larger amount of Fe in the barrels over that in the system inventory was a result of the corrosion of Fe from the mild-steel barrels by the acidic scrub solution accumulated during the later stages of the run. Nonetheless, the relatively good agreement between the two independent methods of inventory calculation lends considerable confidence in the inventories.

4.3.4 Off-Gas HEPA Filters

Samples of the primary and secondary HEPA filters were prepared by PNL and received by ORNL in August 1987. Each HEPA filter was sampled twice in the front, center, and rear by cutting out approximately 30-cm by 30-cm squares of the borosilicate glass fiber material. Each sample was measured for its length and width and weighed into a tared beaker. The filter segments were ashed at 550°C overnight and reweighed after cooling. The filter segments were subjected to a HNO₃ digestion as described in the section on barrel solution analyses. The hydrolyzed filter was extracted with 12% HNO₃, the extract made to 50 mL, and the extracted filter returned to its original container. When Carter et al. (1988) reported considerably greater amounts of Cs in the acid extracts of unheated filter samples than was found in the ORNL acid extracts, complete dissolution of the archived filter segments was attempted. The filter segments readily dissolved on treatment with HF, and HNO₃ plus HF digestions were carried out as described in the section on barrel solution analyses. The dried digests were dissolved into 50 mL of 12% HNO₃ and submitted for Cs and Sr analyses with atomic adsorption spectroscopy.

Table 5. Comparison of scrub solution inventories
(all reported inventories are in grams, except where otherwise noted)

Element or property	Barrel inventory	System inventory	Ratio* (System/Barrel [†])	Imported inventory
Al	17.32	21.14	1.22	10.91
Fe	487.08	117.92	0.24	40.00
Si	160.82	149.75	0.93	19.09
Sr	0.67	0.85	1.27	0.68
Mg	22.13	24.10	1.09	6.00
Ca	35.43	37.94	1.07	5.00
Li	78.97	101.02	1.28	1.09
Na	1,628	1,944	1.19	80.9
Cs	86.02	91.07	1.06	0.64
Solids				
Total	17,138	20,915	1.22	5,526
Dissolved	10,158	12,113	1.19	1,327
Alkalinity	292	299	1.02	335
Acidity	1,663	2,126	1.28	0
Gross beta	824 kBq	896 kBq	1.09	0
Average (excluding Fe)			1.14	

*Ratio of the inventory calculated from the cumulative scrub solution samples and liquid transfer records to the inventory in the 11 barrels of waste scrub solution.

Initially it was hypothesized that the lower Cs in the ORNL samples may have been due to volatilization of Cs from the filters during the 550°C ashing treatment. To test this hypothesis, 1-mL aliquots of a stock ¹³⁷Cs solution (nominally 9.11 kBq/mL) were placed into each of ten 20-mL-capacity borosilicate glass scintillation vials. The carrier for the ¹³⁷Cs was a 0.1 M HCl solution so that the Cs was present as the chloride. The vials were capped and counted in a NaI scintillation detector for 10 min each after being dried at 110°C. Groups of three vials were then heated at 450°, 550°, and 650°C for 16 h. All vials were recounted as before, and, because all vials retained all their ¹³⁷Cs (Fig. 33), an extraction sequence was initiated to determine if the thermal treatments exerted any effect on the extractability of the ¹³⁷Cs. Each vial, including the unashed vial, was extracted with four sequential 5-mL volumes of tapwater. After

Extractability of ¹³⁷Cs from Borosilicate Glass after Heating

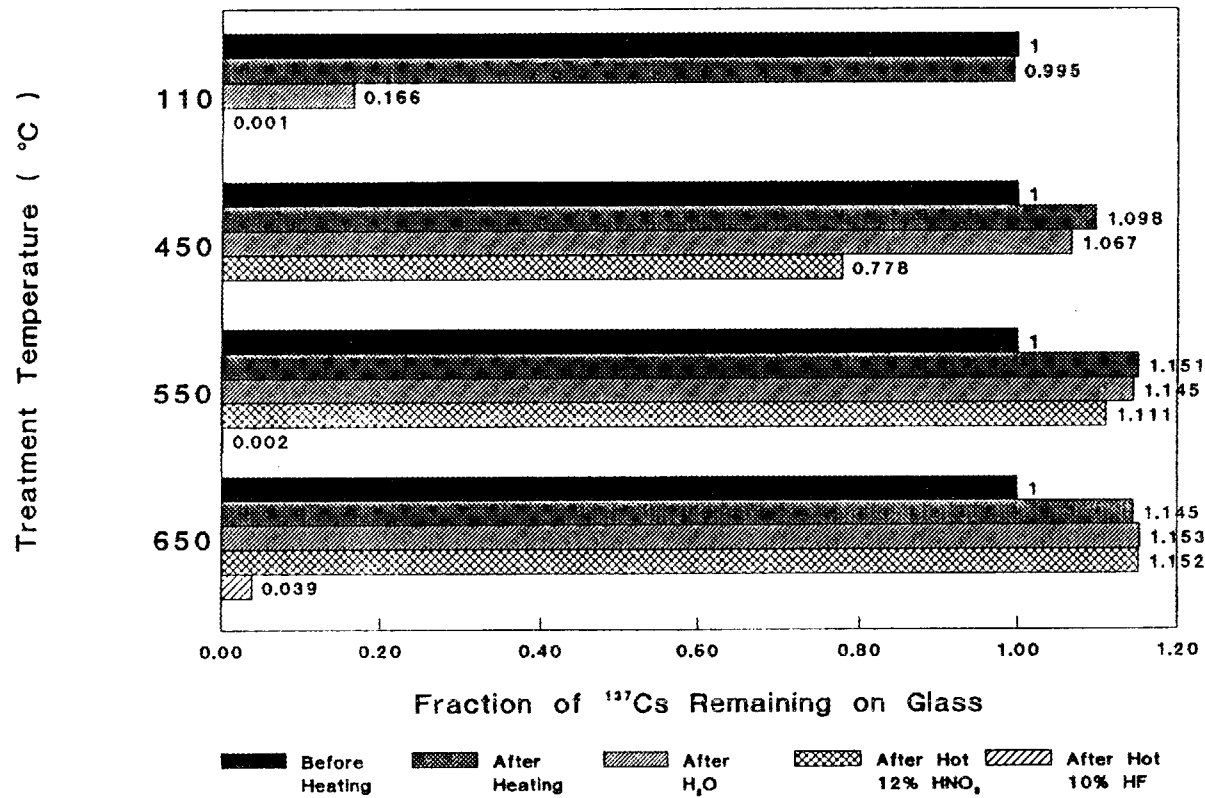


Fig. 33. Leaching of ¹³⁷Cs from borosilicate glass vials following heating to indicated temperatures.

removal of the last tapwater volume, the vials were dried at room temperature, capped, and recounted for activity as above. The vials were then extracted with three 5-mL volumes of 12% HNO_3 , heated to near boiling for the first two volumes by placing the vial on a hot plate, followed by one 5-mL volume of tapwater. After drying and recounting as above, the vials were extracted with two 5-mL volumes of 10% HF also heated to near boiling by placing the vials on a hot plate. The vials were dried for a final time and counted again. The net counts in the ^{137}Cs photopeak of the gamma ray spectrum, corrected for baseline background, were used to compute relative amounts of ^{137}Cs at the different counting times because standards of ^{137}Cs yielded identical counting efficiencies for each counting period.

Results of the thermal treatments are depicted in Fig. 33. After drying at 110°C , tapwater extraction was able to remove all but 17% of the ^{137}Cs , and all of the remainder was extracted with hot HNO_3 . Contrary to the hypothesis of volatilization of ^{137}Cs at the temperatures used for ashing the HEPA filters, all of the ^{137}Cs was retained in the vial after heating up to 650°C . The apparent increase (about 15%) in the activity of ^{137}Cs following the three thermal treatments is probably due to diffusion of the ^{137}Cs into the borosilicate glass at the elevated temperatures, thereby decreasing the shielding afforded by the unheated vial. When the extraction of ^{137}Cs from these heat-treated vials was attempted, essentially none of it was removed from any of the vials. Even hot HNO_3 extraction could extract little of the ^{137}Cs . Only the 450°C heat treatment yielded a glass from which a significant amount (22%) of the ^{137}Cs could be extracted; the 550°C and 650°C thermal treatments resulted in essentially complete resistance of the ^{137}Cs to acid extraction. However, the hot HF was able to remove most of the ^{137}Cs from all of the different thermally treated glass vials. Thus, it appears the ^{137}Cs had diffused into the borosilicate glass, and only dissolution or etching of the glass with HF was capable of removing it. After HF extraction the vials were noticeably etched but were far from completely dissolved. These findings confirm that the extractability of Cs from the ISV off-gas HEPA filters was probably greatly decreased by the ashing temperature, 550°C , experienced before their acid extraction. Quite aside from the analytical inconvenience presented by this fixation of Cs on borosilicate glass filter material in the measurement

of the amount of Cs on the HEPA filters, the effect may present some advantage to the ISV off-gas processing during an actual application to an ORNL seepage trench. As mentioned previously, the placement of a HEPA filter within the off-gas hood, after the initial pulse of particulate release during an ISV run, could well function to prevent volatilized ^{137}Cs from entering the off-gas scrubbing system. Because the off-gas in the hood is often above 300°C , a significant portion of the ^{137}Cs may become fixed on the HEPA filter material in this thermal environment. Such thermal fixation may aid in the removal of ^{137}Cs from the off-gas.

The results of the elemental analyses of the HEPA filter samples are presented in Table 6. First, the extractability of Cs from the HEPA filter segments was apparently quite reduced by the ashing treatment at 550°C . Only about 4% of the total Cs on the primary HEPA filter was extractable via HNO_3 and complete dissolution with HF was required to remove it. The difference in Cs composition between the primary and secondary filters demonstrates that the Cs on the primary filter was deposited by the ISV off-gas and was not a constituent of the borosilicate glass fabric. Carter et al. (1988) reported a similar amount of Cs, 2.32 g, on the primary HEPA filter following sample preparation via water extraction. Their samples were not ashed or thermally treated before the extraction and, therefore, the Cs was water soluble, similar to the findings for ^{137}Cs in glass vials described above. The agreement between the PNL and ORNL Cs inventories on the HEPA filters is reassuring. The confirmation that complete filter dissolution did not release significantly more Cs than was found in the aqueous extracts confirms that residual Cs did not remain on the filters following aqueous extraction and that the Cs inventory is correct.

Strontium, on the other hand, exhibited little difference in total inventory between primary and secondary HEPA filters although, like Cs, HF dissolution was required to remove it from the HEPA filters. The lack of difference between primary and secondary filters probably results from Sr being a constituent element in the borosilicate glass of the filter fabric. Most Ca-containing minerals, like the lime used in the manufacture of the borosilicate glass, contain Sr at a mass ratio of approximately 1:200 to Ca. Thus, for the purposes of computing the inventory of Sr on the HEPA filters, the acid-extractable amounts were used rather than total amounts, as were used

Table 6. Elemental inventories deposited on the off-gas HEPA filters

Element or Species	Amount		
	Primary HEPA (mg)	Secondary HEPA (mg)	Difference (mg)
Al	122	56	66
Ca	534	250	284
Cs			
Acid*	89	16	73
Total	2,146	57	2,089
Fe	73	6	67
Li	286	40	246
Mg	61	48	13
Mn	4	1	3
Mo	606	8	598
Na	19,620	4,640	14,980
Si	953	836	117
Sr			
Acid Ext*	13	6	7
Total	1,020	1,140	-120
Anions			
F ⁻	839	123	716
Cl ⁻	8,242	1,135	7,107
NO ₃ ⁻	523	286	236
PO ₄ ³⁻	336	0	336
SO ₄ ²⁻	43,080	12,210	30,870

*All elements reported are for HNO₃ extracts of the filter samples except for the Cs and Sr totals, which include the HNO₃ extracts plus that removed by HF dissolution. Anions were analyzed for water extracts of filter samples by Battelle Pacific Northwest Laboratory.

for Cs inventory calculation. Inventories of all other elements were also computed by using the HNO₃ extractable analyses. Significant differences for all elements were noted between the primary and secondary filters. Total solids on the HEPA filters were estimated by converting the elemental amounts to their oxide equivalent amounts and summing all the major elements listed in Table 6. It should be emphasized that the calculation will grossly underestimate total solids because the acidic extraction of the

filters will not dissolve much of the siliceous particulates on the filters. Thus, elements like Si and Al will be underestimated in the ducting, scrub solutions, and HEPA filters.

The major difference in anions extractable in water from the HEPA filters was the large amount of sulfate present. As discussed previously, some acid stronger than carbonic acid was required to lower the pH of the scrub solution below 4.0. The large amount of sulfate, particularly on the primary filter, points to SO₂ volatilizing from the melt zone as the likely source of this acidity. The sulfur content and chemical form in the soil and limestone of the trench is not known. However, previous experiments reported by Buelt et al. (1987) indicate that sulfates have a decontamination factor of 70 through the off-gas scrubbing system. Thus, deposition of sulfate from the scrub solution onto the HEPA filters would be expected. Sulfate is the major anion associated with the titratable acidity in the scrub solution samples discussed previously.

4.3.5 Overall Off-Gas System

The actual amounts and distribution of elements within the ISV off-gas handling system have been discussed in the preceding sections describing the various components. The overall off-gas retention factors are listed in Table 7. The retention factors (RFs) for Cs, Na, and Li were low compared to those for the other elements. The low Na and Li RFs were strongly influenced by the soda ash addition early in the run; however, the Cs RF was not influenced by this addition. Increasing the RF for ¹³⁷Cs during ISV represents one of the major challenges in the application of ISV to ORNL seepage pits and trenches. The low RF for Mo is strictly an artifact of its use in the electrode coating and annular packing. The RFs for Si, Al, and Fe are slightly high because the total amounts of these elements in suspended solids were not analyzed in the ISV off-gas scrub solutions; more accurate RFs for these elements would be better reflected in the RF calculated for solids in the system. Carter et al. (1988) performed total elemental analyses on selected samples from the ISV scrub solutions; their analytical results were significantly higher for Si, Al, and Fe but quite similar for Ca, Mg, Sr, Na, Li, and Cs.

Table 7. ISV off-Gas retention factors for elements

Element	Amount in off-gas system (g)	Amount in ISV mass (kg)	Retention factor
Al	27	1472	54,500
Ca	39	2,415	61,900
Cs	92	76	826
Fe	135	655	4,850
Li	91	52	571
Mg	25	329	13,200
Mo	14	0.14	10
Na	1,792	236	132
Si	781	5,377	6,890
Sr	0.8	250	312,000
Solids	18,600	20,000	1,075

The distribution of elements within the components of the off-gas system offers a good overall perspective on the potential radiological hazards, were an actual seepage trench at ORNL to be vitrified with the present hardware and techniques. The distribution of the alkali metal elements is depicted in Fig. 34. The similar partitioning of all of these elements among the ISV components leads to the conclusion that >95% of any ^{137}Cs in the off-gas would reside in the scrub solutions. Increasing amounts of Na, which might be present in the melt zone as an additive to lower melt temperatures, would not result in additional transport of ^{137}Cs from ducting to scrub solution to HEPA filters. The added Na, however, might affect the amount of ^{137}Cs volatilized from the melt zone; such effects must be determined in bench-scale tests before a radioactive field demonstration. The major sink for Cs in the off-gas system will be the scrub solutions. The potential exists to recycle this scrub solution below the melt zone to be incorporated into the final vitrified mass. This procedure could be done by pumping the scrub solution into well casings driven at an angle into the trench bottom. Such a technique would minimize the radiation field around the scrub tank or waste storage

Distribution of Alkali Metal Elements in ISV Off-Gas System

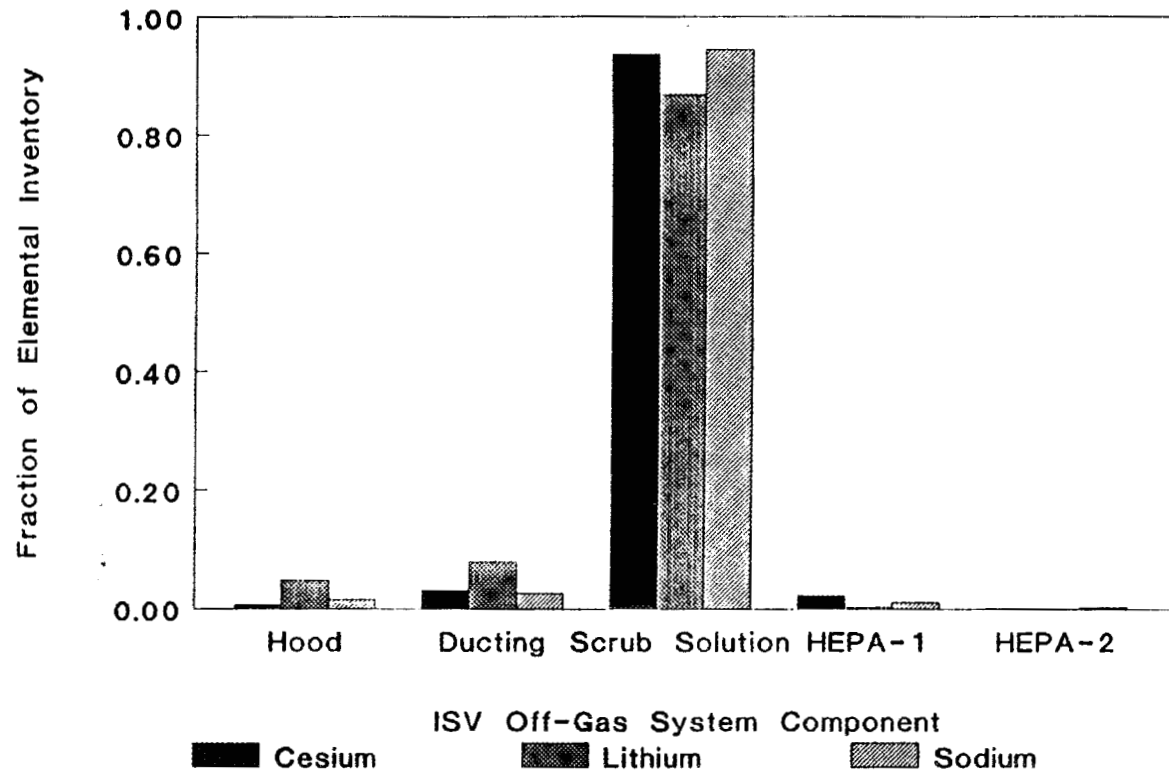


Fig. 34. Distribution of alkali metal elements in the ISV off-gas system components after the ORNL ISV demonstration.

tanks and also minimize the volume and activity of waste generated by the ISV process. A significant amount of ^{137}Cs would be expected to deposit on the inside walls of the ducting. The only method to prevent this deposition from building a significant radiation field during an actual application would be to insert HEPA filters into the off-gas line as it exits the hood as discussed previously. The HEPA filter material would need to be dropped into the melt zone in either a continuous or batch fashion as its ^{137}Cs inventory increased. Such techniques need to be investigated as modifications to the present ISV process to avoid the necessity of handling a large inventory of ^{137}Cs in the off-gas system.

The distribution of the alkaline earth elements in the components of the off-gas system were all similar to each other (Fig. 35) and similar to that of the alkali metals. It should be emphasized that, although the distribution within the off-gas system was similar to the alkali metals, the amounts in the off-gas system relative to the amounts in the vitrified mass were approximately two orders of magnitude lower than the alkali metals (Table 4). The total amount of Sr detected in the entire off-gas system was barely above background amounts contained in the system components (HEPA filters) or imported into the system in the makeup water for the scrub solutions (Table 5). The distribution of elements such as Al, Si, and Fe (Fig. 36) provides some assessment of how transuranic elements will behave in the ISV off-gas system. These elements, like the transuranic elements, will be strongly associated with the particulates in the off-gas. The bulk of the solids in the system ends up in the scrub solutions, and extremely few escape to the HEPA filters. Filtration control of the input of solids to the off-gas, particularly during the middle to later stages of a run when the melt zone enters the contaminated depths of a seepage trench, could minimize the inventory of transuranic isotopes in the processing trailer. The apparent distribution of Al and Si between the hood and ducting and the scrub solution is quite biased by the analytical procedures. The solids from the hood and ducting were subjected to complete dissolution whereas the scrub solutions were subjected to acid hydrolysis and extraction. Thus, complete dissolution of the suspended solids in the scrub solutions would have raised the inventory of Si and Al and resulted in a distribution similar to that of the total solids.

Distribution of Alkaline Earths In ISV Off-Gas System

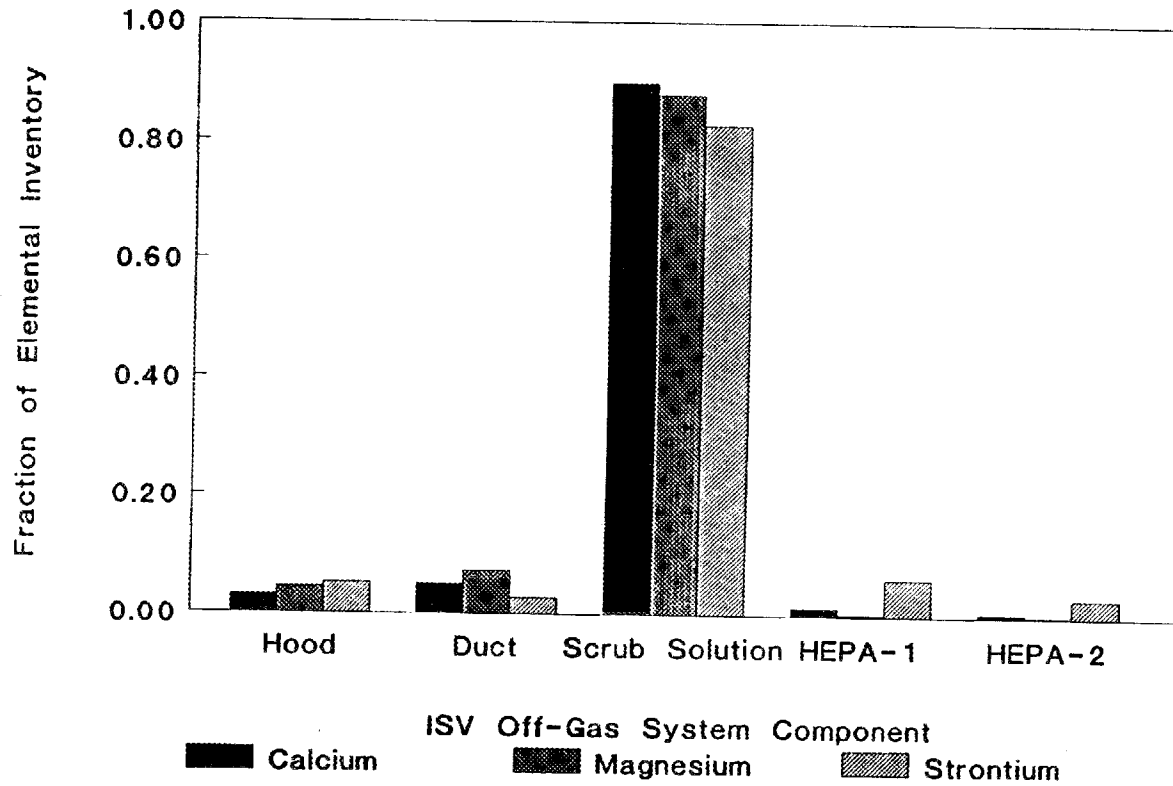


Fig. 35. Distribution of alkaline earth elements in the off-gas system components after the ORNL ISV demonstration.

Distribution of Elements and Solids in ISV Off-Gas System

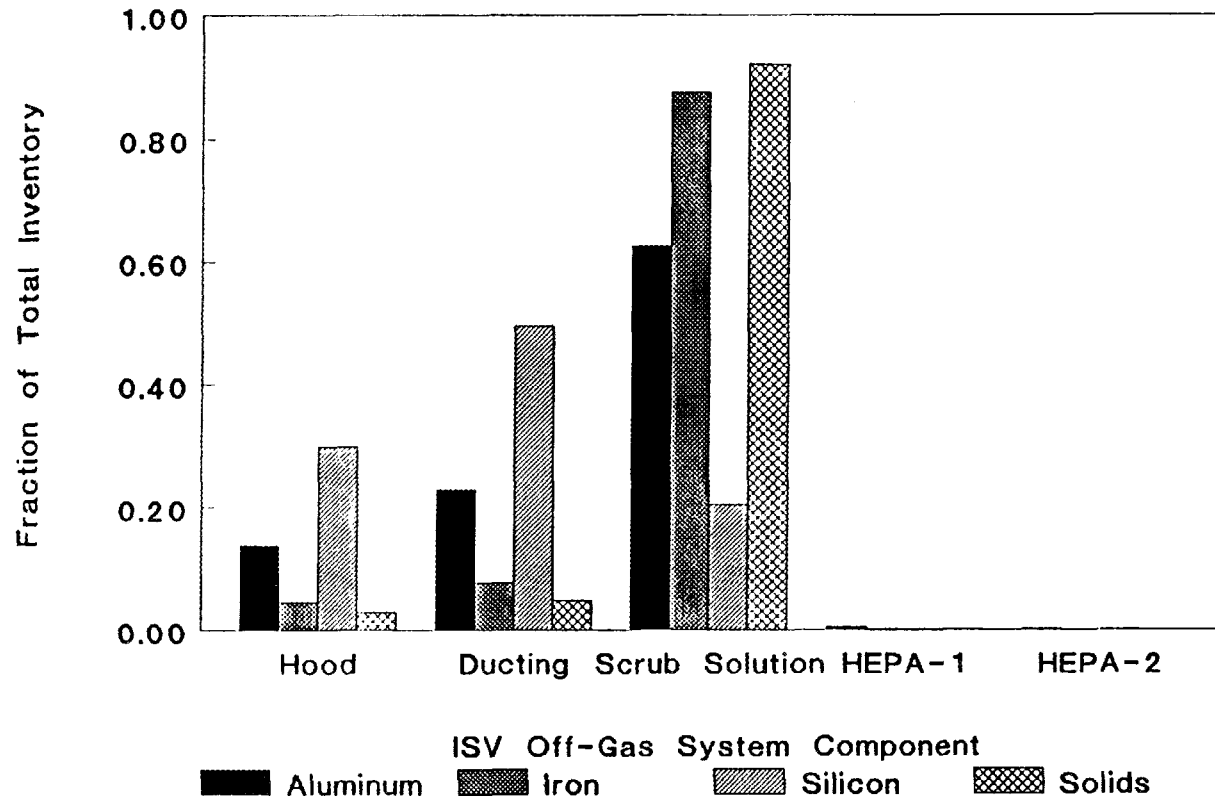


Fig. 36. Distribution of Al, Fe, Si, and solids in the off-gas system components after the ORNL ISV demonstration.

5. ISV PRODUCT CHARACTERIZATION

5.1 FIELD SAMPLING AND CHARACTERIZATION

The off-gas hoods were removed on October 6, 1987, to expose the subsidence zone (Fig. 37). Six cores were taken at the positions illustrated in Fig. 38. Detailed descriptions of the cores are given in Table 8. Because of the unexpected discovery of a multiphase product (see Sect. 5.2), it was decided to excavate a portion of the ISV mass to determine additional detailed information. A longitudinal cross section of the mass was exposed by using a backhoe and pneumatic jack hammer on November 6, 1987. Figure 39 illustrates the final excavated site. Grab samples were taken from several locations (Fig. 40 and Table 9) to complement the samples from the cores.

Some general observations from the excavation of the ISV mass include the following (see Figs. 37 and 39):

1. Subsidence from the ground surface to the top of the vitrified mass was approximately 0.91 m at the center of the trench.
2. Two cold caps were observed. The upper cold cap occurred at a depth of 0.41 m from the surface of the soil. The lower cold cap was at the surface of the melt at a depth of 0.91 m. The upper cold cap was up to 5.0 cm thick and had little structural strength (predominantly a frothy, porous green material) and would collapse upon backfilling of the trench so that future subsidence would be eliminated.
3. The side walls of the subsided surfaces were vertical and were 1.3 cm thick. The upper surface of the ISV mass along the length of the trench was quite level, suggesting that the melting process created a void space between the upper soil and the crushed limestone of the trench. This configuration is consistent with the behavior of the thermocouples (see Sect. 4.2) in which the 0.6-m deep thermocouples indicated lower temperatures than the thermocouples at depths of 1.2 m and 1.5 m. This sloughing of the limestone probably contributed to the longitudinal melting.



Fig. 37. View of the ORNL ISV demonstration trench after removal of the off-gas hood. Subsidence is evident within the array of the electrodes and graphite sleeves.

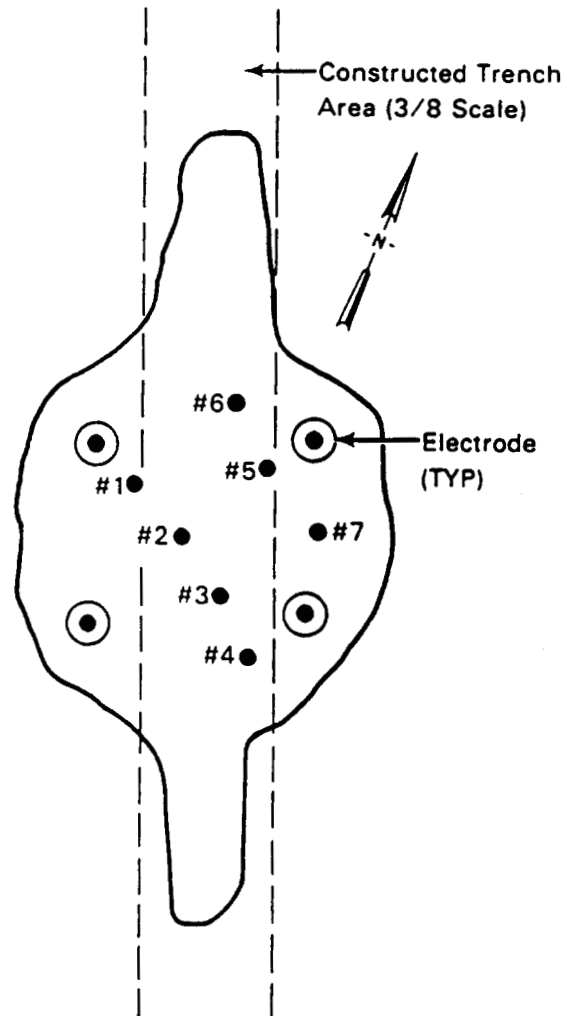


Fig. 38. Relative positions of cores into the ISV mass following the ORNL ISV demonstration.

Table 8. Description of ISV cores^a

Core H1:	<p>Located approximately 33 cm from NW electrode diagonally toward the center of the trench. Frothy cold cap material was broken into pieces and removed. Hole was started at a depth of 94 cm from the surface. Total depth of the hole was 107 cm (201 cm from surface).</p> <p>0-41 cm: Approximately 5 cm of porous green glass; remainder of section was a mixture of pieces of dark green glass and gray spherulites; no estimate on core recovery.</p> <p>41-107 cm: Virtually no recovery of intact core; a mixture of chips of dark green glass and gray spherulites.</p>
Core H2:	<p>Located toward center of trench, 83 cm from NW electrode and 74 cm from SW electrode. Subsidence was 76 cm to the top of the melt. Total depth of core hole was 169 cm (245 cm from surface).</p> <p>0-58 cm: 23 cm of porous green glass; one piece of dense glass; one piece of a mixture of glass and spherulites; one 8-cm-long section of gray spherulites at bottom of section.</p> <p>58-91 cm: 29 cm of core recovered; predominantly dense gray rock (spherulites).</p> <p>91-119 cm: 18 cm of core recovered in three pieces: 7.6-cm piece of spherulites with some blebs of glass; 7.6-cm piece of spherulites with less glass than previous piece; 2.5-cm piece consisting of spherulites only.</p> <p>119-169 cm: Only 18 cm of core recovered from this section; bottom of melt zone is reached; sample consists of glass and oxidized saprolite; intermediate zone of porous, dark gray-to-black altered saprolite (partially melted and degassed).</p>
Core H3:	<p>Located within square array of electrodes 66 cm from SE electrode and 65 cm from SW electrode. Top of melt was at a depth of 76 cm. Total depth of hole was 152 cm (total depth from ground surface of 228 cm).</p> <p>0-94 cm: Only \approx56 cm of core recovered; upper section consists of porous green glass; next section consists of dark green glass; some small (<0.5-cm-diam) spherulites present in this section; lower part of section has higher concentration of spherulites, and they increase in size (some >2 cm diameter).</p>

Table 8. (continued)

	94-132 cm: 30 cm of core recovered; mixture of glass and spherulites; bottom of this zone is close to basal contact with altered soil.
	132-152 cm: Limited recovery of core; mixture of broken pieces; porous, dark gray-to-black altered saprolite; pieces from bottom of section are oxidized, reddish-brown saprolite.
Core H4:	Located just outside a line between the SW and SE electrodes; 38 cm from SE electrode and 81 cm from SW electrode; 13 cm from line between SE and SW electrodes. Top of melt was at 91-cm depth. Total depth of hole was 104 cm (195-cm total depth from ground surface).
	0-33 cm: Recovered \approx 26 cm of core; 5 cm of porous green glass; 2 cm of spherulite zone; \approx 11 cm of pieces of dark green glass; and 8 cm of intact green glass.
	33-79 cm: Recovered 25 cm of core; virtually all green glass with only a few small spherulites.
	79-104 cm: Recovered most of core; 10 cm of glass; transition zone with altered saprolite and some spherulites; metallic iron blebs found at base of section.
Core H5:	Located within square array of electrodes; 32 cm from NE electrode, 112 cm from NW electrode; and 23 cm from centerline between NE-NW electrodes. Subsidence to top of cold cap was 74 cm. Total depth of hole was 150 cm (total depth from ground surface was 224 cm).
	0-53 cm: Recovered only porous crust material (\approx 20 cm).
	53-89 cm: No intact core; all broken pieces; mixture of spherulites and glass.
	89-150 cm: Recovered only \approx 15 cm of altered saprolite (both dark gray-to-black and reddish-brown oxidized material) below the melt zone.
Core H6:	Located just north of center between the NW and NE electrodes, 94 cm from NW electrode, 61 cm from NE electrode, and 30 cm north of line between NW and NE electrodes. Subsidence to top of melt was 79 cm; total depth of hole was 145 cm (224 cm from ground surface).
	0-99 cm: Poor core recovery, mostly broken pieces; \approx 15 cm of porous crust; pieces of glass grading into pieces of glass with more spherulites.

Table 8. (continued)

	99-145 cm: Poor recovery again; mostly broken pieces of glass and spherulites grading into apparently nearly unaltered saprolite (recovered little of altered saprolite zone).
Core H7:	Located near line between SE and NE electrodes, 155 cm from NW electrode, 66 cm from NE electrode, 132 cm from SW electrode, and 51 cm from SE electrode. Subsidence to top of melt was 99 cm. Total depth of hole was 114 cm (total depth from surface of 213 cm).
	0-114 cm: Only one segment of core was pulled; poor recovery of core. Approximately 4 cm of porous crust; pieces of glass and spherulites; and approximately 12 cm of the transition zone from the melt to the altered saprolite.

*See Fig. 38 for location map.

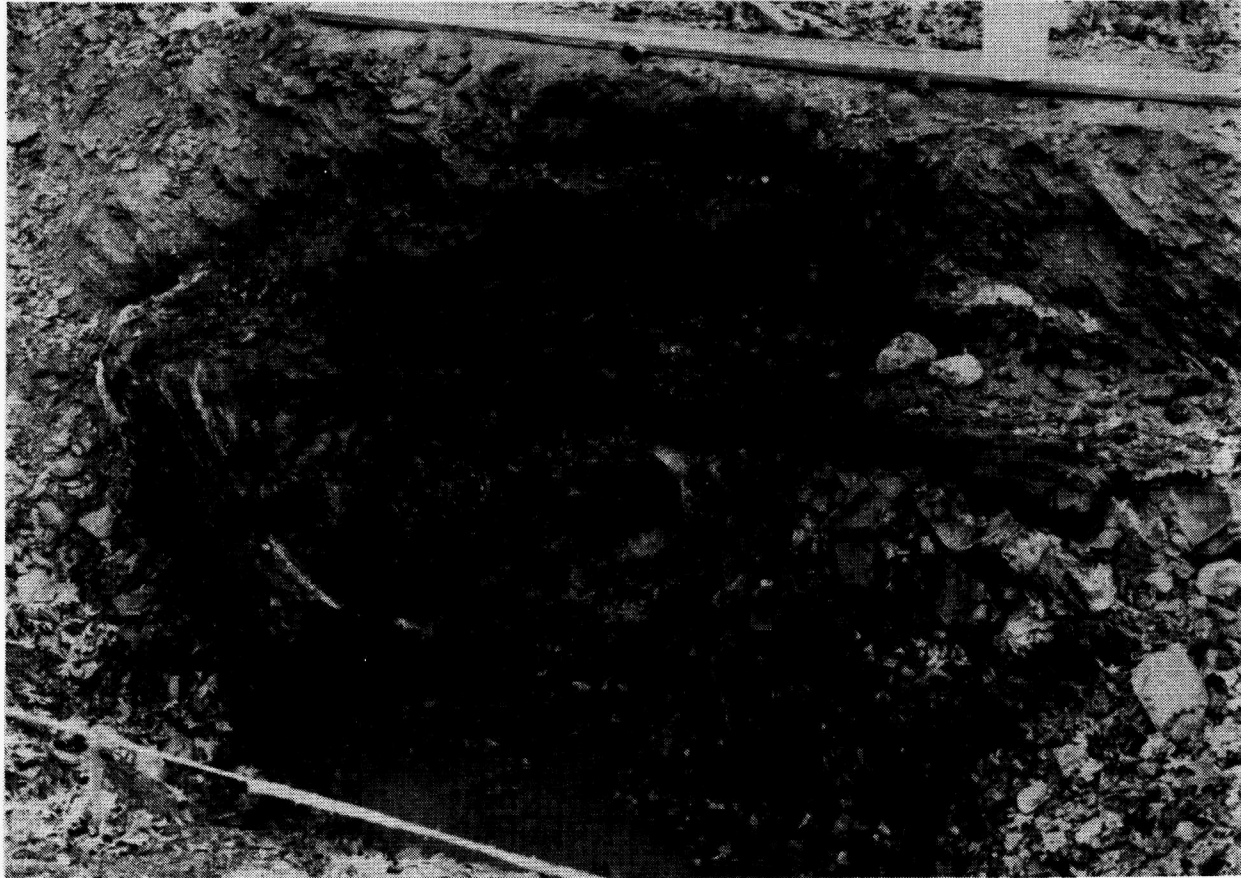


Fig. 39. View of the vitrified mass (looking east) after excavation following the ORNL ISV demonstration. Total length of the mass is approximately 5.3 m. Note concentration of crystalline material (light colored) in the central portion of the mass.

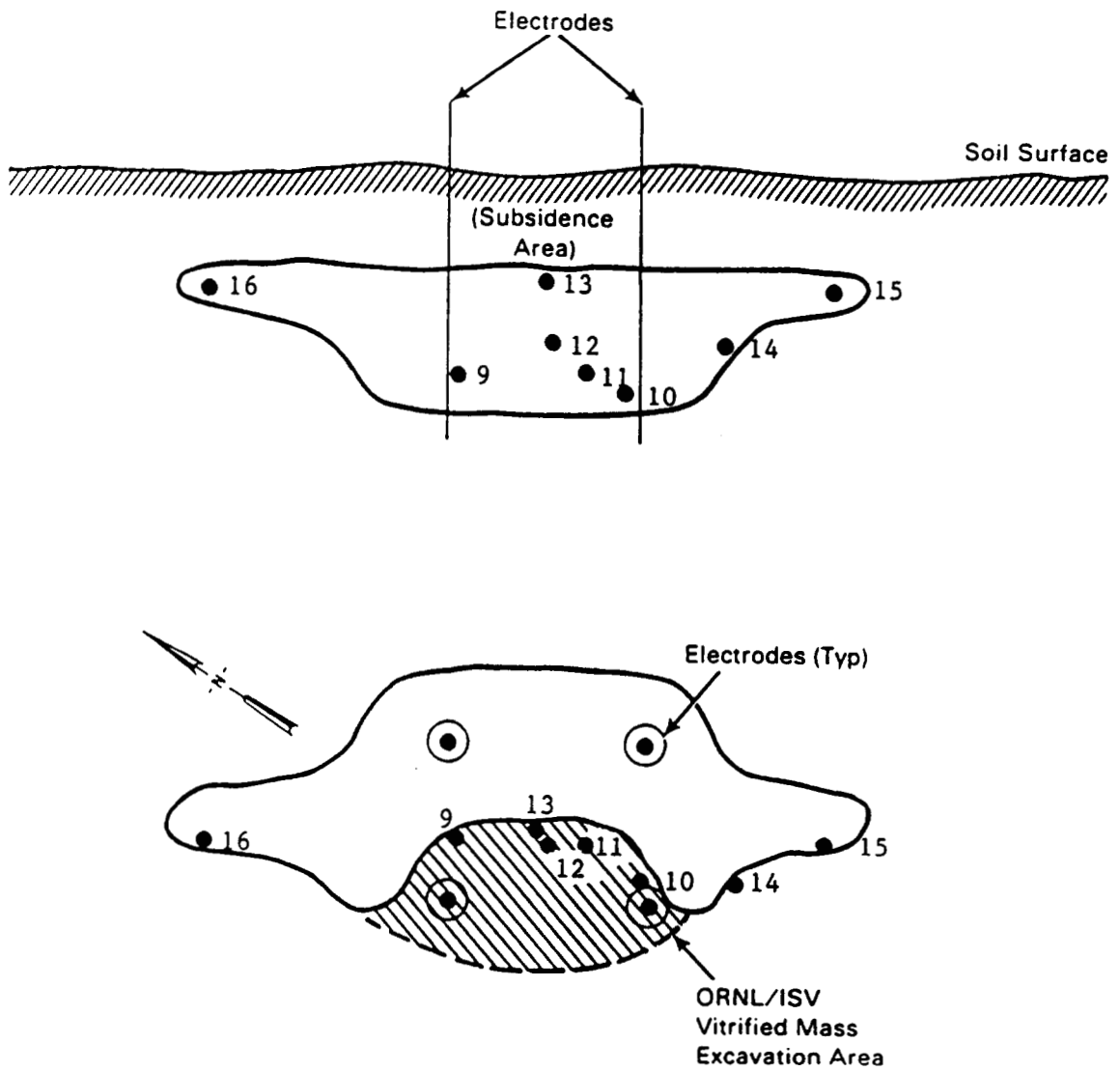


Fig. 40. Position of the grab samples taken after excavation of vitrified mass.

Table 9. Description of grab samples from ISV mass^a

-
- G9: Located 5 cm toward center of trench from line between NW and NE electrodes; 20 cm from base of melt zone. Massive gray rock consisting of coalesced spherulites.
- G1: White substance taken from thin (\approx 10-cm-thick) layer at southern end of ISV mass.
- G10: Sample taken from just inside the SW electrode. Mixture of green glass and spherulites.
- G11: Located 5 cm toward center of trench from line between SE and SW electrodes. Sample consists of mostly glass from within a larger zone that is mostly coalesced spherulites.
- G12: Sample pulled from central portion of melt zone approximately 30 cm from basal contact.
- G13: Dense glass taken from the central portion of the melt zone near the contact with the porous green crust.
- G14: Homogeneous glass sample taken approximately 30 cm south of the SW electrode; 30 cm below upper surface of the ISV mass.
- G15: Homogeneous glass sample taken from the southern end of the ISV mass.
- G16: Homogeneous glass sample taken from the northern end of the ISV mass.
- CC1: Upper cold cap material from within subsidence zone.
- CC2: Material from near-surface zone. Part of upper cold cap with a smooth, greenish coating.
- CC3: Material from the upper cold cap near the surface. Dull, pale green smooth textured substance.
- QG1: Quenched glass removed on steel bar used to manually probe the depth of the melt at the end of the run.
-

^aSee Fig. 40 for locations.

4. The upper zone of the ISV mass was a green, porous layer approximately 7 cm in thickness.
5. The soil around the vitrified mass altered to a reddish-brown color, indicating oxidation of the iron in the soil. The thickness of this layer was approximately 40 cm. The temperatures associated with this type of color alteration in laboratory-heated specimens are typically 200-300°C.
6. The mass was approximately 5.3 m in length and asymmetrically longer to the south. The depth of melting in the center of the trench was approximately 2.1 m; thus the target depth was reached, and all of the chemical addition should have been incorporated into the melt. The approximate width of the melt at the center of the trench position is 2.1 m. This value is an estimate as the entire block was not excavated. The length of the mass is consistent with the temperature data obtained with the thermocouples located north and south of the center of the trench.
7. The southern thermocouples 2.2 m from the center and at depths of 1.2 and 1.5 m burned out, indicating the melt reached this distance. The northern thermocouples 2.2 m from the center of the trench reached several hundred degrees (Celsius), indicating the melt approached this distance to the north. At 3.1 m from the center of the trench, several thermocouples in the southern portion of the trench reached temperatures $>100^{\circ}\text{C}$. This behavior indicated that the melt may have almost reached this distance to the south. The length of the melt would be predicted to be approximately 5.3 m long (assuming the southern thermocouples 3.1 m from the center of the trench were almost reached by the melt and that the melt approached the 2.2 m distance to the north). Thus, the physical measurements and temperature data are consistent and illustrate that temperature monitors can be used to reliably estimate the extent and shape of melting (important when performing radioactive applications).

5.2 PHYSICAL DESCRIPTION OF ISV PRODUCT

Core recovery varied from core to core (see Table 8), and the characteristics varied from sample to sample. In general, however, the characteristics of the ISV mass in the central portion of the oblong mass can be described as follows. The upper 5-20 cm consists of a frothy, porous, green layer (Figs. 39 and 41). The porosity is from the rapid quenching of gases in this layer after power to the electrodes was discontinued. A layer of dark green glass occurs below the porous zone (Figs. 39 and 41). This layer was generally ≈ 25 cm thick. A mixture of glass and gray crystalline material is encountered below this layer (Fig. 39). This zone is approximately 75 cm thick and extends to the bottom of the mass. The amount of glass versus gray crystalline material varies considerably according to position relative to the center of the melt. The gray crystalline material varies from distinct single spherulites (Fig. 42) to more massive growths of coalesced spherulites. The spherulites range in size from < 0.1 cm up to ≈ 3 cm in diameter.

A thin layer (≈ 10 cm thick) of portlandite (Ca(OH)_2), confirmed by X-ray diffraction analysis, was found at the ends of the mass (Fig. 43). This material is rehydrated lime (CaO) formed through the calcination of the crushed limestone placed in the trench. The basal contact of the vitrified mass with the saprolite was quite distinct (Fig. 44). The transition from glass to altered saprolite (with original structure partially retained, but much darker in color and with degassing bubbles present) was only a few centimeters thick. A number of small (< 0.5 -cm-diameter) spherulites were found along this contact. Near the basal contact several blebs of metal were found. These blebs consist of either metallic iron (magnetic) or coalesced pools of thermocouple metal (nonmagnetic). Previous ISV experience (Buelt et al. 1987) suggests that the degassing of the system during processing results in an oxygen-poor melt that promotes the separation and formation of small immiscible melts of metallic nature. These metallic samples were found only in the central portion of the melt zone and generally near the contact with the saprolite. A zone of bright reddish-brown alteration is found around the entire mass and is generally ≈ 40 cm in thickness. The ends of the mass consist almost entirely of glassy material (Figs. 39 and 43) with few spherulites. However, along the contact with the saprolite and at the contact between the frothy porous layer and the glass are numerous small (< 0.5 -cm-diam) spherulites (Fig. 44).

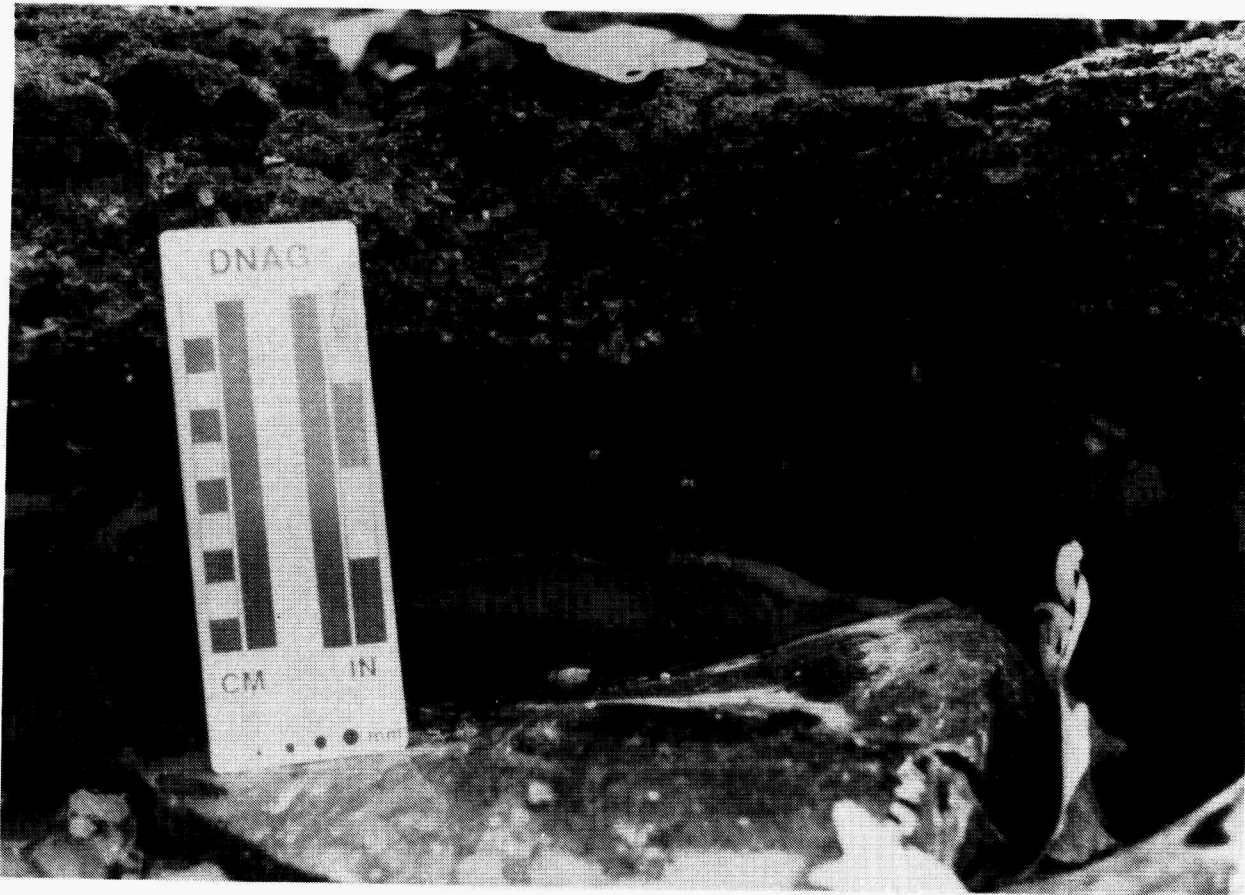


Fig. 41. Dark green porous (upper) and dense (lower) glass phases found in the vitrified mass in the ORNL ISV demonstration trench.

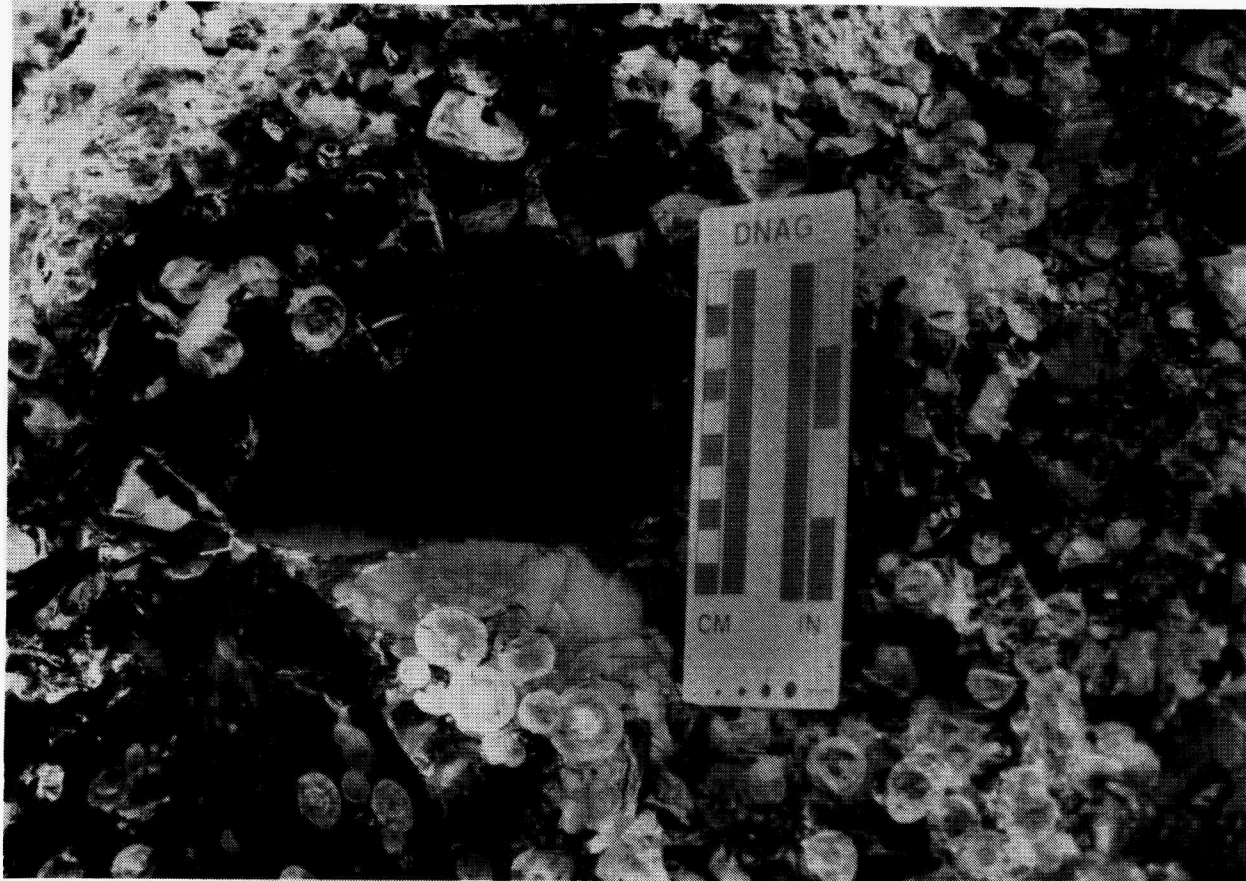


Fig. 42. Gas cavity and spherulites found in the vitrified mass from the ORNL ISV demonstration trench.

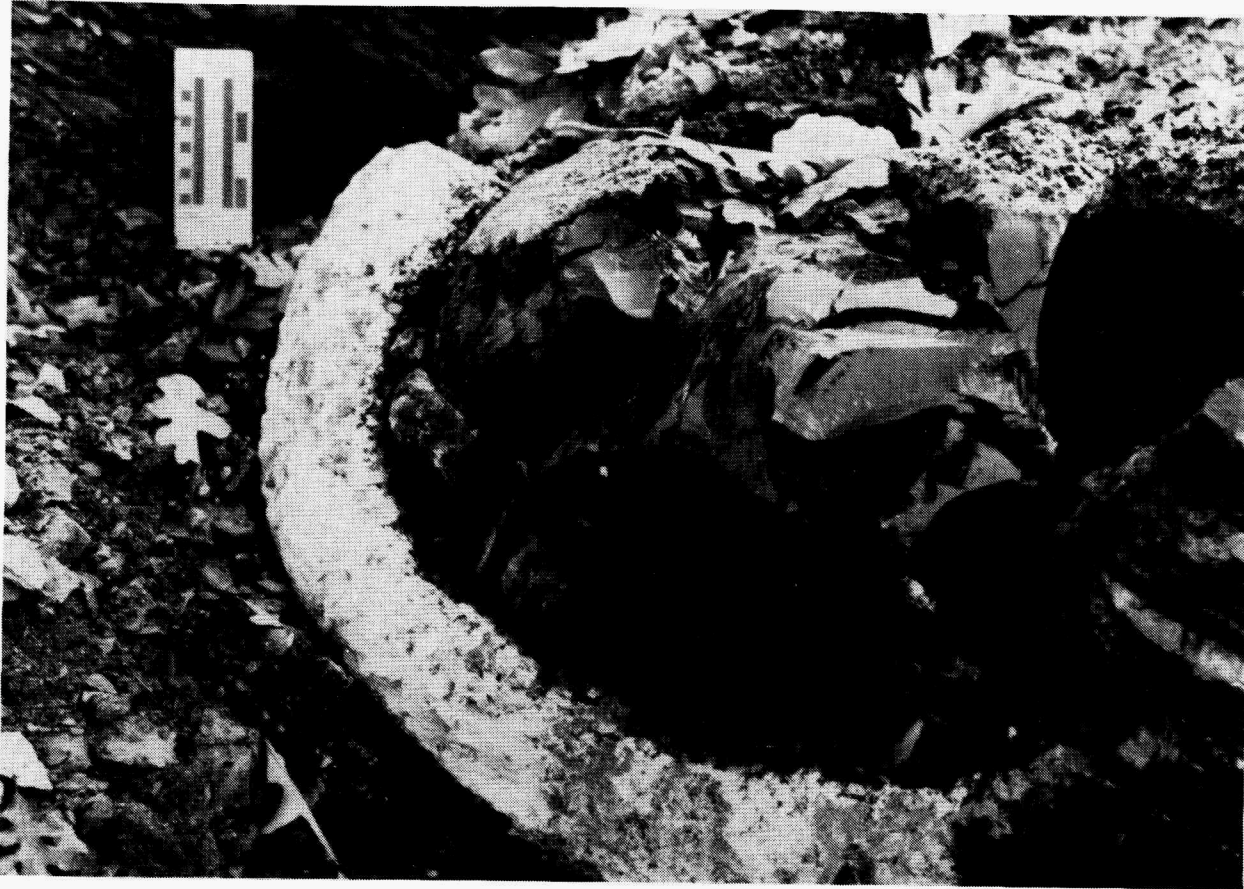


Fig. 43. Portlandite ($\text{Ca}(\text{OH})_2$) found at the contact between the vitrified material and the limestone cobble in the ORNL ISV demonstration trench.



Fig. 44. Contact zone between the saprolite and the vitrified material near the SW electrode in the ORNL ISV demonstration trench.

The spherulites are concentrated in the central portion of the ISV mass but also occur along the entire basal contact and near the contact with the porous zone at the top. This relationship suggests that both relatively slow cooling and a source of nucleation sites are important to their formation. Spherulites are a crystallization feature (Nockolds et al. 1978; Jackson 1970) commonly found in siliceous lavas and siliceous furnace slags. The texture usually results from the crystallization of acicular crystals in a radial pattern and generally indicates a moderate degree of undercooling and a large growth rate. Additional details on the micromorphology and chemistry of the glass and spherulites can be found in Sect. 5.4.

5.3 BULK CHEMICAL COMPOSITION

Samples of ISV material from the cores and grab samples were obtained for whole-rock chemical analysis (Table 10). In addition, samples of the original soil/saprolite and crushed limestone were analyzed. The samples were analyzed with several techniques: (1) digestion and/or fusion with subsequent analysis of solutions with inductively coupled plasma spectroscopy (ICP) for most elements and atomic absorption spectrophotometry (AA) for K, Cs, and Sr (EPA method 200.7); (2) X-ray fluorescence (XRF) analyses of powdered samples; and (3) electron microprobe (EMP) analyses of selected thin sections for bulk chemistry. Some systematic errors occurred in the results of the silica analyses from the original ICP analyses. Analyses of reference U.S. Geological Survey (USGS) rock specimens, submitted with the ISV product samples, yielded SiO₂ compositions that were a minimum of 12 wt % too high. All other elements exhibited better agreement between analyzed and reference compositions. Therefore, additional samples were fused with NaOH and the silica analyses rerun using the molybdate-blue spectrophotometric technique (ASA 1982). Tables 11-22 list the results of the various analyses.

As a control on the accuracy of the Cs and Sr analyses of rock, glass and soil digests, simulated digests were prepared and incremental additions of Cs and Sr were made to cover the range of concentrations encountered in the rock and glass samples. The synthetic digest solution contained the following chemicals (per liter): AlCl₃·6H₂O

Table 10. Samples from ISV cores and grab samples selected for bulk chemical analysis. H# designates core

Sample #	Description
H2-1	Dense, gray rock (spherulites) from 0-58 cm (bottom section).
H2-2	Dense, gray rock (spherulites) from 58-91 cm (top section).
H2-3	Dense, gray rock (spherulites) from 58-91 cm (middle section).
H2-4	Dense, gray rock (spherulites) from 58-91 cm (bottom section).
H2-5	Dense, gray rock (spherulites) from 91-119 cm (top section).
H2-6	Dense, gray rock (spherulites) from 91-119 cm (bottom section).
H2-7	Dark, altered soil from 119-169 cm (top section).
H2-8	Oxidized soil from 119-169 cm (bottom section).
H3-1	Porous crust from top of core.
H3-2	Glass from 0-94 cm (upper middle section).
H3-3	Massive gray rock (spherulites) from 0-94 cm (bottom section).
H3-4	Glass from 94-132 cm (middle section) (lots of spherulites in this section also, but none were included in sample for analysis).
H3-5	Dark, gray, altered soil from 132-152 cm (top section).
H4-1	Porous crust from top of core.
H4-2	Gray rock (spherulites) layer near top of core in contact with some glass.
H4-3	Glass from 0-33 cm.
H4-4	Glass from 79-104 cm (top section).
H4-5	Mixture of glass and spherulites near soil contact from 79-104 cm (middle).
H4-6	Dark, altered soil just below glass.
H5-1	Porous crust from top of core.
H5-2	Glass from 0-53 cm (top section).
H5-3	Glass and gray rock (spherulites) from 0-53 cm (bottom section).
H5-4	Glass from 53-89 cm.
H5-5	Dark, altered soil with some gray rock (spherulites) from 89-150 cm (middle section).
H5-6	Soil zone from 89-150 cm (bottom section).
H6-1	Porous crust from top of core.
H6-2	Glass from 0-99 cm (middle section).
H6-3	Near-natural soil from 99-145 cm (bottom section).
H7-1	Glass fragments from middle of core.
H7-2	Gray rock (spherulites) from middle of core.
H7-3	Oxidized soil from bottom of core.
H7-4	Dark, altered rock from bottom of core.
H7-5	Apparent melt-soil contact zone.
CC1	Sample of upper cold cap with many tiny gas vesicles.
CC2	Near-surface cold cap material with dull, greenish coating.
CC3	Dull, greenish-gray cold cap material.
QG1	Quenched glass from melt (material stuck on the end of the steel rod used to manually probe the depth of melting).

Table 11. Bulk composition of ISV samples

Oxide	230 ^a	231 ^b	232 ^c	233 ^d	Soil ^e	Limestone ^f
SiO ₂	51.8	51.5	52.0	52.4	63.1	2.95
Al ₂ O ₃	12.8	13.1	13.2	13.2	18.3	0.97
TiO ₂	0.58	0.60	0.60	0.60	0.83	--
Fe ₂ O ₃	4.30	4.41	4.46	4.52	6.32	1.37
MgO	2.02	2.15	2.16	2.16	1.83	6.8
MnO	0.11	0.11	0.11	0.12	0.10	0.32
CaO	17.2	18.6	18.7	18.7	3.09	87.3
SrO	1.30	1.40	1.40	1.39	0.13	0.05
Na ₂ O	1.50	1.38	1.47	1.74	0.77	0.65
K ₂ O	2.36	2.66	2.34	2.86	2.7	--
Cs ₂ O	0.33	0.34	0.34	0.37	--	--
Total	94.30	96.25	96.78	98.06	97.17	100.41

^aPorous crust from core H3.

^bGlass from core H4, top section of 33- to 79-cm interval.

^cGlass with $\approx 5\%$ spherulites from core H3, upper-middle portion of 0- to 94-cm interval.

^dSpherulites from core H3, bottom section of 0- to 94-cm interval.

^eSoil/saprolite from trench construction. Samples heat treated (1000°C for 24 h) prior to analysis so that the composition does not include CO₂ or water content.

^fLimestone from trench construction. Samples were heat treated (1000°C for 24 h) prior to analysis so that the composition does not include CO₂ or water content.

Source: J. G. Carter, S. S. Koegler, and S. O. Bates, Process Performance of the Pilot-Scale In Situ Vitrification of a Simulated Waste Disposal Site at the Oak Ridge National Laboratory, NL-6530, Pacific Northwest Laboratory, Richland, Washington, 1988.

Table 12. Bulk chemical composition of crushed limestone and soil from ISV trench^a

Oxide	Limestone	Soil 1	Soil 2	Soil 3	Soil 4
SiO ₂	5.41	54.45	54.45	54.45	54.45
Al ₂ O ₃	1.59	16.25	18.51	17.76	15.30
TiO ₂	0.06	0.80	0.82	0.75	0.70
Fe ₂ O ₃	0.70	6.43	7.01	6.58	6.43
MgO	3.65	1.54	1.82	1.66	1.49
MnO	0.02	0.13	0.10	0.10	0.09
CaO	50.37	4.20	2.10	2.10	3.22
SrO	0.06	0.02	0.01	0.01	0.01
Na ₂ O	0.04	0.92	0.89	1.10	1.13
K ₂ O	1.02	3.96	4.14	3.88	3.54
P ₂ O ₅	0.07	0.21	0.18	0.21	0.20
Cs ₂ O	0.00	0.00	0.00	0.00	0.00
CO ₂ ^b	40.06	--	--	--	--
H ₂ O ^c	--	5.55	5.55	5.55	5.55
Total	103.05	94.46	95.58	94.14	92.12

^aData from ORNL Analytical Chemistry Division. Samples were dried at 100°C for several hours prior to analysis. All values from ICP analyses of digested samples except for Na, Cs, Sr, and K, which are from AA analyses, and Si, which is from molybdate-blue method.

^bWeight loss at 1000°C for 24 h.

^cWeight loss at 1000°C for 24 h (average of two samples).

Table 13. Bulk chemical composition of soil (duplicate and replicate analyses) from ORNL ISV demonstration trench^a

Oxide	1A ^b	1B ^b	1A ^c	1B ^c	SEC ^d	Average
SiO ₂	58.79	59.26	55.46	55.85	0.92	57.34
Al ₂ O ₃	17.96	18.04	18.62	18.76	0.52	18.35
TiO ₂	0.81	0.80	0.81	0.80	0.06	0.81
Fe ₂ O ₃	6.19	6.20	6.24	6.27	0.20	6.23
MgO	1.79	1.77	1.89	1.88	0.40	1.83
MnO	0.08	0.08	0.09	0.09	0.02	0.09
CaO	2.37	2.37	2.69	2.70	0.14	2.53
SrO	0.01	0.01	0.01	0.01	0.003	0.01
Na ₂ O	1.02	1.22	0.99	0.89	0.46	1.03
K ₂ O	3.67	3.67	3.85	3.83	0.04	3.76
P ₂ O ₅	0.24	0.24	0.2	0.24	0.04	0.24
Cs ₂ O	--	--	--	--	--	--
H ₂ O ^e	1.81	2.40	1.81	2.40	--	2.11
H ₂ O ^f	5.51	5.55	5.51	5.55	--	5.53
Total	100.25	101.61	98.19	99.27	--	99.86

^aX-ray fluorescence analyses from O. C. Kopp, the University of Tennessee.

Weight loss data from G. K. Jacobs.

^bXRF analysis run May 19, 1988.

^cXRF analysis run May 20, 1988.

^dSEC = standard error of calibration (2σ).

^eWeight loss at 105°C for 1 h.

^fWeight loss at 1000°C for 24 h.

Table 14. Bulk chemical composition of crushed limestone (duplicate and replicate analyses) from ORNL ISV demonstration trench^a

Oxide	1A ^b	1B ^b	1A ^c	1B ^c	SEC ^d	Average
SiO ₂	4.35	4.24	4.21	4.30	0.44	4.28
Al ₂ O ₃	--	--	--	--	0.32	--
TiO ₂	0.08	0.08	0.08	0.08	0.07	0.08
Fe ₂ O ₃	0.74	0.71	0.70	0.72	0.10	0.72
MgO	3.11	3.13	3.10	3.17	0.32	3.13
MnO	0.03	0.03	0.03	0.03	0.03	0.03
CaO	46.32	45.56	45.09	45.72	0.60	45.67
SrO	0.04	0.04	0.04	0.04	0.003	0.04
Na ₂ O	0.08	0.06	0.05	0.05	0.06	0.06
K ₂ O	1.07	1.02	1.01	1.04	0.08	1.04
P ₂ O ₅	0.06	0.07	0.06	0.05	0.04	0.06
Cs ₂ O	--	--	--	--	--	--
CO ₂ ^e	40.06	40.33	40.72	40.77	--	40.47
Total	95.94	95.27	95.09	95.97	--	95.58

^aX-ray fluorescence analyses from O. C. Kopp, the University of Tennessee.

Weight loss data from G. K. Jacobs.

^bXRF analysis run May 19, 1988.

^cXRF analysis run May 20, 1988.

^dSEC = standard error of calibration (2σ).

^eWeight loss at 1200°C for 24 h.

Table 15. Bulk chemical composition of ISV core samples from ORNL ISV demonstration trench^a

Oxide	CC1	CC2	CC3	H2-1	H2-2	H2-3	H2-4
SiO ₂	50.90	53.90	50.35	52.47	50.38	50.74	52.15
Al ₂ O ₃	13.22	13.79	12.66	13.22	13.60	13.41	13.41
TiO ₂	0.45	0.47	0.43	0.53	0.55	0.55	0.55
Fe ₂ O ₃	4.29	4.58	4.15	4.58	4.86	4.72	4.86
MgO	2.16	2.32	2.49	2.16	2.16	2.16	2.16
MnO	0.14	0.14	0.14	0.12	0.13	0.12	0.13
CaO	19.59	20.99	25.19	18.19	18.19	19.59	19.59
SrO	1.49	0.14	0.90	1.53	1.47	1.51	1.47
Na ₂ O	1.12	1.23	1.06	1.32	1.35	1.35	1.48
K ₂ O	2.58	2.81	2.64	2.73	2.67	2.75	2.66
P ₂ O ₅	0.18	0.21	0.19	0.16	0.16	0.17	0.17
Cs ₂ O	0.41	0.01	0.23	0.37	0.38	0.39	0.39
Total	96.53	100.57	100.43	97.38	95.90	97.46	99.01

Oxide	H2-5	H2-6	H2-7	H2-8	H3-1	H3-2	H3-3
SiO ₂	56.18	52.90	57.14	64.33	52.84	52.83	50.02
Al ₂ O ₃	13.41	13.98	15.49	10.01	13.41	13.41	13.41
TiO ₂	0.55	0.57	0.68	0.23	0.55	0.55	0.55
Fe ₂ O ₃	4.86	5.15	6.72	2.72	4.58	4.58	4.86
MgO	2.16	2.32	1.48	0.55	2.16	2.16	2.16
MnO	0.12	0.13	0.12	0.15	0.12	0.13	0.13
CaO	19.59	20.99	3.50	9.79	18.19	19.59	18.19
SrO	1.47	1.55	0.02	0.02	1.43	1.48	1.45
Na ₂ O	1.48	1.48	1.62	3.24	1.35	1.48	1.35
K ₂ O	2.69	2.82	3.04	1.06	2.71	2.67	2.72
P ₂ O ₅	0.17	0.18	0.30	0.30	0.18	0.18	0.17
Cs ₂ O	0.37	0.41	0.00	0.06	0.48	0.39	0.37
Total	103.05	102.47	90.09	92.46	97.99	99.44	95.39

Oxide	H3-4	H3-5	H4-1	H4-2	H4-3	H4-4	H4-5
SiO ₂	54.20	48.94	52.36	53.42	48.86	46.10	52.22
Al ₂ O ₃	13.60	14.17	13.60	13.60	13.79	13.98	14.73
TiO ₂	0.55	0.55	0.55	0.55	0.57	0.57	0.62
Fe ₂ O ₃	4.58	4.86	4.58	4.58	4.58	4.58	4.86
MgO	2.32	1.51	2.16	2.16	2.16	2.32	2.16
MnO	0.13	0.17	0.13	0.13	0.13	0.13	0.12
CaO	19.59	13.99	18.19	18.19	18.19	18.19	16.79
SrO	1.45	0.02	1.40	1.47	1.50	1.51	0.04
Na ₂ O	1.48	2.56	1.48	1.48	1.48	1.48	1.35
K ₂ O	2.57	2.16	2.82	2.77	2.69	2.67	2.57
P ₂ O ₅	0.18	0.25	0.17	0.17	0.18	0.18	0.17
Cs ₂ O	0.37	0.20	0.40	0.39	0.39	0.38	0.01
Total	101.02	89.38	97.83	98.90	94.50	92.09	95.65

Table 15. (continued)

Oxide	H4-6	H5-1	H5-2	H5-3	H5-4	H5-5	H5-6
SiO ₂	84.49	48.15	51.08	52.27	45.59	58.38	64.11
Al ₂ O ₃	14.55	14.17	13.60	13.60	13.98	18.51	16.25
TiO ₂	0.60	0.57	0.52	0.52	0.53	0.65	0.48
Fe ₂ O ₃	6.29	4.86	4.43	4.43	4.43	6.43	5.43
MgO	1.66	2.16	2.16	2.16	2.16	1.82	1.38
MnO	0.13	0.13	0.14	0.14	0.14	0.06	0.15
CaO	6.72	18.19	18.19	19.59	19.59	5.04	4.90
SrO	0.01	1.40	1.49	1.47	1.50	0.01	0.01
Na ₂ O	1.89	1.62	1.24	1.24	1.25	1.25	1.75
K ₂ O	3.01	2.75	2.71	2.65	2.71	3.85	3.01
P ₂ O ₅	0.23	0.18	0.18	0.18	0.18	0.19	0.21
Cs ₂ O	0.00	0.39	0.39	0.40	0.43	0.02	0.00
Total	119.57	94.55	96.13	98.64	92.50	96.22	97.69

Oxide	H6-1	H6-2	H6-3	H7-1	H7-2	H7-3	H7-4
SiO ₂	51.32	39.41	53.12	50.42	48.96	61.62	54.78
Al ₂ O ₃	13.60	13.60	11.33	13.41	13.41	11.52	14.92
TiO ₂	0.52	0.53	0.32	0.52	0.47	0.30	0.47
Fe ₂ O ₃	4.43	4.43	4.43	4.29	4.72	6.72	5.15
MgO	2.16	2.16	1.16	2.16	2.16	1.49	1.46
MnO	0.13	0.14	0.19	0.13	0.15	0.17	0.18
CaO	19.59	19.59	12.59	18.19	19.59	5.32	11.19
SrO	1.49	1.45	0.10	1.49	1.48	0.01	0.03
Na ₂ O	1.31	1.29	1.89	1.21	1.20	1.62	2.02
K ₂ O	2.71	2.54	1.58	2.43	2.65	1.20	2.45
P ₂ O ₅	0.16	0.18	0.32	0.17	0.19	0.17	0.34
Cs ₂ O	0.55	0.42	0.02	0.38	0.38	0.00	0.18
Total	97.96	85.74	87.06	94.80	95.36	90.15	93.17

Oxide	H7-5	QG1
SiO ₂	52.70	52.97
Al ₂ O ₃	15.49	13.03
TiO ₂	0.53	0.43
Fe ₂ O ₃	5.00	4.29
MgO	2.16	1.99
MnO	0.08	0.14
CaO	13.85	16.79
SrO	1.01	1.29
Na ₂ O	1.04	1.25
K ₂ O	3.17	2.79
P ₂ O ₅	0.19	0.19
Cs ₂ O	0.29	0.42
Total	95.51	95.61

^aData from the ORNL Analytical Chemistry Division. All values from ICP analyses of digested samples except for Cs, Sr, and K, which are from AA analyses and Si, which is from the molybdate-blue method. Low totals on altered saprolite samples may be partially attributable to lack of data on CO₂ and H₂O weight loss.

Table 16. Bulk chemical composition of ISV glass (note duplicate analyses)^a

Oxide	H3-4	H3-4	H4-3	H4-3	H4-4	H4-4	Average ^b	SEC ^c
SiO ₂	56.87	57.10	57.60	57.50	57.71	57.98	57.45(0.43)	0.74
Al ₂ O ₃	13.68	13.70	13.80	13.75	13.56	13.71	13.70(0.08)	0.40
TiO ₂	0.77	0.78	0.80	0.77	0.76	0.78	0.78(0.01)	0.07
Fe ₂ O ₃	4.58	4.62	4.54	4.56	4.53	4.56	4.57(0.03)	0.46
MgO	2.74	2.72	2.79	2.78	2.75	2.73	2.75(0.03)	0.40
MnO	0.09	0.09	0.09	0.09	0.09	0.09	0.09(0.00)	0.02
CaO	17.15	17.20	16.83	16.84	16.66	16.72	16.90(0.22)	0.20
SrO	0.96	0.98	0.98	0.99	0.97	0.97	0.97(0.01)	0.01
Na ₂ O	1.63	1.32	1.50	1.43	1.37	1.44	1.45(0.11)	0.54
K ₂ O	1.99	2.00	2.04	2.03	2.02	2.02	2.02(0.02)	0.12
P ₂ O ₅	0.31	0.33	0.31	0.32	0.31	0.30	0.31(0.01)	0.06
Cs ₂ O ^d	--	--	--	--	--	--	--	--
Total	100.77	100.84	101.28	101.06	100.73	101.30	100.99	--

^aX-ray Fluorescence analyses from O. C. Kopp, the University of Tennessee.

^bValues in parentheses are standard deviations from mean.

^cSEC = standard error of calibration (2σ).

^dNo cesium standard was available for the XRF analyses, but a small peak was identified as present at the appropriate energy for cesium.

Table 17. Bulk chemical composition of ISV spherulites (note duplicate analyses)^a

Oxide	H2-1	H2-1	H2-6	H2-6	H3-3	H3-3	Average ^b	SEC ^c
SiO ₂	57.64	57.61	57.55	57.47	57.48	57.60	57.56 (0.07)	0.74
Al ₂ O ₃	14.35	14.25	14.04	14.06	14.25	14.26	14.20 (0.12)	0.40
TiO ₂	0.79	0.81	0.75	0.75	0.78	0.76	0.77 (0.02)	0.07
Fe ₂ O ₃	4.76	4.75	4.81	4.79	4.80	4.84	4.79 (0.03)	0.46
MgO	2.75	2.74	2.68	2.74	2.63	2.67	2.70 (0.05)	0.40
MnO	0.10	0.09	0.09	0.09	0.09	0.09	0.09 (0.00)	0.02
CaO	16.84	16.83	16.82	16.80	16.98	16.99	16.88 (0.09)	0.20
SrO	0.99	1.00	0.99	0.99	0.99	1.00	0.99 (0.01)	0.01
Na ₂ O	1.92	1.76	1.63	1.75	1.74	1.64	1.74 (0.10)	0.54
K ₂ O	2.03	2.03	2.03	2.03	2.02	2.03	2.03 (0.00)	0.12
P ₂ O ₅	0.33	0.31	0.32	0.33	0.31	0.32	0.32 (0.01)	0.06
Cs ₂ O ^d	--	--	--	--	--	--	--	--
Total	102.50	102.18	101.71	101.80	102.07	102.20	102.07	--

^aX-ray fluorescence analyses from O. C. Kopp, The University of Tennessee.

^bValues in parentheses are standard deviations from mean.

^cSEC = standard error of calibration (2σ).

^dNo cesium standard was available for the XRF analyses, but a small peak was identified as present at the appropriate energy for cesium.

Table 18. Bulk chemical composition of ISV glass sample QG1
(note duplicate analyses)^a

Oxide	QG1	QG1	SEC ^b
SiO ₂	60.20	59.95	0.74
Al ₂ O ₃	13.39	13.32	0.40
TiO ₂	0.74	0.76	0.07
Fe ₂ O ₃	4.51	4.53	0.46
MgO	2.61	2.54	0.40
MnO	0.09	0.09	0.02
CaO	15.07	14.95	0.20
SrO	0.93	0.91	0.01
Na ₂ O	1.54	1.47	0.54
K ₂ O	2.19	2.19	0.12
P ₂ O ₅	0.33	0.29	0.06
Cs ₂ O ^c	--	--	--
Total	101.60	101.00	--

^aX-ray fluorescence analyses from O. C. Kopp, the University of Tennessee.

^bSEC = standard error of calibration (2σ).

^cNo cesium standard was available for the XRF analyses, but a small peak was identified as present at the appropriate energy for cesium.

Table 19. Bulk chemical composition of ISV spherulite in thin section sample H1-1^a

Oxide	Zone 1 [3] ^b	Zone 2 [9]	Zone 3 [8]	Zone 4 [7]	Zone 5 [7]	Zone 6 [9]	Average [43]
SiO ₂	54.5 (8) ^c	55.1 (4)	55.4 (5)	55.0 (5)	55.0 (2)	55.0 (3)	55.1 (3)
Al ₂ O ₃	13.4 (6)	14.0 (10)	14.2 (13)	13.7 (1)	13.4 (3)	13.2 (1)	13.7 (9)
TiO ₂	0.56 (7)	0.62 (4)	0.63 (5)	0.62 (3)	0.64 (5)	0.60 (2)	0.62 (4)
Fe ₂ O ₃ ^d	4.38 (16)	4.13 (40)	4.07 (44)	4.27 (9)	4.26 (16)	4.49 (13)	4.22 (31)
MgO	1.91 (3)	1.80 (23)	1.81 (33)	2.11 (3)	2.09 (5)	2.16 (2)	1.96 (24)
MnO	0.12 (3)	0.10 (3)	0.12 (3)	0.11 (4)	0.12 (2)	0.13 (2)	0.12 (2)
CaO	18.8 (9)	17.8 (10)	17.5 (12)	18.2 (3)	18.3 (6)	18.3 (1)	18.0 (8)
SrO	1.20 (4)	1.13 (10)	1.23 (13)	1.12 (6)	1.15 (5)	1.19 (3)	1.17 (12)
Na ₂ O	1.44 (2)	1.50 (9)	1.47 (13)	1.40 (3)	1.39 (2)	1.38 (2)	1.44 (9)
K ₂ O	2.73 (36)	2.97 (22)	3.07 (35)	2.80 (7)	2.87 (14)	2.80 (6)	2.91 (22)
P ₂ O ₅	0.17 (5)	0.15 (3)	0.19 (2)	0.17 (2)	0.18 (2)	0.19 (1)	0.17 (2)
Cs ₂ O	0.52 (23)	0.49 (6)	0.27 (4)	0.45 (11)	0.38 (11)	0.38 (8)	0.40 (13)
Total	99.73	99.79	99.96	99.95	99.78	99.82	99.81

^aElectron microprobe analyses by L. A. Taylor, H. Y. McSween, and Y. Jin of The University of Tennessee. The six zones were established from the center of the spherulite to the margin in approximately evenly spaced steps (2 mm wide) from one to six. The total distance from the center to margin is approximately 1.25 cm. Analyses were performed by using a defocused beam with a diameter of 50 μ m.

^bValues in [] denote number of analyses used in the average.

^cValues in () represent 1 σ standard deviation of replicate analyses in terms of the least units cited.

^dAll iron was determined as Fe and is reported as Fe₂O₃.

Table 20. Comparison of the average chemical compositions of ISV spherulites and glass^a

	Spherulites		Glass		
	H1-1 ^b [43] ^e	H3-8 ^c [5]	H3-8 ^d [1]	H3-8 ^e [8]	H7-7 ^f [3]
SiO ₂	55.1 (3) ^h	55.0 (1)	54.9	54.9 (1)	54.9 (1)
Al ₂ O ₃	13.7 (9)	13.5 (2)	13.3	13.1 (4)	13.2 (1)
TiO ₂	0.62 (4)	0.61 (3)	0.61	0.61 (5)	0.61 (3)
Fe ₂ O ₃ ⁱ	4.22 (31)	4.36 (17)	4.41	4.38 (2)	4.55 (5)
MgO	1.96 (24)	2.07 (10)	2.17	2.17 (1)	2.17 (2)
MnO	0.12 (2)	0.11 (3)	0.09	0.11 (2)	--
CaO	18.0 (8)	18.0 (2)	18.2	18.2 (5)	18.1 (1)
SrO	1.17 (12)	0.86 (3)	0.82	0.86 (1)	1.17 (2)
Na ₂ O	1.44 (9)	1.41 (6)	1.44	1.27 (2)	1.29 (2)
K ₂ O	2.91 (22)	2.86 (7)	2.80	2.77 (6)	2.85 (5)
P ₂ O ₅	0.17 (2)	0.18 (5)	0.14	0.17 (4)	0.20 (6)
Cs ₂ O	0.40 (13)	--	--	0.41 (15)	0.40 (12)
Total	99.81	98.85	98.86	98.93	99.10

^aElectron microprobe analyses by L. A. Taylor, H. Y. McSween, and Y. Jin of the University of Tennessee. Analyses performed using a defocused beam with a diameter of 50 μ m.

^bAverage from six zones analyzed in sample H1-1 (see Table 19).

^cAnalyses taken from center to margin of spherulite.

^dRepresentative analysis of glass at contact with spherulite.

^eGlass near contact of two spherulites.

^fTypical glass in thin section.

^gValues in [] denote number of analyses used in the average.

^hValues in () represent 1 σ standard deviation of replicate analyses in terms of the least units cited.

ⁱAll iron was determined as Fe and is reported as Fe₂O₃.

Table 21. Average chemical composition of the ISV product

Oxide	EMP analysis ^a	ICP/AA analysis ^b	XRF analysis ^c
SiO ₂	55.1 (0.2) ^d	50.6 (3.6)	57.5 (0.3)
Al ₂ O ₃	13.6 (0.7)	13.6 (0.2)	13.9 (0.3)
TiO ₂	0.62 (0.04)	0.54 (0.02)	0.78 (0.02)
Fe ₂ O ₃	4.27 (0.3)	4.64 (0.2)	4.68 (0.12)
MgO	2.01 (0.2)	2.18 (0.06)	2.73 (0.05)
MnO	0.12 (0.02)	0.13 (0.01)	0.09 (0.00)
CaO	18.04 (0.7)	18.95 (0.83)	16.89 (0.16)
SrO	1.10 (0.09)	1.48 (0.04)	0.98 (0.01)
Na ₂ O	1.41 (0.07)	1.38 (0.12)	1.59 (0.18)
K ₂ O	2.88 (0.18)	2.69 (0.09)	2.02 (0.01)
P ₂ O ₅	0.17 (0.03)	0.17 (0.01)	0.32 (0.01)
Cs ₂ O	0.38 (0.13)	0.40 (0.04)	--
Total	99.70	96.76	101.48

^aWeighted average of analyses in Table 20.

^bAverage of glass and spherulite analyses of Table 15. SiO₂ via molybdate-blue method; K, Cs, and Sr via AA, others via ICP.

^cAverage of glass and spherulite analyses from Table 16 and 17.

^dValues in () are standard deviations.

Table 22. Average chemical compositions of the two major phases identified in spherulite H1-1^a

	Wollastonite-like phase			Feldspar-like phase		
	Zone -3 ^b [8] ^d	Zone +3 ^c [7]	Zone -2 [6]	Zone -3 [8]	Zone +3 [5]	Zone -2 [8]
SiO ₂	51.0 (13) ^e	52.6 (10)	51.7 (7)	53.7 (19)	53.5 (19)	58.4 (56)
Al ₂ O ₃	2.60 (265)	1.58 (154)	3.65 (301)	26.1 (17)	26.4 (35)	22.5 (42)
TiO ₂	0.62 (50)	0.30 (21)	0.65 (51)	0.22 (15)	0.21 (18)	0.40 (27)
Fe ₂ O ₃ ^f	6.69 (204)	7.33 (118)	7.84 (143)	0.76 (21)	0.67 (18)	0.78 (24)
MgO	7.15 (341)	4.48 (63)	6.10 (233)	0.30 (9)	0.29 (5)	0.21 (14)
MnO	0.23 (10)	0.29 (4)	0.24 (12)	0.02 (1)	0.01 (1)	0.02 (3)
CaO	30.7 (60)	32.2 (27)	28.2 (533)	9.76 (136)	9.72 (180)	6.78 (24)
SrO	<0.03 (0)	<0.03 (0)	<0.03 (0)	2.75 (42)	3.02 (56)	2.13 (64)
Na ₂ O	0.12 (8)	0.12 (11)	0.35 (36)	2.60 (24)	2.55 (34)	2.06 (64)
K ₂ O	0.32 (19)	0.54 (49)	0.49 (14)	2.94 (14)	3.24 (361)	5.92 (37)
P ₂ O ₅	0.14 (13)	0.08 (7)	0.15 (13)	0.05 (5)	0.03 (3)	0.05 (9)
Cs ₂ O	<0.03 (0)	0.04 (4)	0.03 (4)	0.05 (5)	0.08 (14)	0.70 (62)
Total	99.57	99.56	99.40	99.25	99.72	99.95

^aElectron microprobe analyses by L. A. Taylor, H. Y. McSweeney, and Y. Jin of the University of Tennessee.

^bAverage of eight different crystals. Zone -3/+3 indicates that these two zones are the same but on opposite sides of the center of the spherulite.

^cAverage of seven analyses on a single crystal (50 by 70 μm in size).

^dValues in [] denote number of analyses used in the average.

^eValues in () represent 1 σ standard deviation of replicate analyses in terms of the least units cited.

^fAll iron was determined as Fe and is reported as Fe₂O₃.

(3.715 g), CaCl₂ (2.261 g), Fe(NH₄)₂SO₄·6H₂O (1.301 g), KCl (0.239 g), MgSO₄·7H₂O (2.553 g), MnO₂ (0.015 g), Na₂SiO₃·9H₂O (14.730 g), and TiO₂ (0.034 g) in 12% HNO₃ (Ultrex). Standard solutions of Cs₂CO₃ (>99.9% assay) and SrCO₃ (reagent grade) were prepared in 12% HNO₃, and dilutions into the synthetic rock digest were prepared in the range 2 to 45 and 7 to 165 mg/L for Cs and Sr, respectively. The solutions were then submitted for AA analyses of Cs and Sr. The regression of the analytical determination of Cs (Y) on the standard concentration (X), in milligrams per liter was $Y = 0.975X - 0.195$ ($r = 0.9999$, $n = 8$). A similar regression was calculated for Sr: $Y = 0.943X - 0.266$ ($r = 0.995$, $n = 8$). Neither regression slope was significantly different from 1.000, leading to the conclusion that the AA analyses for Cs and Sr are quite accurate both in 12% HNO₃ and in the acid containing rock, soil, or glass digests.

Analyses of the soil and limestone are listed in Tables 11-14. The low totals for the soil analyses in Table 12 indicate some problem (unidentified) with the analyses. The limestone analysis appears to be reliable. The analyses of the limestone via XRF (Table 14) have low totals. (The reason is unknown.) The XRF analyses for the soil samples are in excellent agreement (when calculated on a H₂O-free basis) with the values from Carter et al. (1988) in Table 11. In all subsequent calculations, the composition of the limestone is assumed to be that of Table 12, and the composition of the soil is assumed to be that of the average in Table 13. These analyses were chosen because of the good totals and consistency with the anhydrous values of Carter et al. (1988).

The concentrations of the major elements (especially CaO and SiO₂) in the ISV material varies depending on the analysis method (see Table 21). For a given method, however, the concentrations of the various constituents are fairly consistent. The variation among methods is not likely to be a result of sample heterogeneity (note consistency among samples in Table 15), but rather may be attributed to actual differences in the methods. For Cs₂O and SrO, important to the analysis of ISV performance, the results from the AA methods appear to be most reliable and consistent (and also compare favorably with analyses from Carter et al. 1988). The distribution of Cs and Sr was extremely uniform throughout all regions of the melt; a plot of Cs and Sr compositions in all samples of melted material from various cores and depths exhibited quite constant values (Fig. 45). Based on the better summation (99.70) of the EMP

Strontium and Cesium Concentrations in Samples of ORNL Vitrified Block

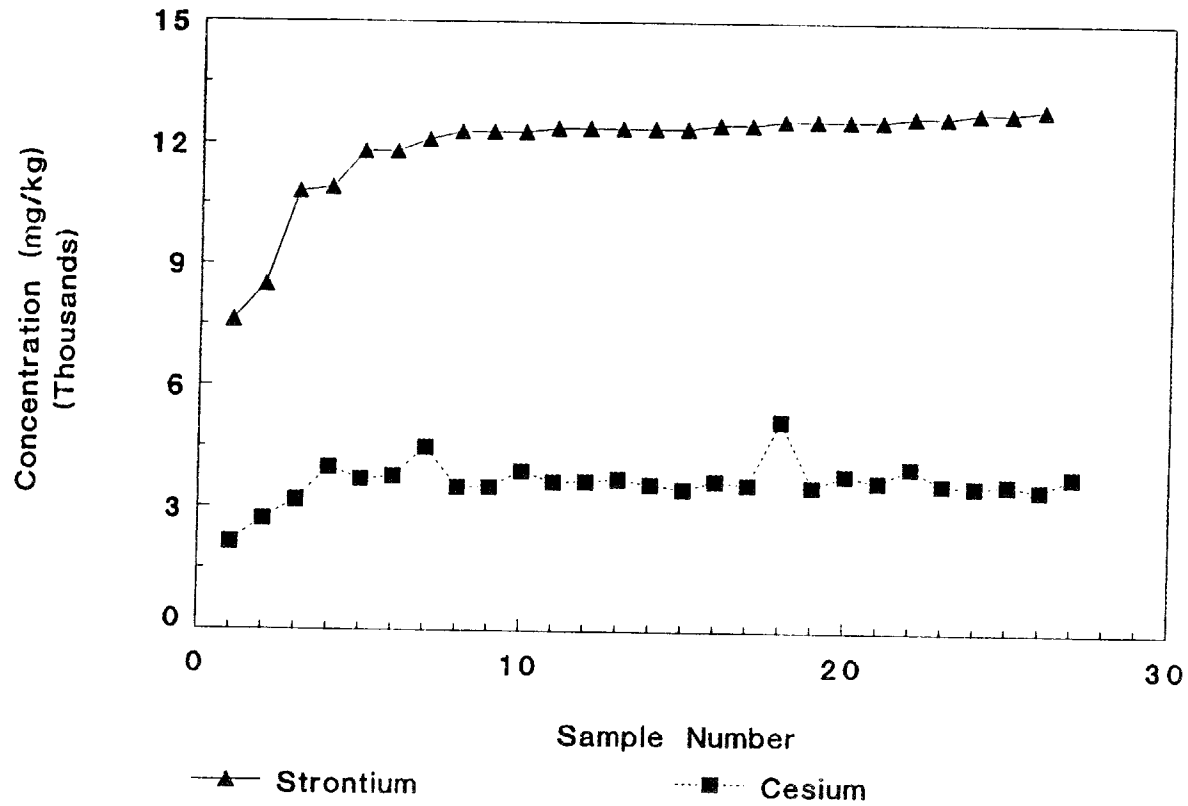


Fig. 45. Cesium and strontium composition of all vitrified samples from ORNL ISV demonstration trench.

results and the large standard deviation for the results of the molybdate-blue method, the SiO_2 values from the EMP method are considered best. The other elements generally are comparable between the EMP and ICP methods with the XRF results somewhat more inconsistent, although they are in good agreement when standard deviations are accounted for.

The data in Tables 12 and 15 indicate that the samples of the saprolite from the cores (e.g., samples H2-8, H5-6, and H7-3) did not contain Cs or Sr above background levels; supporting a conclusion that significant migration of these contaminants during processing did not occur. Some of the samples of the melt-saprolite transition zone (e.g., H3-5, H7-4, and H7-5) did contain slightly elevated levels of Cs and/or Sr; suggesting that some of the chemical addition may have washed into lower zones prior to melting (especially because the more soluble Cs is found in greater abundance than the Sr) or that a small amount of migration into this transition zone may have occurred during processing. Although the ISV trench was covered with plastic during the 2-month period between the placement of the chemicals in the trench and the start of the ISV run, some infiltration of water into the trench may have occurred from areas at the edge of the plastic.

Using the difference in major element composition between the soil and limestone, the ratio of limestone-to-soil consumed during the melting can be calculated (Table 23). The elements Ca, Al, Fe, and K are best suited for this analysis because of their consistent values and relative abundances in the phases. Silica was not used because of the uncertainty in the values for the soil and limestone. Using the average of the analyses in Table 21, an approximate ratio of 30 wt % limestone and 70 wt % soil is calculated. (Silica gives a value of approximately 6 wt % limestone.)

As discussed in Sect. 5.4, the ISV product consists of two macroscopic phases, the glass and the spherulites. The bulk composition of these two phases is essentially identical within the uncertainties of the various analytical methods (Tables 15-20). The data in Table 15 suggest that the ISV mass is quite homogeneous in composition. Little difference is found between analyses from various cores and depths within cores. In support of these data, Carter et al. (1988) surveyed several of the grab samples (Fig. 40 and Table 9) for Cs and Sr by using XRF and found that the concentrations appeared to be similar to those of the core samples, indicating that the mass was well

Table 23. Calculation of limestone-to-soil mixing ratio in the ORNL ISV demonstration product

Oxide	Soil ^a	Limestone ^b	ISV product ^c (wt %)	Limestone ^d in ISV product (wt %)
Al ₂ O ₃	18.35	1.59	13.7	28
CaO	2.53	50.37	18.0	32
Fe ₂ O ₃	6.23	0.7	4.5	31
K ₂ O	3.76	1.02	2.5	46

^aAverage value from Table 13.

^bValue from Table 12.

^cAverage of values from Table 21.

^d $[(\text{ISV-soil})/(\text{limestone-soil})] \times 100\%$.

homogenized by the convection currents known to occur during processing (Buelt et al. 1987). Although there are systematic differences in the concentrations of several elements (e.g., Si, Cs, Sr) between the various methods, the data from any one method support the conclusion that there is no significant partitioning of Cs or Sr on a macroscopic scale (i.e., a few centimeters) between the glass and crystalline phases. The average concentrations of Cs₂O and SrO in the ISV products (only samples which had undergone complete melting) are taken to be 0.40 and 1.48 wt %, respectively (Table 21). These values, based on the AA analysis of digested samples, were used in all calculations because of the reliability and sensitivity of the method and the good agreement with previous analyses reported by Carter et al. (1988).

5.4 MINERALOGICAL PHASE CHARACTERIZATION

Samples of the glass and spherulite phases were prepared for petrographic, x-ray diffraction (XRD), and EMP analysis. The purpose of this characterization was to determine whether there was any microscopic partitioning of Cs or Sr even though there was no evidence of macroscopic fractionation between the two major phases. Figure 46 is a photomicrograph of a single spherulite within the glass phase. The radial growth of acicular crystals is readily apparent, as well as the presence of a series of concentric growth zones. The crystals are larger in the center of the spherulite and become smaller toward the edges. XRD analysis of the ISV glass shows that it is completely amorphous. The spherulites are a mixture of a feldspar-like phase [(Na,K,Ca)Al(Al,Si)Si₂O₈] and a wollastonite-like phase (CaSiO₃). A third, unidentified pyroxene-like phase may be present, but the XRD patterns were not conclusive.

A few thin sections of the homogeneous green glass and the spherulites were selected for detailed microprobe analysis. One spherulite (≈2.5 cm in diameter) was chosen for detailed analysis. Six concentric zones from the center of the spherulite to the edge (identified as -1/+1, -2/+2, etc.) were analyzed by using a wide, defocused beam (50 μm diameter). The width of the zones was approximately 2 mm. From the outside edge of the spherulite to its center, the crystal sizes decreased (10 μm maximum width, down to a glass-crystalline [(grain size < 0.5 μm] transition zone with no identifiable crystals]). Table 19 lists the chemical composition of these zones. There is no apparent fractionation of any element at this scale (2 mm) as a result of the

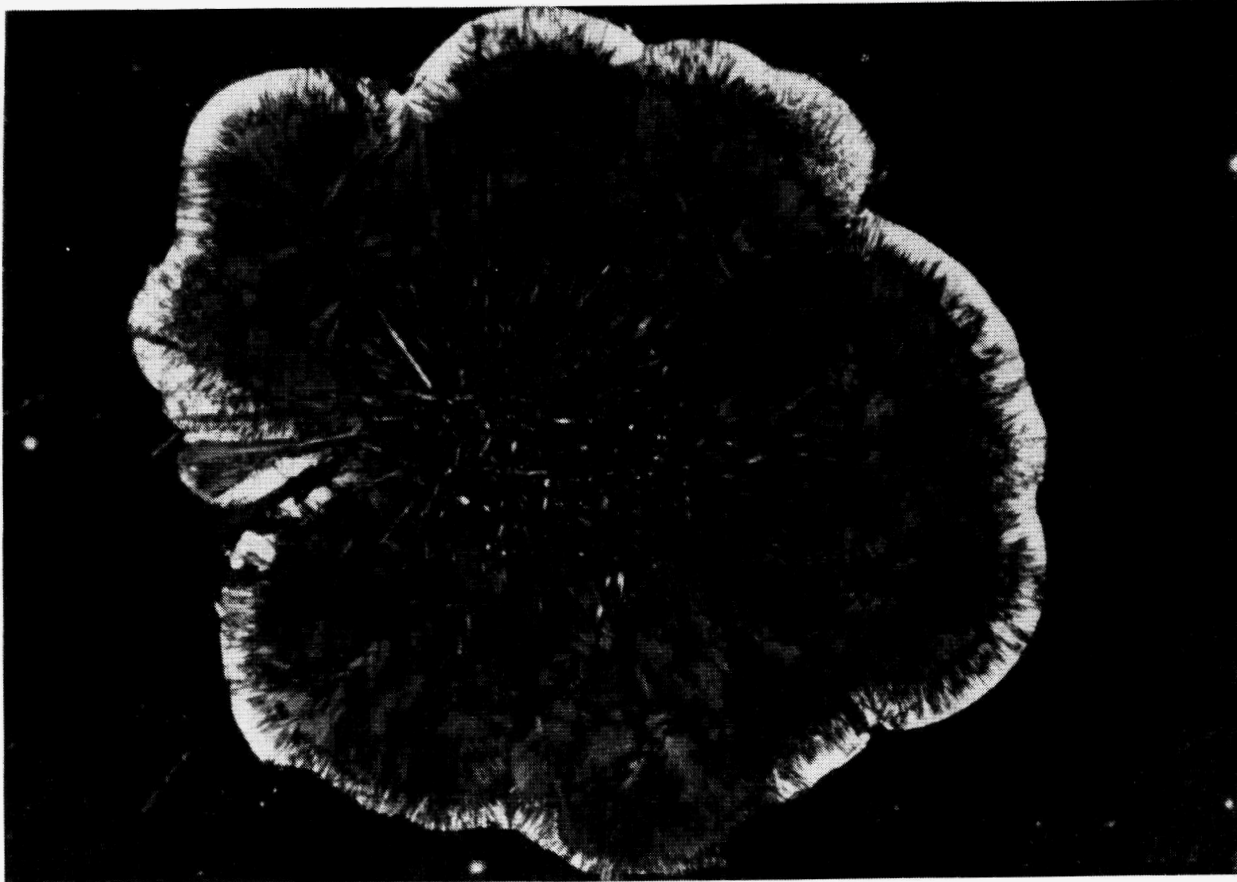


Fig. 46. Photomicrograph of a single spherulite within the glass phase from the ORNL ISV demonstration trench ($\times 10$ polarized light). Field of view is approximately 12 mm.

crystallization process. Table 20 compares the bulk composition (using 50 μm beam diameter) of two spherulites and three glass samples. Again, no significant differences exist, indicating that the crystallization process did not fractionate any elements on the scale of a few centimeters. The Cs values may indicate some small degree of variation, but the data are not conclusive. The large beam diameter that averages the compositions may be partly the reason for the variation in the trace elements. In addition, with a multiphase specimen such as this, the beam will hit some grains and not others with each analysis, so that variations in composition are common.

The individual feldspar-like and wollastonite-like phases were also analyzed in one of the spherulites (Table 22). The textural relationship between these phases is illustrated in Fig. 47. The overall radial nature of the growth is typical of spherulitic textures. The composition of the ISV material bounds the wollastonite-feldspar-silica eutectic in the ternary system $\text{CaO-SiO}_2\text{-Al}_2\text{O}_3$. Carter et al. (1988) suggest that the lamellar texture in the spherulites may be a function of near-eutectic crystallization. The composition of these phases varies significantly from one location to the next, and this behavior is reflected in the large standard deviations. The compositions of these phases are not known to occur naturally. In fact, many of the feldspar-like phases fall within the plagioclase-alkali feldspar immiscible compositional zone, a region of compositions where a single phase is unstable and the feldspar-like phase should have separated into two feldspars with distinct compositions. These unusual compositions of the wollastonite-like and feldspar-like phases indicate that the crystallization was a nonequilibrium process that occurred rapidly. It is interesting to note that the Sr, although macroscopically homogeneous, is heavily partitioned into the feldspar-like phase. Cesium is much lower in concentration in both phases when compared to the bulk composition of the spherulites, indicating that either a third crystalline phase that is not clearly observable via petrography or scanning electron microscopy (SEM) exists which contains the Cs, or that a residual interstitial glass phase is present in the spherulites into which the Cs is partitioned. This partitioning is not reflected in significant preferential leaching of Cs or Sr from the bulk samples of the spherulites compared to the glass and should not significantly compromise the performance of the ISV product for the long-term isolation of contaminants. (See Sect. 5.5 for additional details on leach characteristics.)

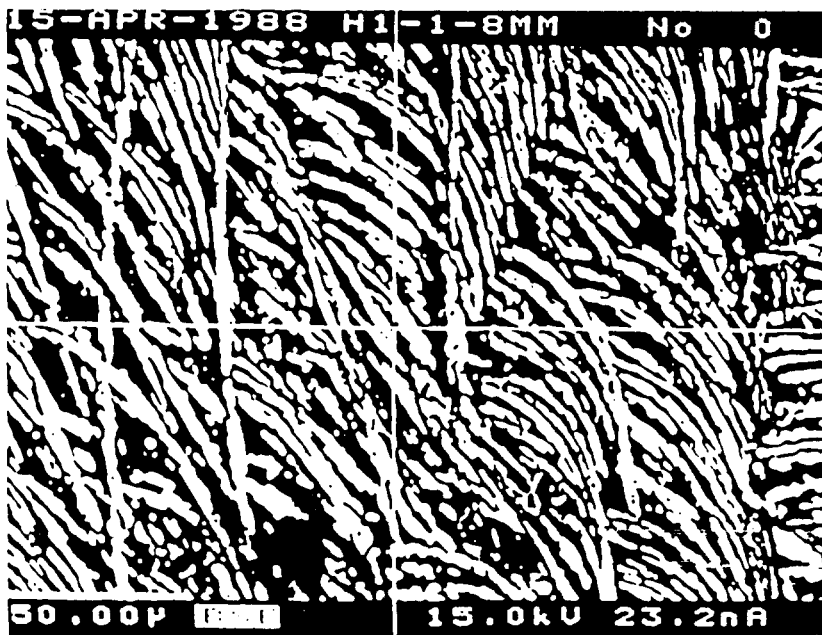
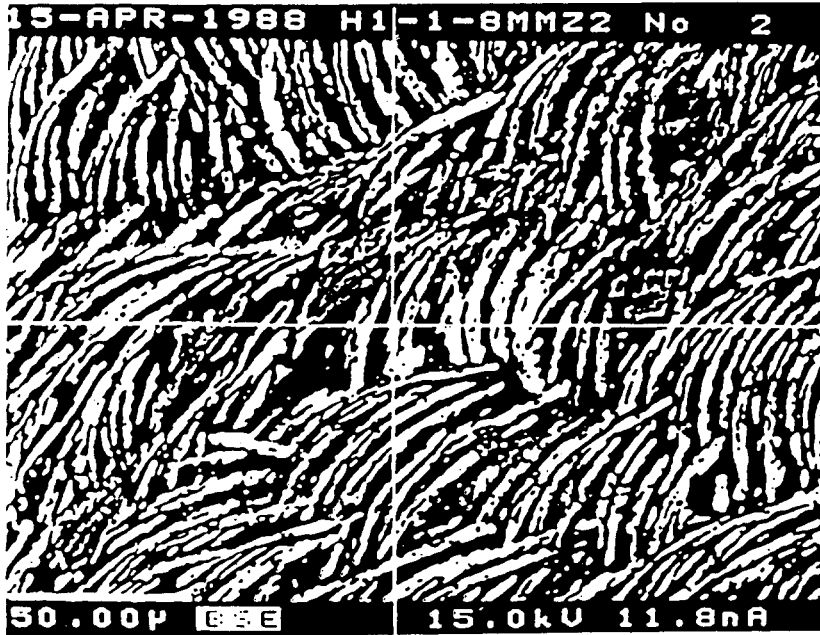


Fig. 47. Backscattered electron image of a spherulite, showing the textural relationship between the feldspar-like (dark zones) and wollastonite-like (light zones) phases in the ORNL ISV demonstration trench. Scale bar (50 μm) is located in lower left of each photograph.

5.5 CHEMICAL DURABILITY OF ISV PRODUCT

The durability of the ISV products (the glass and the spherulite phases) has been evaluated by several methods. Carter et al. (1988) reported results employing four standardized test procedures for evaluation of durability of the resulting phases. First, Material Characterization Center (MCC) Static Leach Test Method 1P (Battelle Pacific Northwest Laboratory 1986), MCC-1P, was performed on small cubic specimens immersed in deionized water at 90°C for 28 d. Second, an MCC-3 Agitated Powder Leach Test was performed on pulverized (-100/+200 mesh) samples of glass and crystalline phases at 90°C in deionized water for 28 d. Third, a modified MCC-3 agitated powder leach test was performed on the same materials at surface area to volume of leachant ratios of 50, 2000, and 10000 m⁻¹ in 90°C deionized water for various time intervals between 30 min and 28 d. Fourth, the extraction procedure toxicity test (USEPA 1986) was performed on both phases, verifying that the ISV products were not hazardous wastes. All of these tests indicated that both the glass and crystalline phases in the ISV product were quite resistant to leaching of all elements, including the Cs and Sr which are of primary interest in the evaluation of waste form performance for ORNL applications.

The present investigation involved additional testing to evaluate the two phases in the ISV product. First, the MCC-1P tests were repeated using a typical groundwater for leaching at the more realistic temperatures that would be experienced by the ISV product in the field environment. A bulk sample of streamwater was characterized and employed for these tests because it represents a chemical composition similar to what a shallow subsurface waste would encounter. It has higher concentrations of dissolved constituents than rainwater yet lower concentrations than a deep groundwater which, in the Oak Ridge geologic setting, generally means considerable hardness as a result of the weathering of limestone. Second, this same bulk streamwater sample was used to carry out the modified MCC-3 tests also at ambient, ~22°C, temperature. Third, an agitated acidic dissolution test, described subsequently, was employed on the pulverized glass and crystalline phases. This more aggressive test was employed in order to compare the ISV field products with unmelted soils that were contaminated with radioisotopes and with melted and pulverized soils also containing radioisotopes that had been tested by the acidic extraction procedure. The use of radioisotopically labeled soils and glasses in

leach testing is important so that the durability of an actual ORNL waste trench product can be predicted. The elemental tracers used in the ISV field demonstration make a significant contribution to its composition; the product averaged 0.4 and 1.48 wt % Cs_2O and SrO , respectively. The product of a vitrified waste seepage trench, however, would contain these elements at only trace levels but would contain quite high activities of ^{137}Cs and ^{90}Sr . It is important to verify that the Cs and Sr in the ISV field product behave similarly to the radioisotopes in an actual application.

5.5.1 MCC-1 Static Leach Test

On June 10, 1988, a 25-L sample of streamwater was collected from the weir of Melton Branch Monitoring Station 2B (Building 7867) by pouring through glass wool. The entire sample was taken to the laboratory, where it was filtered through Whatman no. 1 paper in batches of 2 L. On June 13-14, 1988, the streamwater was filtered through borosilicate glass microfiber filters (GC50 Micro Filtration Systems) in 1-L batches. The bulk sample exhibited an electrical conductivity = 358 dS/m, pH = 8.2, hardness = 158 mg CaCO_3/L , and an alkalinity = 132 mg CaCO_3/L (APHA 1980). The chemical composition of this water is listed in Table 24. This water was modeled using the geochemical model EQ3NR (Wolery 1983) and found to be undersaturated with respect to calcite and silica phases. It is, however, apparently supersaturated with respect to several clay minerals and aluminum hydroxides/oxides. A 125-mL volume of streamwater was placed into a 4-oz. Teflon bottle (Nalgene 2100-0004) along with a cubic specimen of ISV vitreous or crystalline phase. Material for the specimens was prepared from bulk samples collected during excavation of the ISV trench; cubes approximately 1.6 cm on a side were trimmed from larger fragments using a diamond-tip rock saw. Surface areas of each specimen were calculated from measured dimensions, and each specimen was weighed before suspension in the leachant via nylon threads. The leach test was initiated on June 29, 1988, and completed on July 25, 1988. Three specimens of both the crystalline and glass phases were included in the test along with three blank leachants without solid specimens. Sample containers were kept undisturbed on the laboratory bench during the immersion period, and temperature within the laboratory varied only slightly around 22°C. After removal, the specimens were allowed to dry in air before reweighing. Leachant was filtered through 0.45 μm nitrocellulose

Table 24. Chemical composition (milligrams per liter) of the initial leach solution use for Material Characterization Center testing of ORNL ISV demonstration products (three analyses via ICP; Cs, K, and Sr via AA)

Element	11AB	11BB	11CB
Al	0.35	0.28	0.27
Ba	0.45	0.45	0.44
Ca	53.	53.	51.
Fe	0.02	0.02	0.02
Mg	13.	12.	9.8
Na	13.	13.	12.
K	2.55	2.51	2.56
Si	2.5	2.4	2.4
Cs	0.05	0.05	0.05
Sr	0.11	0.11	0.11

Table 25. Analytical data (milligrams per liter except where noted) from MCC-1 28-d leach tests

Sample	Al	Ca	Mg	Na	Si	Cs	Sr	K	pH	Duration (h)	Mass (g)	Volume (mL)	Surface Area (cm ²)
MCC1A ^a	0.36	49	10	9.8	2.0	0.05	0.12	2.75	7.9	668.5	11.337	125	15.68
MCC1B ^a	0.36	51	10	9.7	2.2	0.05	0.13	2.77	8.1	668.5	11.473	125	15.33
MCC1C ^a	0.38	49	10	10	2.2	0.05	0.14	2.88	8.0	668.4	11.541	125	16
MCC1D ^b	0.55	50	10	9.8	2.1	0.05	0.13	2.64	8.1	668.4	10.06	125	15.17
MCC1E ^b	0.36	49	10	9.4	1.9	0.05	0.13	2.63	8.0	668.4	10.778	125	15.39
MCC1F ^b	0.36	49	10	9.4	2.5	0.05	0.13	2.65	8.1	668.4	10.797	125	15.46
MCC1G ^c	0.36	49	10	9.5	2.0	0.05	0.12	2.57	8.1	668.2	0	125	0
MCC1H ^c	0.36	49	10	9.5	1.9	0.05	0.12	2.52	8.2	668.2	0	125	0
MCC1I ^c	0.36	49	10	9.6	1.9	0.05	0.11	2.53	8.2	668.2	0	125	0

^aSpherulite samples.

^bGlass samples.

^cBlanks; initial solution (same as in MCC3-modified tests) in vessel with no solid sample present.

membranes in disposable polystyrene filter units. The leachant pH was also measured. The analytical data from this test are presented in Table 25.

MCC-1 results are usually reported as normalized release (NR) values (grams per square meter). By normalizing the quantity leached to the amount of the element in the solid, one can evaluate whether the release of elements is congruent or incongruent. For congruent releases, the NR values are the same for different elements. These values are calculated as follows:

$$NR_i = m_i / (F_i \times SA)$$

where

NR = normalized release of element i (grams per square meter),

m_i = mass of element i in leachate (grams),

F_i = (wt % oxide/100) (mol. wt element/mol. wt oxide),

SA = surface area of sample (square meter).

For the MCC-1 tests using the streamwater, m_i was calculated by using the net change in the mass of each element (i.e., between the sample and the initial solution). For some elements, this approach yielded negative values, as precipitation must have occurred during these tests. Calculated NR values are presented in Table 26. The blanks indicate changes due to precipitation and provide an estimate of the detection limits for changes in each element. The maximum NR values for Cs were calculated by assuming a concentration of 0.06 mg/L (just above the estimated detection limit of 0.05 mg/L). The NR values for Sr and Cs from these tests are approximately 10-20 times lower than those reported in Carter et al. (1988). This difference may be attributed to either the distilled water or higher temperatures (90°C), or both, used by Carter et al. (1988). Within the limits of the data in our tests, there is no difference between the NR values for Sr or Cs from the glass versus the spherulite samples. Carter et al. (1988) found slightly lower (factor of ≈ 4) NR values for Sr in the one spherulite sample they tested than in their glass samples. In summary, the NR values from the MCC-1 tests indicate the ISV waste form is at least equal to or better than other waste forms used for

Table 26. Normalized release (grams per square meter) values for ISV samples in MCC-1 28-d leach tests^a

	Al	Ca	Mg	Na	Si	Sr	Cs	K
Samples								
MCC1A ^b	0.01	-2.5	-21.0	-23.0	-0.16	0.08	<0.20 ^c	0.66
MCC1B ^b	0.01	-1.3	-20.0	-24.0	-0.10	0.16	<0.20	0.75
MCC1C ^b	0.03	-2.4	-20.0	-21.0	-0.09	0.23	<0.20	1.10
MCC1D ^d	0.23	-1.9	-21.0	-24.0	-0.13	0.16	<0.20	0.31
MCC1E ^d	0.01	-2.5	-20.0	-27.0	-0.19	0.16	<0.20	0.27
MCC1F ^d	0.01	-2.5	-20.0	-26.0	0.00	0.16	<0.20	0.34
Blanks								
MCC1G	0.01	-2.6	-21.0	-27.0	-0.16	0.08	0.00	0.07
MCC1H	0.01	-2.6	-21.0	-27.0	-0.19	0.08	0.00	- 0.10
MCC1I	0.01	-2.6	-21.0	-26.0	-0.19	0.00	0.00	- 0.07

^aConditions: MCC-1, natural stream water (see Table 24); 28 d; specimen surface area to leachant volume = 10 m²; 22°C; normalized release calculated using change in mass of element in leachate from starting solution to final solution.

^bSpherulite samples.

^cMaximum values calculated using concentration of 0.06 mg/L; detection limit is 0.05 mg/L.

^dGlass samples.

nuclear wastes and should be more than adequate for the isolation of the radionuclides found in the pits and trenches at ORNL.

5.5.2 MCC-3 Agitated Powder Leach Tests

The bulk sample of streamwater, described previously, was also used for the MCC-3 tests. Samples of crystalline and glass phases were prepared in bulk by first passing a specimen through a rock crusher and then through a rotating disc grinder with carborundum plates. Samples were then dry sieved through 100 mesh, and the material that was retained on a 200-mesh sieve was saved for the powder tests. For the 10,000 m⁻¹ specimen surface area to leachant volume (SA/V) treatment, 10.000 g of the -100/+200 mesh powder was placed into a 30-mL capacity polycarbonate "Oak Ridge" centrifuge tube with 20 mL of streamwater. For the 2000 m⁻¹ treatment, 7.000 g of powder was placed in a 4-oz. Teflon bottle with 70 mL of streamwater; for the 50 m⁻¹ treatment, 1.000 g of powder was placed in a 500-mL polyethylene bottle with 400 mL of streamwater. Samples were shaken lengthwise at 100 oscillations per minute for 28 d at ambient laboratory temperature (22°C). The leachant was then filtered through 0.45 μm nitrocellulose membranes and submitted for metals analysis via ICP emission spectroscopy and for Cs, K, and Sr analysis via atomic absorption spectroscopy. Analytical results from these tests are presented in Table 27.

Results from MCC-3 agitated tests are reported as normalized concentrations (NC; milligrams per liter) and are typically plotted versus $t \cdot SA/V$ (Bunnell et al. 1987). This parameter, obtained by multiplying the time of reaction by the SA/V ratio, can be thought of as "accelerated" reaction time. Increasing SA/V in an experiment tends to accelerate the reaction, and results can be obtained in shorter times that approach results from longer tests at lower SA/V ratios. These parameters are calculated as follows:

$$NC_i = c_i/F_i$$

where

NC_i = normalized concentration of element i (milligrams per liter),

Table 27. Analytical data (milligrams per liter except where noted) from MCC-3 modified agitated powder leach tests

Sample	Al	Ca	Mg	Na	Si	Cs	Sr	K	pH	Duration (h)	Mass (g)	Volume (mL)	Surface Area (cm ²)
1AR ^a	0.37	34	9.2	19	20	0.49	1.18	13	9.4	15	10	20	2000
1BG ^a	0.39	56	14	18	6.4	0.21	0.48	6.7	8.9	15	10	20	2000
1CR	0.33	60	14	15	9.3	0.22	0.69	5.4	9.0	15	7	70	1400
1DG	0.38	58	13	13	3.8	0.08	0.62	3.49	8.5	15	7	70	1400
1ER	0.29	54	13	12	2.8	0.05	0.14	2.68	8.2	15	1	400	200
1FG	0.29	55	13	13	2.6	0.05	0.13	2.62	8.1	15	1	400	200
2AR	0.34	56	15	17	11	0.36	1.28	10.5	9.0	0.5	10	20	2000
2BG	0.43	65	14	14	4.6	0.18	1.48	5.6	8.9	0.5	10	20	2000
2CR	0.32	60	13	12	4.4	0.17	0.59	4.55	8.6	0.5	7	70	1400
2DG	0.34	59	13	14	3.0	0.06	0.51	3.39	8.4	0.5	7	70	1400
2ER	0.29	54	13	12	2.5	0.05	0.14	2.65	8.0	0.5	1	400	200
2FG	0.29	55	13	11	2.5	0.05	0.13	2.61	8.1	0.5	1	400	200
3AR	0.36	47	14	16	13	0.42	1.43	11.3	9.1	1.5	10	20	2000
3BG	0.45	64	14	15	5.0	0.18	1.51	5.9	8.9	1.5	10	20	2000
3CR	0.32	59	14	13	5.2	0.18	0.61	4.88	8.7	1.5	7	70	1400
3DG	0.34	58	13	14	3.1	0.07	0.55	3.49	8.5	1.5	7	70	1400
3ER	0.29	56	13	12	2.7	0.05	0.14	2.7	8.1	1.5	1	400	200
3FG	0.28	53	9.9	11	2.4	0.05	0.13	2.65	8.1	1.5	1	400	200
4AR	0.36	39	13	20	16	0.47	1.29	12.1	9.2	5	10	20	2000
4BG	0.43	64	15	18	6.1	0.21	0.53	6.35	8.9	5	10	20	2000
4CR	0.34	60	14	14	7.1	0.20	0.69	4.95	8.9	5	7	70	1400
4DG	0.37	58	13	21	3.4	0.09	0.58	3.81	8.5	5	7	70	1400
4ER	0.29	55	13	14	2.7	0.05	0.14	2.71	8.1	5	1	400	200
4FG	0.28	53	10	11	2.5	0.05	0.14	2.6	8.1	5	1	400	200
5AR	0.47	31	6.4	21	29	0.53	1.05	14.7	9.5	96.2	10	20	2000
5BG	0.36	36	13	18	6.5	0.23	1.26	7.65	8.5	96.2	10	20	2000
5CR	0.26	30	13	15	18	0.22	0.6	6.15	9.3	96.2	7	70	1400
5DG	0.40	51	13	13	4.0	0.1	0.6	4.04	8.4	96.2	7	70	1400
5ER	0.35	57	13	13	4.0	0.05	0.19	2.76	8.3	96.2	1	400	200
5FG	0.31	53	9.9	11	2.6	0.05	0.14	2.59	7.9	96.2	1	400	200
6AR	0.47	32	7.1	18	27	0.53	1.14	14.4	9.5	48	10	20	2000
6BG	0.41	44	14	17	6.2	0.22	1.37	7.15	8.7	48	10	20	2000
6CR	0.30	39	14	15	15	0.22	0.67	5.8	9.2	48	7	70	1400
6DG	0.38	53	13	13	3.8	0.07	0.66	3.9	8.3	48	7	70	1400
6ER	0.33	57	13	13	3.4	0.05	0.16	2.69	8.2	48	1	400	200
6FG	0.32	53	10	12	2.6	0.05	0.14	2.65	8.1	48	1	400	200
7AR	0.50	31	3.7	21	28	0.61	1.26	15.8	9.6	191.5	10	20	2000
7BG	0.37	29	13	18	6.2	0.24	1.13	8.05	8.5	191.4	10	20	2000
7CR	0.31	28	12	15	24	0.26	0.72	6.65	9.4	191.2	7	70	1400
7DG	0.36	47	13	13	4.2	0.11	0.74	4.15	8.1	191.	7	70	1400
7ER	0.35	58	13	12	4.6	0.05	0.21	2.8	8.2	190.5	1	400	200
7FG	0.36	53	12	13	2.8	0.05	0.15	2.61	7.9	190.5	1	400	200
8AR	0.43	30	3.3	22	27	0.63	1.27	16.5	9.7	333	10	20	2000
8BG	0.35	23	10	18	5.8	0.26	1.1	8.75	8.6	333	10	20	2000
8CR	0.29	26	9.6	15	20	0.27	0.7	6.8	9.4	333	7	70	1400
8DG	0.36	48	13	14	4.8	0.13	0.81	4.34	8.3	332.5	7	70	1400
8ER	0.33	59	13	13	5.0	0.05	0.22	2.81	8.0	332.1	1	400	200
8FG	0.34	53	9.9	11	2.7	0.05	0.15	2.61	7.7	332.1	1	400	200
9AR	0.59	27	3.1	22	25	0.50	1.04	15.8	9.4	669.4	10	20	2000
9BG	0.36	22	9.7	17	5.4	0.25	1.04	8.45	8.5	669.3	10	20	2000
9CR	0.36	22	8.2	11	19	0.27	0.72	7.05	9.3	669.2	7	70	1400
9DG	0.53	49	11	11	5.3	0.13	0.91	4.05	8.3	669	7	70	1400
9ER	0.64	53	10	9.5	4.6	0.05	0.25	2.5	7.6	668.6	1	400	200
9FG	0.36	51	10	9.7	2.3	0.05	0.16	2.6	7.4	668.6	1	400	200
BLANKA ^b	0.36	49	9.7	9.3	1.7	0.05	0.12	2.55	8.3	669.5	0	70	0
BLANKB ^b	0.36	49	9.8	9.3	1.8	0.05	0.11	2.57	8.2	669.4	0	70	0

^aR designates spherulite samples; G designates glass samples.^bBlanks: initial solution (see Table 24) in vessel with no solid.

c_i = concentration of i in leachate (milligrams per liter),

F_i = (wt % oxide/100) \times (mol. wt element/mol. wt oxide).

The NC values of elements in these tests using streamwater were calculated by using the difference in concentration between the sample and initial solutions. Thus, the NC values calculated here are really the normalized change in concentration. As with the NR values from the MCC-1 tests, negative values of NC result when precipitation or sorption effects outweigh the leaching of elements from the solids.

Figure 48 presents the data for Al, Ca, and Mg. The values for the blanks (i.e., no solids present) are plotted on the right axis of the figure and indicate the behavior of the streamwater alone. Aluminum concentrations change little in the experiments and the concentrations are relatively constant in all samples and blanks. Calcium appears to initially increase and then decrease to values below the blanks in both the glass and spherulite tests. Magnesium behaves similarly to Ca in the spherulite tests but has quite a bit of scatter in the glass samples, especially at low t^*SA/V values. Figure 49 illustrates the leach results for Sr, Cs, and Si from the glass and spherulite samples. The scatter in the data is significant, and the well-behaved trends found by Carter et al. (1988) using distilled water at 90°C are not present. The data suggest that for the glass samples the release of these elements is incongruent ($Sr > Cs > Si$). The NC values at larger t^*SA/V for all three elements are generally higher in the spherulite samples than the glass samples. Although the scatter is significant, it appears that releases may be more congruent from the spherulite samples than from the glass samples. Steady-state concentrations (i.e., no change in concentration with time) at large values of t^*SA/V , typically found in tests such as these (Carter et al. 1988), are not really apparent, indicating that dynamic adjustments to the chemistry of the system are still occurring.

The solution compositions from two tests with a duration of 669 h (9CR and 9DG, Table 27) were modeled with EQ3NR (Wolery 1983). These solutions are calculated to be saturated with respect to quartz, and supersaturated with respect to several zeolite phases. The solution from the spherulite test is also supersaturated with respect to strontianite ($SrCO_3$), while the solution from the glass test is undersaturated with respect to this phase. The pH of the solutions for both the glass and spherulite samples increases over the time of the tests from an initial value of ≈ 8.0 to values

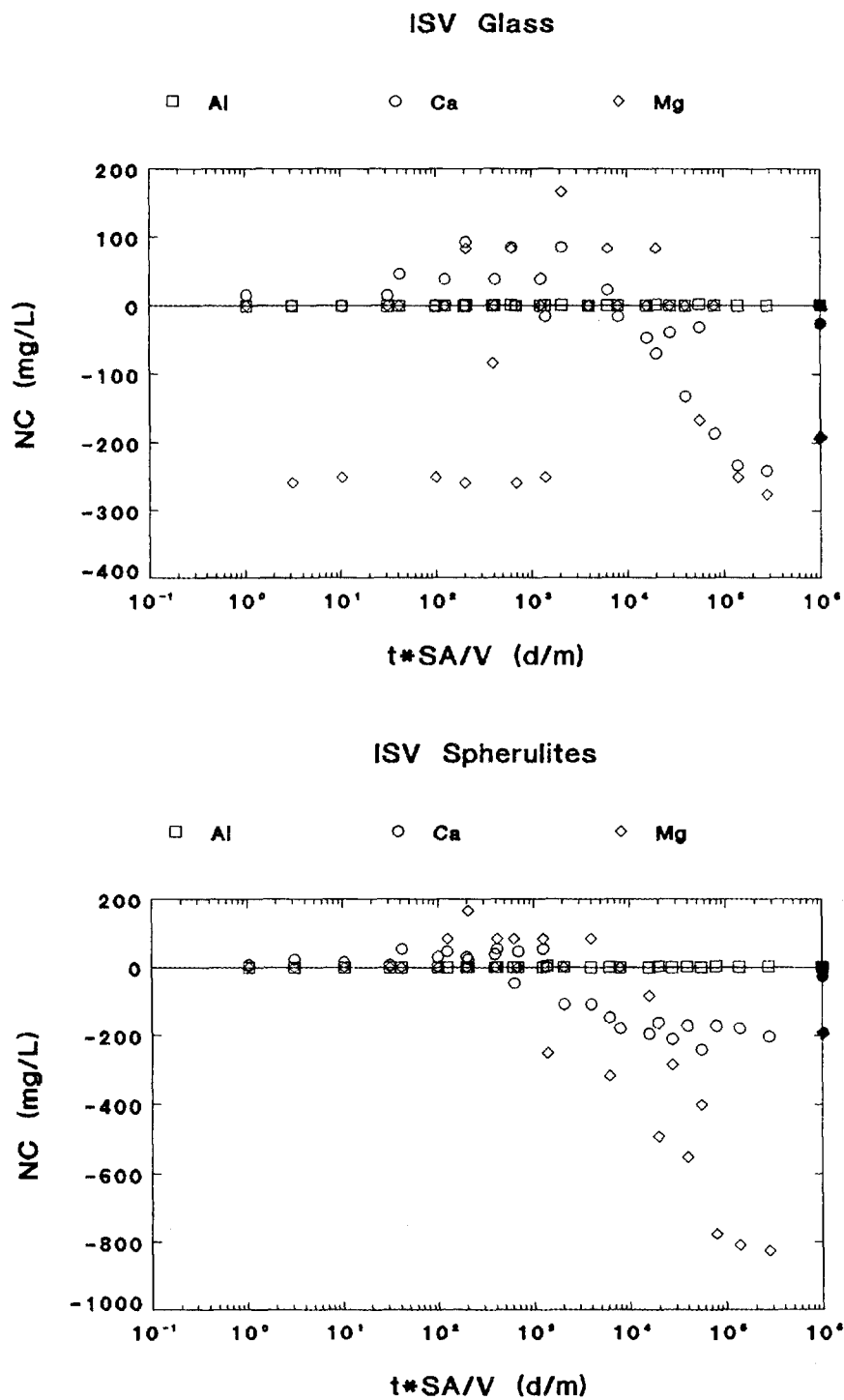


Fig. 48. Results for Al, Ca, and Mg from MCC-3 agitated powder leach tests. Change in normalized concentration (between NC of sample and NC of initial solution) versus (time \times surface area/volume). Filled symbols on right axis are values for blanks.

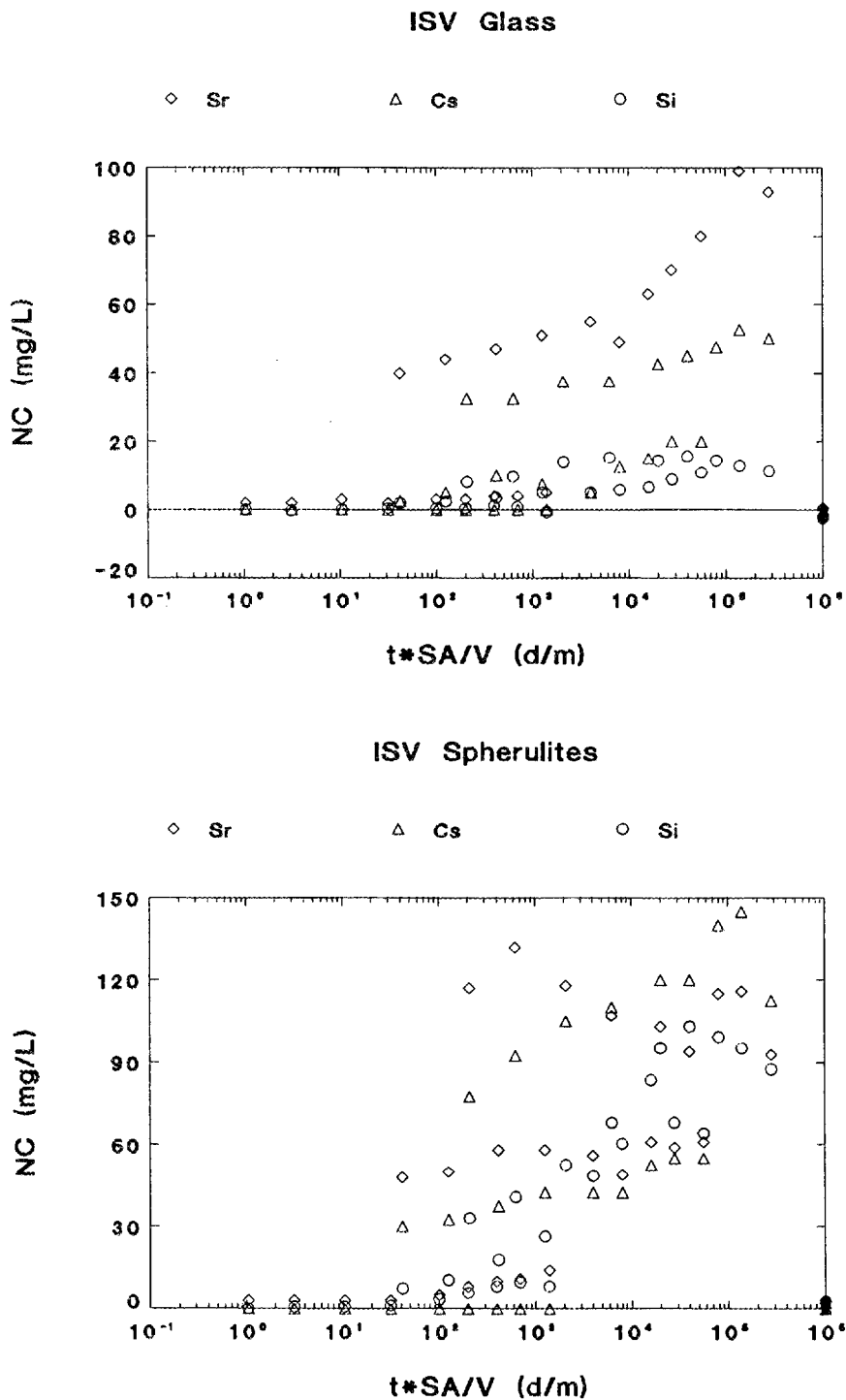


Fig. 49. Results for Sr, Cs, and Si from MCC-3 agitated powder leach tests. Change in normalized concentration (between NC of sample and NC of initial solution) versus (time \times surface area/volume). Filled symbols on right axis are values for blanks.

of 9-9.5. The high silica concentrations, high pH, and source of Ca are consistent with the possible formation of zeolite phases. The ISV material itself is unstable and will continue to dissolve even though the solution becomes saturated with silica, although the rate of matrix dissolution decreases significantly. Several samples of both glass and spherulite material that had been reacted with distilled water at 25°C for several weeks were examined with a scanning electron microscope. No positive identification of secondary products could be made. However, it is possible that such small quantities formed would not be detectable. Longer-term tests will be necessary to grow enough secondary mineral products to identify with XRD or SEM techniques.

As discussed in Carter et al. (1988), the leaching of the ISV mass in the field, where flow rates will be high and contact time with groundwater will be short, will be best represented by the results of the MCC-3 agitated powder test before saturation effects begin to dominate (i.e., at small values of t^*SA/V). In this period the major mechanism of release is assumed to be matrix dissolution with congruent release of all elements. To calculate a dissolution rate, the change in silica concentration as a function of t^*SA/V is plotted on a log scale (Fig. 50). Many of the samples at low t^*SA/V values had silica concentrations near or even below those of the initial solutions, creating significant scatter. Therefore, only positive NC values were included in this analysis. A line is fit to the linear portion of the resulting curve and extrapolated back to $\log(t^*SA/V) = 0$. This y-intercept value is the forward dissolution rate. Forward dissolution rates of 0.07 and 0.32 $\text{g}\cdot\text{m}^{-2}\cdot\text{d}^{-1}$ are obtained for the glass and spherulite samples, respectively. Values of r for these fits were 0.6 and 0.85 for the glass and spherulites, respectively. The scatter in the data and low r value for the glass prevents making a firm conclusion about the apparent difference in dissolution rates. Carter et al. (1988) derived a value of 0.4 $\text{g}\cdot\text{m}^{-2}\cdot\text{d}^{-1}$ for both the glass and spherulite samples in distilled water at 90°C. In theory, the values from our tests should have been lower by a factor of at least ten, but the scatter in the data may mask any real differences. As with the MCC-1 test results, the results from these tests indicate the ISV product will have excellent performance characteristics for isolating radionuclides that dominate the activity in the pits and trenches at ORNL.

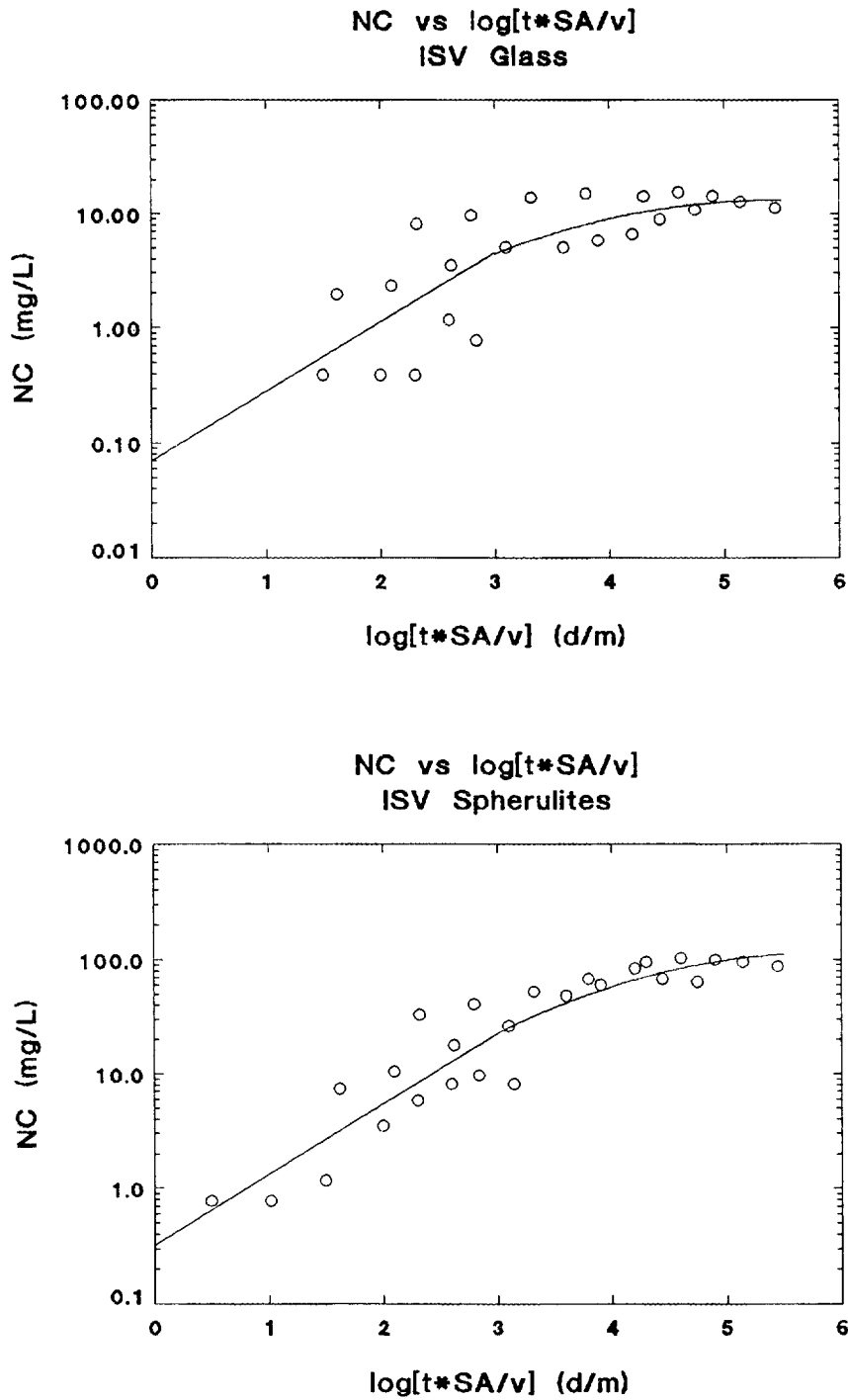


Fig. 50. Change in normalized concentration of Si (between NC of sample and NC of initial solution) versus \log (time \times SA/V) for MCC-3 agitated powder leach tests. Negative values (generally within limits of detection based on blank values) not included.

5.5.3 Pulverized Product Leaching with 0.1 N HCl

A 1.000-g sample of -100/+200 mesh powder of either the crystalline or glass phase material was placed into a 30-mL "Oak Ridge" centrifuge tube to which 20.0 mL of 0.1 N HCl was added. The tubes were then shaken lengthwise for 16 h at 100 oscillations per minute at ambient laboratory temperature. The tubes were then centrifuged at 5000 rpm (3550 relative centrifugal force) and the clear supernatant filtered through 0.45- μ m nitrocellulose membranes in a disposable filter holder unit. The filtered supernatants were placed in polyethylene scintillation vials with polyethylene-lined caps for storage. An additional 20 mL of 0.1 N HCl was added to the centrifugal pellet and the resulting suspension shaken as above for 30 min. A second extract of each sample was then prepared as above. Sequential extractions were repeated three more times on each sample for a total of five 20-mL sequential extracts from each sample. All samples were analyzed for ICP detectable elements and for Cs, K, and Sr via AA.

The results for the leaching of alkaline earths, alkali metals, and silicon for the glass and crystalline phases are presented in Figs. 51 and 52, respectively. The scale of the vertical axis in each of these graphs is identical to facilitate comparisons between the two phases. Every element except Cs, was more extractable into 0.1 N HCl from the crystalline than from the glass phase. Although the absolute magnitude of the fractions of Cs and Sr released by acidic extraction is not necessarily interpretable as a leachable quantity in the field environment, it does support the conclusion that most elements will be more susceptible to acidic leaching from the crystalline phase than from the glass phase. The aggressiveness of this acidic extraction can be seen when the fraction of Ca and Sr extracted is compared with the fractions extracted by the MCC-1 or MCC-3 tests (Table 28). In general, the acidic extraction removed between 20 and 100 times more Cs or Sr than the MCC-3 tests, however, the latter tests are more useful for waste form assessment in the field environment particularly when expressed in the normalized release format. However, the tests using soil glasses containing radioisotopes, described subsequently, required a more substantial fraction of the ^{137}Cs and ^{90}Sr to be extracted in order to detect the amount released. Thus, this acidic extraction test was performed mainly to compare the leachability of Cs and Sr from the field-produced products with that of laboratory-produced products containing radioisotopes.

Cumulative Leaching of Elements from Pulverized ISV Crystalline Phase

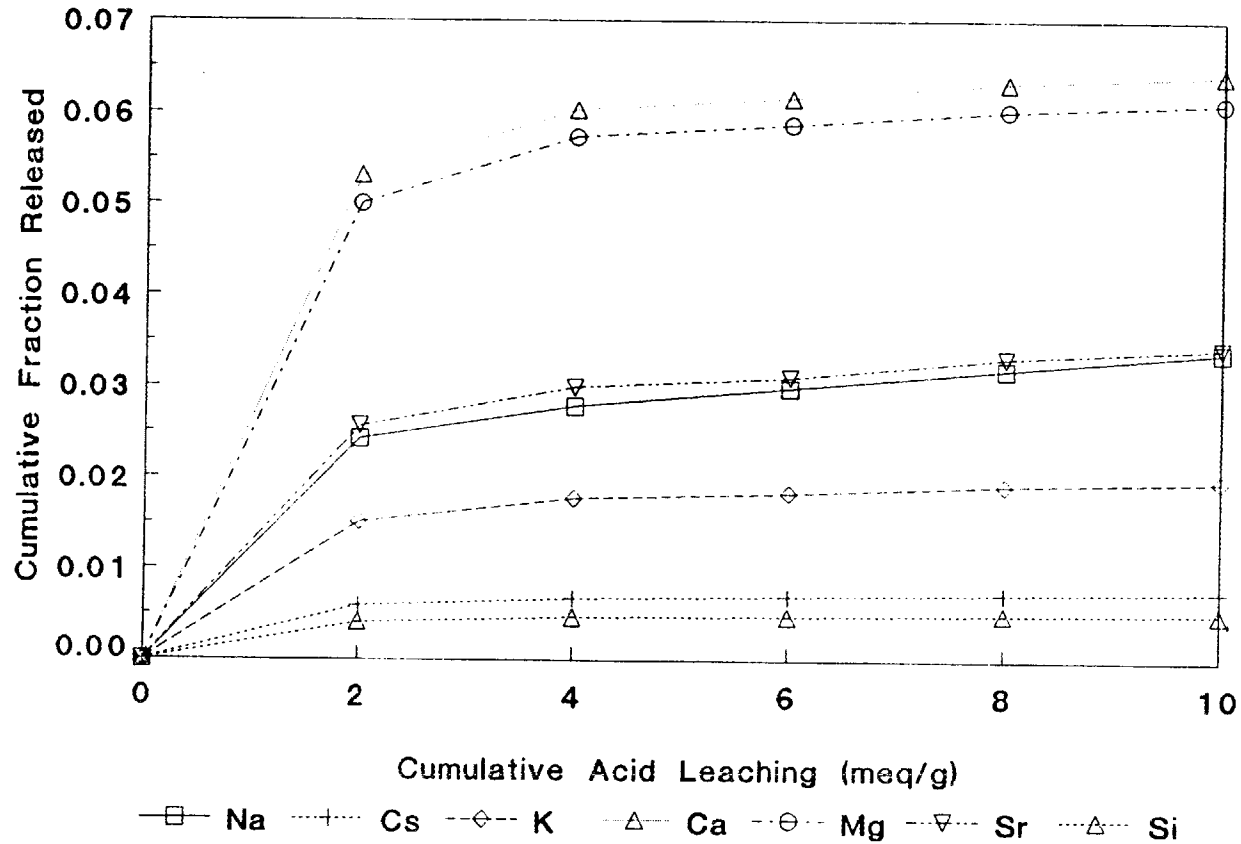


Fig. 51. Leaching of elements from pulverized crystalline phase of the ORNL ISV demonstration trench product with 0.1 N HCl.

Leaching of Elements from Pulverized
ISV Glass with 0.1N HCl

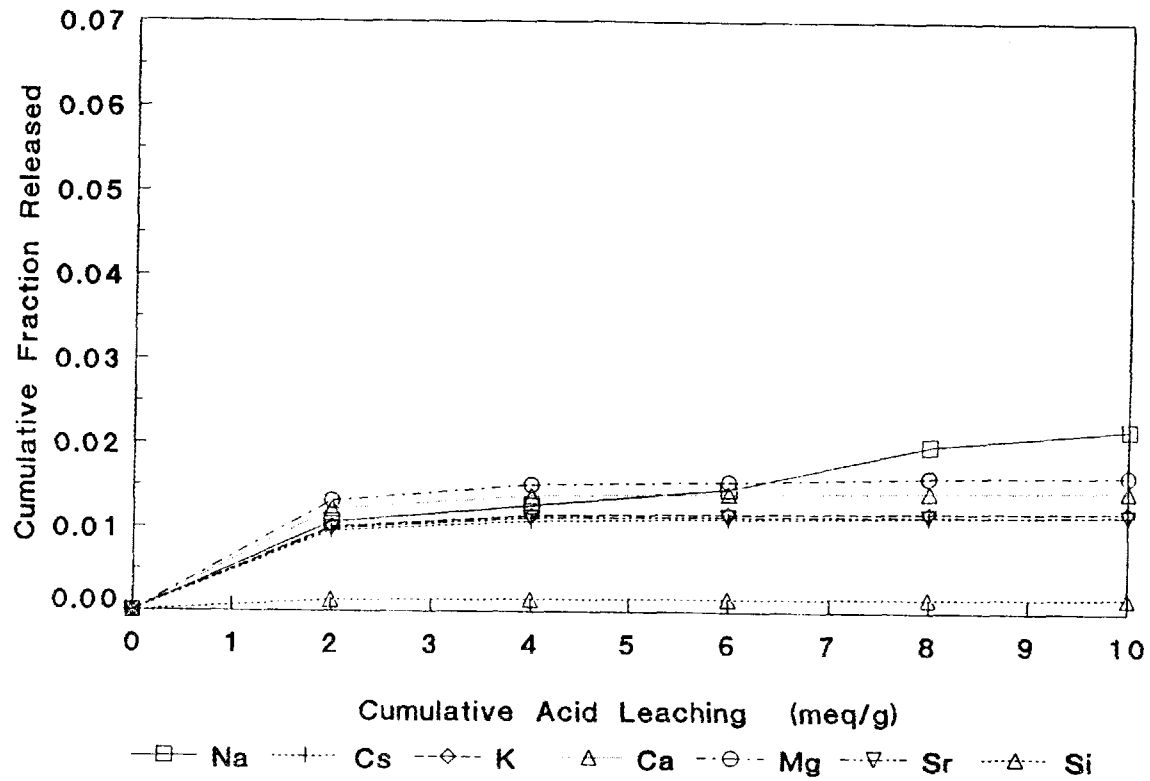


Fig. 52. Leaching of elements from pulverized glass phase of the ORNL ISV demonstration trench product with 0.1 N HCl.

Table 28. Extraction of cesium and strontium from ISV crystalline and glass phases by alternate leaching procedures

Phase	Test	Fraction released	
		Cesium	Strontium
Glass	0.1 <u>N</u> HCl	0.0116	0.0115
Crystalline	0.1 <u>N</u> HCl	0.0076	0.0343
Glass	MCC-3/Streamwater	0.000162	0.00102
Crystalline	MCC-3/Streamwater	0.000418	0.00161
Glass	MCC-1/Streamwater	<10 ⁻⁵	<10 ⁻⁵
Crystalline	MCC-1/Streamwater	<10 ⁻⁵	<10 ⁻⁵

5.5.4 Leaching of ^{137}Cs -, ^{90}Sr -, and ^{60}Co -Labeled Soil Glasses

Soil samples were collected from ORNL areas known to be contaminated with particular radioisotopes (Cerling and Spalding 1981): the floodplain of White Oak Creek east of solid waste storage area (SWSA) 4 (^{137}Cs), the seep area east of ORNL liquid seepage pit 7 (^{60}Co), and the sump near the foot of low-level solid waste trench 117, SWSA 5 (^{90}Sr , Spalding 1984). All samples were dried at 80°C to constant weight and sieved to -10 mesh (2 mm). Activities of ^{137}Cs and ^{60}Co were determined by NaI-gamma ray spectroscopy (30-min counting intervals) using 10.0-g samples in 25-mL plastic scintillation vials (Cerling and Spalding 1981). The activity of ^{90}Sr was determined via bremsstrahlung emission in the NaI gamma ray spectrum by summing the counts in the energy region below the ^{137}Cs photopeak. Compton counts in this bremsstrahlung window from ^{137}Cs or ^{60}Co in the sample were subtracted using Compton correction factors determined from ^{137}Cs and ^{60}Co standards in soil. Background in the bremsstrahlung window was subtracted using soil blanks not containing radioisotopes. Standards of ^{90}Sr in soil were prepared to determine bremsstrahlung counting efficiency, which generally averaged around 4.4%. This bremsstrahlung method, although quite dependent on the type of sample container, weight of soil, and counting geometry, provided a nondestructive method to determine ^{90}Sr activity in soil on the same sample before and after heating and again after extraction. More reliable methods of ^{90}Sr activity determination involve destructive sampling (i.e., soil dissolution or extraction, radiochemical fractionation, and beta activity counting). Samples of each soil were digested for total elemental analyses by the same techniques described under the ISV product characterization (ICP for metals and colorimetric determination of silica) following NaOH fusion and dissolution (ASA 1982). Particle size analysis of these soil samples was also carried out to determine sand, silt, and clay contents via the hydrometer method (ASA 1986). Results of these analyses are presented in Table 29.

To prepare the radioisotopically labeled glasses, 30.0 g of each soil was mixed with 13.0 g of ground limestone from the ISV trench starting material (see chemical analysis in the product characterization section) in a Pt crucible. This ratio of soil:limestone would produce a glass of about 72:28; the 13.0 g of CaCO_3 is equivalent to 7.3 g of CaO . Hence, each glass would be approximately equivalent to the ISV field product in soil:limestone ratio and elemental composition except for the significant Cs and Sr

Table 29. Characteristics of radionuclide-contaminated soils used for preparing radionuclide-labeled soil glasses

Characteristic	Soil		
	¹³⁷ Cs	⁹⁰ Sr	⁶⁰ Co
¹³⁷ Cs (dpm/g)	16280	1370	ND ^a
⁹⁰ Sr (dpm/g)	384	135500	ND
⁶⁰ Co (dpm/g)	32	ND	5530
Elemental oxides (g/kg)			
Al ₂ O ₃	141	147	139
CaO	25	21	11
Fe ₂ O ₃	57	68	55
MgO	13	64	14
MnO	1	2	2
Na ₂ O	4	4	8
SiO ₂	558	566	611
Total	800	873	838
Texture			
Sand (%)	2.3	39.9	38.5
Silt (%)	43.9	28.3	38.2
Clay (%)	53.7	31.7	23.3

^aND = not detected.

elemental contents. The crucibles were placed in a furnace and the temperature held at 1100°C for 2 h to calcine the CaCO₃. The furnace temperature was then raised to 1500°C for 16 h, after which the crucibles were removed with tongs and the molten glass poured out on a stainless steel tray. After cooling, the glass was broken up with a hammer and initially pulverized in a mild-steel manual hammer mill. Grinding was continued with an agate mortar and pestle until all material passed a 100-mesh sieve. Quite a substantial fraction of each glass adhered to the Pt crucible as it flash cooled while pouring; final decontamination of the crucibles required several HF dissolutions. Yields of the final -100-mesh glass were 16.09 g (¹³⁷Cs soil), 21.891 g (⁹⁰Sr soil), and 16.66 g (⁶⁰Co soil). Ten-gram samples of these glasses were analyzed for radioisotopes and found to contain 10,200 (¹³⁷Cs soil), 117,300 (⁹⁰Sr soil), and 4,870 dpm/g (⁶⁰Co soil), which were 63, 87, and 88%, respectively, of the soils starting activities of radioisotope. The potential volatilization of ¹³⁷Cs, indicated by the below 82% of starting activity per gram, represents a significant concern for the ISV process.

Samples of each pulverized soil glass were subjected to the same leach test with 0.1 N HCl as the ground ISV crystalline and glass phases (Sect. 5.5.3). Results are depicted in Fig. 53, where the cumulative amounts of each isotope leached were 11.8, 7.1, and 4.4% for the ¹³⁷Cs-, ⁶⁰Co-, and ⁹⁰Sr-labeled soil glasses, respectively. This result contrasts with the cumulative amounts of elemental Cs and Sr, 1.2 and 1.2%, respectively, leached by the same test from the pulverized ISV glass. The radioisotopically labeled materials were glass and not crystalline because of the flash cooling used in their preparation. However, a major difference between them was that the radioisotopically labeled glasses were not retained on a 200-mesh sieve and, hence, may contain finer material and greater surface area than the ISV glass, which was -100/+200 mesh sized. Nonetheless, the relative leachability of the three isotopes from essentially identical glasses is represented by the data in Fig. 53 where, ¹³⁷Cs continued to be released even after a total of 10 meq of HCl/g of glass had been added.

To assess the improvement in waste form durability when a soil is converted to a glass, specimens of the starting soil were subjected to an identical leaching procedure as the ground soil glasses. In order to elucidate the differing form of the radioisotope in soils and soil glasses, samples were first leached with dilute CaCl₂ to remove cation-exchangeable radioisotopes prior to the acidic extraction. For this procedure, 5.00 g of

Leaching of ⁹⁰Sr, ¹³⁷Cs, and ⁶⁰Co from Pulverized Soil Glass

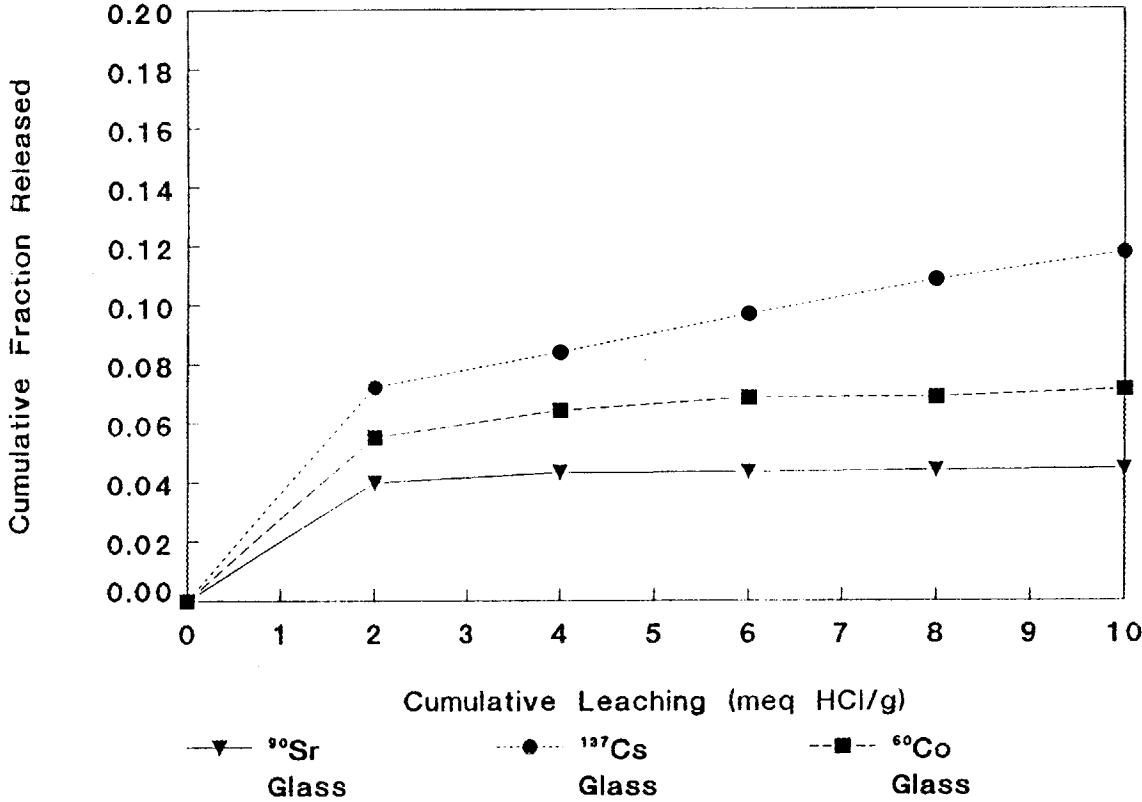


Fig. 53. Leaching of radionuclides from pulverized specimens of radioisotopically labeled soil glasses.

soil or ground soil glass was placed in a 25-mL capacity "Oak Ridge" centrifuge tube with 20 mL of 0.1 N CaCl₂. The samples were shaken, centrifuged, and filtered as described in Sect. 5.5.3 for a total of five 20-mL volumes of extract. The centrifugal pellet was then extracted as above with five 20-mL volumes of 0.1 N HCl. Each 20-mL extract volume was analyzed for ¹³⁷Cs, ⁹⁰Sr, and ⁶⁰Co as described above. The cumulative leaching curves are depicted in Fig. 54. First, the majority of ⁹⁰Sr in the starting soil was in a cation-exchangeable form, with some additional in a coprecipitate with CaCO₃ which was removed by the HCl. After melting the soil to a glass, essentially no ⁹⁰Sr remained in a cation-exchangeable form. This transformation is the major benefit in considering applying ISV to seepage pits and trenches at ORNL. The ⁹⁰Sr in the pits and trenches exists largely in either a cation-exchangeable form or as a coprecipitate with CaCO₃ in the alkaline sludge. Either of these forms is susceptible to significant leaching of ⁹⁰Sr by infiltrating precipitation. Thus, the ⁹⁰Sr, in its present form in the pits and trenches, is potentially quite mobile and, therefore, represents a significant long-term risk of environmental release. By converting the ⁹⁰Sr to a glass or crystalline waste form, it can be essentially immobilized with little risk of significant environmental release at any time in the future.

The behavior of ⁹⁰Sr contrasts with that of ¹³⁷Cs, which is essentially unleachable in its present form in the pits and trenches, a result of its specific adsorption by illitic clay minerals in the soils and saprolite in the waste disposal areas at ORNL (Tamura and Jacobs 1960). Virtually none of the soil ¹³⁷Cs was extractable with either the CaCl₂ or HCl. As a matter of fact, the extractability of ¹³⁷Cs was actually greater in the soil glass than in the starting soil on an equivalent surface area basis. However, this conclusion is somewhat misleading for assessing the ISV waste form in the field. The ISV waste form is not ground to <100 mesh, and the surface area of the field-produced waste form will probably have a specific surface area that is orders of magnitude lower than this ground glass. The starting soils have minimum surface areas of 0.6, 0.4, and 0.6 m²/g for ¹³⁷Cs, ⁹⁰Sr, and ⁶⁰Co soils, respectively. These are minimum surface areas because they are calculated from the measured textures, assuming no particles are smaller than the sedimentation diameters for the sand, silt, and clay fractions. The surface area of an ISV block in the field would probably have a surface area of approximately 10⁻⁶ m²/g. Thus, even with an order of magnitude increase in equivalent surface area extractability

Leachability of ¹³⁷Cs, ⁹⁰Sr, and ⁶⁰Co from Soil and Vitrified Soil

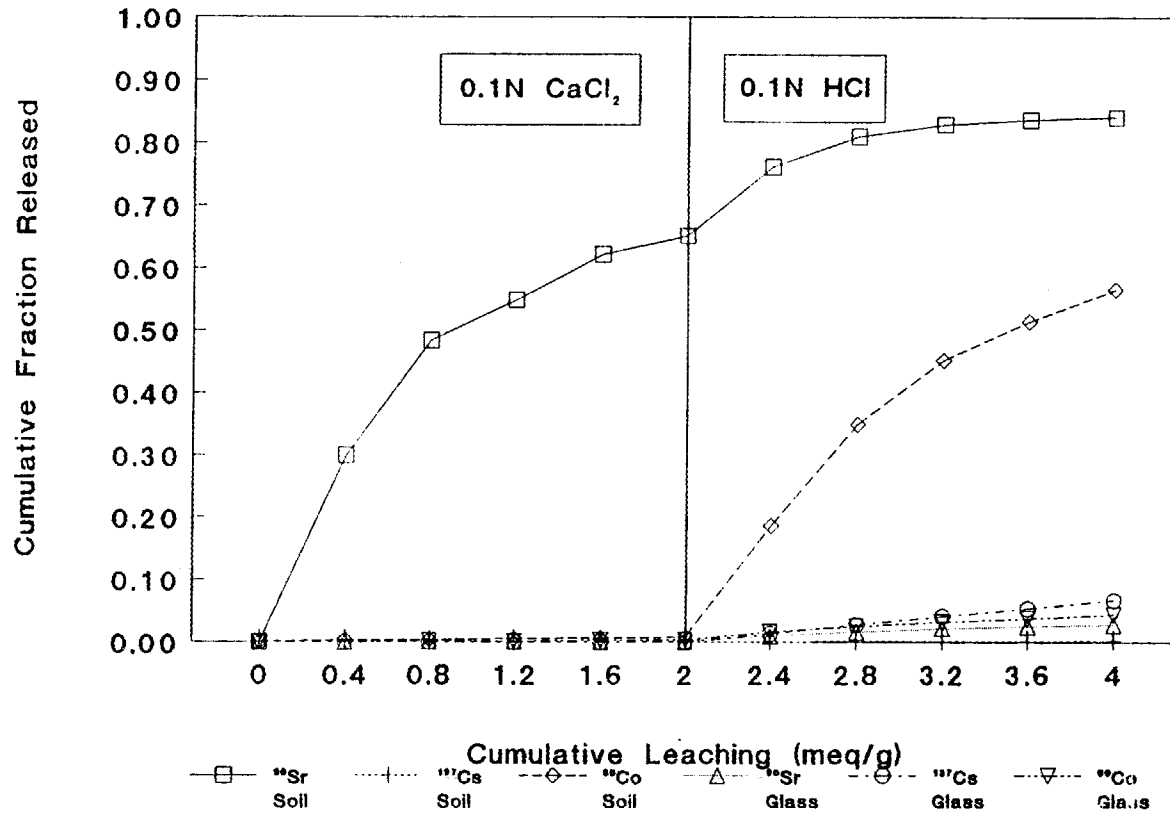


Fig. 54. Cumulative leaching of radioisotopes from soil and pulverized soil glass with CaCl₂ and dilute acid.

of ^{137}Cs , because the surface of the contaminated soil decreases by six orders of magnitude upon vitrification, resulting in a net improvement of five orders of magnitude in waste durability in the field.

The effect of surface area can be seen in the behavior of ^{137}Cs in melted soil which has not been pulverized (Table 30). The large increase in extractability of both ^{137}Cs and ^{90}Sr due to pulverization is quite apparent. The unpulverized specimens of radioisotopically labeled soil glasses were prepared as described subsequently. The surface areas of these unpulverized samples were estimated from the open area of their alumina crucible containers. The areas of the pulverized samples were calculated based on the particle diameter of particles passing the 100-mesh sieve. The leachabilities of both ^{137}Cs and ^{90}Sr from these soil glasses were generally greater than that observed for the ISV glass or crystalline phases but within the same order of magnitude. These soil glasses were only sieved to <100 mesh and hence may contain finer particles than the ISV glass, which was sieved to <100 mesh but retained on 200 mesh. The acidic extraction removed a considerably larger fraction of the ^{137}Cs and ^{90}Sr from these soil glasses than the MCC-3 procedure removed from the ISV products, a result of the aggressiveness of the HCl versus a neutral streamwater extractant. Because virtually none of the ^{137}Cs and ^{90}Sr in the pulverized soil glasses was extractable with 0.1 N CaCl_2 , MCC-3 tests on these pulverized soil glasses would likely show a similar result. Such MCC-3 tests will be carried out on the pulverized soil glasses in the future. The leachability of ^{60}Co from soil decreased significantly following vitrification. Although a significant fraction of the soil ^{60}Co was not present in a cation-exchangeable form, it was readily leached by the dilute acid (Fig. 54). Its leachability from the vitrified soil was considerably lower and approximately equivalent to that of ^{137}Cs and ^{90}Sr . Thus, the effect of vitrification of contaminated soil is to greatly reduce the leachability of all three radioisotopes.

The improvement in the leach resistance of ^{90}Sr in particular was found to be gradual following increasing thermal treatments (Fig. 55). In these tests (see Sect. 5.5.5), 5.00-g specimens of soil were placed in nickel crucibles and heated for 4 h at the indicated temperatures. The treated soil was then transferred to a 50-mL

Table 30. Leachability of ^{137}Cs and ^{90}Sr from soil and soil glass

Treatment	Surface area (estd. m^2/g)	Leachable fraction	
		^{137}Cs	^{90}Sr
1600°C, not pulverized, HCl leach	<.0001	0.00307	0.00032
1600°C, pulverized, HCl leach	>0.02	0.1176	0.0444
1600°C, pulverized, CaCl_2 + HCl Leach	>0.02	0.0671	0.0278
Unheated soil, HCl leach	>0.40	0.00457	0.7469
Unheated soil, CaCl_2 + HCl leach	>0.40	0.0015	0.8418

Temperature Effects on Leachability of ⁹⁰Sr from Soil

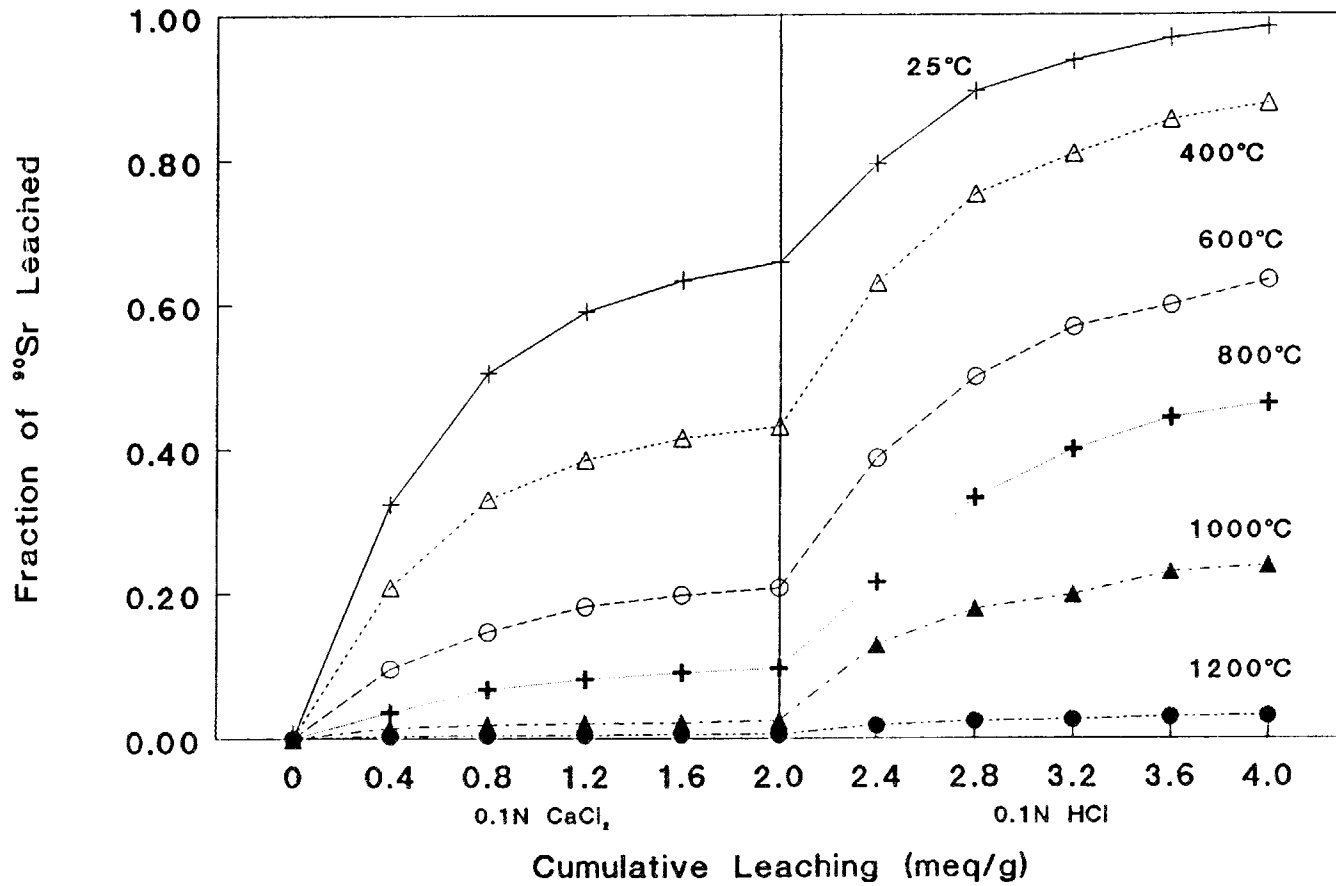


Fig. 55. Leachability of ⁹⁰Sr from soil following treatments of increasing temperature.

"Oak Ridge" centrifuge tube and subjected to the sequential CaCl_2 plus HCl extraction procedure described previously.

At the highest temperature feasible with Ni crucibles, 1200°C , the soil had not vitrified but had fused (i.e., the soil particles were no longer suspendable in the extractant without being manually broken up during transfer from the Ni crucibles). Thus, there appears to be a sintering or partial melting during these fusing temperatures that results in a reduction of surface area and a change in ^{90}Sr from an exchangeable cationic form. Thus, complete soil melting is not necessary to achieve considerable improvement in the fixation of ^{90}Sr . Because of the nature of the ISV process, soil melting must be completed to allow the process to engulf additional contaminated regions, and there is no method to regulate the thermal environment of the target zone below the melting point.

However, contaminated soil, once removed from the ground could be thermally treated below its melting point by a variety of techniques to achieve improvement in ^{90}Sr leachability before disposal. Alternately, soils may be heated in situ via a variety of techniques to attain the desired degree of thermally induced improvement in ^{90}Sr leachability.

5.5.5 Retention and Leachability of ^{137}Cs , ^{90}Sr , and ^{60}Co from Thermally Treated Soils

The soils described in the previous section also were used to study the effect of thermal treatments on the retention and extractability of the radioisotopes. Prior to thermal treatment, a 1-g soil sample was placed in a crucible which was contained within a 25-mL polyethylene scintillation vial and counted for 10 min to measure the activities of ^{137}Cs , ^{60}Co , and ^{90}Sr as described previously. Each crucible was weighed with its soil before and after each thermal treatment; blank crucibles were exposed to the 1600°C thermal treatment, and no detectable weight loss was observed. All thermal treatments were carried out in 12-mm-diam by 25-mm-high cylindrical crucibles (2-mL capacity) made of 99.8% recrystallized alumina (Coors Porcelain Co.). Duplicate samples were run for each soil at each temperature (every 100°C between 200 and 1700°C). For temperatures below 1100°C , the crucibles were placed directly into the high temperature furnace for 16 h. For temperatures above 1100°C , the crucible was placed inside either a Pt or larger alumina crucible fitted with a lid for thermal treatment; the secondary

containment was necessitated by the tendency of the small crucibles to crack or shatter during cooling. The melted soils did not appear to react significantly with the alumina crucible, but they did adhere strongly to the crucible walls. Presumably, the differential contraction of the crucible and the adhering soil glass caused the stresses which resulted in the occasional shattering of crucibles. After cooling, the crucibles were placed in 30-mL "Oak Ridge" centrifuge tubes and counted for 10 min to measure activities of ^{137}Cs , ^{60}Co , and ^{90}Sr as described previously. Each soil crucible was then subjected to five successive extractions with 20 mL of 0.1 N HCl as described previously. Following these extractions, the residue of crucible and soil was counted again for residual activity as above. Each 20-mL volume of extract also was counted for each radioisotope, and the cumulative amount of radioisotope in the five extract volumes was determined.

Retention of each isotope following a thermal treatment was calculated as the ratio of the activity after treatment to that before treatment (Fig. 56). First, the apparent increase in activity of ^{90}Sr , following thermal treatments above 1300°C , resulted from the shattering of the crucibles. As discussed previously, the determination of ^{90}Sr activity via Bremsstrahlung emission is sensitive to the geometry and materials of sample containment. For example, when the activity of ^{90}Sr in 1-g soil samples was attempted without containment in the crucibles, there was a 57% increase in apparent activity over that measured with containment in crucibles. If the activity of ^{90}Sr in the soil was determined by using 5 g instead of 1 g of soil, the apparent activity was 11% less (i.e., 135,500 versus 151,600 dpm/g, respectively). Thus, the unshielding of the ^{90}Sr soil, following crucible shattering at these higher temperatures, explains the apparent increase in activity after thermal treatment. However, there is no quantitative or unbiased method to correct these apparent activities for the differing degrees of shattering so correction was not attempted. The two samples of ^{90}Sr soil raised to 1700°C did not shatter and the apparent activity was only slightly greater than that observed before heating; the densification of the soil after melting could account for the approximate 5% increase in activity after heating due to sensitivity of bremsstrahlung emission to sample geometry. When the activities of ^{137}Cs and ^{60}Co were determined on samples with and without crucible containment, results were not significantly different (i.e., within 2%, which is the approximate uncertainty in the counting rate for the experimental technique). Thus, although the crucibles containing ^{137}Cs and ^{60}Co also shattered to

Residual Radioisotopes in Soil After One-Day Thermal Treatments

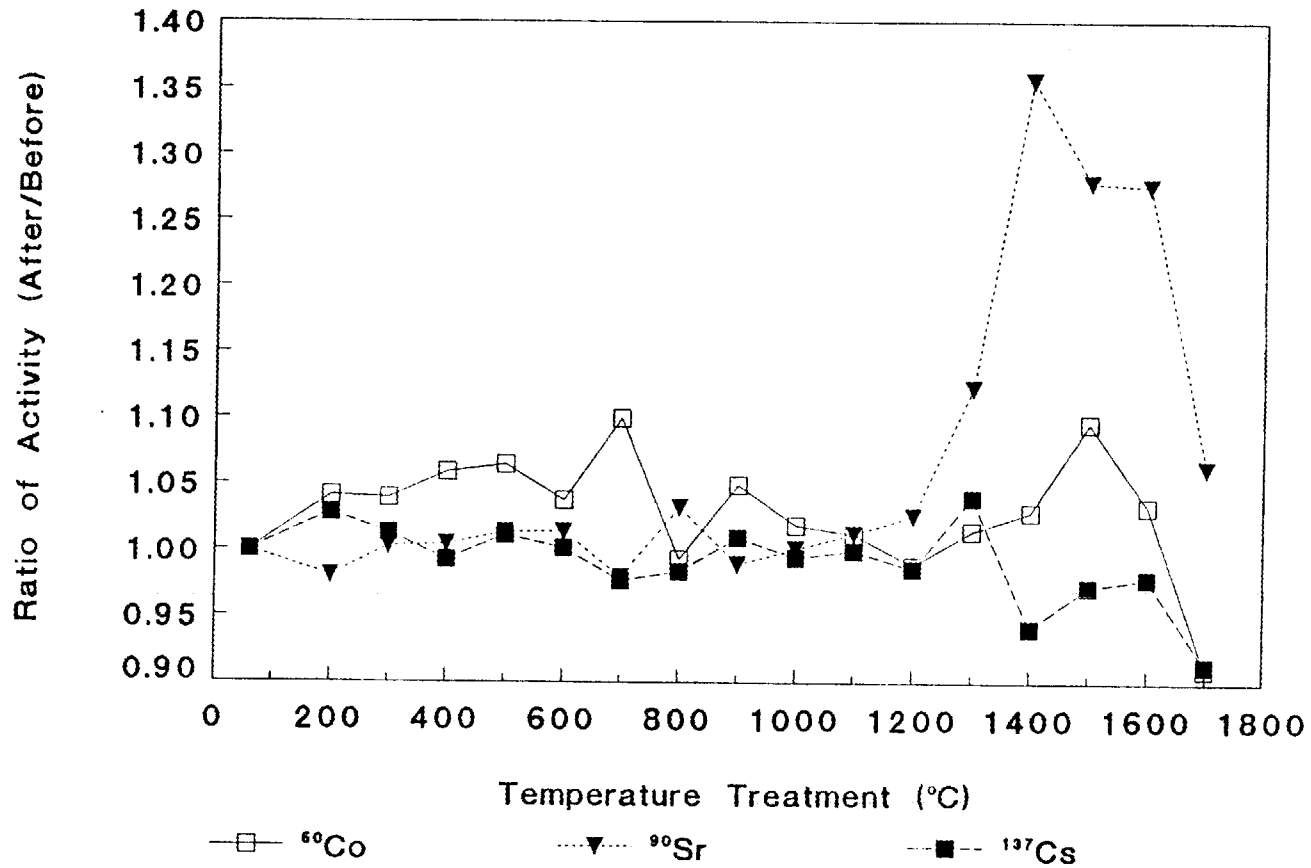


Fig. 56. Retention of radioisotopes in soil following heat treatments of increasing temperature.

varying degrees at these higher temperatures, little effect on the apparent post-treatment activities would be expected.

The activities of ^{137}Cs remained relatively constant before and after thermal treatment up to about 1400°C , where the apparent activity of ^{137}Cs declined (Fig. 56). There was a significant loss of ^{137}Cs activity above this temperature with only 91% retention at 1700°C , the upper temperature limit of the furnace. Thus, the potential for volatilization of ^{137}Cs during ISV is quite significant if melt temperatures approach 1400°C . The viscosity of the molten material is a function of temperature, and the characteristic temperature at which the viscosity is 100 poise (T100P) is useful in assessing ISV operating temperatures. When a melt reaches this temperature, convective flow of the melt is rapid enough to maintain a relatively constant temperature because the energy additions from the power system will be used to melt additional material via convectively transferred heat. Below the T100P, viscosity is high enough to retard convective heat flow, and melt temperatures rise in response to energy input from the electrical power system. Evidence for good convective flow in the field ISV product is the extremely uniform compositions of both Cs and Sr in samples taken from various locations and depths in the final melted block. Measured values of the T100P for a 1:1 mixture of ORNL soil and limestone are 1265°C while that for the unamended soil is 1720°C (Carter et al. 1987). Thus, operating temperatures during the ISV field demonstration, where a 7:3 ratio of soil to limestone was estimated, were probably low enough to yield the small volatilization of Cs observed (0.12%). Because good thermal convection, as evidenced by the uniform distribution of Cs and Sr in the ISV mass, is caused by thermal gradients, areas of the melt were probably quite hotter than the T100P. Such areas probably center around the electrodes, and such hot spots may be the primary sites of ^{137}Cs volatilization.

However, the volatilization of ^{137}Cs would not be expected to be solely a function of temperature. Obviously, the duration of the melt at an elevated temperature must be somewhat important in determining the extent of ^{137}Cs volatilization. The time dependence of ^{137}Cs retention at 1600°C was investigated by maintaining alumina crucibles containing soil in the furnaces for periods up to 13 d (Fig. 57). Although the ^{90}Sr data are quite useless due to the inability to correct for changing bremsstrahlung counting efficiency when sample crucibles shatter, the ^{137}Cs and ^{60}Co data did show a

Effect of Duration of Soil Melting Time at 1600°C on Radioisotope Retention

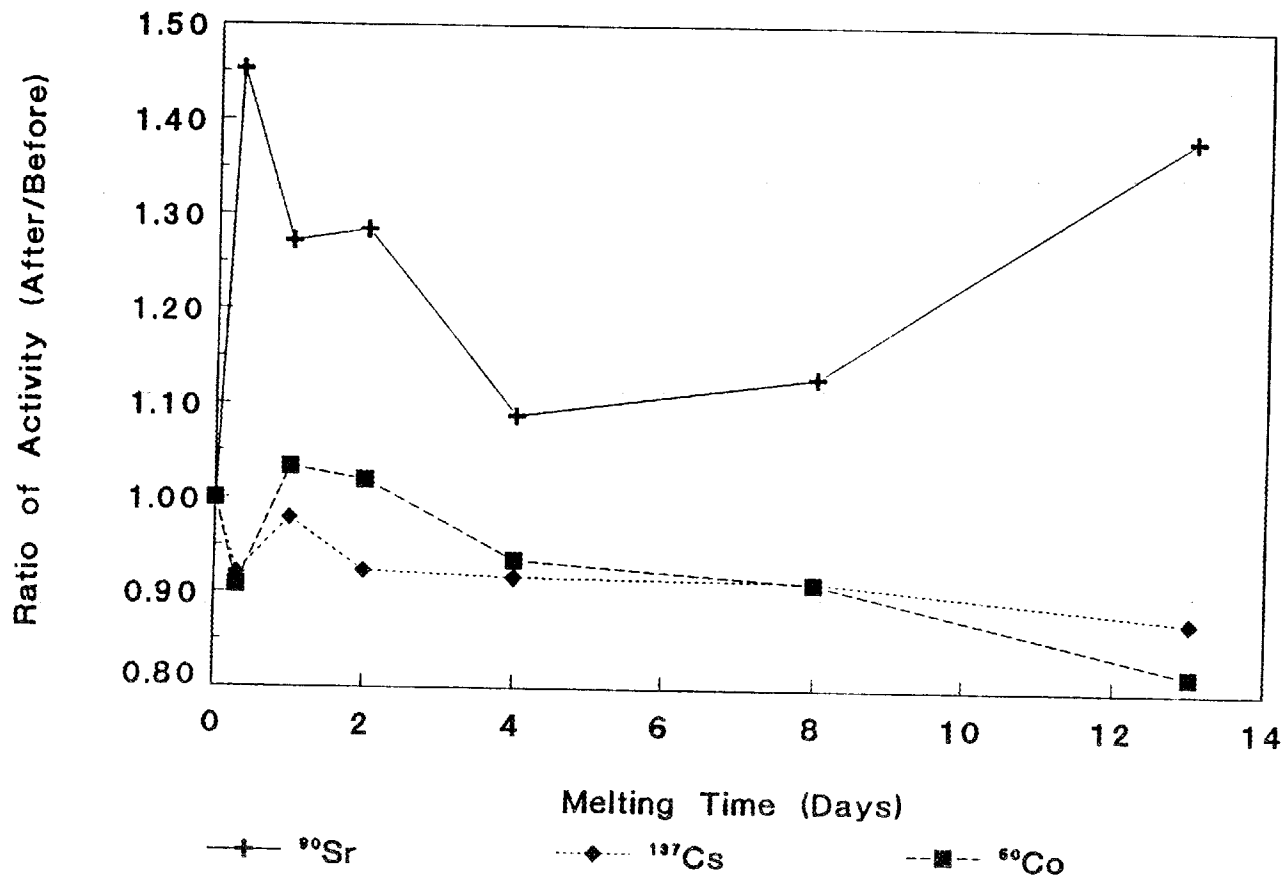


Fig. 57. The retention of ^{137}Cs in soil following heating to 1600°C for increasing periods of time.

significant time trend. Linear regression for ^{137}Cs content versus time was $-0.5\%/d$ ($r = 0.7$); for ^{60}Co , the slope of the linear regression was $-1.26\%/d$ ($r = 0.7$). Thus, volatilization does show a time dependency when the melt is maintained at temperature of 1600°C . However, in addition to the duration of the thermal treatment, the rate of heating also appeared to be important. There is only qualitative information on this effect at present. All of the samples in Fig. 57 were heated in one of two high-temperature furnaces; at maximum heating rates, the smaller furnace usually heated to its setpoint within 2 h while the larger furnace usually required > 8 h to reach its setpoint. It was this more massive furnace which showed the greater ^{137}Cs volatilization at 8 h (1/3 d). If the volatilization of ^{137}Cs depends on the surface area of the specimen, then significantly more volatilization could occur if a specimen were maintained in the porous sintered state between 1200°C and 1500°C . Thus, a more slowly heated specimen would be expected to volatilize more ^{137}Cs even though it attained the same final temperature. In future work, such heating rate effects on ^{137}Cs volatilization will be investigated more quantitatively. Hopefully some of the variation among time intervals in Fig. 57 can be eliminated by reproducible heating intervals.

The weight loss of soil samples, when heated to various temperatures, is depicted in Fig. 58. After heating these soils to about 700°C , further weight loss was not detectable. These soil samples did contain organic matter and possibly secondary CaCO_3 , which would contribute to the weight loss in addition to the dehydration of hydrous mineral phases. Overall, these data affirm the expected weight loss of soil during ISV to be about 10%.

After treatment of the soils to the various temperatures, they were extracted with HCl as described previously (Fig. 59). The cumulative fraction of both ^{90}Sr and ^{60}Co which could be extracted decreased with increasing temperature above $\sim 300^\circ\text{C}$. Virtually no difference in the extractability of these isotopes was detected above 1200°C , the temperature at which fusion of the soil particles started. In contrast, the extractability of ^{137}Cs increased, reaching a maximum of about 3% in the $800\text{-}900^\circ\text{C}$ range. These temperatures are in the range in which clay minerals, such as illite, dehydrate, and apparently lose their specific adsorption capacity for ^{137}Cs (Tamura and Jacobs 1960). As temperatures are further increased, the ^{137}Cs begins to fuse into the incipient glass and behave like Cs in the ISV product. It should be noted that all the

Weight Loss of Soils Following Thermal Treatment

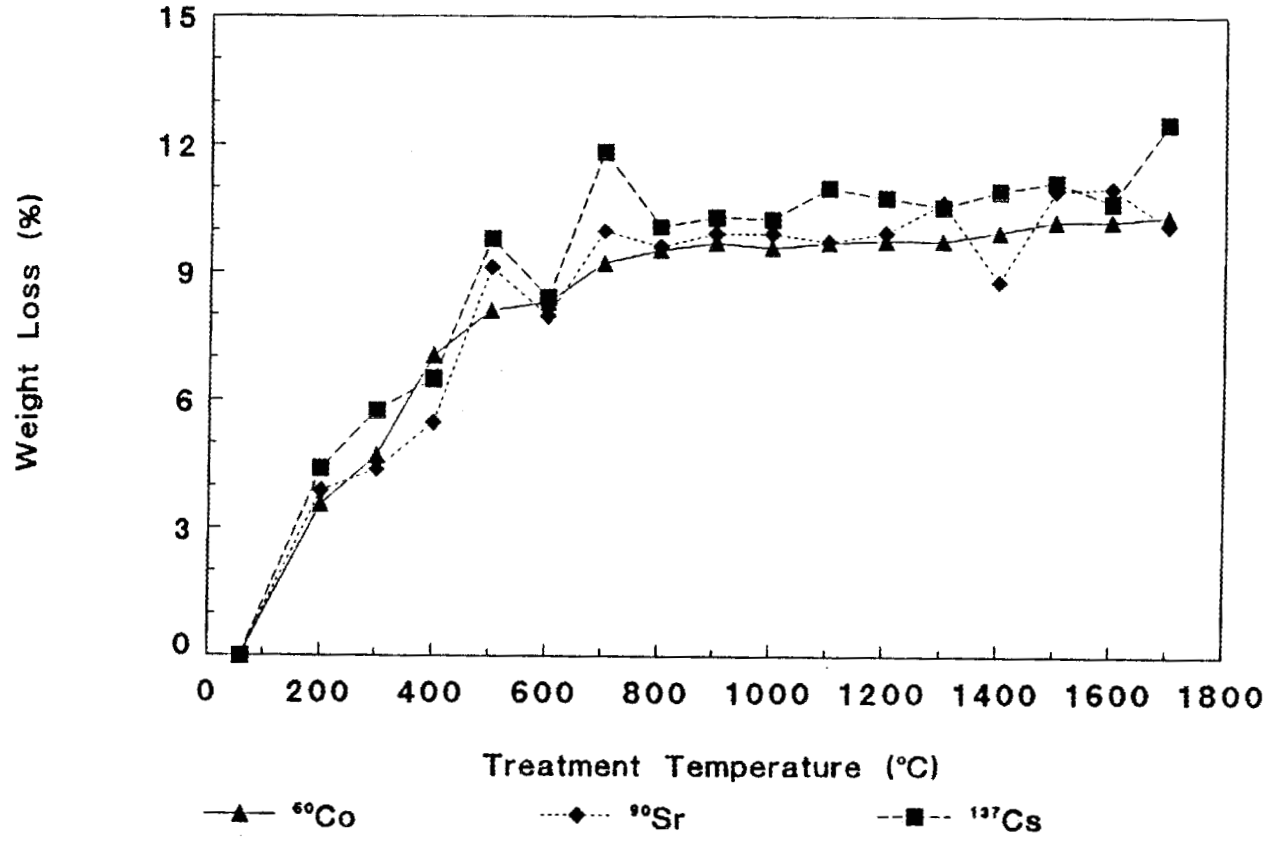


Fig. 58. Weight loss of radionuclide-labeled soils following heat treatments of increasing temperature.

Extraction of Radionuclides from Soil With 0.1N HCL After Thermal Treatment

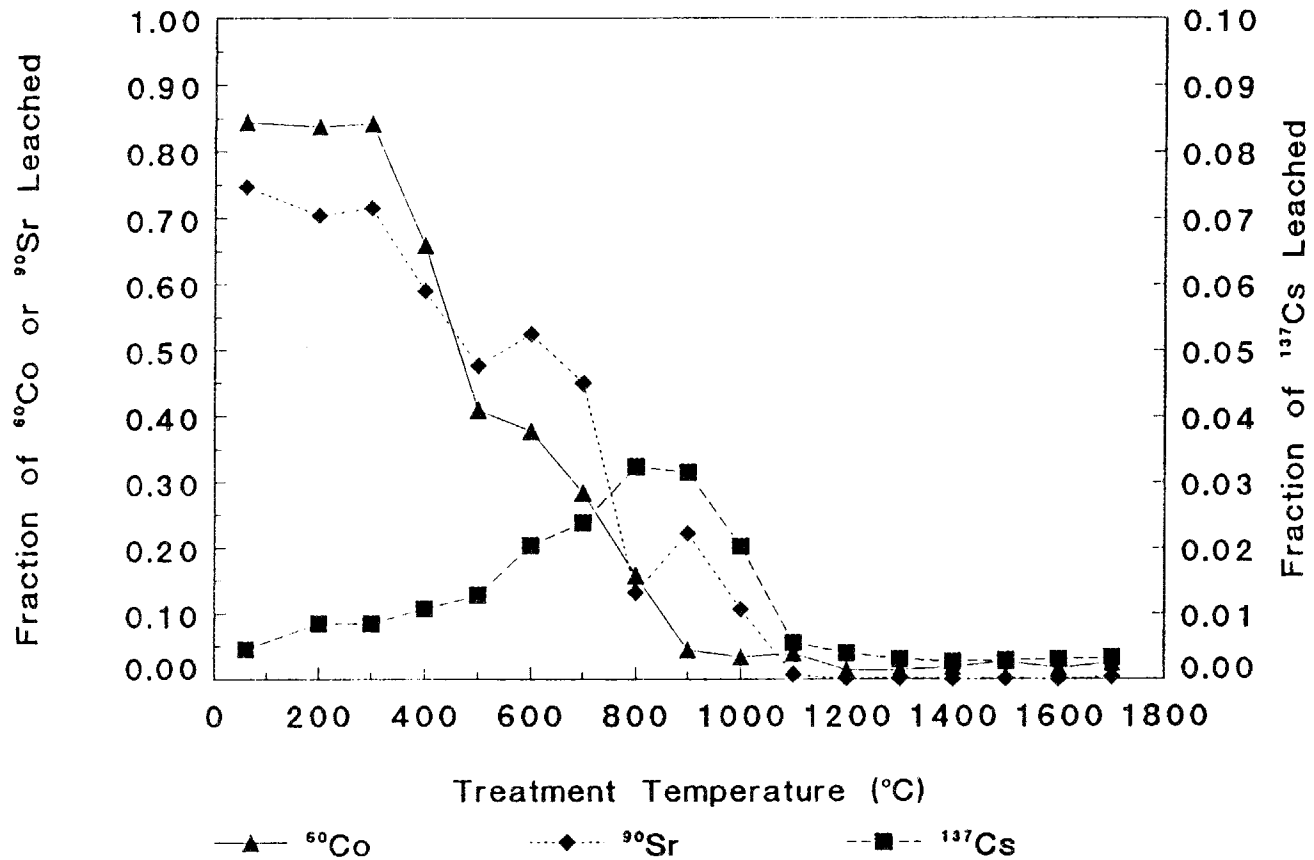


Fig. 59. Extraction of radionuclides from soil with 0.1 N HCl following heat treatments of increasing temperature.

extractions indicated in Fig. 59 were performed on specimens which had not been pulverized, so the effects of decreasing or differing surface area have not been taken into account.

6. RADIOLOGICAL AND OPERATIONAL SAFETY ASSESSMENT OF ISV FOR APPLICATION TO ORNL SEEPAGE PITS AND TRENCHES

Although it appears that the ISV field-produced material is an extremely durable waste form and potentially presents an excellent technique to stabilize and close the seepage pits and trenches at ORNL, several concerns remain in the field operation of the ISV process. Perhaps the greatest concern for an actual ISV application to a seepage trench derives from the retention of only 99.88% of the Cs within the melted mass. Such Cs retention within the melt is an excellent starting point, but Cs retention needs to be improved for an application of ISV to seepage trenches. Were ISV to be applied to liquid waste seepage trench 7 with process performance similar to that achieved for this "cold" pilot-scale demonstration, a significant radiological hazard due to the volatilization of ^{137}Cs would be encountered. Application of ISV to trench 7 would probably require about ten settings of electrodes to complete the entire trench volume, which contains a total inventory of about 100,000 Ci of ^{137}Cs . Thus, each electrode array setting would be producing a vitrified mass with about 10,000 Ci. If 99.88% of this were retained in the melt, then approximately 12 Ci of ^{137}Cs would enter the off-gas system and process trailer, and most of this would be contained in the off-gas scrub solutions (Table 31).

Without performing any dose calculations, it would appear that these quantities of ^{137}Cs represent a hazard for the process operators and would also produce a significant amount of waste for disposal by other means. Although the scrub solutions could probably be disposed of through the radioactive liquid waste disposal system at ORNL, and the HEPA filters through the solid waste disposal system, the hood and ducting, heavily contaminated with fine particulates, would present several problems. Decontamination would be desirable but is not presently possible at ORNL. Reuse of ducting and hood would cause even further accumulation of deposited ^{137}Cs and result in increasing exposure rates. Thus, it is desirable to achieve a net melt retention of 99.999% of the ^{137}Cs . Such a net retention would result in only 0.1 Ci in the process trailer and off-gas system which could be accommodated without extreme shielding or waste handling precautions. There are several possible methods by which such a larger melt retention of ^{137}Cs might be achieved.

Table 31. Hypothetical Distribution of ^{137}Cs activity in ISV off-gas system after vitrifying 10,000 Ci

Off-gas System component	Amount of ^{137}Cs (Ci)	Amount per unit area
Hood	0.079	0.24 $\mu\text{Ci}/\text{cm}^2$
Ducting	0.401	5.5 $\mu\text{Ci}/\text{cm}^2$
Scrub solutions	11.74	0.5 $\mu\text{Ci}/\text{mL}$
Primary HEPA filter	0.293	1.46 $\mu\text{Ci}/\text{cm}^2$
Secondary HEPA filter	0.008	0.04 $\mu\text{Ci}/\text{cm}^2$

Firstly, unlike the "cold" test where elemental Cs analyses in the process off-gas scrub samples were determined after the demonstration, real-time monitoring of ^{137}Cs within the process trailer is available and necessary during a "hot" test. The process trailer is equipped with several radiation monitors within the off-gas train. If significant volatilization of ^{137}Cs were observed, then power to the melt could be lowered. The volatilization of ^{137}Cs is temperature dependent and power regulation, in theory, could be employed to regulate the temperature of the melt. It should be noted that the method used in the cold demonstration did not attempt to minimize Cs volatilization because power delivery to the melt was maximized at all times. Thus, this cold test can be interpreted as measuring the maximum Cs volatilization potential, or worst-case scenario, were the ISV process applied to a trench containing actual radioactive waste. Most Cs volatilization probably occurs in hot spots near the electrodes where power density and, hence, temperatures are greatest. As discussed previously, the extremely uniform distribution of Cs and Sr in the ISV product is indicative of the thorough mixing of materials during vitrification as a result of convective heat transfers. Such convective mass movements within the melt would require significant thermal gradients to drive the process. Direct measurement of temperatures at various positions within the vitrification zone would be highly desirable in future tests. Measurement of the response of ^{137}Cs volatilization to electrical power adjustments and correlation with measured thermal gradients in the melt would provide the assurance needed for safe application of ISV to a seepage trench at ORNL. Production of a given mass of ISV product would require greater time at lower power, compared to the maximum power available, but such an increase in production time may be justified if it results in a significant reduction in the fraction of ^{137}Cs volatilized. Thus, a demonstration of ISV with radioactive ^{137}Cs will provide an excellent test of the feasibility of such a feedback control procedure to minimize ^{137}Cs volatilization by reducing power yet maintaining enough power to continue to enlarge the melted mass.

Several possible techniques may also help to minimize Cs volatilization during ISV and will be evaluated prior to their incorporation into a hot demonstration. Because the seepage trenches were constructed with crushed limestone gravel to maintain their liquid waste holding capacity, they have significant voids, probably about 40% of the trench volume, into which glass-forming or modifying materials might be introduced. Of

particular interest would be materials which could produce a glass of significantly lower melting temperature. Sodium hydroxide would be an interesting choice as an additive because it could be introduced as a liquid solution (e.g., 40% solids) and provide enough Na to yield a glass of significantly lower melting temperature. In addition, the introduction of NaOH could provide an electrically conductive subsurface path between the electrodes within the trench so that surface melt initiation could be obviated. A subsurface melt initiation has the additional potential benefit of starting ISV with a cold cap already between the melt and the ground surface to aid in both particulate and ^{137}Cs filtering of the off-gas. A risk associated with addition of NaOH to a trench may result from increased ^{137}Cs volatilization caused by Na volatilization carrying the ^{137}Cs . Potential benefits and risks from a subsurface melt initiation and glass melt temperature lowering will be tested in the laboratory before being incorporated into a hot field demonstration.

A net reduction in the ambient aboveground inventory of ^{137}Cs during an ISV test could also be attained by recycling scrub solution to the bottom of the trench via a well driven at an angle into the test trench. Thus, only the ^{137}Cs volatilized during the last stages of an ISV run would be retained within the process trailer. The remainder would be incorporated into the melted mass as it engulfed the well discharge point(s) at the trench bottom. Alternately, placement of a HEPA filter within the off-gas hood at the ducting intake could prevent ^{137}Cs from depositing on the ducting and entering the scrub solutions. As discussed previously (Sect. 4.3), most of the solids in the off-gas originate in the early part of the run before the melt has progressed to a depth where it encounters contamination. The HEPA filter could be bypassed during the early portion of the run to prevent its clogging and then switched into the off-gas line when ^{137}Cs volatilization begins. The operation of the HEPA filter at the elevated temperatures of the hood environment could also result in significant fixation of ^{137}Cs in its borosilicate glass fabric. Such filtration of ^{137}Cs would, of course, not affect the amount of ^{137}Cs volatilized, but it could reduce the volume of radioactive waste from an application. Thus, several techniques may be developed and applied in combination to increase the net retention of ^{137}Cs with the melted mass during ISV.

Two additional concerns, not related to the volatilization of ^{137}Cs , need to be addressed before considering application of ISV to seepage trenches at ORNL. First,

the uniform distribution of ^{137}Cs and ^{90}Sr in the ISV product will produce a considerable beta-gamma field, particularly if ISV is initiated from the ground surface, resulting in no shielding between the vitrified material and the ground surface. Considering only the gamma emissions, 10,000 Ci of ^{137}Cs in a 2-m-diam spherical mass would have a surface reading of about 12 R/h. After removal of the off-gas hood, soil or concrete could be placed into the subsidence crater to reduce this exposure rate. But there would also be coatings of vitrified material on the walls of the subsidence cavity, presumably contaminated with ^{137}Cs , which would need to be collapsed into the crater. However, if a subsurface vitrification could be attained, a "cold" soil cap could be maintained to minimize exposure rate at the ground surface. A subsurface initiation of ISV would probably result in subsurface cavities which would need to be collapsed for final site stabilization. Thus, stabilization and closure of the resulting trench after its vitrification do pose some operational concerns.

Second, ISV requires placement of electrodes into the ground to supply power to the melt. For application to trenches 5, 6, and 7 at ORNL, which are long and narrow [<4 ft (1.2 m) wide], electrodes would be placed outside the actual trench into the host soil formation. Presently, ISV electrode placement involves lowering them into a previously constructed borehole. For this pilot-scale ISV demonstration, an 8-in.- (20-cm-) diam auger was used to construct boreholes to accommodate the 6-in.- (15-cm-) diam graphite sleeves of the electrodes. However, augering near the edges of seepage trenches would encounter considerable activity; Olsen et al. (1983) observed many discrete contaminated strata in boreholes 30-50 ft (9-16 m) from trench 7. Contamination levels would be expected to be quite high in boreholes close to the trench. Thus, augering in close proximity to these trenches would probably prove to be unsafe. Characterization of the potential electrode environment would be required before initiating ISV on any trench and would probably be accomplished by driving narrow [<2 -in.- (5-cm-) diam] pipe into the ground around the trench and logging the cased holes for beta-gamma activity. Should radioactivity levels prove to be low enough, then augering of ISV electrode boreholes could be carried out as previously described. Alternately, driving the electrodes into the ground or driving electrically conductive casing to house the electrodes needs to be considered. The placement of grout injection lances around trench 7 in 1985 was accomplished by hammering a 1-in. (2.5-cm) pipe,

fitted with 60° solid drive points, with an air-powered vibratory hammer; depths greater than 35 ft (11 m) were often achieved. For ISV electrodes, a similar operation can be envisioned where 8-in.- (20-cm-) diam steel pipe is driven to the desired depth using pile-driving heavy equipment. The graphite molybdenum electrode could then be lowered into the steel pipe. The steel pipe would melt during the ISV process. Thus, a potential method exists to install ISV electrodes into highly contaminated subsurface regions without exposing personnel or the environment to auger cuttings. This electrode placement method would be extremely important for pits 1-4, which are much wider [50 - 100 ft (15-31 m)] than trenches 5-7, because electrodes would need to be positioned within the pit itself.

Many of the potential hazards of performing a complete vitrification of a trench are a result of the need to move the off-gas collection hood after completing each segment of a trench. For example, the vitrification of trench 7 would require a maximum of ten settings. However, if a single hood were constructed over the entire trench and all electrodes emplaced before initiating ISV, then no movement of the hood would be required. Reconnection of the electrical cables would be all that was required between settings. Final site cleanup, stabilization, and any required decontamination of hood and off-gas ducting would be required only once.

Based on the encouraging results from the cold demonstration and probable improvements in ISV operational effectiveness, it is recommended that a hot demonstration of ISV be performed on a model seepage trench containing a sample of seepage pit waste. Such a hot demonstration will verify the potential ability for feedback control of ^{137}Cs volatilization. The demonstration will also allow a field verification of the performance of a melt temperature depressant such as NaOH and the ability to initiate ISV within the trench rather than at the ground surface. Such a demonstration should provide the information needed to determine whether or not to pursue ISV as a technique for the final stabilization and closure of the pits and trenches at ORNL.

Several operational problems were encountered during the ISV demonstration which need to be resolved through additional investigation and through the proposed hot test. During the July 1987 demonstration, the starter path for the melt was interrupted several times due to subsidence of the trench cap during melting, which resulted in

electrical discontinuities and, therefore, operational interruptions. Additional soil material had to be added through the hood to build up the surface for new starter path material to reinitiate the melt. Although this can be considered merely an inconvenience during the cold test, opening the hood and placing material over a partially exposed trench or in the middle of a sequence of electrode settings within a multisetting hood, may pose a significant risk for operator exposure to radioactivity. Either compaction of the cap prior to initiation of the starter path or a technique to initiate melting within the subsurface needs to be considered to overcome this problem for an actual hot test, where entry or access to the hood must be avoided.

The electrical power delivery system malfunctioned twice during the operation of the demonstration. The first malfunction caused a 3-week delay while the transformer in the PNL process trailer was repaired by a factory representative. A specific cause for the malfunction of the failed components has not been determined. A second malfunction occurred during the second startup of the demonstration when the control circuitry for the amperage regulation of the power delivery to the melt failed. Manual control and data recording of the power were required for the remainder of the demonstration. Although the components which failed have been identified and repaired, no specific cause has been determined.

Spurious alarms by the area-radiation monitors in the process trailer occurred sporadically during the test, particularly during voltage tap changes on the power delivery transformer. Although such spurious alarms posed no safety problem for this cold demonstration, a repeat occurrence during a hot test or actual application would necessitate a decision to shut down. In addition, spurious alarms by area-radiation monitors downline at the new hydrofracture facility were noted during the ISV operation. No cause for these disturbances in the electrical service lines to the site have been identified. These problems need to be solved before a hot test or actual application can be attempted.

During the cold demonstration the depth of melting was monitored by the burn-out of thermocouples specifically buried at selected depths and locations within the trench. Although a similar placement for a hot test may be possible, such placement would be extremely difficult for an actual application to an ORNL seepage trench. PNL has developed a depth-monitoring system based on a radio transmitter attached to one

or more of the electrodes coupled to fiber optic strands strapped to the electrodes at various depths. Successful performance of such a melt depth monitoring system needs to be demonstrated before an actual application of ISV to seepage trenches at ORNL. The backup depth monitoring system used during the cold demonstration (i.e., probing with a steel rod) would not be safe for either a hot test or an actual application.

Nondestructive geophysical tests, (e.g., seismic profiling) need to be evaluated for real-time depth monitoring. The contrast in density, and, hence, acoustic velocity, between the porous trench gravel and soil formation (bulk density 1.4 and 1.8 g/cm³, respectively) and the melted material (bulk density 2.7 g/cm³) makes seismic detection look quite feasible. Moreover, during operation the liquid melt will have significantly different geophysical behavior than the surrounding materials (i.e., the liquid would not transmit S waves).

7. REFERENCES

- APHA (American Public Health Association). 1980. Standard methods for the examination of water and wastewater. American Public Health Association, Washington, D.C.
- ASA (American Society of Agronomy). 1982. Methods of soil analysis, part 2, chemical and microbiological properties. 2d ed. American Society of Agronomy, Madison, Wisconsin.
- ASA (American Society of Agronomy). 1986. Methods of soil analysis, part 1, physical and mineralogical methods. 2d ed. American Society of Agronomy, Madison, Wisconsin.
- BPNL (Battelle Pacific Northwest Laboratory). 1986. Nuclear Waste Materials Handbook Test Methods. DOE/TIC-11400. Battelle Pacific Northwest Laboratory, Richland, Washington.
- Buelt, J. L., and J. G. Carter. 1986. Description and capabilities of the large-scale in situ vitrification process. PNL-5738. Pacific Northwest Laboratory, Richland, Washington.
- Buelt, J. L., and S. T. Freim. 1986. Demonstration of in situ vitrification for volume reduction of zirconia/lime sludges. Pacific Northwest Laboratory, Richland, Washington.
- Buelt, J. L., C. C. Chapman, S. M. Barnes, and R. D. Dierks. 1979. A review of continuous ceramic-lined melters and associated experience at PNL. pp. 107-113. IN Ceramics and Nuclear Waste Management. CONF-790420. Technical Information Center, Springfield, Virginia.
- Buelt, J. L., C. L. Timmerman, K. H. Oma, V. F. Fitzpatrick, and J. G. Carter. 1987. In situ vitrification of transuranic wastes: Systems evaluation and applications assessment. PNL-4800, Supplement 1. Pacific Northwest Laboratory, Richland, Washington.
- Bunnell, L. R., G. D. Maupin, and K. H. Oma. 1987. High-temperature glasses for nuclear waste isolation. pp. 167-173. Nuclear Waste Management II: Advances in Ceramics, Vol. 20. IN D. E. Clark, W. B. White, and A. J. Machiels, (eds.), American Ceramic Society, Columbus, Ohio.

- Carter, J. G., S. O. Bates, and G. D. Maupin. 1987. In situ vitrification of Oak Ridge National Laboratory soil and limestone. PNL-6174. Pacific Northwest Laboratory, Richland, Washington.
- Carter, J. G., S. S. Koegler, and S. O. Bates. 1988. Process performance of the pilot-scale in situ vitrification of a simulated waste disposal site at the Oak Ridge National Laboratory. PNL-6530. Pacific Northwest Laboratory, Richland, Washington.
- Cerling, T. E. and B. P. Spalding. 1981. Areal distribution of ^{60}Co , ^{137}Cs , and ^{90}Sr in streambed gravels of White Oak Creek Watershed, Oak Ridge, Tennessee. ORNL/TM-7318.
- Jacobs, G. K., B. P. Spalding, J. G. Carter, and S. S. Koegler. 1988. In situ vitrification demonstration for the stabilization of buried wastes at the Oak Ridge National Laboratory. Nucl. Chem. Waste Manage. 8:249-259.
- Jackson, K. C. 1970. Textbook of Lithology. McGraw-Hill Book Company, New York, p. 273.
- Lomenick, T. F., D. G. Jacobs, and E. G. Struxness. 1967. The behavior of strontium-90 and cesium-137 in seepage pits at ORNL. Health Phys. 13:897.
- Nockolds, S. R., R. W. O'B. Knox, and G. A. Chimner. 1978. Petrology for Students. Cambridge University Press, New York, p. 36.
- Olsen, C. R., P. D. Lowry, S. Y. Lee, I. L. Larsen, and N. H. Cutshall. 1983. Chemical, ecological, and hydrological factors governing radionuclide migration from a formerly used seepage trench: A field study. ORNL/TM-8839.
- Oma, K. H., D. R. Brown, J. L. Buelt, V. F. FitzPatrick, K. A. Hawley, G. B. Mellinger, B. A. Napier, D. J. Silveira, S. L. Stein, and C. L. Timmerman. 1983. In situ vitrification of transuranic wastes: Systems evaluation and applications assessment. PNL-4800. Pacific Northwest Laboratory, Richland, Washington.
- Spalding, B. P. 1980. Adsorption of radiostrontium by soil treated with alkali metal hydroxides. Soil Sci. Soc. Am. J. 44:703-709.
- Spalding, B. P. 1981. Chemical treatments of soil to decrease radiostrontium leachability. J. Environ. Qual. 10:42-46.

- Spalding, B. P. 1984. Field demonstration of in situ treatment of buried low-level radioactive solid waste with caustic soda and soda ash to immobilize ⁹⁰Sr. ORNL/TM-8990.
- Tamura, T., and D. G. Jacobs. 1960. Structural implications in cesium adsorption. *Health Phys.* 2:391.
- Timmerman, C. L., and K. H. Oma. 1984. An in situ vitrification pilot-scale radioactive test. PNL-5240. Pacific Northwest Laboratory, Richland, Washington.
- Timmerman, C. L., R. A. Brouns, J. L. Buelt, and K. H. Oma. 1983. In situ vitrification: Pilot-scale development. *Nucl. Chem. Waste Manage.* 4:267-276.
- USEPA (United States Environmental Protection Agency). 1986. Test methods for evaluating solid waste. SW-846, Vol. 1. United States Environmental Protection Agency, Washington, D.C.
- Wolery, T. J. 1983. EQ3NR: A computer program for geochemical aqueous speciation-solubility calculations: User's guide and documentation. UCRL-53414. Lawrence Livermore National Laboratory, Livermore, California.

APPENDIX

Analytical Data for ISV Samples

Chemical and Radiochemical Characteristics of ISV Off-Gas Scrub Solution Samples [In the sample number, the first number, 1-x, indicates that the sample came from tank 1 (the venturi scrubber), or 2-x indicates that the sample came from tank 2 (the Hydrosonic scrubber)]. Run Time is the hours from 9:48 AM on July 14, 1987. Negative run times indicate samples collected during the initial abortive start of the ISV test.

Sample Number	pH	El. Cond. (dS/m)	Total Solids (mg/L)	Dissolved Solids (mg/L)	Total Alpha (Bq/L)	Total Beta (Bq/L)	Run Time (hours)
ORNL 1-1	7.07	1750	6080	1460	186	2348	-451.8
ORNL 1-2	7.08	1950	6560	1740	172	2247	-450.5
ORNL 1-3	7.53	2050	7760	1880	186	2104	-448.5
ORNL 1-4	6.51	2300	9940	2320	184	2438	-446.5
ORNL 1-5	5.04	2950	13820	3520	197	2850	-444
ORNL 1-6	5.08	3150	14560	5500	229	2947	-442.5
ORNL 1-7	6.18	3050	13500	3440	213	2583	-441.5
ORNL 1-8	6.19	3450	15080	3920	222	2869	-438.5
ORNL 1-9	6.33	2550	14740	3920	209	2639	-436.6
ORNL 1-10	6.25	3500	15120	3620	190	2312	-434.6
ORNL 1-11	6.28	3600	14620	3960	175	2673	-424.5
ORNL 1-12	6.37	1000	3580	1280	102	748	-19
ORNL 1-13	6.39	1170	4480	1560	75	778	-17.7
ORNL 1-14	6.45	1100	5280	1740	77	829	-16.5
ORNL 1-15	6.61	1200	6140	1700	68	860	-14.1
ORNL 1-16	6.27	950	4080	1240	65	624	1.5
ORNL 1-17	6.45	1400	8760	1820	54	639	3.5
ORNL 1-18	6.89	1450	11580	2140	43	605	5.5
ORNL 2-1	6.97	1550	3860	1300	136	1180	-451.8
ORNL 2-2	6.97	1800	4680	1560	150	1230	-450.5
ORNL 2-3	7.27	2300	6240	1980	111	1062	-448.5
ORNL 2-4	7.31	2400	7760	2100	127	951	-446.5
ORNL 2-5	7.53	2550	10880	2580	145	1346	-444
ORNL 2-6	7.56	2650	13220	2700	152	1401	-442.5
ORNL 2-7	7.79	3200	13100	3460	134	1342	-441.5
ORNL 2-8	7.83	2900	15800	5440	190	1377	-438.5
ORNL 2-9	8.04	3150	12700	3540	129	1092	-436.6
ORNL 2-10	8.07	3100	11220	3440	131	1023	-434.6
ORNL 2-11	7.99	3300	12560	3360	136	1655	-424.5
ORNL 2-12	6.34	1250	4100	1500	79	775	-19
ORNL 2-13	6.69	1300	5780	2060	56	638	-17.7
ORNL 2-14	6.64	1500	7920	1860	84	695	-16.5
ORNL 2-15	6.65	1550	7980	2080	54	589	-14.1
ORNL 2-16	6.49	1550	8300	2540	86	606	1.5
ORNL 2-17	7.02	2100	16520	3380	68	657	3.5
ORNL 2-18	7.36	2350	22360	2980	52	549	5.5

Continued

Sample Number	pH	El. Cond. (dS/m)	Total Solids (mg/L)	Dissolved Solids (mg/L)	Total Alpha (Bq/L)	Total Beta (Bq/L)	Run Time (hours)
ORNL 2-19	9.32	4600	38520	6780	18	425	7.5
ORNL 2-20	10.15	12000	55200	15440	72	63	9.5
ORNL 2-21	10.05	15000	79940	23640	68	804	11.5
ORNL 2-2	9.92	24500	119220	31240	68	1146	13.5
ORNL 2-23	9.37	14000	50240	20140	36	477	15.8
ORNL 2-24	8.92	14000	47900	18380	43	430	17.6
ORNL 1-20	8.42	13500	43940	19640	65	427	19.5
ORNL 1-21	8.04	9550	43160	18940	61	402	21.5
ORNL 1-22	7.94	12000	42260	18260	59	380	23.5
ORNL 1-23	7.36	14000	40920	16500	43	345	25.5
ORNL 1-24	4.58	16000	41880	21060	70	414	28
ORNL 2-25	3.63	13000	39940	20460	36	427	30.2
ORNL 2-26	3.28	13000	39340	19100	63	481	31.6
ORNL 2-27	3.04	15000	36720	18200	47	493	33.4
ORNL 2-28	2.61	14500	34500	18000	34	509	35.5
ORNL 2-29	2.28	14500	30200	16960	40	453	37.7
ORNL 2-30	2.11	14500	25640	15580	34	473	39.5
ORNL 2-31	2.06	12500	22280	13100	34	443	41.5
ORNL 2-32	1.95	12000	12980	12380	31	438	43.5
ORNL 2-33	1.9	12000	16820	11080	45	374	45.5
ORNL 2-34	1.94	11500	13880	9080	25	351	47.8
ORNL 2-35	1.92	11000	12800	7980	25	354	49.5
ORNL 2-36	1.91	10500	11280	7620	38	317	51.5
ORNL 2-37	1.89	10000	10940	8240	29	318	53.5
ORNL 2-38	1.94	10000	9840	7340	54	302	55.6
ORNL 2-39	1.98	9400	9540	7120	38	327	57.5
ORNL 2-40	2.02	8900	8560	6820	65	309	59.5
ORNL 2-41	2.06	8000	8020	6280	63	281	61.5
ORNL 2-42	2.12	8500	7560	6940	63	279	63.5
ORNL 2-43	2.05	8600	7040	5920	36	235	65.5
ORNL 2-44	2.05	8600	6780	5580	84	218	67.5
ORNL 2-45	2.08	7100	6660	5140	36	203	69.5
ORNL 2-46	2.14	7000	5220	5000	77	157	71.8
ORNL 2-47	2.17	6900	5140	4600	65	170	73.5
ORNL 2-48	2.19	6100	5040	5460	29	171	75.5
ORNL 2-49	2.27	6200	4980	4760	52	156	77.5
ORNL 2-50	2.31	5900	4920	4160	50	174	79.5
ORNL 2-51	2.43	5800	5280	3540	63	145	81.5

Continued

Sample Number	pH	El. Cond. (dS/m)	Total Solids (mg/L)	Dissolved Solids (mg/L)	Total Alpha (Bq/L)	Total Beta (Bq/L)	Run Time (hours)
ORNL 2-52	2.46	5500	4700	4440	45	148	83.5
ORNL 2-53	2.42	5600	4680	4000	63	154	85.5
ORNL 2-54	2.33	5600	4380	4120	45	142	87.5
ORNL 2-55	2.21	6500	4260	3360	47	125	89.5
ORNL 2-56	2.09	7600	4460	3500	22	99	91.5
ORNL 2-57	2.07	7500	4240	3260	43	110	93.5
ORNL 2-58	2.15	6300	3720	3440	38	108	95.5
ORNL 2-59	3.04	4950	2900	2940	81	129	97.5
ORNL 2-60	2.98	4800	3740	3240	63	138	99.5
ORNL 2-61	2.77	5100	3680	3300	54	97	101.5
ORNL 2-62	2.38	6500	4180	3660	65	134	103.5
ORNL 2-63	2.2	8000	6220	5000	72	158	105.5
ORNL 2-64	2.11	8500	5940	5180	72	190	107.5
ORNL 2-65	2.01	7600	6340	5240	59	224	109.5
ORNL 2-66	2.01	8400	6320	5140	63	213	110.5
ORNL 2-67	2.03	7300	6340	6040	68	220	111.5
ORNL 2-68	7.18	1950	2540	1820	97	92	112.6
ORNL 2-69	6.85	1750	6720	1460	311	3557	112.8
ORNL 2-70	7.08	1500	4980	1140	188	1794	112.9
DRUM-1	6.65	3050	9940	3820	197	2055	
DRUM-2	6.28	1600	8480	2320	43	493	
DRUM-3	6.13	12000	19520	12740	45	316	
DRUM-4	2.76	9900	12200	9200	38	355	
DRUM-5	2.86	6900	10460	5680	18	253	
DRUM-6	4.57	5700	5960	4580	45	196	
DRUM-7	3.1	5100	4760	3840	29	130	
DRUM-8	3.29	6200	7760	4580	79	238	
DRUM-9	4.73	5900	6180	3780	31	181	
DRUM-10	6.85	2500	3940	1480	61	89	
DRUM-11	6.91	2400	2720	1940	9	50	
WELL-NE	6.9	570	1540	240	-2	2	
WELL-SE	6.8	710	280	160	0	-1	
WELL-SW	7	580	220	280	-2	0	
WELL-NW	6.9	520	640	240	-2	-2	

Drum Numbers indicate the sequential drum number from which samples were taken after transfer of the scrubber solutions from the ISV process trailer. Well numbers indicate the four groundwater monitoring wells surrounding the ISV site.

Sample	Soluble Alkalinity (mg/L)	Soluble Acidity (mg/L)	Total Alpha (cp10min)	Total Beta (cp10min)	Soluble Alpha (cp10min)	Soluble Beta (cp10min)	Run Time (hours)
ORNL 1-1	369		85	4046	9	540	-451.8
ORNL 1-2	451	22	79	3869	19	586	-450.5
ORNL 1-3	467	9	85	3615	3	385	-448.5
ORNL 1-4	96	174	84	4162	11	779	-446.5
ORNL 1-5	10	449	90	4816	17	620	-444
ORNL 1-6	10	460	104	4970	11	540	-442.5
ORNL 1-7	11	327	97	4371	8	590	-441.5
ORNL 1-8	33	478	101	4834	6	559	-438.5
ORNL 1-9			95	4452	7	520	-436.6
ORNL 1-10	24	360	87	3903	8	493	-434.6
ORNL 1-11	28	398	80	4510	11	625	-424.5
ORNL 1-12	136	60	48	1321	9	358	-19
ORNL 1-13	213	49	36	1371	8	448	-17.7
ORNL 1-14	212	97	37	1456	5	403	-16.5
ORNL 1-15	205	81	33	1505	13	455	-14.1
ORNL 1-16	181	68	32	1107	8	418	1.5
ORNL 1-17	272	141	27	1122	5	416	3.5
ORNL 1-18	338	132	22	1058	7	362	5.5
ORNL 2-1	580	5	63	2062	6	297	-451.8
ORNL 2-2	720	0	69	2144	6	303	-450.5
ORNL 2-3	860	0	52	1849	13	302	-448.5
ORNL 2-4	1650	0	59	1654	6	318	-446.5
ORNL 2-5	720	75	67	2310	3	318	-444
ORNL 2-6	670	34	70	2390	6	312	-442.5
ORNL 2-7	850	0	62	2292	3	279	-441.5
ORNL 2-8	900	0	87	2336	10	283	-438.5
ORNL 2-9	880	43	60	1873	4	271	-436.6
ORNL 2-10	810	81	61	1764	7	277	-434.6
ORNL 2-11	820	69	63	2820	8	274	-424.5
ORNL 2-12	190	58	38	1367	4	327	-19
ORNL 2-13	310	160	28	1127	9	320	-17.7
ORNL 2-14	330	169	40	1219	7	309	-16.5
ORNL 2-15	330	108	27	1039	6	329	-14.1
ORNL 2-16	340	64	41	1067	14	353	1.5
ORNL 2-17	540	157	33	1132	6	306	3.5
ORNL 2-18	650	130	26	940	7	279	5.5
ORNL 2-19	2630	0	11	709	6	105	7.5
ORNL 2-20	9070	0	35	993	3	128	9.5
ORNL 2-21	15170	0	33	1178	5	110	11.5

Continued

Sample	Soluble Alkalinity (mg/L)	Soluble Acidity (mg/L)	Total Alpha (cp10min)	Total Beta (cp10min)	Soluble Alpha (cp10min)	Soluble Beta (cp10min)	Run Time (hours)
ORNL 2-22	22600	0	33	1488	8	164	13.5
ORNL 2-23	10600	0	19	770	7	122	15.8
ORNL 2-24	10510	0	22	702	3	179	17.6
ORNL 1-20	948	0	32	703	4	156	19.5
ORNL 1-21	776	0	30	666	5	233	21.5
ORNL 1-22	592	0	29	632	6	192	23.5
ORNL 1-23	267	0	22	579	5	138	25.5
ORNL 1-24	0	1209	34	687	16	297	28
ORNL 2-25	0	1550	19	710	21	473	30.2
ORNL 2-26	0	1526	31	797	13	506	31.6
ORNL 2-27	0	1540	24	821	17	673	33.4
ORNL 2-28	0	1946	18	850	14	637	35.5
ORNL 2-29	0	2054	21	769	26	725	37.7
ORNL 2-30	0	2080	18	809	11	802	39.5
ORNL 2-31	0	0	18	766	12	678	41.5
ORNL 2-32	0	2240	17	773	14	688	43.5
ORNL 2-33	0	2140	23	661	14	638	45.5
ORNL 2-34	0	2040	14	627	17	564	47.8
ORNL 2-35	0	1840	14	632	17	545	49.5
ORNL 2-36	0	1880	20	273	11	526	51.5
ORNL 2-37	0	1950	16	575	12	499	53.5
ORNL 2-38	0	1760	27	549	14	551	55.6
ORNL 2-39	0	1660	20	592	16	442	57.5
ORNL 2-40	0	1520	32	563	12	430	59.5
ORNL 2-41	0	1310	31	516	12	431	61.5
ORNL 2-42	0	1450	31	512	7	390	63.5
ORNL 2-43	0	1480	19	438	15	309	65.5
ORNL 2-44	0	1560	40	409	8	301	67.5
ORNL 2-45	0	1340	19	384	8	298	69.5
ORNL 2-46	0	1190	37	307	7	281	71.8
ORNL 2-47	0	1080	32	329	9	252	73.5
ORNL 2-48	0	1210	16	330	7	241	75.5
ORNL 2-49	0	1030	26	305	7	253	77.5
ORNL 2-50	0	1050	25	336	11	250	79.5
ORNL 2-51	0	1020	31	286	8	243	81.5
ORNL 2-52	0	1000	23	292	10	239	83.5
ORNL 2-53	0	1080	31	301	7	228	85.5
ORNL 2-54	0	1080	23	281	12	202	87.5
ORNL 2-55	0	1280	24	252	8	191	89.5
ORNL 2-56	0	1540	13	207	7	209	91.5

Continued

Sample	Soluble Alkalinity (mg/L)	Soluble Acidity (mg/L)	Total Alpha (cp10min)	Total Beta (cp10min)	Soluble Alpha (cp10min)	Soluble Beta (cp10min)	Run Time (hours)
ORNL 2-57	0	1430	22	227	14	159	93.5
ORNL 2-58	0	1370	20	223	12	200	95.5
ORNL 2-59	0	810	39	260	4	178	97.5
ORNL 2-60	0	740	31	275	13	181	99.5
ORNL 2-61	0	810	27	204	14	151	101.5
ORNL 2-62	0	1330	32	268	5	171	103.5
ORNL 2-63	0	1740	35	308	2	216	105.5
ORNL 2-64	0	2010	35	363	11	263	107.5
ORNL 2-65	0	2110	29	420	1	298	109.5
ORNL 2-66	0	2217	31	402	4	296	110.5
ORNL 2-67	0	2450	33	413	7	260	111.5
ORNL 2-68	550	15	46	197	3	79	112.6
ORNL 2-69	370	0	140	6100	6	475	112.8
ORNL 2-70	530	0	86	3107	8	228	112.9
DRUM-1	425	210	90	3514	5	595	
DRUM-2	282	157	22	875	10	327	
DRUM-3	198	697	23	561	8	224	
DRUM-4	0	1661	20	636	18	594	
DRUM-5	0	1350	11	466	9	412	
DRUM-6	0	1020	23	373	4	326	
DRUM-7	0	1080	16	261	12	229	
DRUM-8	0	1320	38	442	8	323	
DRUM-9	0	980	17	346	6	143	
DRUM-10	450	86	30	190	3	75	
DRUM-11	519	137	7	123	2	74	
WELL-NE	246	0	2	41	3	35	
WELL-SE	273	0	3	35	1	25	
WELL-SW	260	0	2	36	2	24	
WELL-NW	219	0	2	32	2	27	

Sample	Total (Solids	Dissolved mg/5mL)	Sample Month	Sample Day	Sample Hour	Sample Minute	Tank Volume (liters)
ORNL 1-1	30.4	7.3	6	25	13	40	100
ORNL 1-2	32.8	8.7	6	25	15	0	103
ORNL 1-3	38.8	9.4	6	25	17	0	126
ORNL 1-4	49.7	11.6	6	25	19	0	139
ORNL 1-5	69.1	17.6	6	25	21	30	118
ORNL 1-6	72.8	27.5	6	25	23	0	116
ORNL 1-7	67.5	17.2	6	26	0	0	115
ORNL 1-8	75.4	19.6	6	26	3	0	106
ORNL 1-9	73.7	19.6	6	26	4	50	114
ORNL 1-10	75.6	18.1	6	26	6	50	125
ORNL 1-11	73.1	19.8	6	26	17	0	1
ORNL 1-12	17.9	6.4	7	13	14	30	135
ORNL 1-13	22.4	7.8	7	13	15	45	153
ORNL 1-14	26.4	8.7	7	13	17	0	130
ORNL 1-15	30.7	8.5	7	13	19	20	122
ORNL 1-16	20.4	6.2	7	14	11	0	133
ORNL 1-17	43.8	9.1	7	14	13	0	118
ORNL 1-18	57.9	10.7	7	14	15	0	133
ORNL 2-1	19.3	6.5	6	25	13	40	150
ORNL 2-2	23.4	7.8	6	25	15	0	116
ORNL 2-3	31.2	9.9	6	25	17	0	117
ORNL 2-4	38.8	10.5	6	25	19	0	122
ORNL 2-5	54.4	12.9	6	25	21	30	112
ORNL 2-6	66.1	13.5	6	25	23	0	106
ORNL 2-7	65.5	17.3	6	26	0	0	110
ORNL 2-8	79	27.2	6	26	3	0	105
ORNL 2-9	63.5	17.7	6	26	4	50	121
ORNL 2-10	56.1	17.2	6	26	6	50	125
ORNL 2-11	62.8	16.8	6	26	17	0	118
ORNL 2-12	20.5	7.5	7	13	14	30	136
ORNL 2-13	28.9	10.3	7	13	15	45	135
ORNL 2-14	39.6	9.3	7	13	17	0	139
ORNL 2-15	39.9	10.4	7	13	19	20	128
ORNL 2-16	41.5	12.7	7	14	11	0	159
ORNL 2-17	82.6	16.9	7	14	13	0	171
ORNL 2-18	111.8	14.9	7	14	15	0	180
ORNL 2-19	192.6	33.9	7	14	17	0	197
ORNL 2-20	276	77.2	7	14	19	0	274
ORNL 2-21	399.7	118.2	7	14	21	0	261
ORNL 2-22	596.1	156.2	7	14	23	0	286

Continued

Sample	Total Solids (mg/5mL)	Dissolved (mg/5mL)	Sample Month	Sample Day	Sample Hour	Sample Minute	Tank Volume (liters)
ORNL 2-23	251.2	100.7	7	15	1	15	299
ORNL 2-24	239.5	91.9	7	15	3	5	301
ORNL 1-20	219.7	98.2	7	15	5	0	314
ORNL 1-21	215.8	94.7	7	15	7	0	319
ORNL 1-22	211.3	91.3	7	15	9	0	283
ORNL 1-23	204.6	82.5	7	15	11	0	316
ORNL 1-24	209.4	105.3	7	15	13	30	250
ORNL 2-25	199.7	102.3	7	15	15	40	307
ORNL 2-26	196.7	95.5	7	15	17	5	313
ORNL 2-27	183.6	91	7	15	18	55	319
ORNL 2-28	172.5	90	7	15	21	0	276
ORNL 2-29	151	84.8	7	15	23	8	318
ORNL 2-30	128.2	77.9	7	16	1	0	257
ORNL 2-31	111.4	65.5	7	16	3	0	310
ORNL 2-32	64.9	61.9	7	16	5	0	222
ORNL 2-33	84.1	55.4	7	16	7	0	304
ORNL 2-34	69.4	45.4	7	16	9	15	311
ORNL 2-35	64	39.9	7	16	11	0	271
ORNL 2-36	56.4	38.1	7	16	13	0	305
ORNL 2-37	54.7	41.2	7	16	15	0	320
ORNL 2-38	49.2	36.7	7	16	17	5	239
ORNL 2-39	47.7	35.6	7	16	19	0	305
ORNL 2-40	42.8	34.1	7	16	21	0	322
ORNL 2-41	40.1	31.4	7	16	22	55	262
ORNL 2-42	37.8	34.7	7	17	1	0	308
ORNL 2-43	35.2	29.6	7	17	3	0	319
ORNL 2-44	33.9	27.9	7	17	5	0	293
ORNL 2-45	33.3	25.7	7	17	7	0	236
ORNL 2-46	26.1	25	7	17	9	15	310
ORNL 2-47	25.7	23	7	17	11	0	265
ORNL 2-48	25.2	27.3	7	17	13	0	300
ORNL 2-49	24.9	23.8	7	17	15	0	305
ORNL 2-50	24.6	20.8	7	17	17	0	314
ORNL 2-51	26.4	17.7	7	17	19	0	250
ORNL 2-52	23.5	22.2	7	17	21	0	310
ORNL 2-53	23.4	20	7	17	23	0	280
ORNL 2-54	21.9	20.6	7	18	1	0	247
ORNL 2-55	21.3	16.8	7	18	3	0	307
ORNL 2-56	22.3	17.5	7	18	5	0	322
ORNL 2-57	21.2	16.3	7	18	7	0	258

Continued

Sample	Total Solids (mg/5mL)	Dissolved (mg/5mL)	Sample Month	Sample Day	Sample Hour	Sample Minute	Tank Volume (liters)
ORNL 2-58	18.6	17.2	7	18	9	0	248
ORNL 2-59	14.5	14.7	7	18	11	0	305
ORNL 2-60	18.7	16.2	7	18	13	0	307
ORNL 2-61	18.4	16.5	7	18	15	0	323
ORNL 2-62	20.9	18.3	7	18	17	0	326
ORNL 2-63	31.1	25	7	18	19	0	309
ORNL 2-64	29.7	25.9	7	18	21	0	314
ORNL 2-65	31.7	26.2	7	18	23	0	313
ORNL 2-66	31.6	25.7	7	19	0	0	89
ORNL 2-67	31.7	30.2	7	19	1	0	332
ORNL 2-68	12.7	9.1	7	19	2	5	34
ORNL 2-69	33.6	7.3	7	19	2	15	49
ORNL 2-70	24.9	5.7	7	19	2	20	49
DRUM-1	49.7	19.1	8	5	10	0	
DRUM-2	42.4	11.6	8	5	10	0	
DRUM-3	97.6	63.7	8	5	10	0	
DRUM-4	61	46	8	5	10	0	
DRUM-5	52.3	28.4	8	5	10	0	
DRUM-6	29.8	22.9	8	5	10	0	
DRUM-7	23.8	19.2	8	5	10	0	
DRUM-8	38.8	22.9	8	5	10	0	
DRUM-9	30.9	18.9	8	5	10	0	
DRUM-10	19.7	7.4	8	5	10	0	
DRUM-11	13.6	9.7	8	5	10	0	
WELL-NE	7.7	1.2	8	4	10	0	
WELL-SE	1.4	0.8	8	4	10	0	
WELL-SW	1.1	1.4	8	4	10	0	
WELL-NW	3.2	1.2	8	4	10	0	

Transfer Volume is the volume of solution transferred from Tank 1 to Tank 2 or from Tank 2 to the waste drums. Total Solids in Tank is the recorded tank volume x total solids in the sample taken nearest to the tank volume measurement. Total Solids Transfer is the product of transfer volume and concentration. Cum Total Solids Transfer is the cumulative solids transferred to that time. Cum Total Solids is the cumulative amount of solids resident in or transferred from a given tank. System Total Solids is the cumulative solids in the system (tank 1 + tank 2 + transfers to drums) at a given time. Similar inventory quantities are calculated for the other water quality characteristics.

Sample	Transfer Volume (liters)	Total Solids in Tank (mg)	Total Solids Transfer (mg)	Cum Total Solids Transfer (mg)	Cum Total Solids (mg)	System Total Solids (mg)	Dissolved Solids in Tank (mg)
ORNL 1-1	0	60800	0	0	608000	146000	
ORNL 1-2	0	675680	0	0	675680	179220	
ORNL 1-3	0	977760	0	0	977760	236880	
ORNL 1-4	0	1381660	0	0	1381660	322480	
ORNL 1-5	0	1630760	0	0	1630760	415360	
ORNL 1-6	0	1688960	0	0	1688960	638000	
ORNL 1-7	0	1552500	0	0	1552500	395600	
ORNL 1-8	0	1598480	0	0	1598480	415520	
ORNL 1-9	0	1680360	0	0	1680360	446880	
ORNL 1-10	0	1890000	0	0	1890000	452500	
ORNL 1-11	130	14620	1900600	1900600	1915220	3960	
ORNL 1-12	0	483300	0	1900600	2383900	172800	
ORNL 1-13	0	685440	0	1900600	2586040	238680	
ORNL 1-14	0	686400	0	1900600	2587000	226200	
ORNL 1-15	0	749080	0	1900600	2649680	207400	
ORNL 1-16	0	542640	0	1900600	2443240	164920	
ORNL 1-17	0	1033680	0	1900600	2934280	214760	
ORNL 1-18	0	1540140	0	1900600	3440740	284620	
ORNL 2-1	0	579000	0	0	579000	1187000	195000
ORNL 2-2	0	542880	0	0	542880	1218560	180960
ORNL 2-3	0	730080	0	0	730080	1707840	231660
ORNL 2-4	0	946720	0	0	946720	2328380	256200
ORNL 2-5	0	1218560	0	0	1218560	2849320	288960
ORNL 2-6	0	1401320	0	0	1401320	3090280	286200
ORNL 2-7	0	1441000	0	0	1441000	2993500	380600
ORNL 2-8	0	1659000	0	0	1659000	3257480	571200
ORNL 2-9	0	1536700	0	0	1536700	3217060	428340
ORNL 2-10	0	1402500	0	0	1402500	3292500	430000
ORNL 2-11	0	1482080	0	0	1482080	3397300	396480
ORNL 2-12	0	557600	0	0	557600	2941500	204000
ORNL 2-13	0	780300	0	0	780300	3366340	278100
ORNL 2-14	0	1100880	0	0	1100880	3687880	258540

Continued

Sample	Transfer Volume (liters)	Total Solids in Tank (mg)	Total Solids Transfer (mg)	Cum Total Solids Transfer (mg)	Cum Total Solids (mg)	System Total Solids (mg)	Dissolved Solids in Tank (mg)
ORNL 2-15	0	1021440	0	0	1021440	3671120	266240
ORNL 2-16	0	1319700	0	0	1319700	3762940	403860
ORNL 2-17	0	2824920	0	0	2824920	5759200	577980
ORNL 2-18	0	4024800	0	0	4024800	7465540	536400
ORNL 2-19	0	7588440	0	0	7588440	11029180	1335660
ORNL 2-20	0	15124800	0	0	15124800	18565540	4230560
ORNL 2-21	0	20864340	0	0	20864340	24305080	6170040
ORNL 2-22	0	34096920	0	0	34096920	37537660	8934640
ORNL 2-23	0	15021760	0	0	15021760	18462500	6021860
ORNL 2-24	0	14417900	0	0	14417900	17858640	5532380
ORNL 1-20	0	13797160	0	0	13797160	17237900	6166960
ORNL 1-21	0	13768040	0	0	13768040	17208780	6041860
ORNL 1-22	56	11959580	2366560	2366560	14326140	17766880	5167580
ORNL 1-23	0	12930720	0	2366560	15297280	18738020	5214000
ORNL 1-24	69	10470000	2889720	5256280	15726280	19167020	5265000
ORNL 2-25	0	12261580	0	5256280	17517860	20958600	6281220
ORNL 2-26	0	12313420	0	5256280	17569700	21010440	5978300
ORNL 2-27	0	11713680	0	5256280	16969960	20410700	5805800
ORNL 2-28	50	9522000	1725000	6981280	16503280	19944020	4968000
ORNL 2-29	0	9603600	0	6981280	16584880	20025620	5393280
ORNL 2-30	67	6589480	1717880	8699160	15288640	18729380	4004060
ORNL 2-31	0	6906800	0	8699160	15605960	19046700	4061000
ORNL 2-32	101	2881560	1310980	10010140	12891700	16332440	2748360
ORNL 2-33	0	5113280	0	10010140	15123420	18564160	3368320
ORNL 2-34	0	4316680	0	10010140	14326820	17767560	2823880
ORNL 2-35	53	3468800	678400	10688540	14157340	17598080	2162580
ORNL 2-36	0	3440400	0	10688540	14128940	17569680	2324100
ORNL 2-37	0	3500800	0	10688540	14189340	17630080	2636800
ORNL 2-38	87	2351760	856080	11544620	13896380	17337120	1754260
ORNL 2-39	0	2909700	0	11544620	14454320	17895060	2171600
ORNL 2-40	0	2756320	0	11544620	14300940	17741680	2196040
ORNL 2-41	60	2101240	481200	12025820	14127060	17567800	1645360
ORNL 2-42	0	2328480	0	12025820	14354300	17795040	2137520
ORNL 2-43	0	2245760	0	12025820	14271580	17712320	1888480
ORNL 2-44	40	1986540	271200	12297020	14283560	17724300	1634940
ORNL 2-45	91	1571760	606060	12903080	14474840	17915580	1213040
ORNL 2-46	0	1618200	0	12903080	14521280	17962020	1550000
ORNL 2-47	50	1362100	257000	13160080	14522180	17962920	1219000
ORNL 2-48	0	1512000	0	13160080	14672080	18112820	1638000

Continued

Sample	Transfer Volume (liters)	Total Solids in Tank (mg)	Total Solids Transfer (mg)	Cum Total Solids Transfer (mg)	Cum Total Solids (mg)	System Total Solids (mg)	Dissolved Solids in Tank (mg)
ORNL 2-49	0	1518900	0	13160080	14678980	18119720	1451800
ORNL 2-50	0	1544880	0	13160080	14704960	18145700	1306240
ORNL 2-51	81	1320000	427680	13587760	14907760	18348500	885000
ORNL 2-52	0	1457000	0	13587760	15044760	18485500	1376400
ORNL 2-53	53	1310400	248040	13835800	15146200	18586940	1120000
ORNL 2-54	76	1081860	332880	14168680	15250540	18691280	1017640
ORNL 2-55	0	1307820	0	14168680	15476500	18917240	1031520
ORNL 2-56	0	1436120	0	14168680	15604800	19045540	1127000
ORNL 2-57	99	1093920	419760	14588440	15682360	19123100	841080
ORNL 2-58	74	922560	275280	14863720	15786280	19227020	853120
ORNL 2-59	0	884500	0	14863720	15748220	19188960	896700
ORNL 2-60	0	1148180	0	14863720	16011900	19452640	994680
ORNL 2-61	0	1188640	0	14863720	16052360	19493100	1065900
ORNL 2-62	0	1362680	0	14863720	16226400	19667140	1193160
ORNL 2-63	0	1921980	0	14863720	16785700	20226440	1545000
ORNL 2-64	0	1865160	0	14863720	16728880	20169620	1626520
ORNL 2-65	0	1984420	0	14863720	16848140	20288880	1640120
ORNL 2-66	235	562480	1485200	16348920	16911400	20352140	457460
ORNL 2-67	0	2104880	0	16348920	18453800	21894540	2005280
ORNL 2-68	347	86360	881380	17230300	17316660	20757400	61880
ORNL 2-69	0	329280	0	17230300	17559580	21000320	71540
ORNL 2-70	0	244020	0	17230300	17474320	20915060	55860
DRUM-1	199	0	1978060			0	
DRUM-2	140	0	1187200			0	
DRUM-3	197	0	3845440			0	
DRUM-4	193	0	2354600			0	
DRUM-5	185	0	1935100			0	
DRUM-6	196	0	1168160			0	
DRUM-7	194	0	923440			0	
DRUM-8	199	0	1544240			0	
DRUM-9	196	0	1211280			0	
DRUM-10	199	0	784060			0	
DRUM-11	76	0	206720			0	

Total Drum Inventory: 17138300

Sample	Dissolved Solids Transfer (mg)	Cum Dis. Solids Transfer (mg)	Cum Dis. Solids (mg)	System Dissolved Solids (mg)	System Suspended Solids (mg)	Gross Beta in Tank (Bq)	Gross Beta Transfer (Bq)
ORNL 1-1	0	0	146000		234800	0	
ORNL 1-2	0	0	179220		231441	0	
ORNL 1-3	0	0	236880		265104	0	
ORNL 1-4	0	0	322480		338882	0	
ORNL 1-5	0	0	415360		336300	0	
ORNL 1-6	0	0	638000		341852	0	
ORNL 1-7	0	0	395600		297045	0	
ORNL 1-8	0	0	415520		304114	0	
ORNL 1-9	0	0	446880		300846	0	
ORNL 1-10	0	0	452500		289000	0	
ORNL 1-11	514800	514800	518760		2673	347490	
ORNL 1-12	0	514800	687600		100980	0	
ORNL 1-13	0	514800	753480		119034	0	
ORNL 1-14	0	514800	741000		107770	0	
ORNL 1-15	0	514800	722200		104920	0	
ORNL 1-16	0	514800	679720		82992	0	
ORNL 1-17	0	514800	729560		75402	0	
ORNL 1-18	0	514800	799420		80465	0	
ORNL 2-1	0	0	195000	341000	846000	177000	0
ORNL 2-2	0	0	180960	360180	858380	142680	0
ORNL 2-3	0	0	231660	468540	1239300	124254	0
ORNL 2-4	0	0	256200	578680	1749700	116022	0
ORNL 2-5	0	0	288960	704320	2145000	150752	0
ORNL 2-6	0	0	286200	924200	2166080	148506	0
ORNL 2-7	0	0	380600	776200	2217300	147620	0
ORNL 2-8	0	0	571200	986720	2270760	144585	0
ORNL 2-9	0	0	428340	875220	2341840	132132	0
ORNL 2-10	0	0	430000	882500	2410000	127875	0
ORNL 2-11	0	0	396480	915240	2482060	195290	0
ORNL 2-12	0	0	204000	891600	2049900	105400	0
ORNL 2-13	0	0	278100	1031580	2334760	86130	0
ORNL 2-14	0	0	258540	999540	2688340	96605	0
ORNL 2-15	0	0	266240	988440	2682680	75392	0
ORNL 2-16	0	0	403860	1083580	2679360	96354	0
ORNL 2-17	0	0	577980	1307540	4451660	112347	0
ORNL 2-18	0	0	536400	1335820	6129720	98820	0
ORNL 2-19	0	0	1335660	2135080	8894100	83725	0
ORNL 2-20	0	0	4230560	5029980	13535560	172620	0
ORNL 2-21	0	0	6170040	6969460	17335620	209844	0
ORNL 2-22	0	0	8934640	9734060	27803600	327756	0

Continued

Sample	Dissolved Solids Transfer (mg)	Cum Dis. Solids Transfer (mg)	Cum Dis. Solids (mg)	System Dissolved Solids (mg)	System Suspended Solids (mg)	Gross Beta in Tank (Bq)	Gross Beta Transfer (Bq)
ORNL 2-23	0	0	6021860	6821280	11641220	142623	0
ORNL 2-24	0	0	5532380	6331800	11526840	129430	0
ORNL 1-20	0	0	6166960	6966380	10271520	134078	0
ORNL 1-21	0	0	6041860	6841280	10367500	128238	0
ORNL 1-22	1022560	1022560	6190140	6989560	10777320	107540	21280
ORNL 1-23	0	1022560	6236560	7035980	11702040	109020	0
ORNL 1-24	1453140	2475700	7740700	8540120	10626900	103500	28566
ORNL 2-25	0	2475700	8756920	9556340	11402260	131089	0
ORNL 2-26	0	2475700	8454000	9253420	11757020	150553	0
ORNL 2-27	0	2475700	8281500	9080920	11329780	157267	0
ORNL 2-28	900000	3375700	8343700	9143120	10800900	140484	25450
ORNL 2-29	0	3375700	8768980	9568400	10457220	144054	0
ORNL 2-30	1043860	4419560	8423620	9223040	9506340	121561	31691
ORNL 2-31	0	4419560	8480560	9279980	9766720	137330	0
ORNL 2-32	1250380	5669940	8418300	9217720	7114720	97236	44238
ORNL 2-33	0	5669940	9038260	9837680	8726480	113696	0
ORNL 2-34	0	5669940	8493820	9293240	8474320	109161	0
ORNL 2-35	422940	6092880	8255460	9054880	8543200	95934	18762
ORNL 2-36	0	6092880	8416980	9216400	8353280	96685	0
ORNL 2-37	0	6092880	8729680	9529100	8100980	101760	0
ORNL 2-38	638580	6731460	8485720	9285140	8051980	72178	26274
ORNL 2-39	0	6731460	8903060	9702480	8192580	99735	0
ORNL 2-40	0	6731460	8927500	9726920	8014760	99498	0
ORNL 2-41	376800	7108260	8753620	9553040	8014760	73622	16860
ORNL 2-42	0	7108260	9245780	10045200	7749840	85932	0
ORNL 2-43	0	7108260	8996740	9796160	7916160	74965	0
ORNL 2-44	223200	7331460	8966400	9765820	7958480	63874	8720
ORNL 2-45	467740	7799200	9012240	9811660	8103920	47908	18473
ORNL 2-46	0	7799200	9349200	10148620	7813400	48670	0
ORNL 2-47	230000	8029200	9248200	10047620	7915300	45050	8500
ORNL 2-48	0	8029200	9667200	10466620	7646200	51300	0
ORNL 2-49	0	8029200	9481000	10280420	7839300	47580	0
ORNL 2-50	0	8029200	9335440	10134860	8010840	54636	0
ORNL 2-51	286740	8315940	9200940	10000360	8348140	36250	11745
ORNL 2-52	0	8315940	9692340	10491760	7993740	45880	0
ORNL 2-53	212000	8527940	9647940	10447360	8139580	43120	8162
ORNL 2-54	313120	8841060	9858700	10658120	8033160	35074	10792
ORNL 2-55	0	8841060	9872580	10672000	8245240	38375	0
ORNL 2-56	0	8841060	9968060	10767480	8278060	31878	0

Continued

Sample	Dissolved Solids Transfer (mg)	Cum Dis. Solids Transfer (mg)	Cum Dis. Solids (mg)	System Dissolved Solids (mg)	System Suspended Solids (mg)	Gross Beta in Tank (Bq)	Gross Beta Transfer (Bq)
ORNL 2-57	322740	9163800	10004880	10804300	8318800	28380	10890
ORNL 2-58	254560	9418360	10271480	11070900	8156120	26784	7992
ORNL 2-59	0	9418360	10315060	11114480	8074480	39345	0
ORNL 2-60	0	9418360	10413040	11212460	8240180	42366	0
ORNL 2-61	0	9418360	10484260	11283680	8209420	31331	0
ORNL 2-62	0	9418360	10611520	11410940	8256200	43684	0
ORNL 2-63	0	9418360	10963360	11762780	8463660	48822	0
ORNL 2-64	0	9418360	11044880	11844300	8325320	59660	0
ORNL 2-65	0	9418360	11058480	11857900	8430980	70112	0
ORNL 2-66	1207900	10626260	11083720	11883140	8469000	18957	50055
ORNL 2-67	0	10626260	12631540	13430960	8463580	73040	0
ORNL 2-68	631540	11257800	11319680	12119100	8638300	3128	31924
ORNL 2-69	0	11257800	11329340	12128760	8871560	174293	0
ORNL 2-70	0	11257800	11313660	12113080	8801980	87906	0
DRUM-1	760180			0	408945		
DRUM-2	324800			0	69020		
DRUM-3	2509780			0	62252		
DRUM-4	1775600			0	68515		
DRUM-5	1050800			0	46805		
DRUM-6	897680			0	38416		
DRUM-7	744960			0	25220		
DRUM-8	911420			0	47362		
DRUM-9	740880			0	35476		
DRUM-10	294520			0	17711		
DRUM-11	147440			0	3800		
Drum Total =	10158060				823522		

Sample	Cum Gross Beta Transfer (Bq)	Cum Gross Beta (Bq)	System Gross Beta (Bq)	Alkalinty in Tank (mg CaCO ₃)	Alkalinity Transfer (mg)	Cum Alkalinity (mg)	Cum Alkalinity Transfer (mg)
ORNL 1-1	0	234800	36900	0	0	36900	
ORNL 1-2	0	231441	46453	0	0	46453	
ORNL 1-3	0	265104	58842	0	0	58842	
ORNL 1-4	0	338882	13344	0	0	13344	
ORNL 1-5	0	336300	1180	0	0	1180	
ORNL 1-6	0	341852	1160	0	0	1160	
ORNL 1-7	0	297045	1265	0	0	1265	
ORNL 1-8	0	304114	3498	0	0	3498	
ORNL 1-9	0	300846	0	0	0	0	
ORNL 1-10	0	289000	3000	0	0	3000	
ORNL 1-11	347490	350163	28	3640	3640	3668	
ORNL 1-12	347490	448470	18360	0	3640	22000	
ORNL 1-13	347490	466524	32589	0	3640	36229	
ORNL 1-14	347490	455260	27560	0	3640	31200	
ORNL 1-15	347490	452410	25010	0	3640	28650	
ORNL 1-16	347490	430482	24073	0	3640	27713	
ORNL 1-17	347490	422892	32096	0	3640	35736	
ORNL 1-18	347490	427955	44954	0	3640	48594	
ORNL 2-1	0	177000	411800	87000	0	0	87000
ORNL 2-2	0	142680	374121	83520	0	0	83520
ORNL 2-3	0	124254	389358	100620	0	0	100620
ORNL 2-4	0	116022	454904	201300	0	0	201300
ORNL 2-5	0	150752	487052	80640	0	0	80640
ORNL 2-6	0	148506	490358	71020	0	0	71020
ORNL 2-7	0	147620	444665	93500	0	0	93500
ORNL 2-8	0	144585	448699	94500	0	0	94500
ORNL 2-9	0	132132	432978	106480	0	0	106480
ORNL 2-10	0	127875	416875	101250	0	0	101250
ORNL 2-11	0	195290	545453	96760	0	0	96760
ORNL 2-12	0	105400	553870	25840	0	0	25840
ORNL 2-13	0	86130	552654	41850	0	0	41850
ORNL 2-14	0	96605	551865	45870	0	0	45870
ORNL 2-15	0	75392	527802	42240	0	0	42240
ORNL 2-16	0	96354	526836	54060	0	0	54060
ORNL 2-17	0	112347	535239	92340	0	0	92340
ORNL 2-18	0	98820	526775	117000	0	0	117000
ORNL 2-19	0	83725	511680	518110	0	0	518110
ORNL 2-20	0	172620	600575	2485180	0	0	2485180
ORNL 2-21	0	209844	637799	3959370	0	0	3959370
ORNL 2-22	0	327756	755711	6463600	0	0	6463600

Continued

Sample	Cum Gross Beta Transfer (Bq)	Cum Gross Beta (Bq)	System Gross Beta (Bq)	Alkalinty in Tank (mg CaCO ₃)	Alkalinity Transfer (mg)	Cum Alkalinity (mg)	Cum Alkalinity Transfer (mg)
ORNL 2-23	0	142623	570578	3169400	0	0	3169400
ORNL 2-24	0	129430	557385	3163510	0	0	3163510
ORNL 1-20	0	134078	562033	297672	0	0	297672
ORNL 1-21	0	128238	556193	247544	0	0	247544
ORNL 1-22	21280	128820	556775	167536	33152	33152	200688
ORNL 1-23	21280	130300	558255	84372	0	33152	117524
ORNL 1-24	49846	153346	581301	0	0	33152	33152
ORNL 2-25	49846	180935	608890	0	0	33152	33152
ORNL 2-26	49846	200399	628354	0	0	33152	33152
ORNL 2-27	49846	207113	635068	0	0	33152	33152
ORNL 2-28	75296	215780	643735	0	0	33152	33152
ORNL 2-29	75296	219350	647305	0	0	33152	33152
ORNL 2-30	106987	228548	656503	0	0	33152	33152
ORNL 2-31	106987	244317	672272	0	0	33152	33152
ORNL 2-32	151225	248461	676416	0	0	33152	33152
ORNL 2-33	151225	264921	692876	0	0	33152	33152
ORNL 2-34	151225	260386	688341	0	0	33152	33152
ORNL 2-35	169987	265921	693876	0	0	33152	33152
ORNL 2-36	169987	266672	694627	0	0	33152	33152
ORNL 2-37	169987	271747	699702	0	0	33152	33152
ORNL 2-38	196261	268439	696394	0	0	33152	33152
ORNL 2-39	196261	295996	723951	0	0	33152	33152
ORNL 2-40	196261	295759	723714	0	0	33152	33152
ORNL 2-41	213121	286743	714698	0	0	33152	33152
ORNL 2-42	213121	299053	727008	0	0	33152	33152
ORNL 2-43	213121	288086	716041	0	0	33152	33152
ORNL 2-44	221841	285715	713670	0	0	33152	33152
ORNL 2-45	240314	288222	716177	0	0	33152	33152
ORNL 2-46	240314	288984	716939	0	0	33152	33152
ORNL 2-47	248814	293864	721819	0	0	33152	33152
ORNL 2-48	248814	300114	728069	0	0	33152	33152
ORNL 2-49	248814	296394	724349	0	0	33152	33152
ORNL 2-50	248814	303450	731405	0	0	33152	33152
ORNL 2-51	260559	296809	724764	0	0	33152	33152
ORNL 2-52	260559	306439	734394	0	0	33152	33152
ORNL 2-53	268721	311841	739796	0	0	33152	33152
ORNL 2-54	279513	314587	742542	0	0	33152	33152
ORNL 2-55	279513	317888	745843	0	0	33152	33152
ORNL 2-56	279513	311391	739346	0	0	33152	33152

Continued

Sample	Cum Gross Beta Transfer (Bq)	Cum Gross Beta (Bq)	System Gross Beta (Bq)	Alkalinty in Tank (mg CaCO ₃)	Alkalinity Transfer (mg)	Cum Alkalinity (mg)	Cum Alkalinity Transfer (mg)
ORNL 2-57	290403	318783	746738	0	0	33152	33152
ORNL 2-58	298395	325179	753134	0	0	33152	33152
ORNL 2-59	298395	337740	765695	0	0	33152	33152
ORNL 2-60	298395	340761	768716	0	0	33152	33152
ORNL 2-61	298395	329726	757681	0	0	33152	33152
ORNL 2-62	298395	342079	770034	0	0	33152	33152
ORNL 2-63	298395	347217	775172	0	0	33152	33152
ORNL 2-64	298395	358055	786010	0	0	33152	33152
ORNL 2-65	298395	368507	796462	0	0	33152	33152
ORNL 2-66	348450	367407	795362	0	0	33152	33152
ORNL 2-67	348450	421490	849445	0	0	33152	33152
ORNL 2-68	380374	383502	811457	18700	190850	224002	242702
ORNL 2-69	380374	554667	982622	18130	0	224002	242132
ORNL 2-70	380374	468280	896235	25970	0	224002	249972
DRUM-1				0	84575		
DRUM-2				0	39480		
DRUM-3				0	39006		
DRUM-4			0	0			
DRUM-5			0	0			
DRUM-6			0	0			
DRUM-7			0	0			
DRUM-8			0	0			
DRUM-9			0	0			
DRUM-10			0	89550			
DRUM-11			0	39444			

Total Drum Inventory=292055

Sample	System Alkalinity (mg)	Acidity in Tank (mg CaCO ₃)	Acidity Transfer (mg)	Cum Acidity (mg)	Cum Acidity (mg)	System Acidity Transfer (mg)
ORNL 1-1		0	0	0	0	
ORNL 1-2		2266	0	0	2266	
ORNL 1-3		1134	0	0	1134	
ORNL 1-4		24186	0	0	24186	
ORNL 1-5		52982	0	0	52982	
ORNL 1-6		53360	0	0	53360	
ORNL 1-7		37605	0	0	37605	
ORNL 1-8		50668	0	0	50668	
ORNL 1-9		0	0	0	0	
ORNL 1-10		45000	0	0	45000	
ORNL 1-11		398	51740	51740	52138	
ORNL 1-12		8100	0	51740	59840	
ORNL 1-13		7497	0	51740	59237	
ORNL 1-14		12610	0	51740	64350	
ORNL 1-15		9882	0	51740	61622	
ORNL 1-16		9044	0	51740	60784	
ORNL 1-17		16638	0	51740	68378	
ORNL 1-18		17556	0	51740	69296	
ORNL 2-1	123900	750	0	0	750	750
ORNL 2-2	129973	0	0	0	0	2266
ORNL 2-3	159462	0	0	0	0	1134
ORNL 2-4	214644	0	0	0	0	24186
ORNL 2-5	81820	8400	0	0	8400	61382
ORNL 2-6	72180	3604	0	0	3604	56964
ORNL 2-7	94765	0	0	0	0	37605
ORNL 2-8	97998	0	0	0	0	50668
ORNL 2-9	106480	5203	0	0	5203	5203
ORNL 2-10	104250	10125	0	0	10125	55125
ORNL 2-11	100428	8142	0	0	8142	60280
ORNL 2-12	47840	7888	0	0	7888	67728
ORNL 2-13	78079	21600	0	0	21600	80837
ORNL 2-14	77070	23491	0	0	23491	87841
ORNL 2-15	70890	13824	0	0	13824	75446
ORNL 2-16	81773	10176	0	0	10176	70960
ORNL 2-17	128076	26847	0	0	26847	95225
ORNL 2-18	165594	23400	0	0	23400	92696
ORNL 2-19	566704	0	0	0	0	21196
ORNL 2-20	2533774	0	0	0	0	21196
ORNL 2-21	4007964	0	0	0	0	21196
ORNL 2-22	6512194	0	0	0	0	21196

Continued

Sample	System Alkalinity (mg)	Acidity in Tank (mg CaCO ₃)	Acidity Transfer (mg)	Cum Acidity (mg)	Cum Acidity (mg)	System Acidity Transfer (mg)
ORNL 2-23	3217994	0	0	0	0	21196
ORNL 2-24	3212104	0	0	0	0	21196
ORNL 1-20	346266	0	0	0	0	21196
ORNL 1-21	296138	0	0	0	0	21196
ORNL 1-22	249282	0	0	0	0	21196
ORNL 1-23	166118	0	0	0	0	21196
ORNL 1-24	81746	302250	83421	83421	385671	406867
ORNL 2-25	81746	475850	0	83421	559271	580467
ORNL 2-26	81746	477638	0	83421	561059	582255
ORNL 2-27	81746	491260	0	83421	574681	595877
ORNL 2-28	81746	537096	97300	180721	717817	739013
ORNL 2-29	81746	653172	0	180721	833893	855089
ORNL 2-30	81746	534560	139360	320081	854641	875837
ORNL 2-31	81746	0	0	320081	320081	341277
ORNL 2-32	81746	497280	226240	546321	1043601	1064797
ORNL 2-33	81746	650560	0	546321	1196881	1218077
ORNL 2-34	81746	634440	0	546321	1180761	1201957
ORNL 2-35	81746	498640	97520	643841	1142481	1163677
ORNL 2-36	81746	573400	0	643841	1217241	1238437
ORNL 2-37	81746	624000	0	643841	1267841	1289037
ORNL 2-38	81746	420640	153120	796961	1217601	1238797
ORNL 2-39	81746	506300	0	796961	1303261	1324457
ORNL 2-40	81746	489440	0	796961	1286401	1307597
ORNL 2-41	81746	343220	78600	875561	1218781	1239977
ORNL 2-42	81746	446600	0	875561	1322161	1343357
ORNL 2-43	81746	472120	0	875561	1347681	1368877
ORNL 2-44	81746	457080	62400	937961	1395041	1416237
ORNL 2-45	81746	316240	121940	1059901	1376141	1397337
ORNL 2-46	81746	368900	0	1059901	1428801	1449997
ORNL 2-47	81746	286200	54000	1113901	1400101	1421297
ORNL 2-48	81746	363000	0	1113901	1476901	1498097
ORNL 2-49	81746	314150	0	1113901	1428051	1449247
ORNL 2-50	81746	329700	0	1113901	1443601	1464797
ORNL 2-51	81746	255000	82620	1196521	1451521	1472717
ORNL 2-52	81746	310000	0	1196521	1506521	1527717
ORNL 2-53	81746	302400	57240	1253761	1556161	1577357
ORNL 2-54	81746	266760	82080	1335841	1602601	1623797
ORNL 2-55	81746	392960	0	1335841	1728801	1749997
ORNL 2-56	81746	495880	0	1335841	1831721	1852917

Continued

Sample	System Alkalinity (mg)	Acidity in Tank (mg CaCO ₃)	Acidity Transfer (mg)	Cum Acidity (mg)	Cum Acidity (mg)	System Acidity Transfer (mg)
ORNL 2-57	81746	368940	141570	1477411	1846351	1867547
ORNL 2-58	81746	339760	101380	1578791	1918551	1939747
ORNL 2-59	81746	247050	0	1578791	1825841	1847037
ORNL 2-60	81746	227180	0	1578791	1805971	1827167
ORNL 2-61	81746	261630	0	1578791	1840421	1861617
ORNL 2-62	81746	433580	0	1578791	2012371	2033567
ORNL 2-63	81746	537660	0	1578791	2116451	2137647
ORNL 2-64	81746	631140	0	1578791	2209931	2231127
ORNL 2-65	81746	660430	0	1578791	2239221	2260417
ORNL 2-66	81746	197313	520995	2099786	2297099	2318295
ORNL 2-67	81746	813400	0	2099786	2913186	2934382
ORNL 2-68	291296	510	5205	2104991	2105501	2126697
ORNL 2-69	290726	0	0	2104991	2104991	2126187
ORNL 2-70	298566	0	0	2104991	2104991	2126187
DRUM-1		0	41790			
DRUM-2		0	21980			
DRUM-3		0	137309			
DRUM-4		0	320573			
DRUM-5		0	249750			
DRUM-6		0	199920			
DRUM-7		0	209520			
DRUM-8		0	262680			
DRUM-9		0	192080			
DRUM-10		0	17114			
DRUM-11		0	10412			

Total Drum Inventory = 1663128

Sample Number	Al (mg/L)	Ca (mg/L)	Cs (mg/L)	Li (mg/L)	Mg (mg/L)	Na (mg/L)	Si (mg/L)
ORNL-1-1	12	5.5	1.4	1.2	6.6	89	21
ORNL-1-2	48	25	4.4	5.2	25	430	54
ORNL-1-3	44	22	4.7	7.7	22	400	40
ORNL-1-4	44	20	4.5	17	23	420	41
ORNL-1-5	51	24	6	23	26	530	52
ORNL-1-6	55	25	5.9	25	28	570	52
ORNL-1-7	45	20	4.8	30	24	520	46
ORNL-1-8	49	22	5.2	36	27	600	48
ORNL-1-9	51	21	4.6	37	28	590	53
ORNL-1-10	52	19	5.7	37	29	580	57
ORNL-1-11	55	21	5.9	38	30	610	61
ORNL-1-12	13	24	1.7	6.3	15	270	25
ORNL-1-13	12	21	1.4	11	14	300	58
ORNL-1-14	11	19	1.3	12	14	300	34
ORNL-1-15	12	21	1.8	14	15	370	49
ORNL-1-16	9.8	25	1.4	9.5	15	260	38
ORNL-1-17	11	24	1.4	29	17	420	46
ORNL-1-18	13	26	1.4	40	18	210	40
ORNL-2-1	7.5	27	1	4.5	17	350	66
ORNL-2-2	7	24	1.2	4.7	17	320	51
ORNL-2-3	9.3	29	1.9	11	20	490	60
ORNL-2-4	9.9	25	1.6	15	19	450	60
ORNL-2-5	13	30	1.8	21	24	560	62
ORNL-2-6	14	30	1.7	28	25	630	58
ORNL-2-7	14	29	2.4	34	25	690	54
ORNL-2-8	14	29	2.1	39	26	750	44
ORNL-2-9	13	27	2	40	24	710	48
ORNL-2-10	13	25	1.9	38	24	680	46
ORNL-2-11	19	28	2.1	40	26	720	48
ORNL-2-12	7.8	30	0.9	7.4	14	290	33
ORNL-2-13	7.7	28	0.9	19	15	360	36
ORNL-2-14	7.8	30	1	24	16	410	41
ORNL-2-15	7.2	28	0.9	23	16	400	41
ORNL-2-16	7.9	30	1.2	23	16	400	40
ORNL-2-17	9.2	27	1.1	59	19	370	49
ORNL-2-18	11	27	1.3	88	20	530	42
ORNL-2-19	13	29	0.7	200	25	1800	36
ORNL-2-20	15	29	2	340	32	4600	39
ORNL-2-21	25	41	1.9	320	50	7900	44
ORNL-2-22	38	67	2.9	330	75	13000	45
ORNL-2-23	16	50	1.4	370	35	6000	47
ORNL-2-24	14	49	1.3	350	33	5700	47

Continued

Sample Number	Al (mg/L)	Ca (mg/L)	Cs (mg/L)	Li (mg/L)	Mg (mg/L)	Na (mg/L)	Si (mg/L)
ORNL-1-20	13	36	1	310	30	4900	51
ORNL-1-21	13	31	1.2	270	27	4300	52
ORNL-1-22	14	44	1.2	370	31	5800	72
ORNL-1-23	14	32	1.9	330	28	5400	79
ORNL-1-24	13	40	3.1	340	30	5400	77
ORNL-2-25	11	36	3.8	240	26	4300	64
ORNL-2-26	10	36	4.4	230	26	4200	61
ORNL-2-27	11	37	4.8	230	26	4100	64
ORNL-2-28	11	35	6.4	200	24	3800	60
ORNL-2-29	10	30	7.7	160	20	3100	50
ORNL-2-30	9.3	26	7.3	130	18	2700	65
ORNL-2-31	9.1	23	8.9	100	15	2300	53
ORNL-2-32	8	19	7.7	82	13	2000	60
ORNL-2-33	7	17	8.9	67	11	1600	60
ORNL-2-34	6.3	13	7.7	49	9.5	1200	59
ORNL-2-35	6.1	13	9	46	9.1	1200	66
ORNL-2-36	5.6	11	13	41	8.5	1100	73
ORNL-2-37	5.9	14	21	45	8.8	1100	82
ORNL-2-38	7.1	14	20	42	8.4	1000	97
ORNL-2-39	5.6	11	21	33	7.3	790	81
ORNL-2-40	5.8	11	26	31	7	750	90
ORNL-2-41	4.2	9.7	31	26	6.3	650	74
ORNL-2-42	4.6	8.6	46	22	5.7	550	77
ORNL-2-43	4.2	6.8	59	17	4.8	390	76
ORNL-2-44	4.2	6.5	62	16	4.4	370	51
ORNL-2-45	4.2	5.9	60	14	4.2	310	72
ORNL-2-46	4.2	5.7	60	13	3.8	290	64
ORNL-2-47	7.2	7.1	66	15	4.2	310	65
ORNL-2-48	4.2	5.7	60	12	3.5	220	71
ORNL-2-49	4.6	6.7	67	13	3.7	280	42
ORNL-2-50	4.2	6.4	73	13	3.7	240	75
ORNL-2-51	4.2	5.3	72	11	3.3	390	72
ORNL-2-52	4.2	5	74	10	3	360	47
ORNL-2-53	4.2	4.3	78	8.3	2.7	320	7.3
ORNL-2-54	4.2	4	83	8	2.5	300	74
ORNL-2-55	4.2	3.4	90	7	2.3	260	23
ORNL-2-56	4.2	3.7	112	7.2	2.2	250	44
ORNL-2-57	4.2	3.6	114	6.6	2	220	89
ORNL-2-58	4.2	3	103	5.6	1.8	190	84
ORNL-2-59	4.2	4.1	100	5.9	1.8	180	81
ORNL-2-60	4.2	3.3	92	4.8	1.6	160	75

Continued

Sample Number	Al (mg/L)	Ca (mg/L)	Cs (mg/L)	Li (mg/L)	Mg (mg/L)	Na (mg/L)	Si (mg/L)
ORNL-2-61	4.2	3.1	93	5.5	1.6	160	94
ORNL-2-62	4.2	3.6	116	6.1	1.9	190	120
ORNL-2-63	4.6	3.4	136	5.7	2.1	200	130
ORNL-2-64	5.1	3.8	141	6.2	2.4	210	130
ORNL-2-65	5.8	4.3	137	7.1	2.5	220	170
ORNL-2-66	5.4	3.9	141	6.8	2.5	220	150
ORNL-2-67	6.4	4.1	145	7	2.8	250	140
ORNL-2-68	4.2	32	15	4.2	10	250	51
ORNL-2-69	57	41	5.7	5.4	31	380	81
ORNL-2-70	15	37	1.1	4.2	20	390	43
DRUM-1	42	39	3.4	29	30	470	67
DRUM-2	9.4	34	1.6	30	17	410	61
DRUM-3	7.3	24	3.2	170	21	3300	91
DRUM-4	6.5	20	12	68	13	1600	85
DRUM-5	4.6	9.4	46	24	6.6	560	78
DRUM-6	4.7	8.7	56	19	5.4	490	78
DRUM-7	2.9	5.4	90	18	2.7	300	87
DRUM-8	6.4	6.2	108	21	3.6	300	100
DRUM-9	4.3	12	90	15	5.2	320	99
DRUM-10	1.6	23	20	12	8.9	460	63
DRUM-11	0.59	18	19	7.9	8.4	440	64

Sample Number	Sr (mg/L)	Fe (mg/L)	Tank Vol (liters)	Trans Vol (liters)	Tank-Cs (mg)	Trans-Cs (mg)	TotranCs (mg)
ORNL-1-1	0.75	44	100	0	140	0	0
ORNL-1-2	2.7	170	103	0	453.2	0	0
ORNL-1-3	2.4	150	126	0	592.2	0	0
ORNL-1-4	2.1	130	139	0	625.5	0	0
ORNL-1-5	0.96	140	118	0	708	0	0
ORNL-1-6	2.5	140	116	0	684.4	0	0
ORNL-1-7	2	110	115	0	552	0	0
ORNL-1-8	2.2	120	106	0	551.2	0	0
ORNL-1-9	2.3	120	114	0	524.4	0	0
ORNL-1-10	2.3	120	125	0	712.5	0	0
ORNL-1-11	2.5	130	1	130	5.9	767	767
ORNL-1-12	0.54	41	135	0	229.5	0	767
ORNL-1-13	0.53	36	153	0	214.2	0	767
ORNL-1-14	0.53	36	130	0	169	0	767
ORNL-1-15	0.61	38	122	0	219.6	0	767
ORNL-1-16	0.51	31	133	0	186.2	0	767
ORNL-1-17	0.55	30	118	0	165.2	0	767
ORNL-1-18	0.52	30	133	0	186.2	0	767
ORNL-2-1	0.49	60	150	0	150	0	0
ORNL-2-2	0.47	54	116	0	139.2	0	0
ORNL-2-3	0.57	64	117	0	222.3	0	0
ORNL-2-4	0.51	54	122	0	195.2	0	0
ORNL-2-5	0.66	70	112	0	201.6	0	0
ORNL-2-6	0.68	72	106	0	180.2	0	0
ORNL-2-7	0.69	73	110	0	264	0	0
ORNL-2-8	0.72	75	105	0	220.5	0	0
ORNL-2-9	0.67	68	121	0	242	0	0
ORNL-2-10	0.66	66	125	0	237.5	0	0
ORNL-2-11	0.81	86	43	75	90.3	157.5	157.5
ORNL-2-12	0.45	33	136	0	122.4	0	157.5
ORNL-2-13	0.44	29	135	0	121.5	0	157.5
ORNL-2-14	0.46	30	139	0	139	0	157.5
ORNL-2-15	0.44	27	128	0	115.2	0	157.5
ORNL-2-16	0.48	30	159	0	190.8	0	157.5
ORNL-2-17	0.45	27	171	0	188.1	0	157.5
ORNL-2-18	0.46	27	180	0	234	0	157.5
ORNL-2-19	0.53	31	197	0	137.9	0	157.5
ORNL-2-20	0.51	33	274	0	548	0	157.5
ORNL-2-21	0.68	55	261	0	495.9	0	157.5
ORNL-2-22	0.92	82	286	0	829.4	0	157.5
ORNL-2-23	0.52	35	299	0	418.6	0	157.5
ORNL-2-24	0.5	32	301	0	391.3	0	157.5

Continued

Sample Number	Sr (mg/L)	Fe (mg/L)	Tank Vol (liters)	Trans Vol (liters)	Tank-Cs (mg)	Trans-Cs (mg)	TotranCs (mg)
ORNL-1-20	0.46	30	314	0	314	0	157.5
ORNL-1-21	0.44	27	319	0	382.8	0	157.5
ORNL-1-22	0.48	27	283	56	339.6	67.2	224.7
ORNL-1-23	0.44	25	316	0	600.4	0	224.7
ORNL-1-24	0.49	24	250	69	775	213.9	438.6
ORNL-2-25	0.48	24	307	0	1166.6	0	438.6
ORNL-2-26	0.49	26	313	0	1377.2	0	438.6
ORNL-2-27	0.51	29	319	0	1531.2	0	438.6
ORNL-2-28	0.51	29	276	50	1766.4	320	758.6
ORNL-2-29	0.47	31	318	0	2448.6	0	758.6
ORNL-2-30	0.44	33	257	67	1876.1	489.1	1247.7
ORNL-2-31	0.42	35	310	0	2759	0	1247.7
ORNL-2-32	0.38	36	222	101	1709.4	777.7	2025.4
ORNL-2-33	0.35	36	304	0	2705.6	0	2025.4
ORNL-2-34	0.3	34	311	0	2394.7	0	2025.4
ORNL-2-35	0.29	35	271	53	2439	477	2502.4
ORNL-2-36	0.28	35	305	0	3965	0	2502.4
ORNL-2-37	0.25	36	320	0	6720	0	2502.4
ORNL-2-38	0.26	39	239	87	4780	1740	4242.4
ORNL-2-39	0.22	38	305	0	6405	0	4242.4
ORNL-2-40	0.22	40	322	0	8372	0	4242.4
ORNL-2-41	0.2	39	262	60	8122	1860	6102.4
ORNL-2-42	0.18	38	308	0	14168	0	6102.4
ORNL-2-43	0.15	37	319	0	18821	0	6102.4
ORNL-2-44	0.15	41	293	40	18166	2480	8582.4
ORNL-2-45	0.14	46	236	91	14160	5460	14042.4
ORNL-2-46	0.13	50	310	0	18600	0	14042.4
ORNL-2-47	0.16	100	265	50	17490	3300	17342.4
ORNL-2-48	0.14	69	300	0	18000	0	17342.4
ORNL-2-49	0.15	83	305	0	20435	0	17342.4
ORNL-2-50	0.15	95	314	0	22922	0	17342.4
ORNL-2-51	0.13	91	250	81	18000	5832	23174.4
ORNL-2-52	0.13	92	310	0	22940	0	23174.4
ORNL-2-53	0.12	87	280	53	21840	4134	27308.4
ORNL-2-54	0.11	86	247	76	20501	6308	33616.4
ORNL-2-55	0.1	86	307	0	27630	0	33616.4
ORNL-2-56	0.11	80	322	0	36064	0	33616.4
ORNL-2-57	0.1	78	258	99	29412	11286	44902.4
ORNL-2-58	0.1	75	248	74	25544	7622	52524.4
ORNL-2-59	0.11	72	305	0	30500	0	52524.4
ORNL-2-60	0.1	61	307	0	28244	0	52524.4

Continued

Sample Number	Sr (mg/L)	Fe (mg/L)	Tank Vol (liters)	Trans Vol (liters)	Tank-Cs (mg)	Trans-Cs (mg)	TotranCs (mg)
ORNL-2-61	0.1	60	323	0	30039	0	52524.4
ORNL-2-62	0.12	70	326	0	37816	0	52524.4
ORNL-2-63	0.13	74	309	0	42024	0	52524.4
ORNL-2-64	0.14	80	314	0	44274	0	52524.4
ORNL-2-65	0.15	82	313	0	42881	0	52524.4
ORNL-2-66	0.15	83	89	235	12549	33135	85659.4
ORNL-2-67	0.16	90	97	0	14065	0	85659.4
ORNL-2-68	0.17	16	34	347	510	5205	90864.4
ORNL-2-69	3.3	220	49	0	279.3	0	90864.4
ORNL-2-70	0.59	99	49	0	53.9	0	90864.4
DRUM-1	1.4	120	0	199	0	676.6	
DRUM-2	0.54	120	0	140	0	224	
DRUM-3	0.41	130	0	197	0	630.4	
DRUM-4	0.32	210	0	193	0	2316	
DRUM-5	0.2	320	0	185	0	8510	
DRUM-6	0.18	570	0	196	0	10976	
DRUM-7	0.1	320	0	194	0	17460	
DRUM-8	0.14	330	0	199	0	21492	
DRUM-9	0.13	360	0	196	0	17640	
DRUM-10	0.11	21	0	199	0	3980	
DRUM-11	0.09	40	0	76	0	1444	

Total Drum Inventory= 85349

Sample Number	Cum-Cs (mg)	SysCumCs (mg)	Run Time (hours)
ORNL-1-1	140		-451.8
ORNL-1-2	453.2		-450.5
ORNL-1-3	592.2		-448.5
ORNL-1-4	625.5		-446.5
ORNL-1-5	708		-444
ORNL-1-6	684.4		-442.5
ORNL-1-7	552		-441.5
ORNL-1-8	551.2		-438.5
ORNL-1-9	524.4		-436.6
ORNL-1-10	712.5		-434.6
ORNL-1-11	772.9		-424.5
ORNL-1-12	996.5		-19
ORNL-1-13	981.2		-17.7
ORNL-1-14	936		-16.5
ORNL-1-15	986.6		-14.1
ORNL-1-16	953.2		1.5
ORNL-1-17	932.2		3.5
ORNL-1-18	953.2		5.5
ORNL-2-1	150	290	-451.8
ORNL-2-2	139.2	592.4	-450.5
ORNL-2-3	222.3	814.5	-448.5
ORNL-2-4	195.2	820.7	-446.5
ORNL-2-5	201.6	909.6	-444
ORNL-2-6	180.2	864.6	-442.5
ORNL-2-7	264	816	-441.5
ORNL-2-8	220.5	771.7	-438.5
ORNL-2-9	242	766.4	-436.6
ORNL-2-10	237.5	950	-434.6
ORNL-2-11	247.8	1020.7	-424.5
ORNL-2-12	279.9	1276.4	-19
ORNL-2-13	279	1260.2	-17.7
ORNL-2-14	296.5	1232.5	-16.5
ORNL-2-15	272.7	1259.3	-14.1
ORNL-2-16	348.3	1301.5	1.5
ORNL-2-17	345.6	1277.8	3.5
ORNL-2-18	391.5	1344.7	5.5
ORNL-2-19	295.4	445.4	7.5
ORNL-2-20	705.5	855.5	9.5
ORNL-2-21	653.4	803.4	11.5
ORNL-2-22	986.9	1136.9	13.5
ORNL-2-23	576.1	726.1	15.8
ORNL-2-24	548.8	698.8	17.6

Continued

Sample Number	Cum-Cs (mg)	SysCumCs (mg)	Run Time (hours)
ORNL-1-20	471.5	621.5	19.5
ORNL-1-21	540.3	690.3	21.5
ORNL-1-22	564.3	714.3	23.5
ORNL-1-23	825.1	975.1	25.5
ORNL-1-24	1213.6	1363.6	28
ORNL-2-25	1605.2	1755.2	30.2
ORNL-2-26	1815.8	1965.8	31.6
ORNL-2-27	1969.8	2119.8	33.4
ORNL-2-28	2525	2675	35.5
ORNL-2-29	3207.2	3357.2	37.7
ORNL-2-30	3123.8	3273.8	39.5
ORNL-2-31	4006.7	4156.7	41.5
ORNL-2-32	3734.8	3884.8	43.5
ORNL-2-33	4731	4881	45.5
ORNL-2-34	4420.1	4570.1	47.8
ORNL-2-35	4941.4	5091.4	49.5
ORNL-2-36	6467.4	6617.4	51.5
ORNL-2-37	9222.4	9372.4	53.5
ORNL-2-38	9022.4	9172.4	55.6
ORNL-2-39	10647.4	10797.4	57.5
ORNL-2-40	12614.4	12764.4	59.5
ORNL-2-41	14224.4	14374.4	61.5
ORNL-2-42	20270.4	20420.4	63.5
ORNL-2-43	24923.4	25073.4	65.5
ORNL-2-44	26748.4	26898.4	67.5
ORNL-2-45	28202.4	28352.4	69.5
ORNL-2-46	32642.4	32792.4	71.8
ORNL-2-47	34832.4	34982.4	73.5
ORNL-2-48	35342.4	35492.4	75.5
ORNL-2-49	37777.4	37927.4	77.5
ORNL-2-50	40264.4	40414.4	79.5
ORNL-2-51	41174.4	41324.4	81.5
ORNL-2-52	46114.4	46264.4	83.5
ORNL-2-53	49148.4	49298.4	85.5
ORNL-2-54	54117.4	54267.4	87.5
ORNL-2-55	61246.4	61396.4	89.5
ORNL-2-56	69680.4	69830.4	91.5
ORNL-2-57	74314.4	74464.4	93.5
ORNL-2-58	78068.4	78218.4	95.5
ORNL-2-59	83024.4	83174.4	97.5
ORNL-2-60	80768.4	80918.4	99.5

Continued

Sample Number	Cum-Cs (mg)	SysCumCs (mg)	Run Time (hours)
ORNL-2-61	82563.4	82713.4	101.5
ORNL-2-62	90340.4	90490.4	103.5
ORNL-2-63	94548.4	94698.4	105.5
ORNL-2-64	96798.4	96948.4	107.5
ORNL-2-65	95405.4	95555.4	109.5
ORNL-2-66	98208.4	98358.4	110.5
ORNL-2-67	99724.4	99874.4	111.5
ORNL-2-68	91374.4	91524.4	112.6
ORNL-2-69	91143.7	91293.7	112.8
ORNL-2-70	90918.3	91068.3	112.9

Anions in Water Extracts of HEPA Filters. Sample labeling according to Battelle where PF=Primary Filter, FF= Final Filter, F=Forward, C=Center, R=Rear (N.B. Labeling was actually reversed and the label PF was actually the final HEPA Filter and FF was actually the primary HEPA filter.) μg =micrograms.

Sample	F ($\mu\text{g}/\text{cm}^2$)	Cl ($\mu\text{g}/\text{cm}^2$)	NO ₂ ($\mu\text{g}/\text{cm}^2$)	NO ₃ ($\mu\text{g}/\text{cm}^2$)	PO ₄ ($\mu\text{g}/\text{cm}^2$)	SO ₄ ($\mu\text{g}/\text{cm}^2$)
PFF-1-1	0.9	8.7		2.5	87.4	
PFC-1-2	0.5	4.8		1	50.1	
PFR-1-3	0.4	4		1	41	
PFF-2-1	0.7	6.3		1.7	61.4	
PFC-2-2	0.6	5.7		1.4	63.8	
PFR-2-3	0.6	4.6		1	63	
Avg.	0.616666	5.683333		1.433333	61.11666	
FFF-1-1	4.3	44.8		2.2	1.8	222
FFC-1-2	3.9	39.7		2.7	1.4	217
FFR-1-3	4.5	40.6		3.1	1.6	227
FFF-2-1	3.6	29.1		2.8	1.2	153
FFC-2-2	4.6	49.3		2.3	1.9	240
FFR-2-3	4.3	44.1		2.6	2.2	235
Avg.	4.2	41.26666		2.616666	1.683333	215.6666

Amount of Anion is the amount per unit area ($\mu\text{g}/\text{cm}^2$) times the total area of the HEPA filter (199,738 cm^2). Net deposition (Dep) on the HEPA filter was calculated as the difference between the amount on the final and primary filters. The number of equivalents (Equivalent) of each anion was calculated by dividing Dep by the anion equivalent weight:

	(g)	(g)	(g)	(g)	(g)	(g)
Amt(PF)	0.123171	1.135177	0.286291	0	12.20732	
Amt(FF)	0.838899	8.242521	0.522647	0.336225	43.07682	Total
Dep (F-P)	0.715727	7.107343	0.236356	0.336225	30.86950	Equivalent.
Equivalent	0.037669	0.200489	0.003810	0.010618	0.642579	20.895168

Distribution of Anions on an charge equivalent basis:

Anion	(%)	(%)	(%)	(%)	(%)	(%)	(%)
Fraction	4.208135	22.39682	0	0.425727	1.186232	71.78309	100.0000

Elemental Inventories in the ISV Waste Drums:

Sample	Volume (L)	Al (mg/L)	B (mg/L)	Ba (mg/L)	Ca (mg/L)	Co (mg/L)	Cs (mg/L)
DRUM-1	199	42	210	0.064	39	0.9	3.4
DRUM-2	140	9.4	130	0.042	34	0.21	1.6
DRUM-3	197	7.3	470	0.042	24	0.21	3.2
DRUM-4	193	6.5	260	0.042	20	0.21	12
DRUM-5	185	4.6	130	0.042	9.4	0.21	46
DRUM-6	196	4.7	99	0.042	8.7	0.21	56
DRUM-7	194	2.9	48	0.048	5.4	0.15	90
DRUM-8	199	6.4	55	0.093	6.2	0.23	108
DRUM-9	196	4.3	41	0.098	12	0.15	90
DRUM-10	199	1.6	19	0.059	23	0.05	20
DRUM-11	76	0.6	16	0.042	18	0.01	19

Sample	Fe (mg/L)	Li (mg/L)	Mg (mg/L)	Mo (mg/L)	Na (mg/L)	P (mg/L)	Si (mg/L)
DRUM-1	120	29	30	3.4	470	36	67
DRUM-2	120	30	17	0.8	410	7.5	61
DRUM-3	130	170	21	0.8	3300	26	91
DRUM-4	210	68	13	0.8	1600	18	85
DRUM-5	320	24	6.6	0.8	560	11	78
DRUM-6	570	19	5.4	0.8	490	6.9	78
DRUM-7	320	18	2.7	0.8	300	4.2	87
DRUM-8	330	21	3.6	8.4	300	4.3	100
DRUM-9	360	15	5.2	4.2	320	2.6	99
DRUM-10	21	12	8.9	17	460	1.8	63
DRUM-11	40	7.9	8.4	7.1	440	0.8	64

Sample	Sr (mg/L)	Zn (mg/L)	Zr (mg/L)	Al-Total (mg)	B-Total (mg)	Ba-Total (mg)	Ca-Total (mg)
DRUM-1	1.4	57	11	8421	42105	12.832	7819.5
DRUM-2	0.54	14	2.5	1330.1	18395	5.943	4811
DRUM-3	0.41	26	1	1449.05	93295	8.337	4764

Continued

Sample	Sr (mg/L)	Zn (mg/L)	Zr (mg/L)	Al-Total (mg)	B-Total (mg)	Ba-Total (mg)	Ca-Total (mg)
DRUM-4	0.32	29	1.1	1264.25	50570	8.169	3890
DRUM-5	0.2	19	0.73	857.9	24245	7.833	1753.1
DRUM-6	0.18	17	0.66	928.25	19552.5	8.295	1718.25
DRUM-7	0.1	14	0.24	566.95	9384	9.384	1055.7
DRUM-8	0.14	28	0.31	1283.2	11027.5	18.6465	1243.1
DRUM-9	0.13	28	0.26	849.25	8097.5	19.355	2370
DRUM-10	0.11	3.5	0.07	320.8	3809.5	11.8295	4611.5
DRUM-11	0.09	1.4	0.03	46.5	1240	3.255	1395
				Total(mg)	Total(mg)	Total(mg)	Total(mg)
				17317.25	281721	113.879	35431.15

Sample	Co-Total (mg)	Cs-Total (mg)	Fe-Total (mg)	Li-Total (mg)	Mg-Total (mg)	Mo-Total (mg)	Na-Total (mg)
DRUM-1	180.45	681.7	24060	5814.5	6015	681.7	94235
DRUM-2	29.715	226.4	16980	4245	2405.5	113.2	58015
DRUM-3	41.685	635.2	25805	33745	4168.5	158.8	655050
DRUM-4	40.845	2334	40845	13226	2528.5	155.6	311200
DRUM-5	39.165	8579	59680	4476	1230.9	149.2	104440
DRUM-6	41.475	11060	112575	3752.5	1066.5	158	96775
DRUM-7	29.325	17595	62560	3519	527.85	156.4	58650
DRUM-8	46.115	21654	66165	4210.5	721.8	1684.2	60150
DRUM-9	29.625	17775	71100	2962.5	1027	829.5	63200
DRUM-10	10.025	4010	4210.5	2406	1784.45	3408.5	92230
DRUM-11	0.775	1472.5	3100	612.25	651	550.25	34100
	Total(mg)						
	489.2	86022.8	487080.5	78969.25	22127	8045.35	1628045

Sample	P-Total (mg)	Si-Total (mg)	Sr-Total (mg)	Zn-Total (mg)	Zr-Total (mg)
DRUM-1	7218	13433.5	280.7	11428.5	2205.5
DRUM-2	1061.25	8631.5	76.41	1981	353.75
DRUM-3	5161	18063.5	81.385	5161	198.5
DRUM-4	3501	16532.5	62.24	5640.5	213.95
DRUM-5	2051.5	14547	37.3	3543.5	136.145
DRUM-6	1362.75	15405	35.55	3357.5	130.35
DRUM-7	821.1	17008.5	19.55	2737	46.92
DRUM-8	862.15	20050	28.07	5614	62.155
DRUM-9	513.5	19552.5	25.675	5530	51.35
DRUM-10	360.9	12631.5	22.055	701.75	14.035
DRUM-11	62	4960	6.975	108.5	2.325
	Total(mg)	Total(mg)	Total(mg)	Total(mg)	Total(mg)
	22975.15	160815.5	675.91	45803.25	3414.98

Ratio of elements in vitrified product to totals in off-gas.

Al	B	Ba	Ca			
Product	Product	Product	Product			
Compostn	Compostn	Compostn	Compostn			
(mg/kg)	(mg/kg)	(mg/kg)	(mg/kg)			
75000	280	640	130000			
Fraction	Fraction	Fraction	Fraction			
(OffGas/ Product)	(OffGas/ Product)	(OffGas/ Product)	(OffGas/ Product)			
0.000011	0.051863	0.000009	0.000014			
Co	Cs	Fe	Li	Mg	Mo	Na
Product						
Compostn						
(mg/kg)						
17	3710	34000	2600	13000	6.9	12000
Fraction						
(OffGas/ Product)						
0.001483	0.001195	0.000738	0.001565	0.000087	0.060102	0.006993
P	Si	Sr	Zn	Zr		
Product	Product	Product	Product	Product		
Compostn	Compostn	Compostn	Compostn	Compostn		
(mg/kg)	(mg/kg)	(mg/kg)	(mg/kg)	(mg/kg)		
770	280000	12400	71	200		
Fraction	Fraction	Fraction	Fraction	Fraction		
(OffGas/ Product)	(OffGas/ Product)	(OffGas/ Product)	(OffGas/ Product)	(OffGas/ Product)		
0.001538	0.000029	0.000002	0.033253	0.000880		

A-38

Elemental analyses of ducting and hood ash smears and HEPA filters.

Sample	Al (mg/kg)	Ca (mg/kg)	Cs-AA (mg/kg)	Fe (mg/kg)	Li (mg/kg)	Mg (mg/kg)	Mn (mg/kg)
DUCTSMEAR ASH 1	5600	2600	3700	5600	8000	2400	180
DUCTSMEAR ASH 2	10000	5200	370	50000	5900	3200	250
DUCTSMEAR ASH 3	7900	3900	3260	11000	8000	2600	370
DUCTSMEAR ASH 4	8800	6100	2090	18000	5500	3000	250
DUCTSMEAR BLANK	19000	58000	80	16000	70	23000	450

Net (-Blank)	Al (mg/kg)	Ca (mg/kg)	Cs (mg/kg)	Fe (mg/kg)	Li (mg/kg)	Mg (mg/kg)	Mn (mg/kg)
DUCTSMEAR ASH1	5297.804	1350.625	3781.637	5365.460	8165.305	1935.431	173.9109
DUCTSMEAR ASH2	9571.488	2686.067	383.8075	51618.82	6149.012	2257.275	240.4775
DUCTSMEAR ASH3	7596.589	2421.214	3346.923	10863.32	8200.360	2042.380	367.8132
DUCTSMEAR ASH4	8448.668	4312.345	2159.232	18068.88	5666.365	2311.115	243.1111
Average	7728.637	2692.563	2417.900	21479.12	7045.260	2136.550	256.3282

Component	(grams)						
Upright	1.384084	0.352859	0.987976	1.401759	2.133236	0.505643	0.045435
Elbow	0.385791	0.108265	0.015469	2.080564	0.247844	0.090982	0.009692
22'Length	4.158934	1.325551	1.832352	5.947388	4.489483	1.118149	0.201368
Adaptor	0.421496	0.215139	0.107722	0.901440	0.282689	0.115299	0.012128
Grand Total (g)	6.350306	2.001815	2.943521	10.33115	7.153253	1.830075	0.268624
Equiv. Oxide g	11.99572	2.800539	3.120132	14.77354	15.40095	3.034264	0.424964

Sample	Mo (mg/kg)	Na (mg/kg)	Si (mg/kg)	Sr-ICP (mg/kg)	Sr-AA (mg/kg)	Sample Ash Wt (mg)	Ducting Area (cm ²)
DUCTSMEAR ASH 1	3600	57000	430000	35	31	1537.1	17380
DUCTSMEAR ASH 2	5800	27000	430000	49	46	745.9	5661
DUCTSMEAR ASH 3	3300	53000	410000	42	40	1274.1	44144
DUCTSMEAR ASH 4	5300	36000	450000	39	37	1018.1	5069
DUCTSMEAR BLANK	130	70000	1800	520	520	33.9	0

Net (-Blank)	Mo (mg/kg)	Na (mg/kg)	Si (mg/kg)	Sr (mg/kg)	Sr (mg/kg)	Weight (mg)	Ducting Line Location
DUCTSMEAR ASH 1	3678.255	56706.82	439656.7	24.06233	19.97212	1503.2	Upright
DUCTSMEAR ASH 2	6069.962	24952.66	405387.6	26.57457	23.43174	712	Elbow
DUCTSMEAR ASH 3	3386.649	52535.31	421157.8	28.93420	26.87953	1240.2	22' Length
DUCTSMEAR ASH 4	5478.076	34828.89	465437.8	22.43233	20.36344	984.2	Adaptor
Average	4653.235	42255.92	444160.0	25.50086	22.66171	0	

Component	(grams)	(grams)	(grams)	(grams)	(grams)	(grams) Oxide Sum
Upright	0.960966	14.81500	114.8630	0.006286	0.005217	261.2561
Elbow	0.244657	1.005750	18.15346	0.001071	0.000944	40.30632
22' Length	1.854102	28.76171	230.5729	0.015840	0.014715	547.4738
Adaptor	0.273296	1.737582	23.22027	0.001119	0.001015	49.88909
Grand Total (g)	3.333023	46.32005	386.8097	0.024317	0.021894	898.9254
Equiv. Oxide g	4.999534	62.43943	827.3859	0.028767	0.025900	946.4038

SAMPLE	100cm2	Cs-HNO3 Extract (mg/L)	Cs-HF Extract (mg/L)	Cs-Total Extract (mg/L)	Cs-Total (microgm)	Cs Fraction (mg/g)
	Ash Weight (mg)					
HOODSMEAR-1	107.8	1.14	1.84	2.98	149	1.382189
HOODSMAER-2	212281.9	0.64	4.64	5.28	264	0.936502
HOODSMEAR-3	172.5	0.58	2.74	3.32	166	0.962318
HOODSMEAR-4	210.6	0.4	2.09	2.49	124.5	0.591168
HOODSMEAR-5	235	1.12	3.15	4.27	213.5	0.908510
BLANK	34	0.05	0.05	0.1	5	0.147058
Average(-Blank)	167.56				178.4	0.809078
	Hood Ash Inventory (grams)					Cs Hood Inventory (grams)
	541.6594					0.576701

SAMPLE	Sr-HNO3 Extract (mg/L)	Sr-HF Extract (mg/L)	Sr-Total Extract (mg/L)	Sr-Total (microgm)	Sr Fraction (mg/g)
HOODSMEAR-1	0.2	0.1	0.3	15	0.139146
HOODSMAER-2	0.2	0.1	0.3	15	0.053210
HOODSMEAR-3	0.1	0.1	0.2	10	0.057971
HOODSMEAR-4	0.2	0.1	0.3	15	0.071225
HOODSMEAR-5	0.2	0.1	0.3	15	0.063829
BLANK	0.01	0.01	0.02	1	0.029411
Average(-Blank)				13	0.047664
					Sr Hood Inventory (grams)
					0.042024

HEPA Filter Sample	HNO3 Extract						
	Al (mg/kg)	Ca (mg/kg)	Cs (microgm)	Fe (mg/kg)	Li (mg/kg)	Mg (mg/kg)	Mn (mg/kg)
FILTER FFC-1-2	95	410	16.8	35	160	38	2.3
FILTER FFC-2-2	51	320	12.5	47	210	33	2.4
FILTER FFF-1-1	81	310	13.3	26	150	31	1.7
FILTER FFF-2-1	67	300	12.8	37	130	27	1.5
FILTER FFR-1-3	46	210	13.5	39	170	34	2.5
FILTER FFR-2-3	58	190	8.8	55	110	37	2.7
FILTER PFC-1-2	22	84	2	3.3	22	13	0.56
FILTER PFC-2-2	35	160	2	3	20	34	0.5
FILTER PFF-1-1	29	160	2	4.3	29	34	0.72
FILTER PFF-2-1	26	170	2	3	20	40	0.49
FILTER PFR-1-3	36	100	2	2.9	19	14	0.48
FILTER PFR-2-3	36	140	2	3	20	21	0.5
FFF-1-1PNL			0				
FFC-1-2PNL			0				
Avg. F Filter	66.33333	290	12.95	39.83333	155	33.33333	2.183333
Avg. P Filter	30.66666	135.6666	2	3.25	21.66666	26	0.541666
	(mg)	(mg)	(mg)	(mg)	(mg)	(mg)	(mg)
Avg. F Filter	122.3651	534.963		73.48055	285.9285	61.49	4.027595
Avg. P Filter	56.5708	250.2643		5.995275	39.9685	47.9622	0.999212
Difference	65.7943	284.6987		67.48527	245.96	13.5278	3.028382
Eq. Oxide(mg)	124.2854	398.2934	969.9	96.50394	529.5518	22.42909	4.790901

Sample	Cs-HNO3 (mg/kg)	Cs-HF Extract (microgm)	Sr-HF Extract (microgm)	Cs-Total (microgm)	Sr-Total (microgm)	Total Cs (mg/kg)
FILTER FFC-1-2	54.54545	344	158	360.8	168	1171.428
FILTER FFC-2-2	58.41121	276	109.5	288.5	114.8	1348.130
FILTER FFF-1-1	50	320.5	135.5	333.8	143.8	1254.887
FILTER FFF-2-1	45.71428	335.5	146	348.3	154.5	1243.928
FILTER FFR-1-3	48.91304	304.5	147	318	152.6	1152.173
FILTER FFR-2-3	32.95880	207.5	152	216.3	158	810.1123
FILTER PFC-1-2	8.888888	5	136	7	139	31.11111
FILTER PFC-2-2	7.968127	5	148	7	151.3	27.88844
FILTER PFF-1-1	11.56069	5	103	7	105.8	40.46242
FILTER PFF-2-1	7.905138	NA	NA	2	3.3	
FILTER PFR-1-3	7.722007	5	156	7	159.3	27.02702
FILTER PFR-2-3	8.064516	5	158.5	7	161.5	28.22580
FFF-1-1PNL	159	62.5	159		62.5	1012.738
FFC-1-2PNL	177	86.5	177		86.5	931.5789
Avg. F Filter	48.42380					1163.443
Avg. P Filter	8.684895					30.94296
	(mg)					
Avg. F Filter	89.32738					2146.204
Avg. P Filter	16.02102					57.08048
Difference	73.30635					972.1589
Eq. Oxide(mg)	77.70473					1793.341

Sample	Total Sr (mg/kg)	HNO3-Ext Sr (mg/kg)
FILTER FFC-1-2	545.4545	32.46753
FILTER FFC-2-2	536.4485	24.76635
FILTER FFF-1-1	540.6015	31.20300
FILTER FFF-2-1	551.7857	30.35714
FILTER FFR-1-3	552.8985	20.28985
FILTER FFR-2-3	591.7602	22.47191
FILTER PFC-1-2	617.7777	13.33333
FILTER PFC-2-2	602.7888	13.14741
FILTER PFF-1-1	611.5606	16.18497
FILTER PFF-2-1	NA	13.04347
FILTER PFR-1-3	615.0579	12.74131
FILTER PFR-2-3	651.2096	12.09677
FFF-1-1PNL	398.0891	NA
FFC-1-2PNL	455.2631	NA
Avg. F Filter	553.1582	26.92596
Avg. P Filter	619.6789	13.42454
Avg. F Filter	1020.410	49.67033
Avg. P Filter	1143.121	24.76426
Difference	426.6761	
Eq. Oxide(mg)	787.0895	

Elemental inventories in ISV Process Trailer Components:

Element	Al (g)	Ca (g)	Cs (g)	Fe (g)	Li (g)	Mg (g)	Mo (g)
Hood	3.829	1.207	0.577	6.229	4.313	1.103	2.01
Ducting	6.35	2.002	2.944	10.331	7.153	1.83	3.333
Scrub Sol	17.317	35.431	86.022	117.917	78.969	22.127	8.045
HEPA-P	0.122	0.535	2.146	0.073	0.286	0.061	0.605
HEPA-F	0.057	0.25	0.057	0.006	0.04	0.048	0.008
Total	27.675	39.425	91.746	134.556	90.761	25.169	14.001

	Fraction of Total						
Hood	0.138355	0.030615	0.006289	0.046292	0.047520	0.043823	0.143561
Ducting	0.229448	0.050779	0.032088	0.076778	0.078811	0.072708	0.238054
Scrub Sol	0.625727	0.898693	0.937610	0.876341	0.870076	0.879137	0.574601
HEPA-P	0.004408	0.013570	0.023390	0.000542	0.003151	0.002423	0.043211
HEPA-F	0.002059	0.006341	0.000621	0.000044	0.000440	0.001907	0.000571

Element	Na (g)	Si (g)	Sr (g)	Solids (g)
Hood	27.928	233.22	0.042	542
Ducting	46.32	386.81	0.022	899
Scrub Sol	1693.418	159.506	0.67	17138
HEPA-P	19.615	0.953	0.05	23.484
HEPA-F	4.642	0.836	0.025	0
Total	1791.923	781.325	0.809	18602.48

Continued

	Na Fraction of Total	Si Fraction of Total	Sr Fraction of Total	Solids Fraction of Total
Hood	0.015585	0.298492	0.051915	0.029135
Ducting	0.025849	0.495069	0.027194	0.048326
Scrub Sol	0.945028	0.204148	0.828182	0.921274
HEPA-P	0.010946	0.001219	0.061804	0.001262
HEPA-F	0.002590	0.001069	0.030902	0

Concentrations of elements in sequential 0.1N HCl extracts of pulverized ISV products: G=glass and R=rock (crystalline phase).

Sample	Al	Ca	Mg	Na	Si	Sr	Cs
	(------ mg/L -----)						
G11	30	76	8.1	5.8	17	5.82	1.68
G12	3.5	11	1.3	1.2	2.1	0.74	0.21
G13	0.54	1.9	0.32	1.2	1.2	0.09	0.05
G14	0.67	1.6	0.29	3.7	1.2	0.08	0.05
G15	0.36	1.2	0.14	1.2	1.2	0.05	0.05
G21	31	81	8.9	6.9	18	5.99	1.8
G22	4.2	11	1.3	1.2	2.5	0.81	0.26
G23	0.61	1.9	0.27	1.2	1.2	0.11	0.05
G24	0.68	1.7	0.46	2.6	1.2	0.08	0.05
G25	0.36	1.2	0.1	1.2	1.2	0.05	0.05
R11	79	340	32	14	56	15.5	1.1
R12	13	48	4.8	2.4	8.9	2.62	0.17
R13	3.5	8.7	0.95	1.2	1.7	0.7	0.05
R14	6	9.9	0.95	1.2	2.9	1.17	0.05
R15	3.6	5.6	0.53	1.2	1.4	0.7	0.05
R21	78	350	33	15	58	15.2	1.06
R22	13	46	4.7	2	8.6	2.51	0.15
R23	3.4	8.2	0.88	1.2	1.6	0.67	0.05
R24	6.8	11	1	1.2	3.3	1.35	0.05
R25	3.9	5.7	0.54	1.2	1.5	0.72	0.05

FRACTION OF TOTAL ELEMENT RELEASED:

	Al	Ca	Mg	Na	Si	Sr	Cs
G11	0.008	0.011692	0.012461	0.009666	0.001214	0.009708	0.009147
G12	0.000933	0.001692	0.002	0.002	0.00015	0.001234	0.001143
G13	0.000144	0.000292	0.000492	0.002	0.000085	0.000150	0.000272
G14	0.000178	0.000246	0.000446	0.006166	0.000085	0.000133	0.000272
G15	0.000096	0.000184	0.000215	0.002	0.000085	0.000083	0.000272
G21	0.008266	0.012461	0.013692	0.0115	0.001285	0.009991	0.009801
G22	0.00112	0.001692	0.002	0.002	0.000178	0.001351	0.001415
G23	0.000162	0.000292	0.000415	0.002	0.000085	0.000183	0.000272
G24	0.000181	0.000261	0.000707	0.004333	0.000085	0.000133	0.000272
G25	0.000096	0.000184	0.000153	0.002	0.000085	0.000083	0.000272
R11	0.021066	0.052307	0.049230	0.023333	0.004	0.025854	0.005989
R12	0.003466	0.007384	0.007384	0.004	0.000635	0.004370	0.000925
R13	0.000933	0.001338	0.001461	0.002	0.000121	0.001167	0.000272
R14	0.0016	0.001523	0.001461	0.002	0.000207	0.001951	0.000272

Continued

	Al	Ca	Mg	Na	Si	Sr	Cs
R15	0.00096	0.000861	0.000815	0.002	0.0001	0.001167	0.000272
R21	0.0208	0.053846	0.050769	0.025	0.004142	0.025354	0.005771
R22	0.003466	0.007076	0.007230	0.003333	0.000614	0.004186	0.000816
R23	0.000906	0.001261	0.001353	0.002	0.000114	0.001117	0.000272
R24	0.001813	0.001692	0.001538	0.002	0.000235	0.002251	0.000272
R25	0.00104	0.000876	0.000830	0.002	0.000107	0.001201	0.000272

Elements released from ISV samples by extraction with 0.1N HCl:
 Fraction:

	Al	Ca	Mg	Na	Si	Sr	Cs
G1TOTAL	0.009352	0.014107	0.015615	0.021833	0.001621	0.011309	0.011108
G2TOTAL	0.009826	0.014892	0.016969	0.021833	0.001721	0.011743	0.012033
GAVERAGE	0.009589	0.0145	0.016292	0.021833	0.001671	0.011526	0.011570
R1TOTAL	0.028026	0.063415	0.060353	0.033333	0.005064	0.034512	0.007732
R2TOTAL	0.028026	0.064753	0.061723	0.034333	0.005214	0.034111	0.007405
RAVERAGE	0.028026	0.064084	0.061038	0.033833	0.005139	0.034311	0.007568

SUMMATION TOTALS:

G1AVGSUM	0.008133	0.012076	0.013076	0.010583	0.00125	0.009849	0.009474
G2AVGSUM	0.00916	0.013769	0.015076	0.012583	0.00141	0.011142	0.010754
G3AVGSUM	0.009313	0.014061	0.015530	0.014583	0.0015	0.011309	0.011026
G4AVGSUM	0.009493	0.014315	0.016107	0.019833	0.001585	0.011442	0.011298
G5AVGSUM	0.009589	0.0145	0.016292	0.021833	0.001671	0.011526	0.011570
R1AVGSUM	0.020933	0.053076	0.05	0.024166	0.004071	0.025604	0.005880
R2AVGSUM	0.0244	0.060307	0.057307	0.027833	0.004696	0.029883	0.006751
R3AVGSUM	0.02532	0.061607	0.058715	0.029833	0.004814	0.031025	0.007024
R4AVGSUM	0.027026	0.063215	0.060215	0.031833	0.005035	0.033127	0.007296
R5AVGSUM	0.028026	0.064084	0.061038	0.033833	0.005139	0.034311	0.007568

Sample	K (mg/L)	Fraction of Total K
G11	11.2	0.009824
G12	1.47	0.001289
G13	0.27	0.000236
G14	0.22	0.000192
G15	0.15	0.000131
G21	11.6	0.010175
G22	1.67	0.001464
G23	0.31	0.000271
G24	0.23	0.000201
G25	0.23	0.000201
R11	17.3	0.015175
R12	2.95	0.002587
R13	0.74	0.000649
R14	0.9	0.000789
R15	0.58	0.000508
R21	17.2	0.015087
R22	2.93	0.992570
R23	0.7	0.000535
R24	1.03	0.000903
R25	0.61	0.000535

SUMMATION

G1TOTAL	0.011675
G2TOTAL	0.012315
GAVERAGE	0.011995
R1TOTAL	0.019710
R2TOTAL	0.019710
RAVERAGE	0.019710
G1AVGSUM	0.01
G2AVGSUM	0.011377
G3AVGSUM	0.011631
G4AVGSUM	0.011828
G5AVGSUM	0.011995
R1AVGSUM	0.015131
R2AVGSUM	0.017710
R3AVGSUM	0.018342
R4AVGSUM	0.019188
R5AVGSUM	0.019710

A-50

Radioisotope Activity in Starting Materials for Leaching:

Sample	Weight	cp30min SrInteg	cp30min Cs-Area	cp30min Co-Area	dpm/g Sr-act	dpm/g Cs-act	dpm/g Co-act
Sr1Soil	10.011	1862453	17671	-14456	136231.2	439.7504	
Sr2Soil	10.017	1846323	19128	-15192	134799.0	475.7234	
Cs3Soil	10.004	925456	649442	-55		16172.95	
Cs4Soil	10.013	939531	658901	-51		16393.76	
Co5Soil	10.011	281230	-172	133730		5545.166	
Co6Soil	10.029	281238	886	133350		5519.485	
Sr7Glass	10.006	1607358	13882	-10605	117776.7	345.6321	
Sr8Glass	10.032	1600664	15086	-13002	116848.1	374.6357	
Cs9Glass	10.029	622782	419660	356		10424.67	
Cs10Glas	5.019	297642	201772	357		10015.35	
Co11Glas	10.035	258989	537	118887		4917.905	
Co12Glas	5.028	126677	-687	58437		4824.539	

Leaching Results: Sequential (A-E) extractions with 0.1N HCl.

Sample	cp10min SrInteg	cp10min Cs-Area	cp10min Co-Area	Counting Date	Extractable		
					Sr-dpm/g	Cs-dpm/g	Co-dpm/g
Sr7GlassA	2775	5	36	7-5-88	4558.758		
B	860	38	-13	7-5-88	312.6385		
C	701	-3	-3	7-5-88	-39.9113		
D	756	15	-11	7-5-88	82.03991		
E	756	2	34	7-5-88	82.03991		
Sr8GlassA	2858	17	26	7-5-88	4742.793		
B	949	62	60	7-5-88	509.9778		
C	761	25	9	7-5-88	93.12638		
D	746	30	-13	7-5-88	59.86696		
E	726	18	16	7-5-88	15.52106		
Cs9GlassA	345	991	15	6-21-88		743.9939	
B	994	140	7	6-21-88		105.1051	
C	904	181	2	6-21-88		135.8858	
D	979	127	-14	6-21-88		95.34534	
E	888	119	6	6-21-88		89.33933	

Continued

Sample	cp10min SrInteg	cp10min Cs-Area	cp10min Co-Area	Counting Date	Extractable		
					Sr-dpm/g	Cs-dpm/g	Co-dpm/g
Cs10GlasA	2115	972	-34	6-21-88		729.7297	
B	901	180	-28	6-21-88		135.1351	
C	944	174	68	6-21-88		130.6306	
D	950	187	29	6-21-88		140.3903	
E	922	132	26	6-21-88		99.09909	
Co11GlasA	1269	49	205	6-21-88			281.9807
B	758	-25	-5	6-21-88			-6.87757
C	720	29	52	6-21-88			71.52682
D	757	16	-10	6-21-88			-13.7551
E	759	16	19	6-21-88			26.13480
Co12GlasA	1306	-11	185	6-21-88			254.4704
B	805	-14	70	6-21-88			96.28610
C	770	22	-21	6-21-88			-28.8858
D	684	-5	11	6-21-88			15.13067
E	761	9	-1	6-21-88			-1.37551

Leaching results with sequential extracts of 0.1N CaCl₂ (A-E) and HCl (F-J):

Sample	cp10min SrInteg	cp10min Cs-Area	cp10min Co-Area	Counting Date	Extractable		
					Sr-dpm/g	Cs-dpm/g	Co-dpm/g
Sr1SoilA	92100	-181	-502	7-5-88	40523.72		
B	54809	-58	-454	7-5-88	23986.69		
C	20074	124	-232	7-5-88	8583.148		
D	25747	-181	-50	7-5-88	11098.89		
E	9505	-56	-155	7-5-88	3896.230		
F	34346	-83	-131	7-5-88	14912.19		
G	16141	44	-70	7-5-88	6839.024		
H	7040	84	16	7-5-88	2803.104		
I	3479	61	-27	7-5-88	1223.946		
J	2169	95	40	7-5-88	643.0155		
Sr2SoilA	92626	-70	-606	7-5-88	40756.98		
B	59283	-62	-352	7-5-88	25970.73		
C	20858	-137	-105	7-5-88	8930.820		

Continued

Sample	cp10min SrInteg	cp10min Cs-Area	cp10min Co-Area	Counting Date	Extractable		
					Sr-dpm/g	Cs-dpm/g	Co-dpm/g
D	20543	-50	-243	7-5-88	8791.130		
E	10268	-28	-4	7-5-88	4234.589		
F	34334	-158	-258	7-5-88	14906.87		
G	15013	-68	-1	7-5-88	6338.802		
H	6114	28	15	7-5-88	2392.461		
I	2734	-67	-28	7-5-88	893.5698		
J	1686	6	27	7-5-88	428.8248		
Cs3SoilA	1132	22	17	6-20-88		3.303303	
B	854	-32	48	6-20-88		-4.80480	
C	792	22	8	6-20-88		3.303303	
D	791	28	23	6-20-88		4.204204	
E	788	0	-41	6-20-88		0	
F	791	-8	10	6-20-88		-1.20120	
G	800	25	36	6-20-88		3.753753	
H	822	59	-17	6-20-88		8.858858	
I	809	37	5	6-20-88		5.555555	
J	779	58	40	6-20-88		8.708708	
Cs4SoilA	1092	28	-63	6-20-88		4.204204	
B	988	17	-14	6-20-88		2.552552	
C	840	24	6	6-20-88		3.603603	
D	782	-9	26	6-20-88		-1.35135	
E	788	-37	26	6-20-88		-5.55555	
F	795	58	47	6-20-88		8.708708	
G	809	8	30	6-20-88		1.201201	
H	825	3	75	6-20-88		0.450450	
I	800	16	15	6-20-88		2.402402	
J	775	5	-6	6-20-88		0.750750	
Co5SoilA	796	9	60	6-20-88			16.50618
B	836	12	35	6-20-88			9.628610
C	717	-6	27	6-20-88			7.427785
D	760	10	26	6-20-88			7.152682
E	741	18	21	6-20-88			5.777166
F	9433	47	3716	6-20-88			1022.283
G	8287	-93	3457	6-20-88			951.0316
H	6226	106	2131	6-20-88			586.2448
I	3624	52	1261	6-20-88			346.9050
J	3398	-26	1099	6-20-88			302.3383

Continued

Sample	cp10min SrInteg	cp10min Cs-Area	cp10min Co-Area	Counting Date	Extractable		
					Sr-dpm/g	Cs-dpm/g	Co-dpm/g
Co6SoilA	816	24	52	6-20-88			14.30536
B	757	11	10	6-20-88			2.751031
C	724	-5	21	6-20-88			5.777166
D	724	9	17	6-20-88			4.676753
E	778	2	63	6-20-88			17.33149
F	9141	-78	3467	6-20-88			953.7826
G	8224	-165	3118	6-20-88			857.7716
H	5619	-71	2000	6-20-88			550.2063
I	3905	-29	1248	6-20-88			343.3287
J	3258	-34	967	6-20-88			266.0247
Sr7GLASSA	844	11	-32	7-5-88	55.43237		
B	748	-26	-3	7-5-88	12.86031		
C	638	-3	-8	7-5-88	-35.9201		
D	719	19	0	7-5-88	0		
E	779	21	-16	7-5-88	26.60753		
F	3098	-7	-21	7-5-88	1054.988		
G	2466	52	-20	7-5-88	774.7228		
H	2284	89	200	7-5-88	694.0133		
I	1526	24	12	7-5-88	357.8713		
J	1480	28	-26	7-5-88	337.4722		
Sr8GLASSA	787	11	23	7-5-88	30.15521		
B	774	23	6	7-5-88	24.39024		
C	768	-3	-19	7-5-88	21.72949		
D	774	34	-10	7-5-88	24.39024		
E	714	23	23	7-5-88	-2.21729		
F	3157	-26	-30	7-5-88	1081.152		
G	2538	72	4	7-5-88	806.6518		
H	2039	81	-13	7-5-88	585.3658		
I	1547	-4	60	7-5-88	367.1840		
J	1411	-24	-42	7-5-88	306.8736		
Cs9GLASSA	744	5	15	6-20-88		0.750750	
B	697	-17	54	6-20-88		-2.55255	
C	724	21	0	6-20-88		3.153153	
D	689	0	13	6-20-88		0	
E	699	12	58	6-20-88		1.801801	
F	1990	937	32	6-20-88		140.6906	
G	2131	1006	-29	6-20-88		151.0510	
H	2127	918	17	6-20-88		137.8378	

Continued

Sample	cp10min SrInteg	cp10min Cs-Area	cp10min Co-Area	Counting Date	Extractable		
					Sr-dpm/g	Cs-dpm/g	Co-dpm/g
I	2012	875	19	6-20-88		131.3813	
J	2140	904	28	6-20-88		135.7357	
Cs10GLASA	732	17	-8	6-20-88		2.552552	
B	718	-2	38	6-20-88		-0.30030	
C	746	0	4	6-20-88		0	
D	759	14	3	6-20-88		2.102102	
E	751	1	13	6-20-88		0.150150	
F	1954	862	33	6-20-88		129.4294	
G	2209	974	-11	6-20-88		146.2462	
H	2059	935	34	6-20-88		140.3903	
I	1893	823	29	6-20-88		123.5735	
J	2042	850	-21	6-20-88		127.6276	
Co11GLASS	720	-27	-3	6-20-88			-0.82530
B	714	-18	34	6-20-88			9.353507
C	732	5	-16	6-20-88			-4.40165
D	714	21	23	6-20-88			6.327372
E	742	18	-9	6-20-88			-2.47592
F	1277	37	217	6-20-88			59.69738
G	1156	-10	130	6-20-88			35.76341
H	971	3	89	6-20-88			24.48418
I	951	-28	81	6-20-88			22.28335
J	940	-57	98	6-20-88			26.96011
Co12GLASS	749	15	-11	6-20-88			-3.02613
B	684	18	56	6-20-88			15.40577
C	718	-2	-24	6-20-88			-6.60247
D	737	-8	37	6-20-88			10.17881
E	729	24	28	6-20-88			7.702888
F	1309	-19	249	6-20-88			68.50068
G	1170	-13	190	6-20-88			52.26960
H	1015	-10	169	6-20-88			46.49243
I	909	56	101	6-20-88			27.78541
J	923	36	113	6-20-88			31.08665

Residual ^{134}Cs Activity in Borosilicate Glass Vials After Heating and Sequential Extractions. Sample replicates (a, b, and c) were heated to 450, 550, or 650°C after initial drying at 110°C.

Sample	Before Heating Extract	After Heating Extract (Net counts per 10 minutes)	After Tapwater Extract	After 12% HNO_3	After 10% HF
a550	235251	272448	268666	264787	42
b550	233981	268205	267303	256230	1273
c550	232745	267153	267564	258919	99
a650	236037	271854	275954	271771	10608
b650	239609	272222	272057	274719	10355
c650	235248	270093	271392	272724	6707
a450	238726	261606	261077	160221	106
b450	236643	259684	251681	199289	105
c450	241451	265696	252060	198101	71
a110	237157	236046	39284	190	-8

Temperature	(Average fraction remaining in vial)				
110	1	0.995315	0.165645	0.000801	-0.00003
450	1	1.097885	1.066959	0.777895	0.000393
550	1	1.150758	1.144671	1.111056	0.002014
650	1	1.145274	1.152637	1.152371	0.038922

A-56

Activities of ^{137}Cs , ^{60}Co , and ^{90}Sr in soil samples following thermal treatment and extraction with 0.1N HCl:

Isotope Soil	Sample Number	Treat. Temp. (deg C)	Sr-90 Crucible Broken	Before Cs-137 Activity (dpm/g)	Before Co-60 Activity (dpm/g)	Before Sr-90 Activity (dpm/g)	After Activity (dpm/g)
CO	33	60	N	0	0	5644.53	.
CO	34	60	N	0	16.8	5487.7	.
CO	36	60	N	0	61.5	5234.64	.
CO	35	60	N	0	27.9	5347.51	.
CO	32	60	N	0	0	5520.28	.
CO	31	60	N	0	84.7	4883.01	.
CO	1	200	N	0	16.1	5126.4	0
CO	2	200	N	0	0	5559.08	0
CO	3	300	N	0	76.3	5053.5	0
CO	4	300	N	0	0	5078.19	0
CO	6	400	N	0	0	5567.31	0
CO	5	400	N	0	10.5	5062.9	0
CO	7	500	N	0	82.6	5039.39	0
CO	8	500	N	0	0	5367.43	0
CO	10	600	N	0	30.1	5008.82	0
CO	9	600	N	0	6.3	5409.76	0
CO	11	700	N	0	0	5062.9	0
CO	12	700	N	0	0	5429.75	0
CO	13	800	N	0	0	5845.97	0
CO	14	800	N	0	120.4	6075.25	0
CO	15	900	N	0	0	4848.52	0
CO	16	900	N	0	97.8	5965.31	0
CO	17	1000	N	0	103.6	5861.26	0
CO	18	1000	N	0	0	5770.72	0
CO	20	1100	N	0	0	5229.86	0
CO	19	1100	N	0	0	5470.9	0
CO	22	1200	N	0	16.8	5259.26	0
CO	21	1200	N	0	102.2	5463.84	0
CO	24	1300	N	0	0	6063.49	0
CO	23	1300	N	0	0	5442.68	0
CO	25	1400	Y	0	0	5580.25	0
CO	26	1400	Y	0	0	5526.16	0
CO	27	1500	Y	0	0	5309.82	0
CO	28	1500	Y	0	0	5008.82	0
CO	30	1600	Y	0	153.3	5213.4	0
CO	29	1600	Y	0	0	6008.23	0
CO	38	1700	Y	0	0	5904.97	0
CO	37	1700	N	0	0	5427.22	0
CS	35	60	N	0	14142.6	0	.

Continued

Isotope Soil	Sample Number	Treat. Temp. (deg C)	Crucible Broken	Before Sr-90 Activity (dpm/g)	Before Cs-137 Activity (dpm/g)	Before Co-60 Activity (dpm/g)	After Sr-90 Activity (dpm/g)
CS	36	60	N	278	13583.2	0	.
CS	32	60	N	1440	14336.7	10.58	.
CS	33	60	N	793	14143.3	0	.
CS	34	60	N	495	15425.7	0	.
CS	31	60	N	3856	14848.4	0	.
CS	2	200	N	5876	14102.3	0	4614
CS	1	200	N	6401	14597.8	0	5545
CS	3	300	N	5750	12849.7	0	5478
CS	4	300	N	4339	14016	0	4530
CS	6	400	N	5320	13927.6	0	0
CS	5	400	N	3305	13093.9	0	4807
CS	7	500	N	4584	12853.9	0	3655
CS	8	500	N	3760	13849	0	3921
CS	10	600	N	5029	16060.5	0	4634
CS	9	600	N	3792	15180.9	0	5240
CS	11	700	N	4011	12927.6	0	5042
CS	12	700	N	4127	14082.1	0	5095
CS	14	800	N	4548	13031.3	0	4669
CS	13	800	N	3765	13711.2	0	4897
CS	15	900	N	4401	13338.2	0	4174
CS	16	900	N	5582	15286	0	4489
CS	18	1000	N	6803	16057.1	0	5609
CS	17	1000	N	3363	13828.8	0	4339
CS	20	1100	N	4661	12123.9	0	3697
CS	19	1100	N	4757	16263	0	4304
CS	21	1200	N	5062	15662.5	0	5341
CS	22	1200	N	5786	15524	0	3608
CS	24	1300	N	3193	12475.3	0	919
CS	23	1300	N	3704	13979.1	0	1913
CS	25	1400	Y	5609	13911.6	0	6562
CS	26	1400	Y	4506	12259.6	0	4835
CS	28	1500	Y	4824	14437	0	7348
CS	27	1500	Y	3534	14565.1	0	2890
CS	29	1600	Y	3831	14478.8	0	3692
CS	30	1600	Y	4648	12315.9	0	3799
CS	37	1700	N	5538	17185.6	74.81	8899
CS	38	1700	N	4574	13325.1	13.13	8228
SR	31	60	N	153566	392	0	153566
SR	32	60	N	154278	260.4	0	154278

Continued

Isotope Soil	Sample Number	Treat. Temp. (deg C)	Crucible Broken	Before Sr-90 Activity (dpm/g)	Before Cs-137 Activity (dpm/g)	Before Co-60 Activity (dpm/g)	After Sr-90 Activity (dpm/g)
SR	36	60	N	148307	414.9	0	148307
SR	34	60	N	152491	515.5	0	152491
SR	35	60	N	146715	602.8	0	146715
SR	33	60	N	154311	115.2	0	154311
SR	1	200	N	101857	338.9	0	99491
SR	2	200	N	99501	480.2	0	97873
SR	4	300	N	94864	327.1	0	94695
SR	3	300	N	92719	303.4	0	93419
SR	5	400	N	93341	473.2	0	94061
SR	6	400	N	99048	345.9	0	99151
SR	8	500	N	97338	338.2	0	98023
SR	7	500	N	91656	293	0	93506
SR	10	600	N	96353	366.7	0	98729
SR	9	600	N	94062	286.7	0	94338
SR	12	700	N	99464	334	0	98968
SR	11	700	N	97560	289.5	0	94058
SR	14	800	N	96476	395.3	0	99116
SR	13	800	N	94363	415.4	0	97863
SR	15	900	N	98660	419.6	0	95546
SR	16	900	N	92680	405	0	93590
SR	18	1000	N	96762	350	0	97885
SR	17	1000	N	103777	391.8	0	102751
SR	20	1100	N	103488	499	0	105764
SR	19	1100	N	95293	409.2	0	95641
SR	21	1200	N	92255	267.9	0	94769
SR	22	1200	N	93370	299.2	0	95708
SR	23	1300	N	94678	296.5	0	95974
SR	24	1300	Y	95355	859.4	0	117507
SR	26	1400	Y	97544	318	0	133086
SR	25	1400	Y	95959	404.3	0	129388
SR	27	1500	Y	95859	347.3	0	129220
SR	28	1500	Y	100198	299.9	0	121264
SR	30	1600	Y	95975	837.9	0	133775
SR	29	1600	Y	97969	463.5	0	113553
SR	37	1700	N	99465	455.4	64.31	99641
SR	38	1700	N	91631	271.2	0	102925

Isotope Soil	Sample Number	After Cs-137 Activity (dpm/g)	After Co-60 Activity (dpm/g)	Residual Sr-90 Activity (dpm/g)	Residual Cs-137 Activity (dpm/g)	Residual Co-60 Activity (dpm/g)	Extract Sr-90 Activity (dpm/g)
CO	33	.	5644.53
CO	34	.	5487.7
CO	36	.	5234.64
CO	35	.	5347.51
CO	32	.	5520.28	0	46.5	1245.33	0
CO	31	.	4883.01	0	0	1100.47	0
CO	1	0	5166.92	0	64	883.14	335
CO	2	0	5972.44	0	34.1	1167.4	0
CO	3	0	5314.24	0	0	1028.91	325
CO	4	0	5213.26	0	0	1128.52	171
CO	6	0	5928.48	0	108.4	2356.66	158
CO	5	0	5330.88	0	18.1	2074.83	0
CO	7	38.4	5474.63	0	37.5	2943.39	22
CO	8	39.8	5598.19	0	0	3188.78	486
CO	10	3.5	5692.05	0	0	3398.93	155
CO	9	0	5077.82	0	69.5	3316.33	393
CO	11	87.6	5866.13	0	27.8	3914.72	319
CO	12	41.7	5651.12	0	9.7	3582.94	0
CO	13	0	5926.87	0	3.5	4226.64	91
CO	14	18.8	5905	0	0	4103.97	506
CO	15	13.9	5372.93	0	26.4	4682.24	0
CO	16	0	5907.43	0	85.4	4956.78	119
CO	17	0	6031.34	0	0	5387.85	205
CO	18	0	5819.97	0	0	5269.86	266
CO	20	0	5174.93	0	0	4794.39	0
CO	19	66.7	5662.05	0	79.2	4789.72	605
CO	22	0	5299.81	0	0	4857.96	0
CO	21	0	5296.09	0	18.9	4942.35	0
CO	24	0	6299.19	0	99.5	5657.91	16
CO	23	7	5390.44	0	57.4	5159.87	480
CO	25	61.2	5872.13	0	71.4	5252.59	82
CO	26	0	5556.8	0	6.3	4976.82	10
CO	27	26.7	5767.85	0	76.3	4704.62	0
CO	28	0	5543.14	0	0	4974.44	0
CO	30	117.5	5297.33	0	0	4903.13	0
CO	29	0	6310.37	0	0	5350.05	417
CO	38	143.9	5112.66	.	.	.	0
CO	37	0	5184.81	.	.	.	161
CS	35	14142.6
CS	36	13583.2

A-60

Continued

Isotope Soil	Sample Number	After Cs-137 Activity (dpm/g)	After Co-60 Activity (dpm/g)	Residual Sr-90 Activity (dpm/g)	Residual Cs-137 Activity (dpm/g)	Residual Co-60 Activity (dpm/g)	Extract Sr-90 Activity (dpm/g)
CS	32	14336.7	.	2305	14272.6	0	187
CS	33	14143.3
CS	34	15425.7
CS	31	14848.4	.	1662	14874.7	26.87	740
CS	2	14674.3	0	7829	13665.1	0	511
CS	1	14825.1	0	8868	14141.1	0	657
CS	3	13166.7	0	8952	12528.5	0	228
CS	4	14032.5	0	8492	13445.9	0	106
CS	6	0	0	8475	13288.6	0	105
CS	5	12903.4	0	8017	12378.2	0	19
CS	7	12879.3	0	10067	11917.4	0	475
CS	8	14129.3	0	7570	13377.8	0	0
CS	10	16422.6	0	10663	15258.2	0	527
CS	9	14887.2	0	8230	14308.6	0	0
CS	11	12581.4	0	7653	11749.7	0	960
CS	12	13798	0	8829	12975.3	0	230
CS	14	12827.8	0	11660	10381.8	16.08	642
CS	13	13481.3	0	10949	10540.8	55.67	0
CS	15	13471.5	0	10304	11343	0	0
CS	16	15416.1	0	12542	12036.6	70.52	432
CS	18	16246.2	0	12166	14712.1	37.11	71
CS	17	13514.8	0	10455	11638.6	22.27	60
CS	20	12164.1	0	7429	11961.8	14.61	171
CS	19	16196.6	0	10056	15629.4	58.44	107
CS	21	14841	0	7674	15509.6	32.87	0
CS	22	15904.4	0	5927	15786	1.22	339
CS	24	12861.8	0	3882	12204.1	54.79	86
CS	23	14657.4	0	8877	13448.9	2.44	204
CS	25	13061.8	0	8972	12664	10.69	453
CS	26	11564.3	26.79	7672	11172.7	0	353
CS	28	13439.8	8.52	9829	13254.2	0	263
CS	27	14771.7	0	8951	13250.7	14.26	209
CS	29	14553.8	62.1	7152	13640.4	0	247
CS	30	11734.8	29.22	5866	11597.4	7.13	316
CS	37	15701.7	20.25	.	.	.	454
CS	38	12168.2	62.03	.	.	.	413
SR	31	.	.	6978	356.5	0	112289
SR	32	.	.	7011	433.1	0	117640
SR	36

A-61

Continued

Isotope Soil	Sample Number	After Cs-137 Activity (dpm/g)	After Co-60 Activity (dpm/g)	Residual Sr-90 Activity (dpm/g)	Residual Cs-137 Activity (dpm/g)	Residual Co-60 Activity (dpm/g)	Extract Sr-90 Activity (dpm/g)
SR	34
SR	35
SR	33
SR	1	360.3	0	18658	363.4	0	108106
SR	2	485.3	0	17780	454.2	0	114226
SR	4	321.9	0	17002	330.5	0	101393
SR	3	299.6	0	16064	326.3	0	109100
SR	5	487.4	0	24244	434.6	0	89002
SR	6	270.2	0	26266	356.4	0	88913
SR	8	382.2	0	36931	344.2	0	70968
SR	7	350.1	0	33089	404.3	0	70311
SR	10	341.7	0	30906	381.2	0	84205
SR	9	351.5	0	34210	333	0	72647
SR	12	441.6	0	38988	446.3	0	69585
SR	11	292.8	0	35245	381.2	0	69610
SR	14	436.7	0	72760	395.1	0	18843
SR	13	413	0	71078	344	0	20604
SR	15	389.2	0	73903	222.1	0	34951
SR	16	474.5	0	72067	397.2	0	31836
SR	18	305	0	69995	252.9	0	13290
SR	17	326.3	0	70861	297.7	0	20582
SR	20	554	0	91562	474.8	0	1666
SR	19	349.7	0	83311	442.1	0	507
SR	21	262.7	0	86663	272.2	19.48	157
SR	22	359.4	0	85658	343.2	0	80
SR	23	292.8	0	88922	261.1	15.83	327
SR	24	951.4	0	116147	803.4	0	53
SR	26	407.3	0	110774	303.8	0	30
SR	25	361.3	0	107526	325.5	0	0
SR	27	628	0	113459	352.7	0	0
SR	28	382.9	0	99031	260.5	0	188
SR	30	1036.8	0	105878	764.8	0	20
SR	29	423.9	0	102207	486.8	0	77
SR	37	543.3	0	.	.	.	495
SR	38	256.1	0	.	.	.	626

Isotope Soil	Sample Number	Extract Cs-137 Activity (dpm/g)	Extract Co-60 Activity (dpm/g)	Soil Weight Loss (%)	Activity Ratio (Before/ After)	Soluble Fraction
CO	33	.	.	.	1	0
CO	34	.	.	.	1	0
CO	36	.	.	.	1	0
CO	35	.	.	.	1	0
CO	32	53.933	4585.76	.	1	0.830711
CO	31	51.131	4191.13	.	1	0.858308
CO	1	62.338	3902.29	4	1.007904	0.761214
CO	2	70.743	5086.18	3.1	1.074357	0.914931
CO	3	77.747	4386.07	5.1	1.051595	0.867927
CO	4	107.866	4143.59	4.3	1.026598	0.815958
CO	6	60.937	3575.42	7.5	1.064873	0.642216
CO	5	126.077	3424.46	6.6	1.052930	0.676383
CO	7	56.034	2137.17	8.5	1.086367	0.424092
CO	8	23.815	2115.77	7.7	1.042992	0.394186
CO	10	32.92	1929.16	7.4	1.136405	0.385152
CO	9	40.625	2001.66	9.2	0.938640	0.370009
CO	11	20.312	1482.23	9.505	1.158650	0.292763
CO	12	70.743	1498.87	8.9286	1.040769	0.276047
CO	13	55.334	829.67	9.4675	1.013838	0.141921
CO	14	70.743	1060.26	9.5945	0.971976	0.174521
CO	15	53.933	219.9	9.3069	1.108158	0.045354
CO	16	9.806	263.88	10.1	0.990297	0.044235
CO	17	28.017	206.82	9.604	1.029017	0.035285
CO	18	65.14	183.05	9.5661	1.008534	0.031720
CO	20	40.625	254.37	9.7633	0.989496	0.048638
CO	19	51.131	159.28	9.6457	1.034939	0.029114
CO	22	11.907	73.7	9.7804	1.007710	0.014013
CO	21	56.735	71.32	9.739	0.969298	0.013053
CO	24	19.612	49.92	9.7633	1.038872	0.008232
CO	23	32.22	106.98	9.7345	0.990401	0.019655
CO	25	53.933	93.9	9.8117	1.052305	0.016827
CO	26	81.95	115.3	10.1101	1.005544	0.020864
CO	27	18.912	166.41	10.2102	1.086260	0.031340
CO	28	30.118	112.92	10.2102	1.106675	0.022544
CO	30	67.941	124.81	10.1	1.016098	0.023940
CO	29	2.802	57.05	10.331	1.050287	0.009495
CO	38	0	151	10.338	0.865823	0.025571
CO	37	2.158	138.18	10.338	0.955334	0.025460
CS	35	.	.	.	1	0
CS	36	.	.	.	1	0

Continued

Isotope Soil	Sample Number	Extract Cs-137 Activity (dpm/g)	Extract Co-60 Activity (dpm/g)	Soil Weight Loss (%)	Activity Ratio (Before/ After)	Soluble Fraction
CS	32	130.98	192.56	.	1	0
CS	33	.	.	.	1	0.009135
CS	34	.	.	.	1	0
CS	31	123.976	93.9	.	1	0
CS	2	120.973	36	3.6779	1.040560	0.008349
CS	1	113.94	76.97	4.0755	1.015570	0.008578
CS	3	118.16	12.41	4.2829	1.024669	0.007805
CS	4	142.777	172.56	4.4821	1.001177	0.009195
CS	6	157.547	115.46	5.4726	1	0.010186
CS	5	108.313	119.18	5.4726	0.985451	0.011311
CS	7	221.55	39.73	9.0728	1.001976	0.008272
CS	8	340.414	54.62	9.1542	1.020239	0.017236
CS	10	260.937	59.59	8.0677	1.022545	0.024580
CS	9	225.067	156.42	7.8685	0.980653	0.016247
CS	11	424.814	40.97	9.98	0.973220	0.014825
CS	12	507.807	125.39	9.98	0.979825	0.032861
CS	14	372.064	16.14	9.5713	0.984383	0.036060
CS	13	368.547	156.42	9.6614	0.983232	0.028551
CS	15	481.08	115.46	9.5808	1.009993	0.026879
CS	16	524.687	37.24	10.2692	1.008511	0.036067
CS	18	99.17	70.76	9.9701	1.011776	0.034324
CS	17	102.687	50.9	9.8802	0.977293	0.006176
CS	20	46.42	151.46	9.6806	1.003315	0.007425
CS	19	43.607	160.15	9.7902	0.995917	0.003828
CS	21	82.29	70.76	9.8901	0.947549	0.002681
CS	22	78.773	47.18	9.99	1.024503	0.005253
CS	24	13.363	139.04	11.3	1.030981	0.005074
CS	23	26.023	18.62	10	1.048522	0.001071
CS	25	49.937	64.56	7.7922	0.938914	0.001861
CS	26	36.573	67.04	9.7902	0.943285	0.003589
CS	28	40.793	108.01	11	0.930927	0.002983
CS	27	56.97	91.87	10.8782	1.014184	0.002825
CS	29	32.353	120.42	10.1898	1.005179	0.003911
CS	30	21.1	55.87	11.8	0.952817	0.002234
CS	37	84.173	76.92	10.3	0.913654	0.001713
CS	38	2.158	59.83	9.9305	0.913178	0.004897
SR	31	165.301	128.37	.	1	0.731210
SR	32	61.638	85.58	.	1	0.762519
SR	36	.	.	.	1	0

Continued

Isotope Soil	Sample Number	Extract Cs-137 Activity (dpm/g)	Extract Co-60 Activity (dpm/g)	Soil Weight Loss (%)	Activity Ratio (Before/ After)	Soluble Fraction
SR	34	.	.	.	1	0
SR	35	.	.	.	1	0
SR	33	.	.	.	1	0
SR	1	22.507	62.07	4.4	0.976771	0.676019
SR	2	116.753	74.49	4.4	0.983638	0.731202
SR	4	59.08	1.24	5.3	0.998218	0.680780
SR	3	17.583	18.62	6.2	1.007549	0.749473
SR	5	57.673	12.41	6.0939	1.007713	0.607334
SR	6	33.76	2.48	6.8931	1.001039	0.571768
SR	8	137.15	70.76	9.8098	1.007037	0.464387
SR	7	126.6	101.8	9.7804	1.020184	0.488610
SR	10	28.837	115.46	8.3166	1.024659	0.556638
SR	9	35.87	151.46	8.5085	1.002934	0.491930
SR	12	80.18	60.83	9.3186	0.995013	0.445605
SR	11	55.563	81.94	14.343	0.964104	0.454464
SR	14	24.617	45.93	10.3206	1.027364	0.124403
SR	13	79.477	100.56	9.8394	1.037090	0.139075
SR	15	26.023	54.62	10.3	0.968437	0.225641
SR	16	61.19	273.12	10.3103	1.009818	0.218792
SR	18	74.553	131.6	10.5	1.011605	0.087482
SR	17	68.223	166.36	10.0301	0.990113	0.126324
SR	20	48.53	139.04	10.4	1.021992	0.010253
SR	19	73.147	161.39	11.6	1.003651	0.003388
SR	21	28.837	120.42	10.6212	1.027250	0.001083
SR	22	47.123	16.14	10.9109	1.025040	0.000545
SR	23	40.09	68.28	10.1101	1.013688	0.002199
SR	24	73.147	59.59	11	1.232310	0.000354
SR	26	58.903	69.13	10.9	1.364368	0.000195
SR	25	54.157	144.01	10.9438	1.348367	0
SR	27	79.849	135.5	10.7	1.348021	0
SR	28	35.021	77.26	11.5768	1.210243	0.001195
SR	30	67.941	137.88	11.3886	1.393852	0.000132
SR	29	25.215	35.66	9.9198	1.159070	0.000500
SR	37	18.625	51.72	10.479	1.001769	0.003169
SR	38	30.802	61.01	14.5436	1.123255	0.004351

Averages:

Temp. (deg C)	Average Co Ratio (Before/ After)	Average Cs Ratio (Before/ After)	Average Sr Ratio (Before/ After)	Average Soluble Fraction Co	Average Soluble Fraction Cs
60	1	1	1	0.844510	0.004567
200	1.041130	1.028065	0.980204	0.838073	0.008463
300	1.039096	1.012923	1.002884	0.841942	0.008500
400	1.058901	0.992725	1.004376	0.659299	0.010749
500	1.064680	1.011107	1.013610	0.409139	0.012754
600	1.037522	1.001599	1.013796	0.377580	0.020413
700	1.099710	0.976522	0.979558	0.284405	0.023843
800	0.992907	0.983808	1.032227	0.158221	0.032306
900	1.049228	1.009252	0.989127	0.044794	0.031473
1000	1.018776	0.994535	1.000859	0.033503	0.020250
1100	1.012218	0.999616	1.012822	0.038876	0.005627
1200	0.988504	0.986026	1.026145	0.013533	0.003967
1300	1.014636	1.039751	1.122999	0.013944	0.003072
1400	1.028925	0.941099	1.356368	0.018845	0.002725
1500	1.096468	0.972556	1.279132	0.026942	0.002904
1600	1.033193	0.978998	1.276461	0.016717	0.003072
1700	0.910578	0.913416	1.062512	0.025516	0.003305

Temperature	Average Soluble Fraction Sr	Weight Loss Co (%)	Weight Loss Cs (%)	Weight Loss Sr (%)
60	0.746864	0	0	0
200	0.703611	3.55	3.8767	4.4
300	0.715126	4.7	4.3825	5.75
400	0.589551	7.05	5.4726	6.4935
500	0.476498	8.1	9.1135	9.7951
600	0.524284	8.3	7.9681	8.41255
700	0.450034	9.2168	9.98	11.8308
800	0.131739	9.531	9.61635	10.08
900	0.222217	9.70345	9.925	10.30515
1000	0.106903	9.58505	9.92515	10.26505
1100	0.006821	9.7045	9.7354	11
1200	0.000814	9.7597	9.94005	10.76605
1300	0.001276	9.7489	10.65	10.55505
1400	0.000097	9.9609	8.7912	10.9219
1500	0.000597	10.2102	10.9391	11.1384
1600	0.000316	10.2155	10.9949	10.6542
1700	0.003760	10.338	10.11525	12.5113

Residual Activity of ^{137}Cs , ^{90}Sr , and ^{60}Co in soil versus duration of treatment at 1,600°C

Sample	Before			After Heating			days
	Sr _{cp10m}	Cs _{cp10m}	Co _{cp10m}	Sr _{cp10m}	Cs _{cp10m}	Co _{cp10m}	
13	42864	18207	4176	60581	17388	3985	0.3
14	44686	21013	4638	67576	19400	3998	0.3
29	43424	20806	5110	50238	20873	5083	1
30	43401	17698	4434	60089	16830	4267	1
11	44458	21536	3901	63798	19990	4211	2
12	41864	20741	4097	48410	19814	3932	2
9	43427	18145	4271	47213	16822	3776	4
10	46885	20351	3845	51968	18888	4013	4
3	43008	19754	4428	48738	18144	4194	8
4	43682	22216	4068	49962	20668	3791	8
7	44082	17247	4172	62148	14586	3511	13
8	44647	21240	4450	61264	19594	3760	13

Sample	Before			After			Ratio Sr(A/B)
	Sr(dpm/g)	Cs(dpm/g)	Co(dpm/g)	Sr(dpm/g)	Cs(dpm/g)	Co(dpm/g)	
13	97293.54	12803.79	5248.868	136539.5	11991.72	5008.798	1.403376
14	101508.2	14777.07	5829.562	152517.1	13379.31	5025.138	1.502510
29	99812.64	14478.77	6008.230	115446.0	14553.75	6310.366	1.156627
30	99758.78	12315.93	5213.403	138451.6	11734.76	5297.330	1.387864
11	100980.8	15144.86	4903.217	143887.6	13786.20	5292.860	1.424900
12	94980.33	14585.79	5149.572	108739.1	13664.82	4942.182	1.144859
9	98345.63	12662.24	5532.383	106005.0	11601.37	4746.103	1.077882
10	106324.4	14201.67	4980.569	116866.1	13026.20	5043.991	1.099146
3	97378.86	13785.06	5735.751	109488.3	12513.10	5271.493	1.124354
4	98934.01	15503.14	5269.430	112284.1	14253.79	4764.957	1.134939
7	99856.94	12035.58	5404.145	140118.7	10059.31	4413.021	1.403195
8	101160.5	14822.05	5764.248	138099.5	13513.10	4725.992	1.365152

Sample	Ratio				
	Cs(A/B)	Co(A/B)	Sr(A/B) (----- average -----)	Cs(A/B)	Co(A/B)
13	0.936575	0.954262	1.452943	0.920992	0.908135
14	0.905409	0.862009	1.272245	0.978995	1.033192
29	1.005178	1.050286	1.284880	0.923573	1.019596
30	0.952811	1.016098	1.088514	0.916724	0.935305
11	0.910289	1.079466	1.129647	0.913571	0.911661
12	0.936858	0.959726	1.384173	0.873743	0.818239
9	0.916218	0.857876			
10	0.917230	1.012733			
3	0.907728	0.919058			
4	0.919413	0.904264			
7	0.835797	0.816599			
8	0.911689	0.819880			

Elemental Compositions of radionuclide-contaminated soil used in preparing specimens of labeled glasses:

Sample	Al (mg/kg)	Ca (mg/kg)	Fe (mg/kg)	Mg (mg/kg)	Mn (mg/kg)	Na (mg/kg)	Si-ICP (mg/kg)
Sr90-1	77000	11000	45000	9500	1500	2600	380000
Sr90-2	79000	23000	50000	10000	1700	3500	350000
Sr90-3	77000	11000	48000	97000	1500	2700	370000
Sr90Avg	77666.66	15000	47666.66	38833.33	1566.666	2933.333	366666.6
Cs137-1	75000	18000	40000	8200	720	3300	280000
Cs137-2	75000	17000	40000	8100	710	3200	350000
Cs137-3	74000	19000	39000	8100	700	3200	340000
Cs137Avg	74666.66	18000	39666.66	8133.333	710	3233.333	323333.3
Co60-1	74000	6900	39000	8700	1000	5300	370000
Co60-2	77000	8400	40000	9000	1100	5600	370000
Co60-3	69000	7900	36000	7700	980	5800	360000
Co60Avg	73333.33	7733.333	38333.33	8466.666	1026.666	5566.666	366666.6
ISV-1	86000	30000	45000	9300	1000	8200	360000
ISV-2	98000	15000	49000	11000	810	7600	400000
ISV-3	94000	15000	46000	10000	750	9200	370000
ISV-4	81000	23000	45000	9000	700	9300	360000
ISVAvg	89750	20750	46250	9825	815	8575	372500
Limestone	8400	360000	4900	22000	140	50	34000

Sample	Al ₂ O ₃ (mg/kg)	CaO (mg/kg)	Fe ₂ O ₃ (mg/kg)	MgO (mg/kg)	MnO ₂ (mg/kg)	Na ₂ O (mg/kg)	SiO ₂ (mg/kg)
Sr90-1	145453	15389	64350	15751	2373	3504.8	
Sr90-2	149231	32177	71500	16580	2689.4	4718	
Sr90-3	145453	15389	68640	160826	2373	3639.6	
Sr90Avg	146712.3	20985	68163.33	64385.66	2478.466	3954.133	
Cs137-1	141675	25182	57200	13595.6	1139.04	4448.4	
Cs137-2	141675	23783	57200	13429.8	1123.22	4313.6	
Cs137-3	139786	26581	55770	13429.8	1107.4	4313.6	
Cs137Avg	141045.3	25182	56723.33	13485.06	1123.22	4358.533	
Co60-1	139786	9653.1	55770	14424.6	1582	7144.4	
Co60-2	145453	11751.6	57200	14922	1740.2	7548.8	
Co60-3	130341	11052.1	51480	12766.6	1550.36	7818.4	
Co60Avg	138526.6	10818.93	54816.66	14037.73	1624.186	7503.866	
ISV-1	162454	41970	64350	15419.4	1582	11053.6	
ISV-2	185122	20985	70070	18238	1281.42	10244.8	

Continued

Sample	Al ₂ O ₃ (mg/kg)	CaO (mg/kg)	Fe ₂ O ₃ (mg/kg)	MgO (mg/kg)	MnO ₂ (mg/kg)	Na ₂ O (mg/kg)	SiO ₂ (mg/kg)
ISV-3	177566	20985	65780	16580	1186.5	12401.6	
ISV-4	153009	32177	64350	14922	1107.4	12536.4	
ISVAvg	169537.7	29029.25	66137.5	16289.85	1289.33	11559.1	
Limestone	15867.6	503640	7007	36476	221.48	714.44	
as	Al ₂ O ₃	CaCO ₃	Fe ₂ O ₃	MgCO ₃	MnCO ₃	Na ₂ O	SiO ₂
carbonate	15867.6	898920	7007	76296	292.88	3504.8	

Sample	Si-WetCh (mg/kg)	SiO ₂ (mg/kg)	Sum Total (mg/kg)
Sr90-1		0	
Sr90-2		0	
Sr90-3		0	
Sr90Avg	264.6096	566000	872678.9
Cs137-1	252.9219	541000	
Cs137-2	269.0687	575538.1	
Cs137-3		0	
Cs137Avg	260.9953	558269.0	800186.5
Co60-1		0	
Co60-2		0	
Co60-3		0	
Co60Avg	285.6474	611000	838328.0
ISV-1	245.4417	525000	
ISV-2	244.0392	522000	
ISV-3	248.2468	531000	
ISV-4	257.1294	550000	
ISVAvg	248.7143	532000	825842.7
Limestone	30.38803	65000	628926.5
as		SiO ₂	K ₂ O
carbonate		65000	1066888

ISV Test Trench Construction Dimensions (length was measured from the south end of the trench). Widths and Depths were measured after filling the trench to the indicated depth below ground surface:

Length (ft)	Depth-1 (in)	Width-1 (in)	Depth-2 (in)	Width-2 (in)	Depth-3 (in)	Width-3 (in)	Depth-4 (in)
2	29	20	29	20	29	18	24
4	58	21	44	23	32	30	24
6	62	21	44	24	33	35	23
8	65	22	46	28	33	30	24
10	67	22	48	24	35	30	23
12	67	22	47	27	33	31	23
14	57	24	47	27	34	32	23
16	52	26	46	26	36	34	24
18	55	22	45	28	35	35	24
20	59	19	45	28	35	34	23
22	65	24	47	29	36	32	25
24	66	25	48	29	37	34	24
26	65	26	48	32	37	38	25
28	64	27	48	34	37	38	25
30	59	26	47	30	38	28	25
32	49	25	49	25	38	23	26

Width-4 (in)	Width-5 (in)	Depth-5 (in)	Vol-1 (in3)	Vol-2 (in3)	Vol-3 (in3)	Vol-4 (in3)
24	44	0	0	0	2520	19584
34	46	0	7392	7632	6144	23040
43	46	0	9720	7788	9360	24564
37	44	0	11400	9048	7236	23328
42	45	0	10488	8424	10368	24012
36	45	0	11760	9744	8040	22356
39	46	0	6120	9204	9372	23460
39	44	0	3744	7200	10512	23904
46	47	0	6000	7560	10692	26784
40	46	0	7896	7440	10656	23736
40	48	0	11448	8052	9504	26400
42	51	0	11664	8316	11856	26784
43	50	0	11832	9240	11664	27900
41	54	0	11712	9504	11376	28500
38	53	0	8064	6264	10296	27300
24	44	0	0	6336	6768	21216
Total Volume			129240	121752	146364	392868

	Vol-1 (L)	Vol-2 (L)	Vol-3 (L)	Vol-4 (L)	Trench Volume
	2118.243 (kg)	1995.515 (kg)	2398.905 (kg)	6439.106 (kg)	12951.77L
Weight to fill	3050.270	2873.542	3454.424	9079.140	
Total Limestone	9378.237kg @ 1.44 kg/L bulk density			Total Soil 9079.14kg @ 1.41 kg/L bulk density	

Anion Concentrations in ISV Waste Scrub Solutions:

Sample	Br	Cl	F	NO ₂ ⁻	NO ₃ ⁻	PO ₄ ³⁻	SO ₄ ²⁻
			(----- mg/L -----)				
ISVDRUM1	<50	84	140	<10	<50	<50	520
ISVDRUM2	<50	40	70	<10	<50	<50	360
ISVDRUM3	<50	560	300	<10	<50	<50	6500
ISVDRUM4	<50	610	230	<10	<50	<50	4100
ISVDRUM5	<50	550	200	<10	<50	<50	2700
ISVDRUM6	<50	480	160	<10	<50	<50	2200
ISVDRUM7	<50	370	130	<10	<50	<50	1700
ISVDRUM8	<50	640	280	<10	<50	<50	2700
ISVDRUM9	<50	580	270	<10	<50	<50	2000
ISVDRUM10	<50	130	61	<10	<50	<50	460
ISVDRUM11	<50	130	63	<10	<50	<50	510

INTERNAL DISTRIBUTION

- | | | | |
|--------|------------------|--------|-----------------------------|
| 1. | T. L. Ashwood | 26-29. | P. T. Owen |
| 2. | J. Autrey | 30. | D. E. Reichle |
| 3. | L. D. Bates | 31. | P. S. Rohwer |
| 4. | W. J. Boegly | 32. | T. H. Row |
| 5. | H. M. Braunstein | 33-42. | B. P. Spalding |
| 6. | T. W. Burwinkle | 43. | S. H. Stow |
| 7. | K. W. Cook | 44. | J. R. Trabalka |
| 8. | A. F. Croff | 45. | S. D. Van Hoesen |
| 9. | G. L. Dippo | 46. | L. D. Voorhees |
| 10. | R. B. Dreier | 47. | Central Research Library |
| 11. | L. D. Eyman | 48-62. | ESD Library |
| 12. | S. G. Hildebrand | 63-64. | Laboratory Records Dept. |
| 13. | D. D. Huff | 65. | Laboratory Records, ORNL-RC |
| 14-23. | G. K. Jacobs | 66. | ORNL Patent Section |
| 24. | C. E. Nix | 67. | ORNL Y-12 Technical Library |
| 25. | N. E. Korte | | |

EXTERNAL DISTRIBUTION

68. R. P. Berube, Deputy Assistant Secretary for Environment, EH-20, U.S. Department of Energy, Washington, DC 20585
69. W. F. Bonner, Battelle Pacific Northwest Laboratories, Battelle Boulevard, Richland, WA 99352
70. J. L. Buel, Battelle Pacific Northwest Laboratories, Battelle Boulevard, Richland, WA 99352
71. S. O. Bates, Battelle Pacific Northwest Laboratories, Battelle Boulevard, Richland, WA 99352
72. C. M. Borgstrom, Director, Office of NEPA Project Assistance, EH-25, U.S. Department of Energy, Washington, DC 20585
73. J. S. Brehm, Office of Surplus Facilities Management, UNC Nuclear Industries, P.O. Box 490, Richland, WA 99352
74. J. G. Carter, Battelle Pacific Northwest Laboratories, Battelle Boulevard, Richland, WA 99352
75. T. C. Chee, R&D and Byproducts Division, DP-124 (GTN), U.S. Department of Energy, Washington, DC 20545
76. R. R. Colwell, Director, Maryland Biotechnology Institute, Microbiology Building, University of Maryland, College Park, MD 20742
77. W. E. Cooper, Department of Zoology, College of Natural Sciences, Michigan State University, East Lansing, MI 48824
78. N. H. Cutshall, 10461 White Granite Dr., Suite 204, Oakton, VA 22124
79. E. C. Davis, East Tennessee State University, Johnson City, TN 37601

80. J. E. Dieckhoner, Acting Director, Operations and Traffic Division, DP-122 (GTN), U.S. Department of Energy, Washington, DC 20545
81. J. Farley, Office of Environmental Process and Effects Research, U.S. Environmental Protection Agency, 401 M Street, SW, RD-682, Washington, DC 20460
82. R. D. Glenn, Bechtel National, Inc., P.O. Box 350, Oak Ridge, TN 37831-0350
83. T. B. Hindman, Director, Office of Defense Waste and Transp. Management, DP-12, U.S. Department of Energy, Washington, DC 20545
84. E. A. Jordon, Office of Defense Programs, U.S. Department of Energy, DP-122, Washington, DC 20545
85. George Y. Jordy, Director, Office of Program Analysis, Office of Energy Research, ER-30, G-226, U.S. Department of Energy, Washington, DC 20545
86. S. D. Koegler, Battelle Pacific Northwest Laboratories, Battelle Boulevard, Richland, WA 99352
87. Emil Kowalski, Division Head, Repository Projects, NAGRA, Parkstrasse 23, CH-401, Baden, Switzerland
88. G. E. Likens, Director, The New York Botanical Garden, Institute of Ecosystem Studies, The Mary Flagler Cary Arboretum, Box AB, Millbrook, NY 12545
89. G. Loomis, EG&G Idaho, Inc., P.O. Box 1625, Idaho Falls, ID 83415
90. Helen McCammon, Director, Ecological Research Division, Office of Health and Environmental Research, Office of Energy Research, ER-75, U.S. Department of Energy, Washington, DC 20545
91. C. E. Miller, Surplus Facilities Management Program Office, U.S. Department of Energy, Richland Operations, P.O. Box 550, Richland, WA 99352
92. W. E. Murphie, Office of Remedial Action and Waste Technology, U.S. Department of Energy, NE-23, Washington, DC 20545
93. E. O'Donnell, Division of Radiation Program and Earth Sciences, U.S. Nuclear Regulatory Commission, NLS-260, Washington, DC 20555
94. R. J. Starmer, HLW Technical Development Branch, Office of Nuclear Material Safety and Safeguards, Nuclear Regulatory Commission, 5E4 (OWFN), Washington, DC 20555
95. Brian Sturt, Geological Survey of Norway, P.O. Box 3006, Trondheim, Norway N7001
96. David H. Thompson, Argonne National Laboratory, Bldg. 206, 9700 S. Cass Avenue, Arlington, IL 60439
97. Frank J. Wobber, Ecological Research Division, Office of Health and Environmental Research, Office of Energy Research, ER-75, U.S. Department of Energy, Washington, DC 20545
98. J. G. Yates, Office of Energy Research, U.S. Department of Energy, ER-42, Washington, DC 20585
99. Office of Assistance Manager for Energy Research and Development, Oak Ridge Operations, P.O. Box 2001, U.S. Department of Energy, Oak Ridge, TN 37831-8600
- 100-109. Office of Scientific and Technical Information, P.O. Box 62, Oak Ridge, TN 37831